

Recovery of dissolved platinum group metals from a pregnant copper sulphate leach solution by precipitation

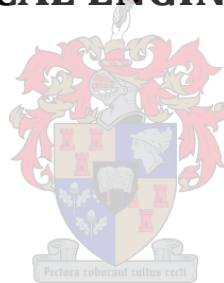
by

James Mulwanda

**Thesis presented in partial fulfillment
of the requirements for the Degree**

of

**MASTER IN ENGINEERING
(CHEMICAL ENGINEERING)**



**in the Faculty of Engineering
at Stellenbosch University**

Supervisor

Dr. Christie Dorfling

April 2014

Declaration

By submitting this thesis electronically, I declare that the entirety of the work contained therein is my own, original work, that I am the sole author thereof (save to the extent explicitly otherwise stated), that reproduction and publication thereof by Stellenbosch University will not infringe any third party rights and that I have not previously in its entirety or in part submitted it for obtaining any qualification.

James Mulwanda
Signature:

20th February 2014

Abstract

In Base Metal Refineries (BMRs), the copper sulphate leach solution produced during the final pressure leaching stage contains impurities such as selenium and tellurium, as well as other precious metals (OPMs, namely Rh, Ru, and Ir). Se and Te are removed by precipitation with sulphur dioxide prior to electrowinning of Cu. While a small percentage of the dissolved OPMs precipitate with the Se and Te, the largest portion remains in solution and is recycled to the first stage leach. If a larger portion of the OPMs in solution can be recovered in the Se/Te precipitation stage, OPM losses and the OPM inventory of the plant can be reduced. The aim of this project was to determine operating conditions that would allow maximum OPM recovery with minimal Cu and Ni co-precipitation in the Se/Te removal section of a BMR.

The effects that the operating temperature, pressure, stirring rate, reagent type, and reagent quantity have on the metal precipitation behavior and precipitate characteristics were determined experimentally. Thio-urea and sulphurous acid were evaluated as precipitation reagents for temperatures of 80°C and 160°C, stirring rates of 250 rpm and 500 rpm, and pressures equal to ambient pressure and 7 bar. 200 % and 320 % excess thio-urea and 720 % and 960 % excess sulphur dioxide were used.

The precipitation of OPMs with sulphur dioxide was generally poor; the maximum percentage Rh, Ru, and Ir precipitated were 35 %, 18 %, and 20 %, respectively. It was, however, found that the OPM precipitation increased as the reagent amount was increased. Increasing the temperature further increased Rh and Ir precipitation but affected the Ru precipitation negatively. Thio-urea precipitated virtually all of the Rh contained in the solution irrespective of the values of the process variables studied. As was the case with sulphur dioxide, increasing the amount of thio-urea added resulted in increased Ru and Ir precipitation, while higher temperatures favored Ir precipitation but not Ru precipitation. The maximum percentage Ru and Ir precipitation achieved with thio-urea were 87 % and 60 %, respectively.

Complete Se precipitation was observed at all process conditions, while Te precipitation increased as the operating temperature and the reagent quantity were increased. Maximum Te precipitation of 98 % and 90 % were achieved when using 320 % excess thio-urea and 960 % sulphurous acid quantities, respectively, at 160°C and a stirring rate of 250 rpm. Increasing the reagent quantity and temperature did, however, also result in increased copper and nickel precipitation.

The statistical analysis of the results allowed regression models to be fitted to predict the percentage metal precipitation as a function of the investigated process variables. These models were used to define an objective function to determine the optimal operating conditions. A temperature of 80°C, a pressure of 7 bar, and 200 % excess thio-urea were proposed as the optimum operating conditions that would yield 98 % Rh, 75 % Ru, and 48 % Ir precipitation with less than 5 % Cu and Ni co-precipitation. Experimental validation tests confirmed the model predicted values and proved repeatability of the experimental data.

Opsomming

Die kopersulfaat logingsoplossing wat tydens die finale drukloging stadium in Basis Metaal Raffinaderye (BMRe) produseer word, bevat onsuiverhede soos selenium en tellurium sowel as ander edelmetale (AEMe, naamlik Rh, Ru, en Ir). Se en Te word voor Cu elektrowinning verwyder deur middel van presipitasie met swaweldioksied. Alhoewel 'n klein persentasie van die opgeloste AEMe saam met die Se en Te presipiteer, bly die grootste gedeelte in oplossing en word gevolglik na die eerste loging stadium hersirkuleer. AEM verliese en die AEM inventaris van die aanleg kan verminder word indien 'n groter gedeelte van die AEMe in die Se/Te presipitasie stadium herwin kan word. Die doel van hierdie projek was om bedryfstoestande te bepaal om maksimum AEM herwinning met minimale Cu en Ni kopresipitasie in die Se/Te verwyderingseksie van 'n BMR te behaal.

Die effekte wat bedryfstoestande soos temperatuur, druk, roerder tempo, tipe reagens, en hoeveelheid reagens op die metaal presipitasiegedrag en presipitaat eienskappe het, is eksperimenteel bepaal. Tio-ureum en swaweligsuur is evalueer as presipitasie reagent vir temperature van 80°C en 160°C, roerder tempo's van 250 rpm en 500 rpm, en drukke gelyk aan omgewingsdruk en 7 bar. 200 % en 320 % oormaat tio-ureum en 720 % en 960 % oormaat swaweldioksied is gebruik.

Die presipitasie van AEMe met swaweldioksied was swak in die algemeen; die maksimum persentasie Rh, Ru, en Ir presipitasie wat behaal is, is 35 %, 18 %, en 20 %, onderskeidelik. Daar is egter gevind dat die AEM presipitasie toeneem indien die hoeveelheid reagens toeneem. 'n Toename in die temperatuur het verder tot 'n toename in Rh en Ir presipitasie gelei, maar dit het Ru presipitasie negatief affekteer. Tio-ureum het basies al die Rh in oplossing laat presipiteer, ongeag die waardes van die ander prosesveranderlikes wat ondersoek is. Soos wat die geval vir swaweldioksied was, het 'n toename in die hoeveelheid tio-ureum 'n toename in die Ru en Ir presipitasie tot gevolg gehad, terwyl hoër temperature Ir presipitasie bevoordeel en Ru presipitasie benadeel het. Die maksimum persentasie Ru en Ir presipitasie wat met tio-ureum behaal is, is 87 % en 60 %, onderskeidelik.

Volledige Se presipitasie is by alle proses toestande waargeneem, terwyl Te presipitasie toegeneem het soos wat die temperatuur en die hoeveelheid reagens toegeneem het. Maksimum Te presipitasie van 98 % en 90 % is behaal toe 320 % oormaat tio-ureum en 960 % oormaat swaweligsuur, onderskeidelik, by 160°C en 'n roerder tempo van 250 rpm gebruik is. 'n Toename in die hoeveelheid reagens en die temperatuur het egter ook meer koper en nikkel presipitasie tot gevolg gehad.

Die statistiese analise van die resultate het dit moontlik gemaak om regressie modelle te pas om die persentasie metaal presipitasie as 'n funksie van die ondersoekte veranderlikes te voorspel. Hierdie modelle is gebruik om 'n doelfunksie te definieer ten einde die optimale bedryfstoeestand te bepaal. 'n Temperatuur van 80°C, 'n druk van 7 bar, en 200 % oormaat tiorureum is voorgestel as die optimale bedryfstoeestand wat 98 % Rh, 75 % Ru, en 48 % Ir presipitasie met minder as 5 % Cu en Ni kopresipitasie tot gevolg sal hê. Eksperimentele geldigheidsbepalingtoetse het die waardes wat deur die modelle voorspel is bevestig en die herhaalbaarheid van die eksperimentele data bewys.

Acknowledgements

I would like to express my appreciation to the following:

- Dr. Christie Dorfling for his invaluable guidance, dedication to the research and inspiration for perfection.
- Lonmin BMR, for providing the materials and financial support for this research.
- All the administrative and technical personnel at the Stellenbosch University Department of Process Engineering for providing administrative and technical assistance.
- My family and all friends both in Zambia and South Africa for their support and encouragements.

I am particularly grateful to God almighty for strengthening, guiding and keeping me throughout this research process.

Table of contents

Declaration	i
Abstract	ii
Opsomming	iv
Acknowledgements	vi
Table of contents.....	vii
List of tables.....	x
List of figures.....	xiii
Nomenclature.....	xviii
1. INTRODUCTION.....	1
1.1. Background.....	1
1.2. Problem statement.....	4
1.3. Objectives	5
1.4. Thesis outline	5
2. LITERATURE REVIEW	6
2.1. Introduction	6
2.2. BMR process solution chemistry	6
2.3. Selenium and tellurium removal operations.....	7
2.3.1. General operations	7
2.3.2. Se/Te removal at Lonmin	9
2.3.3. Reaction of iron with various reagents	10
2.4. Precipitation of metals from acidic solutions.....	11
2.4.1. Precipitation of metals as sulphides	11
2.4.2. Key results from previous OPM chemical precipitation investigations	12
2.5. Key process variables.....	13
2.5.1. Precipitating reagent.....	14
2.5.2. Temperature	15
2.5.3. Pressure	16
2.5.4. Agitation.....	16
2.6. Precipitate characterisation	17
2.7. Chapter Summary	18
3. EXPERIMENTAL	19
3.1. Materials.....	19
3.2. Methodology	19
3.2.1. Equipment.....	19

3.2.2. Experimental procedure	21
3.2.3. Experimental planning	21
3.2.3.1. Experimental tests.....	21
3.2.3.2. Analytical methods.....	22
3.2.3.3. Statistical analysis.....	23
4. REAGENT SCREENING TESTS - RESULTS AND DISCUSSION	24
4.1. Introduction	24
4.2. OPM precipitation.....	24
4.3. Nickel and copper precipitation	27
4.4. Selenium and tellurium precipitation	29
4.5. Conclusion.....	31
5. EFFECTS OF OPERATING PARAMETERS ON THE PRECIPITATION PROCESS	32
5.1. Characterization of the precipitates.....	32
5.2. Thio-urea based experiments	34
5.2.1. Rhodium precipitation.....	34
5.2.2. Ruthenium precipitation.....	36
5.2.3. Iridium precipitation.....	37
5.2.4. Copper precipitation.....	38
5.2.5. Nickel precipitation.....	39
5.2.6. Selenium and tellurium	40
5.3. Sulphurous acid based experiments	40
5.3.1. Rhodium precipitation.....	41
5.3.2. Ruthenium precipitation.....	42
5.3.3. Iridium precipitation.....	42
5.3.4. Copper precipitation.....	43
5.3.5. Nickel precipitation.....	44
5.3.6. Selenium and tellurium	45
5.4. Influence of operating parameters on precipitate characteristics	45
5.4.1. Temperature	46
5.4.2. Reagent quantity	47
5.4.3. Pressure	48
5.4.4. Agitation speed	49

6.	STATISTICAL ANALYSIS OF EXPERIMENTAL RESULTS	51
6.1.	Thio-urea based experimental data	51
6.1.1.	Model selection	51
6.1.2.	Analysis of variance (ANOVA)	57
6.1.3.	Mathematical representation of models	59
6.1.4.	Optimization	60
6.1.5.	Confirmatory test results.....	62
6.1.6.	Process options and practical consideration	66
6.2.	Sulphurous acid based experimental data.....	68
6.2.1.	Model selection	68
6.2.2.	Analysis of variance	71
6.2.3.	Mathematical representation of model.....	73
6.2.4.	Concluding remarks.....	73
7.	CONCLUSIONS AND RECOMMENDATIONS	74
7.1.	Reagent identification	74
7.2.	Effects operating variables.....	74
7.3.	Process variable optimization	75
7.4.	Recommendations for future work	75
	References	77
	APPENDIX: A.....	82
	EXPERIMENTAL DATA.....	82
	Screening experiments.....	82
	Optimisation experiments	85
	APPENDIX: B.....	97
	LIST OF FIGURES	97
	Thio-urea experimental data.....	97
	Sulphurous acid experimental data	105
	APPENDIX: C.....	114
	STATISTICAL ANALYSIS DATA	114

List of tables

<i>Table 1: Typical Merensky and UG-2 concentrate analysis for Lonmin operations (Nell, 2004)</i>	2
<i>Table 2: Typical analysis of the smelter matte produced by Lonmin platinum (Crundwell et al, 2011)</i>	2
<i>Table 3: Typical analysis of the converter matte produced by Lonmin platinum (Jones, 2000)</i>	2
<i>Table 4: Dissolution reactions of PGMs in sulphate solution (Dorfling et al., 2013)</i>	7
<i>Table 5: Chemical compositions of the copper sulphate leach solution supplied by Lonmin Plc</i>	19
<i>Table 6: Chemical reagents and operating temperature for screening tests</i>	22
<i>Table 7: Experimental conditions for the second phase of experiment performed using thio-urea</i>	22
<i>Table 8: Experimental conditions for the second phase of experiment performed using SO₂</i>	22
<i>Table 9: Composition of the precipitates formed at both temperatures after 480 minutes (200 % excess thio-urea, ambient temperature and 250 rpm)</i>	46
<i>Table 10: Composition of the precipitates for the variation in reagent excess quantity (80°C, ambient pressure, and 250 rpm)</i>	47
<i>Table 11: Composition of the precipitates for the variation in reactor pressure (80°C, 200 % excess thio-urea, and 250 rpm)</i>	48
<i>Table 12: Composition of the precipitates for the variation in agitation speed (80°C, 200 % excess thio-urea, and ambient pressure)</i>	49
<i>Table 13: Standardized effects of factors on various precipitation responses (thio-urea data)</i>	58
<i>Table 14: Percentage contribution of standardized effects to the fitted model</i>	58
<i>Table 15: ANOVA table of p-values for the responses</i>	59
<i>Table 16: Constraints varied to obtain optimal conditions</i>	61
<i>Table 17: Combinations of optimal conditions for parameters as generated from numerical optimization for two OPMs and base metal precipitation optimization cases</i>	62
<i>Table 18: Standardized effects of factors on various precipitation responses (sulphurous acid data)</i>	71
<i>Table 19: Percentage contribution of standardized effects to the fitted model (sulphurous acid data)</i>	72
<i>Table 20: ANOVA p-values for OPMs and base metal precipitation responses (sulphurous acid data)</i>	72
<i>Table 21: Screening test 1</i>	82
<i>Table 22: Screening test 2</i>	82
<i>Table 23: Screening test 3</i>	83
<i>Table 24: Screening test 4</i>	83
<i>Table 25: Screening test 5</i>	83

<i>Table 26: Screening test 6</i>	84
<i>Table 27: Screening test 7</i>	84
<i>Table 28: Screening test 8</i>	84
<i>Table 29: Optimization test 1 (thio-urea data)</i>	85
<i>Table 30: Optimization test 2 (thio-urea data)</i>	85
<i>Table 31: Optimization test 3 (thio-urea data)</i>	86
<i>Table 32: Optimization test 4 (thio-urea data)</i>	86
<i>Table 33: Optimization test 5 (thio-urea data)</i>	86
<i>Table 34: Optimization test 6 (thio-urea data)</i>	87
<i>Table 35: Optimization test 7 (thio-urea data)</i>	87
<i>Table 36: Optimization test 8 (thio-urea data)</i>	87
<i>Table 37: Optimization test 9 (thio-urea data)</i>	88
<i>Table 38: Optimization test 10 (thio-urea data)</i>	88
<i>Table 39: Optimization test 11 (thio-urea data)</i>	88
<i>Table 40: Optimization test 12 (thio-urea data)</i>	89
<i>Table 41: Optimization test 13 (thio-urea data)</i>	89
<i>Table 42: Optimization test 14 (thio-urea data)</i>	89
<i>Table 43: Optimization test 15 (thio-urea data)</i>	90
<i>Table 44: Optimization test 16 (thio-urea data)</i>	90
<i>Table 45: Optimization test 1 (sulphurous acid data)</i>	91
<i>Table 46: Optimization test 2 (sulphurous acid data)</i>	91
<i>Table 47: Optimization test 3 (sulphurous acid data)</i>	92
<i>Table 48: Optimization test 4 (sulphurous acid data)</i>	92
<i>Table 49: Optimization test 5 (sulphurous acid data)</i>	92
<i>Table 50: Optimization test 6 (sulphurous acid data)</i>	93
<i>Table 51: Optimization test 7 (sulphurous acid data)</i>	93
<i>Table 52: Optimization test 8 (sulphurous acid data)</i>	93
<i>Table 53: Optimization test 9 (sulphurous acid data)</i>	94
<i>Table 54: Optimization test 10 (sulphurous acid data)</i>	94
<i>Table 55: Optimization test 11 (sulphurous acid data)</i>	94
<i>Table 56: Optimization test 12 (sulphurous acid data)</i>	95
<i>Table 57: Optimization test 13 (sulphurous acid data)</i>	95
<i>Table 58: Optimization test 14 (sulphurous acid data)</i>	95
<i>Table 59: Optimization test 15 (sulphurous acid data)</i>	96
<i>Table 60: Optimization test 16 (sulphurous acid data)</i>	96
<i>Table 61: Rh precipitation- ANOVA for selected factorial model (thio-urea data)</i>	114

<i>Table 62: Ru precipitation- ANOVA for selected factorial model (thio-urea data)</i>	115
<i>Table 63: Ir precipitation- ANOVA for selected factorial model (thio-urea data)</i>	115
<i>Table 64: Cu precipitation- ANOVA for selected factorial model (thio-urea data)</i>	116
<i>Table 65: Ni precipitation-ANOVA for selected factorial model (thio-urea data)</i>	117
<i>Table 66: Se precipitation-ANOVA for selected factorial model (thio-urea data)</i>	117
<i>Table 67: Te precipitation-ANOVA for selected factorial model (thio-urea data)</i>	118
<i>Table 68: Rh precipitation- ANOVA for selected factorial model (sulphurous acid data)</i>	118
<i>Table 69: Ru precipitation- ANOVA for selected factorial model (sulphurous acid data)</i>	119
<i>Table 70: Ir precipitation- ANOVA for selected factorial model (sulphurous acid data)</i>	119
<i>Table 71: Cu precipitation- ANOVA for selected factorial model (sulphurous acid data)</i>	120
<i>Table 72: Ni precipitation- ANOVA for selected factorial model (sulphurous acid data)</i>	121
<i>Table 73: Se precipitation- ANOVA for selected factorial model (sulphurous acid data)</i>	121
<i>Table 74: Te precipitation- ANOVA for selected factorial model (sulphurous acid data)</i>	122

List of figures

<i>Figure 1: Process flow diagram of a typical BMR (Redrawn from Bircumshaw (2008))</i>	3
<i>Figure 2: Experimental setup schematic diagram</i>	20
<i>Figure 3: OPM precipitations for the different screening test reagents at 80°C and 160°C (250 rpm, ambient pressure)</i>	26
<i>Figure 4: Cu and Ni precipitation for the different screening test reagents at 80°C and 160°C (250 rpm, ambient pressure)</i>	28
<i>Figure 5: Se and Te precipitation for the different screening test reagents at 80°C and 160°C (250 rpm, ambient pressure)</i>	30
<i>Figure 6: XRD patterns of the precipitate sample (80°C, 200 % excess thio-urea, ambient pressure, and 250 rpm)</i>	32
<i>Figure 7: XRD patterns of the precipitate sample (160°C, 200 % excess thio-urea, ambient pressure, and 250 rpm)</i>	33
<i>Figure 8: Scanning electron image of precipitates generated from the two reagents at 80°C (a) thio-urea and (b) sulphurous acid</i>	34
<i>Figure 9: Effects of (a) reagent quantity, (b) temperature, (b) pressure, and (d) agitation speed on the rate and extent of Rh precipitation using thio-urea</i>	35
<i>Figure 10: Effects of (a) agitation speed (b) reagent quantity, (c) temperature, and (d) pressure on the rate and extent of Ru precipitation using thio-urea</i>	36
<i>Figure 11: Effects of (a) reagent quantity, (b) temperature, (c) pressure and (d) agitation speed on the rate and extent of Ir precipitation using thio-urea</i>	38
<i>Figure 12: Effects of (a) reagent quantity, (b) temperature, (c) pressure and (d) agitation speed on the rate and extent of Cu precipitation using thio-urea</i>	39
<i>Figure 13: Effects of (a) reagent quantity, (b) temperature, (c) pressure and (d) agitation speed on the rate and extent of Ni precipitation using thio-urea</i>	40
<i>Figure 14: Effects of (a) reagent quantity, (b) temperature (c) pressure, (d) agitation speed on the rate and extent of Rh recovery using sulphurous acid</i>	41
<i>Figure 15: Effects of (a) reagent quantity, (b) temperature (c) pressure, (d) agitation speed on the rate and extent of Ru recovery using sulphurous acid</i>	42
<i>Figure 16: Effects of (a) reagent quantity, (b) temperature (c) pressure, and (d) agitation speed on the rate and extent of Ir precipitation using sulphurous acid</i>	43
<i>Figure 17: Effects of (a) reagent quantity, (b) temperature (c) pressure, and (d) agitation speed on the rate and extent of Cu precipitation using sulphurous acid</i>	44
<i>Figure 18: Effects of (a) reagent quantity, (b) temperature (c) pressure, and (d) agitation speed on the rate and extent of Ni precipitation using sulphurous acid</i>	45

<i>Figure 19: Size distribution of the precipitates obtained at low and high temperature levels (200 % excess thio-urea, ambient pressure, and 250 rpm).....</i>	<i>47</i>
<i>Figure 20: Size distributions of the precipitates obtained using 200 % and 320 % excess thio-urea (80°C, ambient pressure, and 250 rpm)</i>	<i>48</i>
<i>Figure 21: Size distributions of the precipitates obtained at ambient and 7 bar reactor pressure (80°C, 200 % excess thio-urea, and 250 rpm)</i>	<i>49</i>
<i>Figure 22: Size distributions of the precipitates obtained at 250 rpm and 500 rpm agitation speed (80°C, 200 % excess thio-urea, and ambient pressure).....</i>	<i>50</i>
<i>Figure 23: Half-normal probability plot of effects for Rh precipitation by thio-urea</i>	<i>53</i>
<i>Figure 24: Half-normal probability plot of effects for Ru precipitation by thio-urea</i>	<i>53</i>
<i>Figure 25: Half-normal probability plot of effects for Ir precipitation by thio-urea.</i>	<i>54</i>
<i>Figure 26: Half-normal probability plot of effects for Cu precipitation by thio-urea.....</i>	<i>54</i>
<i>Figure 27: Half-normal probability plot of effects for Ni precipitation by thio-urea.</i>	<i>55</i>
<i>Figure 28: Half-normal probability plot of effects for Se precipitation by thio-urea.</i>	<i>55</i>
<i>Figure 29: Half-normal probability plot of effects for Te precipitation by thio-urea.....</i>	<i>56</i>
<i>Figure 30: Interaction plots showing the effects of interactions between (a) agitation speed and pressure -Rh (b) temperature and reagent-Ru (c) pressure and reagent - Ru and (d) agitation speed and pressure -Ir on the precipitation responses.....</i>	<i>57</i>
<i>Figure 31: OPMs recovery confirmatory results obtained at optimized process conditions (200 % excess thio-urea, 80°C, 7bar, and 500 rpm).....</i>	<i>63</i>
<i>Figure 32: Base metal co-precipitation confirmatory results obtained at optimized process conditions (200 % excess thio-urea, 80°C, 7bar, and 500 rpm)</i>	<i>63</i>
<i>Figure 33: Selenium and tellurium precipitation confirmatory results obtained at optimized process conditions (200 % excess thio-urea, 80°C, 7bar, and 500 rpm)</i>	<i>64</i>
<i>Figure 34: Repeatability of Ru recovery experimental results (200 % excess thio-urea, 80°C, 7bar, and 500 rpm).....</i>	<i>64</i>
<i>Figure 35: Repeatability of Ru recovery experimental results (200 % excess thio-urea, 80°C, 7bar, and 500 rpm).....</i>	<i>65</i>
<i>Figure 36: Repeatability of Ir recovery experimental results (200 % excess thio-urea, 80 °C, 7bar, and 500 rpm).....</i>	<i>65</i>
<i>Figure 37: Repeatability of Cu co-precipitation experimental results (200 % excess thio-urea, 80°C, 7 bar, and 500 rpm).....</i>	<i>66</i>
<i>Figure 38: Repeatability of Ni co-precipitation experimental results (200 % excess thio-urea, 80 °C, 7 bar, and 500 rpm).....</i>	<i>66</i>
<i>Figure 39: Half-normal probability plot of effects for Rh precipitation by Sulphurous acid</i>	<i>69</i>
<i>Figure 40: Half-normal probability plot of effects for Ru precipitation by Sulphurous acid</i>	<i>69</i>

Figure 41: Half-normal probability plot of effects for Ir precipitation by Sulphurous acid 70

Figure 42: Half-normal probability plot of effects for Cu precipitation by Sulphurous acid 70

Figure 43: Half-normal probability plot of effects for Ni precipitation by Sulphurous acid 71

Figure 44: Effect of operating variables on precipitation (80°C, 320% excess, 500rpm, ambient pressure) 97

Figure 45: Effect of operating variables on precipitation (80°C, 200% excess, 250rpm, ambient pressure) 98

Figure 46: Effect of operating variables on precipitation (80°C, 320% excess, 250rpm, ambient pressure) 98

Figure 47: Effect of operating variables on precipitation (80°C, 320% excess, 250rpm, 7 bars). 99

Figure 48: Effect of operating variables on precipitation (80°C, 320% excess, 500rpm, 7bars)..... 99

Figure 49: Effect of operating variables on precipitation (80°C, 200% excess, 500rpm, 7 bars) 100

Figure 50: Effect of operating variables on precipitation (80°C, 200% excess, 500rpm, ambient pressure)100

Figure 51: Effect of operating variables on precipitation (80°C, 320% excess, 250rpm, 7 bars) 101

Figure 52: Effect of operating variables on precipitation (160°C, 200% excess, 250rpm, 7 bars)101

Figure 53: Effect of operating variables on precipitation (160°C, 200% excess, 500rpm, ambient pressure)102

Figure 54: Effect of operating variables on precipitation (160°C, 200% excess, 250rpm, ambient pressure)102

Figure 55: Effect of operating variables on precipitation (160°C, 320% excess, 500rpm, 7 bars)103

Figure 56: Effect of operating variables on precipitation (160°C, 200% excess, 500rpm, 7 bars)103

Figure 57: Effect of operating variables on precipitation (160°C, 320% excess, 250rpm, ambient pressure)104

Figure 58: Effect of operating variables on precipitation (160°C, 320% excess, 250rpm, 7 bars)104

Figure 59: Effect of operating variables on precipitation (160°C, 320% excess, 500rpm, ambient pressure)105

Figure 60: Effect of operating variables on precipitation (80°C, 960% excess, 250rpm, ambient pressure)105

Figure 61: Effect of operating variables on precipitation (80°C, 960% excess, 500rpm, ambient pressure)106

<i>Figure 62: Effect of operating variables on precipitation (80°C, 720% excess, 250rpm, ambient pressure)</i>	<i>106</i>
<i>Figure 63: Effect of operating variables on precipitation (80°C, 720% excess, 500rpm, ambient pressure)</i>	<i>107</i>
<i>Figure 64: Effect of operating variables on precipitation (80°C, 960% excess, 500rpm, 7 bars).....</i>	<i>107</i>
<i>Figure 65: Effect of operating variables on precipitation (160°C, 960% excess, 500rpm, ambient pressure)</i>	<i>108</i>
<i>Figure 66: Effect of operating variables on precipitation (160°C, 720% excess, 500rpm, ambient pressure)</i>	<i>108</i>
<i>Figure 67: Effect of operating variables on precipitation (80°C, 960% excess, 250rpm, 7 bars).....</i>	<i>109</i>
<i>Figure 68: Effect of operating variables on precipitation (80°C, 720% excess, 500rpm, 7 bars).....</i>	<i>109</i>
<i>Figure 69: Effect of operating variables on precipitation (160°C, 960% excess, 250rpm, ambient pressure)</i>	<i>110</i>
<i>Figure 70: Effect of operating variables on precipitation (160°C, 960% excess, 500rpm, 7 bars).....</i>	<i>110</i>
<i>Figure 71: Effect of operating variables on precipitation (160°C, 960% excess, 250rpm, 7 bars).....</i>	<i>111</i>
<i>Figure 72: Effect of operating variables on precipitation (80°C, 720% excess, 250rpm, 7 bars).....</i>	<i>111</i>
<i>Figure 73: Effect of operating variables on precipitation (160°C, 720% excess, 250rpm, ambient pressure)</i>	<i>112</i>
<i>Figure 74: Effect of operating variables on precipitation (160°C, 720% excess, 500rpm, 7 bars).....</i>	<i>112</i>
<i>Figure 75: Effect of operating variables on precipitation (80°C, 720% excess, 250rpm, 7 bars).....</i>	<i>113</i>
<i>Figure 76: Pareto plots of effects for the Rh response (thio-urea data)</i>	<i>123</i>
<i>Figure 77: Pareto plots of effects for the Ru response (thio-urea data)</i>	<i>123</i>
<i>Figure 78: Pareto plots of effects for the Ir response (thio-urea data)</i>	<i>124</i>
<i>Figure 79: Pareto plots of effects for the Cu response (thio-urea data).....</i>	<i>124</i>
<i>Figure 80: Pareto plots of effects for the Ni response (thio-urea data)</i>	<i>125</i>
<i>Figure 81: Pareto plots of effects for the Se response (thio-urea data)</i>	<i>125</i>
<i>Figure 82: Pareto plots of effects for the Te response (thio-urea data).....</i>	<i>126</i>
<i>Figure 83: Pareto plots of effects for the Rh response (sulphurous acid data).....</i>	<i>126</i>
<i>Figure 84: Pareto plots of effects for the Ru response (sulphurous acid data).....</i>	<i>127</i>
<i>Figure 85: Pareto plots of effects for the Ir response (sulphurous acid data).....</i>	<i>127</i>
<i>Figure 86: Pareto plots of effects for the Cu response (sulphurous acid data).....</i>	<i>128</i>

Figure 87: Pareto plots of effects for the Ni response (sulphurous acid data).....128

Figure 88 Interaction plots showing the effects of interactions between (a) reagent quantity and pressure -Rh (b) temperature and reagent-Ru (c) pressure and temperature - Ru and (d) pressure and temperature-Ir (e) pressure and temperature-Cu, (f) pressure and temperature-Cu, (f) pressure and temperature-Ni, and (g) temperature and agitation-Ni on the precipitation responses130

Nomenclature

Acronym	Meaning
ACS	America Chemical Society
BMR	Base Metal Refinery
CAF	Central Analytical Facility
ICP-AES	Inductively Coupled Plasma Atomic Emission Spectroscopy
OPMs	Other Precious Metals
PGMs	Platinum Group Metals
ppm	Parts per million
rpm	Revolutions per minute
SEM	Scanning Electron Microscope
XRD	X-ray Diffraction

Symbol	Unit	Meaning
Eh	mV	Oxidation reduction potential
pH	-	Negative log of H ⁺ activity
C _o	mg/L	Initial concentration of species
C _t	mg/L	Concentration of species at the time of sampling
%	-	Percentage

1. INTRODUCTION

1.1. Background

The elements ruthenium (Ru), rhodium (Rh), palladium (Pd), platinum (Pt), osmium (Os), and iridium (Ir) are referred to as platinum group metals (PGMs). In South Africa the mineral ores that are processed to extract PGMs are located in the Bushveld Igneous Complex found in the Northwest, Limpopo, Gauteng, and Mpumalanga provinces. The Bushveld Complex of South Africa is the world's largest known primary deposit of PGMs (Renner et al., 2001; Von Grunewaldt, 1977). Lonmin is among the world's largest platinum producers operating in the Bushveld Complex.

The PGM bearing ores processed at Lonmin Marikana are obtained from the Merensky and Upper Group 2 (UG-2) reefs. The UG-2 ore body lies 40 – 140 meters below the Merensky reef on the western limb of the Bushveld Igneous Complex. In both the Merensky and UG-2 reefs, the major sulphides of base metals associated with the occurrence of PGMs include pentlandite $(\text{Ni,Fe,Co})_9\text{S}_8$, pyrrhotite (Fe_8S_9) , and chalcopyrite (CuFeS_2) . The dominant PGMs in the Merensky reef include the cooperite (PtS), braggite (Pt-Pd)S, sperrylite (PtAs_2) , and Pt-Pd bismuthtelluride. Ru-Os-Ir-bearing laurites, cooperite, braggite, Rh sulphides, and unnamed Pt-Rh-Ir-Cu-S are some of the PGMs present in the in the UG-2 reef. In the Merensky reef, these PGMs are found along the sulphide/silicate grain boundaries or as inclusions in silicate and chromite whereas in the UG-2 PGMs “occur interstitially, along chromite grain boundaries and locked in chromites” (Lamya, 2007; Lindsay, 1988).

According to Crundwell et al. (2011), the mined PGM ores usually contain between 3 – 4 g of PGMs per tonne of ore. The recovery of PGMs and base metal from such ores is achieved via a number of process stages which include comminution, flotation, smelting and refining. Comminution process aims to reduce the ore to manageable size and liberate the ore minerals. The ore is crushed and ground to liberate PGMs and base metal sulphide-bearing mineral grains from the host rock. The minerals are then separated from the gangue rock using flotation. The process of flotation aims to isolate most of the minerals that are rich in PGMs into a small amount of flotation concentrate by rejecting most of the rock barren in PGMs. Table 1 shows the typical composition of Merensky and UG-2 concentrates in the Lonmin operations (Nell, 2004; Crundwell et al., 2011).

Table 1: Typical Merensky and UG-2 concentrate analysis for Lonmin operations (Nell, 2004)

	Al_2O_3 (%)	CaO (%)	Cr_2O_3 (%)	Cu+Ni (%)	Fe (%)	MgO (%)	S (%)	SiO_2 (%)	PGM (g/t)
Merensky	1.8	2.8	0.4	5.0	18.0	18.0	9.0	41	130
UG-2blend	3.6	2.7	2.8	3.3	15.0	21.0	4.1	47	340

The concentrates are then treated in the smelter and converter to obtain a molten sulphide matte. The molten matte produced under smelting stage is relatively richer in PGMs in comparison to the smelter feed concentrate. By melting the concentrate in the furnace, two immiscible molten layers are produced. The dense molten layer is usually a sulphide matte rich in PGMs whereas a less dense layer is silicate slag. The major components of the silicate slag include SiO_2 (44-47%), FeO_2 (9-28%), MgO (19-22%), and CaO (10-13%). The composition of the PGM-rich matte produced by smelting the concentrate at Lonmin is given in Table 2 (Crundwell et al., 2011).

Table 2: Typical analysis of the smelter matte produced by Lonmin platinum (Crundwell et al., 2011)

	S (%)	Ni (%)	Cu (%)	Co (%)	Fe (%)	PGM(g/t)
Merensky	28	17	10	0.5	37	1000
UG-2 blend	28	17	10	0.5	35	2500

To obtain a matte suitable for refining, the PGM-rich sulphide matte is treated in a Peirce-Smith converter where the iron and sulphur contained in the matte are oxidized in the presence of air or oxygen-air mixture. The product obtained from the converter is referred to as converter matte. Typical composition of the converter matte is displayed in Table 3 (Jones, 2000).

Table 3: Typical analysis of the converter matte produced by Lonmin platinum (Jones, 2000)

	Co (%)	Cu (%)	Fe (%)	Ni (%)	S (%)	PGMs (g/t)
Composition	0.6	29	1.4	48	20	6060

The converter matte is transferred to the Base Metal Refinery (BMR) where the base metals contained in the matte are selectively extracted and a high grade PGM concentrate is produced. Figure 1 shows the general process diagram for the recovery of copper, nickel and PGMs in a BMR.

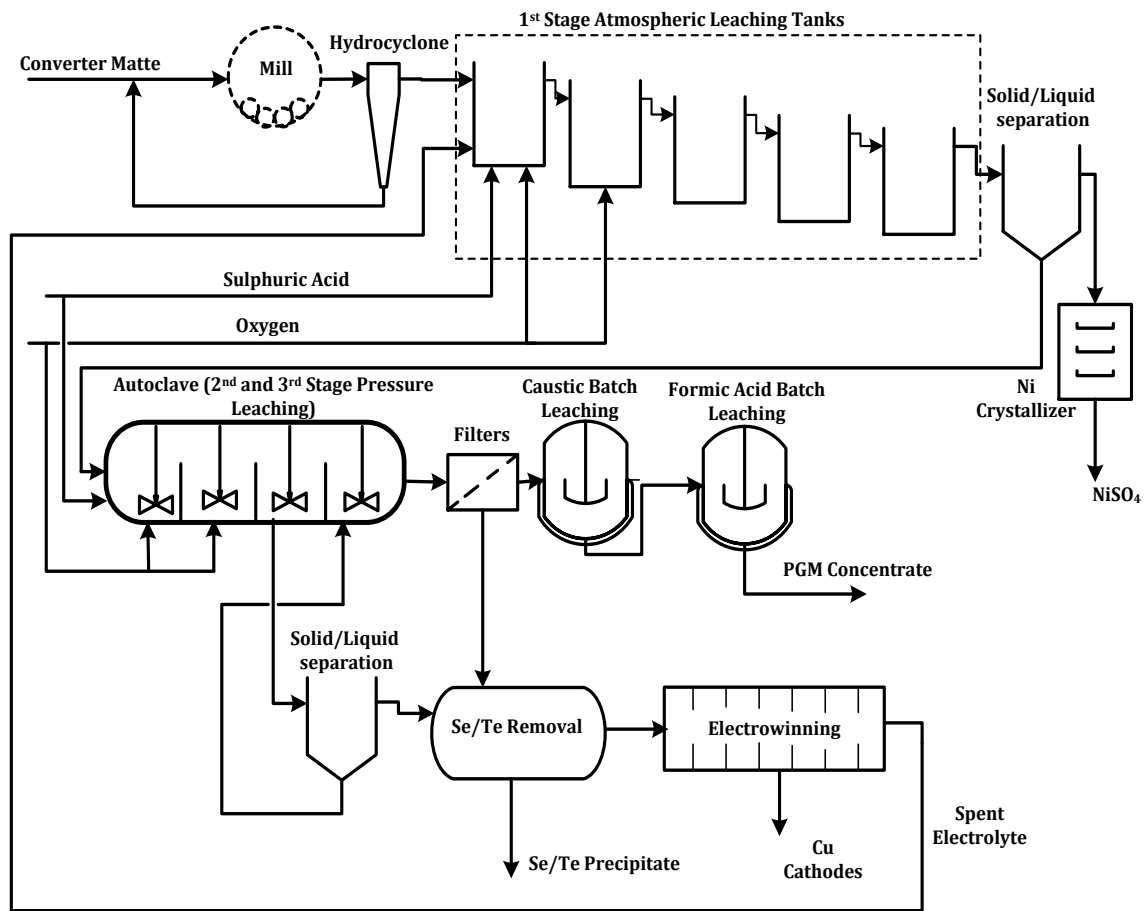


Figure 1: Process flow diagram of a typical BMR (Redrawn from Bircumshaw (2008))

The first step in the treatment of milled nickel-copper matte from the Peirce-Smith converter is sulphuric acid leaching at a temperature of 85°C under atmospheric pressure. This achieves dissolution of the nickel sulphide phases present in the matte as well as precipitation of dissolved Cu and other precious metals (OPMs, which include Rh, Ru and Ir) that are present in the recycled spent electrolyte. Sulphuric acid is also consumed in this leaching stage. The atmospheric leach stage product stream is then sent to a thickener where separation of the pregnant nickel sulphate leach solution from the solid matte residue is achieved. The nickel sulphate leach solution (containing 100 g/L Ni, < 1 g/L Cu, and < 3 mg/L PGMs) is treated in a crystallizer to produce nickel sulphate crystals, while the solid residue (about 13 - 18 % Ni, 48 - 55 % Cu and 0.3 % PGMs) is subjected to high pressure sulphuric acid/oxygen leaching to dissolve the copper sulphide and remaining nickel sulphide phases (Crundwell et al., 2011). During the process of high pressure leaching, impurities such as Se and Te as well as other precious metals (Rh, Ru and Ir) contained in the matte are also dissolved to some extent in addition to copper and nickel. The high pressure leach product stream then undergoes solid-liquid separation to produce a CuSO₄ pregnant leach solution and a PGM-rich solid residue.

The PGM solid residue is treated in batch caustic leaching and formic acid leaching steps before being sent to the precious metal refinery, while the pregnant CuSO_4 solution is treated in pipe reactors prior to the electrowinning of Cu. The objective of this process is to reduce the concentration of Se and Te to less than 5 mg/L and 10 mg/L, respectively. Selenium and tellurium removal from the electrowinning feed solution is important in order to prevent detrimental effects that these impurities have on the copper cathode quality and electrowinning process efficiency. Currently, the removal is achieved by precipitating selenium and tellurium as Cu_2Se and Cu_2Te respectively using sulphurous acid at 85°C and atmospheric pressure. Detailed discussion regarding the removal of Se and Te from process solutions is presented in section 2.3. It has also been observed that minor amounts of the dissolved OPMs are precipitated during the selenium/tellurium removal operations in the BMR. Approximately 20 % of the Rh is precipitated in the Se and Te removal stage (Lottering, 2011). This observation could potentially be used as an OPM recovery mechanism.

The Se and Te precipitates obtained are filtered from the solution and are further treated to recover PGMs while the filtrate is fed to the electrowinning section. The characteristics of the generated precipitate particles are vital for acceptable performance of the filtration process. It is believed that the characteristics (shape, size, and size distribution) of precipitates depend on the operating conditions of the precipitation process and consequently influence the solid-liquid separation processes significantly (Wakeman, 2007).

1.2. Problem statement

Currently, a large portion of the OPMs dissolved during the pressure leaching stages is recycled to the first stage leach as part of the spent electrolyte. This recycling of OPMs could negatively affect the performance of the process in two ways. Firstly, it causes a relatively large amount of OPMs to be locked up in the process and hence increases the time required to recover OPMs from the converter matte. Secondly, a high concentration of OPMs in the spent electrolyte places more stringent requirements on the operation of the first stage leach as any OPMs that are not precipitated will be lost to the nickel sulphate crystal stream. The rates of the OPM precipitation reactions are dependent on, amongst other variables, the composition of the converter matte and the spent electrolyte being fed to the first stage leach. Advanced control strategies and online analytical instruments are not in place to take rapid corrective action in the case of process disturbances (e.g. changes in the converter matte composition). A high OPM concentration in the recycled spent electrolyte would result in higher OPM losses to the nickel sulphate stream when these disturbances occur.

Given the fact that OPM co-precipitation has been observed in the Se/Te removal section of the BMR, it presents an opportunity to recover a large portion of the dissolved OPMs in the copper sulphate leach solution, thereby addressing the abovementioned operational challenges. At present, it is not clear what process configuration and operating conditions should be utilized to maximize OPM precipitation in the Se/Te removal section of the BMR.

1.3. Objectives

The aim of this research project was to propose a precipitation process that could be used to effectively recover dissolved OPMs from the copper sulphate leach solution prior to electrowinning. In order to achieve this aim, the following objectives had to be achieved:

- Evaluate different reagents to compare the OPM precipitation achieved with these reagents with the performance of sulphurous acid, which is currently used as reagent in the Se/Te removal section.
- For the selected reagents, determine the effect of key operating variables such as temperature, pressure, reagent addition and agitation speed on precipitation kinetics, percentage OPM precipitation, extent of nickel and copper co-precipitation, as well as the characteristics of the solid precipitate.
- Propose optimal operating conditions that achieve maximum OPM recovery with minimal copper and nickel co-precipitation.

1.4. Thesis outline

Chapter 2 covers a review of literature relevant to precipitation methods and reactions as well as the influence of key process variables. The materials and experimental methods used in this study will be discussed in chapter 3. Chapter 4 will present the findings of the reagent screening tests while in chapter 5 statistical analyses of data on the effects of process parameters and optimization of key parameters will be discussed. In Chapter 6, the effects of operating parameters on the process of OPMs and base metal precipitation will be discussed, while chapter 7 will address the conclusions from the study along with the recommendations for further work.

2. LITERATURE REVIEW

2.1. Introduction

Knowledge regarding the speciation and reactivity of metal components in process solutions is fundamental to the development of a process for the recovery of such metal values. To develop an understanding of the component speciation involved in base metal refinery solutions, the chemistry of typical BMR process solutions is discussed in section 2.2. The typical techniques used in the removal of selenium and tellurium from process solutions in base metal refineries are discussed in section 2.3. The precipitation process applicable to the recovery of metals from acidic solutions is discussed in section 2.4. One of the objectives of this study was to evaluate the effects of key variables on the precipitation behaviour; to this end, the operating variables affecting the precipitation process are discussed in section 2.5. Section 2.6 discusses the characterisation of precipitate particles while the chapter summary with an overview of the preceding sections is presented in section 2.7.

2.2. BMR process solution chemistry

To completely extract metals from solutions and fully separate them, knowledge of their chemical behaviour in terms of speciation and reactivity in such solutions is necessary. The current project aims to propose a precipitation process and operating conditions that can be used to recover OPMs (Rh, Ru and Ir) from an acidic sulphate solution containing base metals (Cu, Ni, and Fe) as well as impurities (Se and Te).

In BMR, Cu-Ni sulphate solutions are normally obtained from acidic leaching of the Cu-Ni sulphide converter matte. The second stage leaching of the iron, nickel and copper from such converter matte generally produce a sulphate solution containing Ni and Cu in their divalent oxidation states and the iron in its trivalent oxidation state.

The Ni-Cu sulphide mattes processed in BMR also contain the platinum group metals (PGMs). Platinum group metals are believed to exist in numerous oxidation states in their compound form. The principle oxidation states known for Rh, Ru and Ir in such compounds are; Rh (+3), Ru (+3/+4), and Ir (+3/+4) (Habashi, 1997; Renner et al., 2001). It can be expected that when there is no oxidation or reduction of the PGMs in the solution, Rh in such aqueous solutions would mainly be present as Rh^{3+} whereas Ru and Ir would often exist as Ru^{3+} or Ru^{4+} and Ir^{3+} or Ir^{4+} , respectively. Dissolution reactions of platinum group metals contained in Ni-Cu matte during high pressure leaching stage in a BMR have been investigated. Table 4 is a summary of the dissolution reactions that have been proposed (Dorfling et al., 2013). From the information

presented in Table 4 it can be assumed that the PGMs in the Lonmin sulphate solution under investigation in this research would be present as metal (III) ions.

Table 4: Dissolution reactions of PGMs in sulphate solution (Dorfling et al., 2013)

Dissolution Reaction	Equation no.
$Rh_2S_3 + 6O_2 \rightarrow Rh^{3+} + 3SO_4^{2-}$	Equation 1
$4Rh + 3O_2 + 12H^+ \rightarrow 4Rh^{3+} + 6H_2O$	Equation 2
$2RhO_2 + 6H^+ \rightarrow 2Rh^{3+} + 3H_2O + 0.5O_2$	Equation 3
$4Ru + 3O_2 + 12H^+ \rightarrow 4Ru^{3+} + 6H_2O$	Equation 4
$4RuS_2 + 2H_2O + 15O_2 \rightarrow 4Ru^{3+} + 6SO_4^{2-} + 4H^+ + 2SO_4^{2-}$	Equation 5
$RuO_2 + 6H^+ \rightarrow 2Ru^{3+} + 3H_2O + 0.5O_2$	Equation 6
$Ir_2S_3 + 6O_2 \rightarrow 2Ir^{3+} + 3SO_4^{2-}$	Equation 7
$2IrO_2 + 6H^+ \rightarrow 2Ir^{3+} + 3H_2O + 0.5O_2$	Equation 8
$4Ir + 3O_2 + 12H^+ \rightarrow 4Ir^{3+} + 6H_2O$	Equation 9

When selenium and tellurium are also contained in the Ni-Cu sulphide matte, acidic pressure leaching of such converter matte frequently results in the dissolution of Se and Te values. In such leach solutions selenium would usually be present as a mixture of Se^{4+} and Se^{6+} (Weir et al., 1983; Crundwell et al., 2011). Tellurium in such acidic leach solution is also commonly present in its tetravalent (Te^{4+}) and hexavalent (Te^{6+}) oxidation states (Habbashi, 1997). To remove selenium and tellurium from such solutions, the reagent frequently used is sulphur dioxide or sulphurous acid (hydrated form of sulphur dioxide).

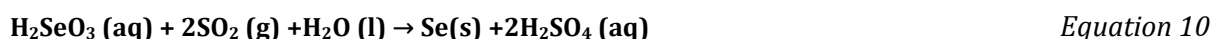
2.3. Selenium and tellurium removal operations

2.3.1. General operations

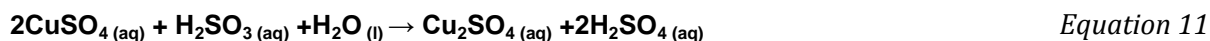
In order to prepare the copper sulphate leach solution for the electrolytic recovery of Cu, it is important to remove dissolved selenium and tellurium from the process solution to prevent detrimental effects on the quality of the copper cathodes. Selenium (IV) tends to co-deposit with Cu at the cathode during the process of copper electrowinning (Crundwell et al., 2011). The presence of selenium in metallic copper decreases its conductivity and ductility (Chou et al., 1985).

There are several methods that are currently employed in the removal of Se and Te from process solutions where the solutions are to be subjected to a copper electrowinning process.

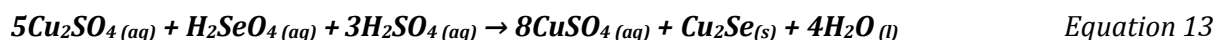
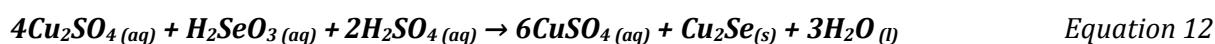
These methods include precipitation of selenium as copper selenide from CuSO_4 solution by reduction with sulphur dioxide at different conditions. Sulphurous acid can reduce tetravalent Se in acidic solution to elemental Se according to the following reaction (Wang et al., 2003):



Sulphurous acid also reduces the cupric sulphate to cuprous sulphate as follows (Crundwell et al., 2011):



The cuprous ions would then react with the tetravalent and hexavalent selenium to produce copper selenide according to equation 12 and equation 13 respectively (Crundwell et al., 2011):

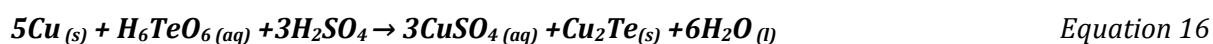
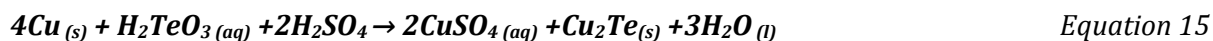


Weir et al. (1983) proposed a process for the removal of Se (IV) and Se (VI) from aqueous acidic copper-nickel sulphate solutions. The process consists of two stages. In the first stage of this process, the process solution at a temperature ranging from 140 to 175°C is passed through a tubular reactor and simultaneously SO_2 or a sulphite-containing solution is injected into the reactor. As a second stage, the slurry obtained from the first stage is maintained at temperature in the range 140 to 200°C and pressure of about 4 to 17.5 bar in an essentially oxygen free environment. The precipitate obtained normally consists of cuprous selenide (Cu_2Se) and metallic copper. This process is normally applicable to copper-nickel sulphate solutions which contains up to 90 g/L Cu, and up to 50 g/L Ni. The amount of Se (IV) and Se (VI) may be up to 210 mg/L and 70 mg/L, respectively and reduces the concentration of total selenium in the solution to less 5 mg/L.

Other known selenium removal operations include the precipitation of selenium (IV) as copper selenide by treating the copper sulphate solution with metallic copper powder at a temperature of about 160°C (Weir et al., 1982). Furthermore, it is known that adding metallic reagent such as Ni and Fe powders (that are above Cu in the electromotive series) to a Ni-Cu sulphate solution containing Se would result in Se precipitation. A temperature of about 190°C and a pressure of more than 12.4 bar are required to rapidly reduce the concentration of Se in the solution to less than 2 ppm within 15 to 30 minutes. This process is applicable to Cu-Ni sulphate solutions

containing about 20 to 100 g/L Cu, up to 70 g/L Ni, 5 g/L Fe, and upwards of about 50 mg/L Se. The solution may also contain about 5 to 250 g/L H₂SO₄ (Nikolic et al., 1977).

Unlike selenium, it is difficult to precipitate tellurium from acidic aqueous solution by direct addition of sulphur dioxide. However, both Se and Te can be cemented as copper selenide and copper telluride respectively using reduced copper in aqueous solutions as shown below (Wang et al., 2003).



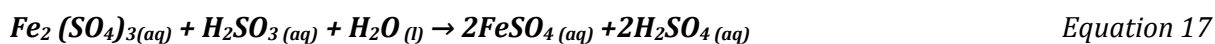
2.3.2. Se/Te removal at Lonmin

At Lonmin BMR, the copper sulphate leach solution obtained from pressure leaching of Cu-Ni sulphide converter matte contains between 30 – 35 g/L Ni, 60 – 65 g/L Cu and 15 – 20 g/L H₂SO₄ as well as impurities such as Se and Te (Crundwell et al., 2011). To remove these impurities, the process solution exiting the pressure leaching section is contacted with sulphurous acid (containing 50 – 60 g/L SO₂) at a temperature of 90°C before passing it through selenium-tellurium removal tubular (pipe) reactors. The added sulphurous acid reduces the cupric to cuprous state which then react with tetravalent Se and Te in solution to produce copper selenide and copper telluride respectively (reaction mechanisms discussed in section 2.3.1, equations 12 to 16). If ferric ions are present in the solution they would also be reduced to ferrous ions by the sulphurous acid reagent. The reaction of iron with sulphurous acid and various reagents pertinent to this study is discussed in section 2.3.4.

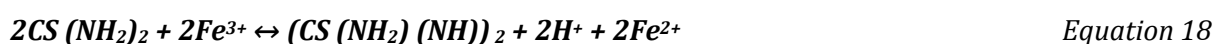
In order to promote agglomeration of solid precipitates to enhance filtration, a flocculant is added to the solution prior to feeding it to the Se/Te reactor. The pipe reactor retention time is approximately 20 seconds. The process solution is then discharged into a tank with relatively larger residence time (typically 24 h) where unreacted SO₂ is displaced by sparging air into the tank. The selenium/tellurium precipitate is then filtered using a recessed plate filter which is normally pre-coated with wood cellulose pulp. The concentration of Se in solution is usually reduced to less than 5 mg/L (Crundwell et al., 2011). The residue produced usually contains 65 % Cu, 25 % Se and 3 % Te (Sherritt Gordon Mines Limited, 1983). The filtered Se/Te residue is finally washed and transferred to the Se/Te residue roaster whereas the CuSO₄ filtrate heads to the electrowinning section via the electrolyte surge tank.

2.3.3. Reaction of iron with various reagents

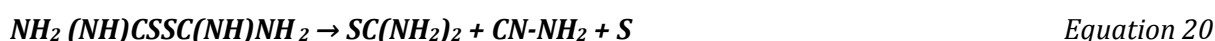
The iron present in the leach solution will always be the first to react and consume the reagent before any other component during the removal of Se and Te in base metal refinery. This is because iron is higher in the electrochemical series and is thus expected to be more reactive than all of the major metal components present in the process solution. Iron is present in the above solution as ferric sulphate and reacts with sulphurous acid according to the following equation (Sherritt Gordon Mines Limited, 1983; Van der Merwe, 2002):



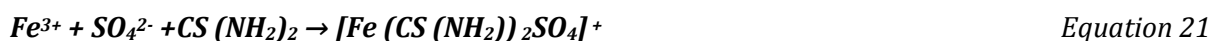
According to Gupta (1963), ferric ions in acidic solutions can also react with thio-urea to produce formamidine disulphide. This product is easily formed in acidic solutions at room temperature according to the reaction given below:



High concentration of oxidising agents would also promote the decomposition of thio-urea to formamidine disulphide. Formamidine disulphide is not stable in acidic solutions and decomposes irreversibly producing elemental sulphur, cyanamide and several sulphur-containing products according to following reactions (Maslowska, 1969; Lacoste-Bouchet et al., 1998):



In weak aqueous solutions, thio-urea can also react with ferric ions to form stable ferric sulphate complex as shown below (Maslowska, 1969; Hiskey, 1984):

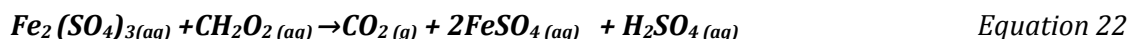


Thio-urea is also known to react with Cu^{2+} in copper sulphate solutions resulting in the formation of Cu^+ , formamidine disulphide and several other cuprous-thio-urea complexes (Javet and Hintermann, 1969). Thio-urea is also known to influence the nucleation and growth of copper in the electro refining of copper (Fabricius et al., 1994)

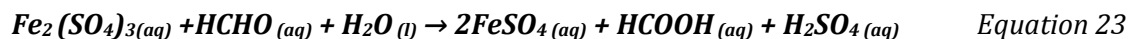
Lottering (2011) developed the reactions for iron with formic acid and formaldehyde based on the redox reactions of these reagents. These set of reactions were based on the assumption that formic acid-iron reaction would take place via ionic precipitation. In the case of formaldehyde, it

was assumed that formaldehyde would likely be oxidised to formic acid which would then react with the iron. These reactions would be as shown below:

- Iron reaction with formic acid (based on redox reaction)



- Formaldehyde reaction with Iron (based on redox reaction)



2.4. Precipitation of metals from acidic solutions

Precipitation can be defined as a physical-chemical process, in which soluble metals and inorganics are converted to relatively insoluble solids known as precipitates. The physical process of precipitation involves adjustment of concentration and or temperature of the solution to an extent where crystallization process takes place. Under physical precipitation, no chemical reagents are added to the solution. Physical precipitation is a slow process and usually the crystal products obtained have high solubility in water and contain water of crystallization. Chemical precipitation on the other hand, involves the addition of reagents to precipitate a desired compound from solution (Habashi, 1999). This work focused on the precipitation of metallic ions through addition of chemical agents.

2.4.1. Precipitation of metals as sulphides

Metal sulphide precipitation can be applied in the separation of impurities from aqueous solution or in the recovery of major metals of interest from solutions. In metal sulphide precipitation process, soluble metal compounds are converted into relatively insoluble sulphide compounds by addition of agents containing sulphurous atom. Such sulphide precipitating agents may be in gaseous (H_2S , SO_2), aqueous (Na_2S , SO_3^{2-} , SO_4^{2-}) and or solid (CaS , FeS) form. Equation 24 illustrates the reaction mechanism involved when a sulphide ion is used in metal sulphide precipitation.



where M^{2+} is the metal cation being removed from the solution.

For the metal ions pertinent to this research the reaction would occur as given below:



The use of metal sulphide precipitation technology is preferred in hydrometallurgical treatment of metal containing aqueous solution to hydroxide precipitation. This is so because metal sulphide precipitates produced have lower solubilities, favourable dewatering characteristics, potential for selective metal removal, and high degree of metal removal at relatively low pH (Bhatthacharyya et. el, 1981, Lewis, 2006, Peters & Ku, 1985). The general solubilities of common metal sulphide in order of most soluble to least soluble are given by: $\text{FeS} > \text{ZnS} > \text{NiS} > \text{CoS} > \text{PbS} > \text{CdS} > \text{CuS} > \text{Ag}_2\text{S} > \text{HgS} > \text{Ir}_2\text{S}_3 > \text{Rh}_2\text{S}_3 > \text{PtS}_2 > \text{RuS}_2 > \text{OsS}_2 > \text{Au}_2\text{S}_3$ (Thomas, 1964).

In addition, sulphide precipitation process requires relatively low detention time in the precipitating reactors because of the high reaction rates of sulphides. Furthermore, sulphide precipitation is less affected by the presence of complexing and chelating agents than hydroxide precipitation (Crear, 2001). The application of sulphide precipitation method in the removal selenium and tellurium from process solution at Lonmin BMR has already been discussed in section 2.3.

2.4.2. Key results from previous OPM chemical precipitation investigations

There are several chemical precipitating processes employed in the recovery of metallic compounds from leach solutions and other aqueous solutions. This section discusses several researches done on the application of chemical precipitation process to recover metals from acidic process solutions using various reducing agents.

Awadalla et al. (1994) investigated the direct recovery of PGMs from thio-urea solutions and other highly acidic leach solutions by reduction precipitation using sodium borohydride at ambient temperature and pressure. Solutions containing 5 ppm – 1000 ppm PGMs and 25 ppm – 250 ppm Cu^{2+} , Pb^{2+} , Zn^{2+} , and Al^{3+} were investigated at temperatures from 25°C to 60°C over a time range of 2 – 15 minutes. The method was observed to be effective over a wide range of solution acidity (from pH <1 to 4). Approximately 95 % maximum PGM recovery was achieved in their study. They also observed that reduction of PGMs was more efficient at lower PGM concentration not less than 25 ppm. They further observed that the presence of Pb^{2+} , Zn^{2+} , and Al^{3+} within the given concentration range had no effect on the PGM precipitation efficiency and kinetics. The Pb^{2+} was, however, observed to co-precipitate with the PGMs. The presence of Cu^{2+} ions in the solution has a negative effect on the use of NaBH_4 to precipitate PGMs. This is because copper ions acts as an active catalyst for the hydrolysis of borohydride ion and rapidly liberate hydrogen before the PGMs are completely reduced. A Cu^{2+} concentration above 25 ppm was observed to have a large effect on PGMs precipitation with Rh being the most affected. It should thus be noted that using NaBH_4 to precipitate PGMs in the current study would produce similar effects on the PGM recoveries due to high Cu^{2+} concentration (above 75 g/L) in the

CuSO₄ process solution under investigation. Furthermore, using sodium borohydride would introduce sodium into the solution which is regarded as an impurity in Ni recovery.

Many other reducing agents that are capable of precipitating metals from aqueous solutions have been discussed. McGeorge et al. (2009) used Na₂S₂O₃ as a source of sulphur atoms to study the mechanism and kinetics of Rh and Cu co-precipitate from aqueous solutions. A synthetic solution containing 13.2 g/L Cu, 5.5 g/L Ni and 90 mg/L of Rh was used for their investigate over a temperature range of 50 – 150°C. In the first phase of their experiment, Rh precipitation in the absence of copper was examined followed by Rh precipitation in the presence of copper.

They found that in the absence of Cu²⁺, ionic Rh precipitation (equation 31) took place. This reaction is fast and it is where most of the Rh is precipitated due to the availability of sulphide ions provided by the precipitating reagent. When copper is present in the solution, ionic co-precipitation occurs. These reactions occurs homogeneously (equations 30 and 31) preceding noticeable nucleation which is followed by heterogeneous crystal growth (equation 32) before Rh co-precipitate with copper (reactions 33 and 34) (McGeorge et al., 2009).

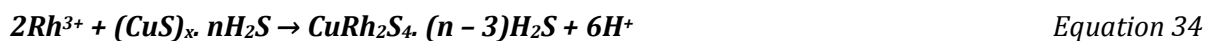
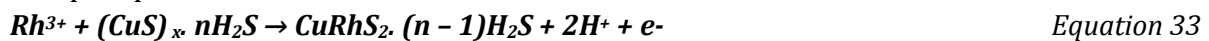
Homogeneous reactions:



Heterogeneous growth:



Co - precipitation



The initial reactions are characterized by high consumption of the reagent since copper initially precipitate faster than Rh because of the large concentration difference between the two components. Large concentration amount of Cu tends to limit the amount Rh³⁺ ionic precipitation by consuming the available sulphide. In such cases the CuS formed continue to precipitate Rh³⁺ via cationic substitution reaction resulting in the enrichment of the Rh³⁺ towards the edge of the CuS particles (Mc George et al., 2009).

2.5. Key process variables

Precipitation being a physical-chemical process is dependent on a number of physical and chemical conditions of the process. In order to properly design and optimise control of

precipitation process, knowledge on the influence of operational materials and parameters on precipitation process is cardinal (Sohnel and Garside, 1992).

This section discusses the most commonly studied process variables (reagent addition, temperature, pressure and agitation) relevant to metal precipitation processes from acid solution.

2.5.1. Precipitating reagent

Precipitation of a desired metal from solution can be effected by addition of a chemical reagent. Chemical precipitating reagent provides anions which interact with cationic metals in the solution to form insoluble compounds. The reagent anions can also reduce the ionic metallic species to their elemental form. Some of the most common anionic species of relevance to the current study includes HS^- , SO_4^{2-} , S^{2-} , and SO_3^{2-} .

It is believed that reagent addition can influence the size and number of precipitated particles (Fischer and Rhinehammer, 1954). Reagent addition influence precipitation processes by providing new available sites that induces nucleation. Reagents may also contain impurities that can impede the precipitation process by competing for sites already available to make them less effective for nuclei formation (Fischer, 1959). The various researchers have investigated the influence of reagent type and reagent addition on the precipitation process.

Lottering et al. (2012) investigated the possibility of precipitating Rh and Ru from a pregnant base metal leach solution using thio-urea and sulphur dioxide as reagents. Different quantities of these reagents were assessed based on their ability to precipitate Rh. They observed that the excess quantity of thio-urea had negligible effect on Rh precipitation except at the highest temperature of 150°C. Though their results regarding the effect of reagent addition using SO_2 were inconclusive, they observed that precipitation of Rh and Ru precipitation depended on the amount of reagent added and temperature variation.

Jayaweera et al., (1989) in their investigation of precipitating copper sulphide using several reagents (hydrogen sulphide (H_2S), thioacetamide (CH_3CSNH_2) and sodium sulphide (Na_2S)) from a copper sulphate solution reported that the precipitates generated from the three reagents were of different particle size and phase compositions. The experiments were carried out at 22°C and 80°C. The particle size of the precipitates produced using H_2S ranged from 0.3 μm to approximately 10 μm whereas those generated using Na_2S were between 0.2 and 100 μm in diameter. CH_3CSNH_2 yielded particles with size ranging from 0.1 to 20 μm . The

observed difference in reagent influence was attributed to the difference in their rates of decomposition reaction to release sulphide atoms.

2.5.2. Temperature

Operating temperature can influence the rates and yields of precipitation reactions. It is well known that for a reversible chemical reaction, the highest conversion that can be achieved is the equilibrium conversion. Increasing temperature would increase the equilibrium conversion of an endothermic reaction and decrease that of an exothermic reaction (Fogler, 2006).

In addition, the solubility of reactant molecules as well as that of the products (precipitates) formed is also influenced by temperature. For the gaseous reagents, in solutions the solubility decreases with increasing temperature (Silberberg, 2010). Generally, chemically controlled precipitation reactions are known to be heavily dependent on temperature (Sohnel and Garside, 1992).

Several researchers have investigated the influence of temperature on the precipitation process. Weir et al. (1983) studied the effect of temperature on the rate of Se (VI) precipitation. A Cu-Ni sulphate solution containing 100 mg/L selenium (VI) and less than 1 mg/L of selenium (IV) was contacted with metallic copper at temperatures of 150 and 175°C. For the nickel-copper sulphate solution containing 20 to 50 g/L sulphuric acid, it was observed that the rate of selenium (VI) precipitation increased with increasing temperature. The concentration of Se (VI) in their solution was reduced to less than 1 mg/L in less than 30 minutes when the process was operated at 175°C whereas at 150°C the selenium concentration was reduced to the same level in about 60 minutes.

Awadalla et al. (1994) investigated the effect of operating temperature on the precipitation efficiency of PGMs from acidic solutions. The study was performed using a solution containing 100 ppm (Pt) over temperature range of 25 to 60°C. They used sodium borohydride as precipitating agent. They reported that increasing temperature from 25°C to 60°C resulted in increased Pt recovery efficiency from 69 % to 95 % respectively.

Lottering et al. (2012) reported the influence of operating temperature on the precipitation of Rh and Ru using sulphur dioxide. The report showed that Rh and Ru precipitation was strongly dependent on the variation of temperature as well as reagent. In their investigation, the average Rh precipitation achieved using SO₂ at 80, 115, and 150°C were approximately 10 %, 25 % and 40 %, respectively.

Ruiz et al. (2007) studied the effect of operating temperature on the extent, rates and particle size distribution of iron precipitation from a sulphuric acid media. They reported that increasing temperature increased the rates and extents of iron precipitation. Approximately 55 % and 89 % iron precipitation was achieved in 10 minutes when the process was operated at 180°C and 220°C, respectively. The results also showed that increasing temperature produced precipitates with smaller particle sizes. The cumulative mass size distribution of the precipitates obtained at 180°C and 220 °C were 37 µm and 14.4 µm, respectively.

Roy and Srivastava (2007) in their study of CuS nanorods synthesis using hydrated copper chloride and carbon sulphide at 105°C reported that the morphology of the particles was affected by the reaction temperature. They explained that at low temperature particle growth is favoured while at higher temperatures nucleation predominates. This is because higher temperatures induce supersaturation which results in increased rates of nuclei formation. Higher nucleation rates often results in the formation of smaller sized particles (Dirksen and Ring, 1991).

2.5.3. Pressure

It is well known that liquids and solids exhibit practically no change in solubility with changes in pressure. Therefore, it is less expected that the solubility of precipitates formed in this research would be significantly affected by the variation in pressure. However, depending on the state of precipitating reagent used (gas or liquid), pressure variation can affect the precipitation reaction process. Solubility of gaseous reagents in the solution containing dissolved metal species is generally expected to increase with increased pressure. This is because the concentration of molecules in the gas phase increases with increasing pressure as a result the concentration of dissolved gas molecules in the solution at equilibrium would also be higher at higher pressures. Dissolving more reagent molecules would promote interaction between the metal ions and reagent molecules which would result in increased chemical reactions to form precipitates.

2.5.4. Agitation

According to Pohorecki and Baldyga (1983), the precipitation process involves three successive stages. These stages consist of mixing reactants on molecular scale which may result in homogeneous reaction. Homogeneous reactions then produce supersaturation which results in precipitation through the mechanisms of nucleation and crystal growth. It is believed that being the first stage of a precipitation process, mixing can significantly affect the course of the process.

Studies that have been done on the effects of agitation on metal precipitation processes show that agitation is an important parameter.

Serdar (2011) investigated the effect of agitation on Rh recovery from rhodium-containing waste rinsing water by cementation using zinc powder. Without agitating the system, a recovery of 9 % Rh was achieved in 10 minutes of experimental run. The recovery increased to 39 % within the same time range when the solution was agitated.

Jha et al. (1978) studied the effect of agitation on the precipitation of NiS from acidic nickel sulphate solution using H₂S. This study was performed using solution containing 6.9 g/L Ni at constant temperature of 90 °C and 0.7 atm for agitation range between 72 rpm – 1250 rpm. It was observed that Ni precipitation efficiency improved with increasing agitation. The nickel ion concentration was decreased to less than 100 ppm at a stirring rate of 500 rpm in less than one hour and in less than 15 minutes at a stirring rate of 1000 rpm.

Roy (1961) investigated the effect of agitation on precipitation rates of Ni from Ni-Co sulphate solution using H₂S gas at a temperature of 90°C. It was observed that increasing the impeller speed from 405 rpm to 643 rpm increased the recovery of nickel from 94.7 % to 98 %.

2.6. Precipitate characterisation

When precipitation process is used to extract metals from process solutions, there is always a necessity to separate the liquid from the precipitate (residue) solid. In the Se/Te removal section at Lonmin Plc, the filtration process is used to separate the Se/Te precipitates from the pregnant copper sulphate solution (Sherritt Gordon Mines Limited, 1983). Some of the requirements for successful application of the filtration process include the magnitude of the process volume being handled, whether the process is continuous or batch, and material the characteristics of the solids being removed (particle size, chemical composition) (Sutherland, 2008). In the present work the characteristics (size distribution and composition) of particles generated from the precipitation process rather than their influence on filtration was investigated.

According to Wakeman (2007), the shape, size, and size distribution of the product particles resulting from processes such as precipitation or crystallisation, are significantly influenced by the process operating conditions. There are several techniques employed in the characterisation of particles. For the majority of particles characterisation applications, PSD analysis is sufficient to provide required information.

The analytical technologies such as laser diffraction and dynamic light scattering are some of the powerful techniques applied in PSD analyses (Horiba scientific, 2012). The PSD data can be represented as median values. For particle size distributions, the median is referred to as the d_{50} . The d_{50} is the value in the size distribution where 50% of the particle size is below this size and 50% is above it (Wills, 1997). The d_{50} value is one of the easier statistics to understand and also provide the most meaningful information for particle size distributions (Horiba scientific, 2012).

2.7. Chapter Summary

Precipitation is a well-known process used in the recovery of dissolved metal ions from solutions. Among the various precipitation methods commonly practiced, the use of reducing reagents to effect precipitation is preferred because it affords selective precipitation of desired metals from solutions containing unwanted species. The precipitation of metals from solutions using sulphide reagents is preferable because the metal sulphide precipitates are generally of low solubility over a wide range of pH and are of good dewatering characteristics.

In order to optimise precipitation processes and produce precipitates of desired quality, knowledge on the effect of operating parameters such as temperature, agitation, and reagent addition as well as reagent type are vital. Different metallic ions in solution respond differently to the change in each of these operating parameters. This difference in behaviour can be explored to recover and separate metals of interest from solutions. The characteristics such as shape and size of the particles generated from precipitation processes are influenced by the precipitating conditions and are consequently influential in the solid-liquid separation process.

3. EXPERIMENTAL

3.1. Materials

Copper sulphate leach solution was supplied by Lonmin Plc. This leach solution was extracted from the process stream feeding the Se/Te removal section of Lonmin BMR. ICP-AES was used to determine the chemical composition of this leach solution. The leach solution's chemical composition was analysed by Stellenbosch University Central Analytical Facility laboratory (CAF). Table 5 summarizes the leach solution's chemical composition.

The amount of reagent needed for each experimental run in this study was determined based on the reaction of iron with each of the proposed reagents. The stoichiometric reaction equations of iron sulphate and the proposed reagents (section 2.3.4) were used to calculate the amount of reagent added. Thus it was vital to know the concentration of iron in the process solution used. The concentration of iron in Lonmin BMR solution is approximately 850mg/l. The chemical reagents thio-urea ($\geq 99.0\%$, ACS reagent), formic acid ($\geq 95\%$ reagent grade), and sulphurous acid ($\geq 6\%$, ACS reagent) were supplied by Sigma Aldrich™. The formaldehyde solution (40%wt in water) was supplied by Saarchem (Pty) Ltd.

Table 5: Chemical compositions of the copper sulphate leach solution supplied by Lonmin Plc.

Solution composition (g/L)												
Cu	Fe	Ni	Ir	Rh	Ru	Se	Te	Zn	Pb	Co	As	Cr
108.4	0.810	53.75	0.043	0.035	0.221	0.057	0.033	0.264	0.039	0.351	0.283	0.027

3.2. Methodology

3.2.1. Equipment

Laboratory tests were carried out in a 2.0 L Büchi pressure reactor. Figure 2 shows the schematic drawing of the experimental setup used in this study. The Büchi polyclave reactor is equipped with a Cyclone 300 magnetic stirrer drive, the speed of which was set manually. The anchor type blade stirrer was used to agitate the solution for all the tests performed in this research. The reactor vessel is also fitted with pressure gauge which was used to monitor the pressure inside the reactor vessel. In order to obtain the desired pressure in the reactor vessel, the volume of nitrogen gas added to the reactor vessel was regulated by the valve fitted to the nitrogen cylinder.

Heating of the reactor vessel was achieved by utilising electric heating elements placed around the reactor shell. Heat provided by these heating elements is controlled by a programmable controller on which desired reactor temperature values are set. The programmable controller use thermal signals from thermocouples located on the reactor vessel to activate and deactivate the heating elements as well as relay valves used to control the flow of cooling water through the reactor shell. This temperature control strategy allowed the reactor vessel temperature to be maintained at levels close to the set value ($\pm 0.5\%$).

For the addition of reagents, a stainless steel reagent cylinder was fitted to the reactor vessel. One open end of this cylinder was attached to the reactor valve fitted on the reactor cover plate (top part of reactor vessel) while the other open end was attached to the nitrogen cylinder stream line. In this way it was possible to pressurise the reagent cylinder after filling it in order to obtain a pressure difference required for the reagent to flow into the reactor vessel at the point of reagent addition.

In order to collect samples the bottom drain valve of the reactor vessel was used. A tube with an additional valve was connected to the reactor drain valve. This allowed samples to be collected without the possibility of solution splashing from the reactor due to sudden pressure drop. The samples collected were allowed to cool down below the solution boiling point by keeping it in between the drain valve and the additional tube valve.

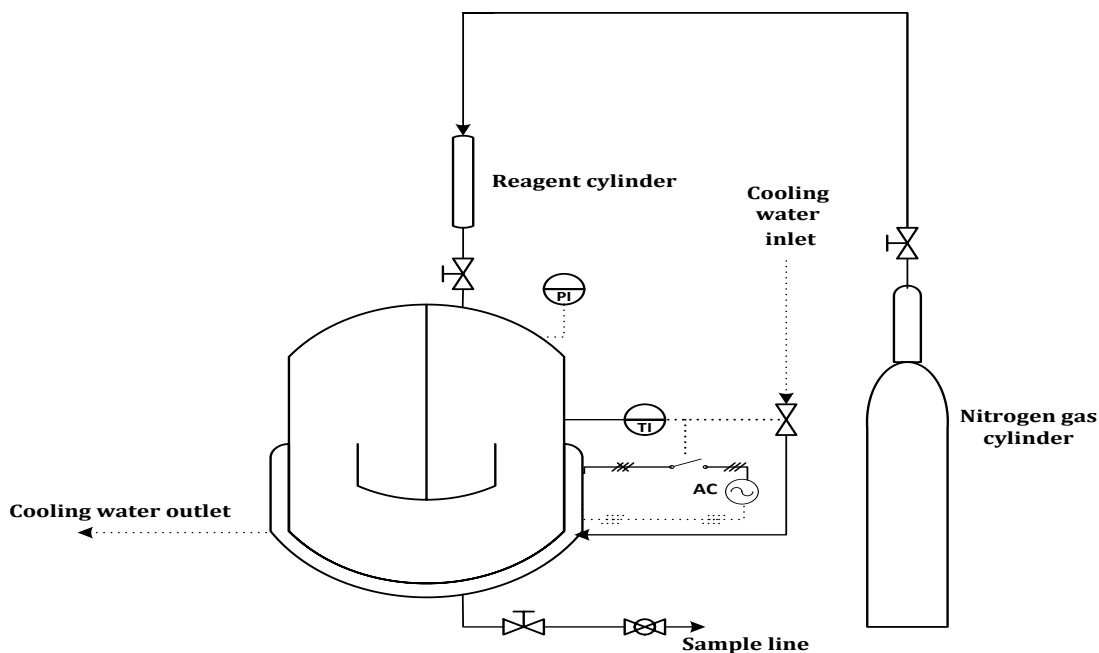


Figure 2: Experimental setup schematic diagram

3.2.2. Experimental procedure

This research involves experimental work on a laboratory scale that was divided into two phases. All experiments were carried out using a similar experimental procedure, but with different operating parameter levels and reagents.

After filling the autoclave with 1 liter of the process solution provided by Lonmin BMR, the required quantity of reagent was measured out and placed into the stainless steel reagent cylinder. The reagent cylinder was then pressurized to the required pressure using nitrogen gas. This cylinder was thereafter attached to the autoclave ensuring that all the valves on both the reagent cylinder and autoclave were tightly closed.

The autoclave's internal agitator was set to the required speed and the power was switched on. Next, the temperature controller was switched on and set to the required temperature value. When the solution temperature in the reactor reached the set value, a solution sample was taken and the reagent cylinder valve was opened to allow the reagent flow into the reactor. The autoclave bottom drain line was used to take 15 ml samples from the reactor.

Samples were taken every 20, 60, 120, and 240 minutes from the time of mixing the reagent and the solution in the reactor, while the last sample was taken at the end of 480 minutes. pH and Eh values were recorded immediately after taking each particular sample. The liquid samples were immediately filtered using a 0.2 μm syringe filter and the filtrate was diluted with distilled water.

3.2.3. Experimental planning

3.2.3.1. Experimental tests

The experimental tests were divided into the screening and optimization phases. In screening tests 200 % excess quantity of each reagent was used in order to identify the reagent(s) with greater potential to provide higher precipitation of OPMs from the leach process solution. The process operating conditions and reagents investigated in the screening phase are summarized in Table 6.

For the optimisation tests, a 2^4 factorial design was employed to evaluate the effects of the variables on the precipitation process and to assess possibility of interaction effects between the chosen control variables. The variables investigated in the second phase of experiments (using thio-urea) and their respective levels are summarised in Table 7. Similar design was considered for the experiments performed with sulphurous acid. Table 8 gives a summary of the variables and their respective levels.

Table 6: Chemical reagents and operating temperature for screening tests

Variable	Value
Temperature (°C)	80, 160
Pressure (bar)	Ambient
Agitation speed (rpm)	250
Reagent excess (%)	200
Reagents	Formaldehyde Formic acid Sulphurous acid Thio-urea

Table 7: Experimental conditions for the second phase of experiment performed using thio-urea

Variable	Low value	High value
Reagent quantity (%excess)	200	320
Temperature (°C)	80	160
Pressure (bar)	Ambient	7
Stirring rate (rpm)	250	500

Table 8: Experimental conditions for the second phase of experiment performed using SO₂

Variable	Low value	High value
Reagent quantity (% excess)	720	960
Temperature (°C)	80	160
Pressure (bar)	Ambient	7
Stirring rate (rpm)	250	500

3.2.3.2. Analytical methods

The following analytical techniques were used in this study:

- ICP-AES analysis was used to obtain the concentrations of rhodium, ruthenium, iridium, selenium, tellurium, copper, iron, and nickel in the liquid samples.

- XRD analyses of the solid samples were done to identify the phases of the precipitate compounds formed. XRD analysis of the samples was done by Central Analytical Facility of Stellenbosch University while the interpretation of XRD data was done by XRD Analytical and Consulting – South Africa.
- To determine the composition of the precipitates, SEM analyses were performed using a MA 15 EVO SEM ZEISS instrument with accelerating voltage of 20KV. This instrument uses INCA software to identify the compositions of the samples. These analyses were done by Central Analytical Facility of Stellenbosch University.
- Particle size distribution analysis was done using the Saturn DigiSizer 5200 particle size analyzer.

3.2.3.3. Statistical analysis

Fitting of statistical models for the experimental data generated from the factorial experiments was achieved by using the half-normal probability and Pareto plot of effects. For the half-normal probability plots, the inactive effects will normally be distributed along a straight line whereas significant effects tend to appear as extreme points falling off each end of the straight line (Montgomery and Runger, 2007).

In the Pareto charts, the effects are plotted in decreasing order of relative frequency from left to right. The heights of bars on the chart represent frequency and clearly illustrate which variables have the greatest cumulative effect on a process that one has to deal with in order to optimize the process (Jiju, 2003). The Pareto chart draws two t-limits reference lines based on the Bonferroni corrected t and standard t (Moradi and Monhemius, 2011). Any effects that extend above the Bonferroni limit are certainly significant and should be included in the model whereas the effects that past the t-value limit are potentially significant and should be added if necessary. On the other hand, the effects falling below the t-value limit are considered to be inactive (Antony2003).

The fitted models were then analysed using a method known as Analysis of Variance (ANOVA) to determine the significance of the models and to verify whether correct model terms were selected. After fitting the models, confirmatory tests were performed to verify the validity of the fitted models.

4. REAGENT SCREENING TESTS - RESULTS AND DISCUSSION

4.1. Introduction

This section presents the findings obtained from reagent screening tests that were performed on a laboratory scale in order to identify the reagent(s) with greater potential to provide complete OPMs (Rh, Ru and Ir) precipitation from a nickel-copper sulphate process solution. The experimental set up, conditions, and procedure that were used are outlined in chapter 3. The quantity of OPMs precipitated from the process solution by each of the four reagents investigated was the criteria used to effect reagent selection.

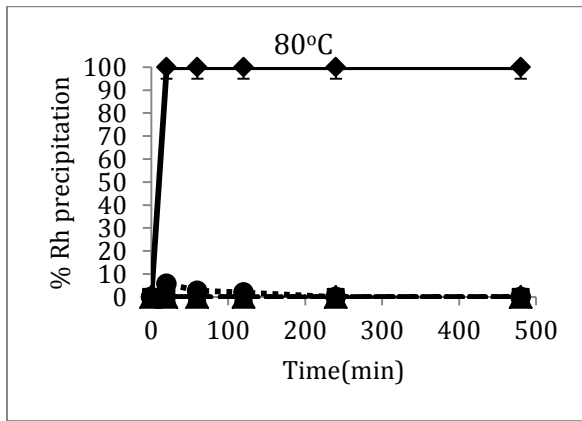
4.2. OPM precipitation

The variations in the quantities of rhodium, ruthenium and iridium precipitated by each of the investigated reagents for the duration of the laboratory experiment performed at the experimental conditions discussed in section 3.2, are displayed in Figure 3. Referring to Figure 3a and b, it can be seen that thio-urea provided the highest Rh precipitation with faster kinetics in comparison to formic acid, formaldehyde and sulphur dioxide at the two temperatures studied. Within the first 20 minutes into the experimental run, thio-urea precipitated virtually all of the Rh contained in the solution regardless of the temperature. The observed better performance by thio-urea can be attributed to its tendency to decompose into several sulphur containing products such as formamidine disulphide and hydrogen sulphide (Fang and Muhammed, 1992) and the consequent precipitation of metallic ions from solutions as metal sulphides. Metal sulphide precipitation is believed to have high degree of metal removal with fast kinetics at relatively low pH values (Bhatthacharyya et. el, 1981, Lewis, 2006, Peters & Ku, 1985). On the other hand, formate reagents are reported to have better performance in terms of Rh precipitation at pH values of about 1.5 unlike the pH values below 1.5 at which the experiments for the current study were conducted (Julsing and McCrindle, 2001).

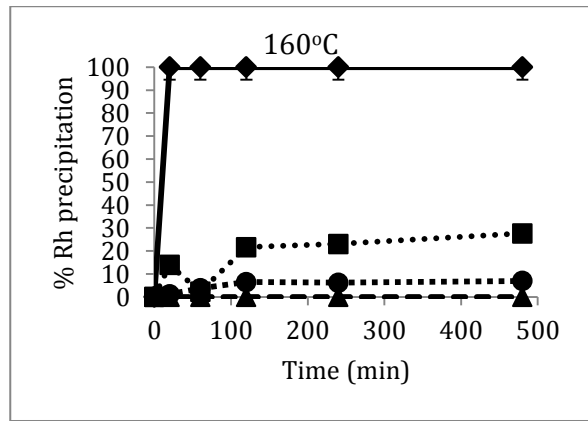
In addition thio-urea also achieved better ruthenium precipitation in comparison to other reagents screened as is evident from Figure 3c. Increasing the temperature also produced a positive effect on ruthenium recovery as can be seen from Figure 3d. Furthermore, when thio-urea was used as precipitating agent, roughly 55 % iridium was precipitated from the solution compared to less than 5 % Ir precipitated by each of the other investigated reagents. Referring to Figure 3 e, and f, approximately 50 % and 60 % iridium recoveries were observed at operating temperatures of 80°C and 160°C respectively in 3 hours of reaction time.

According to Figure 3, the recovery of OPMs using 200 % excess amount of formaldehyde and formic acid increased with increasing temperature. Maximum ruthenium precipitation using formaldehyde and formic acid increased by roughly 28 % and 40 % respectively, after increasing the temperature from 80 to 160°C. Formic acid at this temperature (160°C) would also precipitate approximately 20 % rhodium from the solution (Figure 3b). From the OPM recovery point of view, it seems that selecting formic acid and formaldehyde as the reagents for plant operation would require higher excess reagent quantity and operating temperatures.

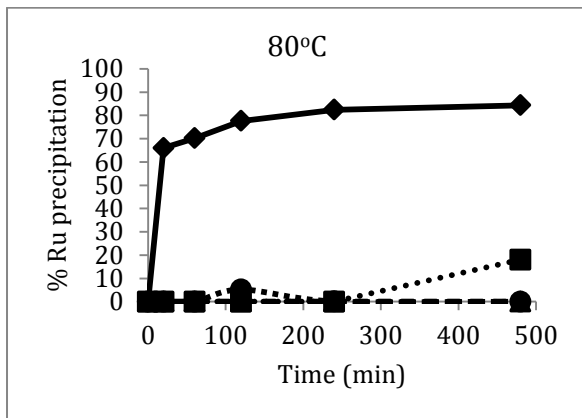
Using sulphurous acid as precipitating agent as is currently practised on site, the OPM recovery remained poor at both temperatures investigated. The observed poor performance in OPM precipitation by sulphurous acid suggested that increasing the reagent quantity would be the best option if one wishes to improved OPM precipitation using this reagent. This was also suggested by Lottering et al. (2012) who reported the dependence of Rh precipitation on the quantity of sulphurous acid addition.



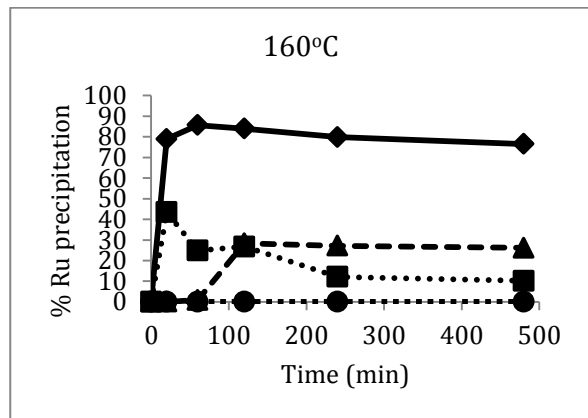
(a)



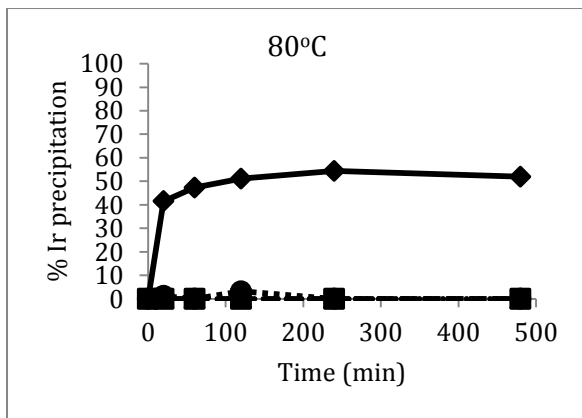
(b)



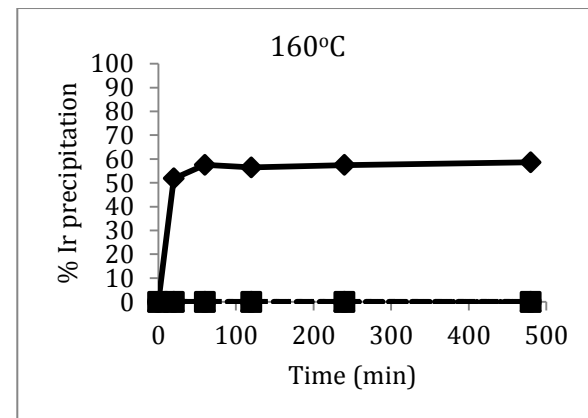
(b)



(d)



(e)



(f)

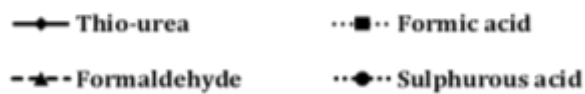


Figure 3: OPM precipitations for the different screening test reagents at 80°C and 160°C (250 rpm, ambient pressure)

4.3. Nickel and copper precipitation

Although copper and nickel precipitation were not used as decisive factors in reagent screening tests, it was necessary to note the behaviour of these components in response to temperature and reagent type variations. This was necessary because the objectives of this research did not only focus on precipitating OPMs but also in ensuring that nickel and copper co-precipitation remained minimal. Although the desirable situation was to prevent copper and nickel precipitation as much as possible, it was expected that the nickel and copper contained in the process solution would co-precipitate along with the rhodium in an ionic precipitation reaction as suggested by McGeorge et al. (2009). The quantity of Cu and Ni precipitated from the process solution by each of the investigated reagents at the two investigated operating temperatures are displayed in Figure 4.

Referring to Figure 4a and Figure 4b, it can be noticed that thio-urea precipitated significant amounts Cu and Ni. Contrary to what was observed in the study done by Lottering (2011), more Cu than Ni was precipitated using thio-urea as reagent in the current study. The possible explanation to this trend could be that beside precipitating as a result of direct interaction between the Cu ions and thio-urea, additional copper may have precipitated by the methathesis reaction with the nickel precipitates present in the solution, as is typically observed in the first stage leach of the base metal refinery (Provis et al, 2003). However, with increased operating temperature and reaction time copper and nickel precipitated by thio-urea and formaldehyde were reduced significantly (Figure 4c and d). From the nickel and copper point of view it thus appears that choosing thio-urea as an ideal reagent would require either operating the process at higher temperatures or running the process at low temperature for at least more than 3 hours of reaction time. The second option appears to be a better alternative as this would also provide maximum recovery of OPMs.

Using formic acid as precipitating reagent also resulted in high copper and nickel precipitation especially at 160°C. Based on its performance on nickel and copper precipitation, formic acid would not be a better option for the ideal reagent.

The performance of formaldehyde on base metal precipitation was generally low at both temperatures. This could probably mean that the quantity of formaldehyde converted to formic acid (Habashi, 1999) under the investigated condition was not sufficient to produce the same effect observed when formic acid was used.

Sulphurous acid on the other hand appears to precipitate a lesser amount of (typically below 10 %) copper and nickel at low temperatures (Figure 4 a and b) although these quantities would increase with increased operating temperature as is evident from Figure 4 c and d.

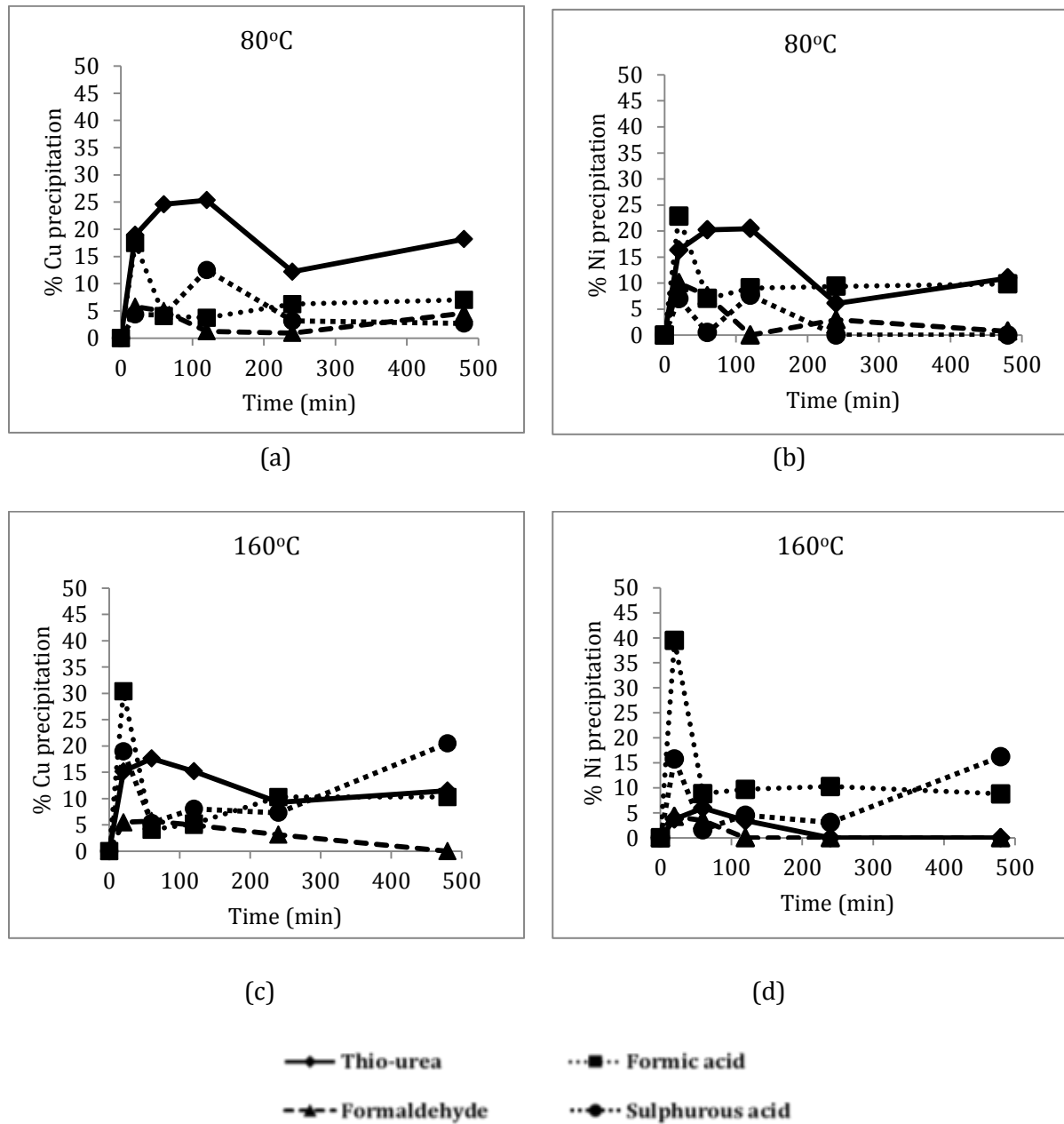


Figure 4: Cu and Ni precipitation for the different screening test reagents at 80°C and 160°C (250 rpm, ambient pressure)

4.4. Selenium and tellurium precipitation

Although selenium and tellurium removal were not the main focus of this research, it was necessary to evaluate the performance of the screened reagent with regard to Se and Te removal. This was necessary in order to obtain relevant information that could be used to modify or improve control of the Se/Te removal stage for the possibility of recovering OPMS along with Se and Te. Figure 5a and c shows that thio-urea removed virtually all the selenium from the solution with relatively fast reaction kinetics regardless of operating temperature. Once again from the Se removal point of view it appears that using thio-urea as a reagent on the plant would be a better option.

Sulphurous acid also resulted in sufficient selenium removal at both temperatures (Figure 5a and c). The observed performance of sulphurous acid can be attributed to its ability to reduce ionic selenium in acid solution to elemental Se according to equation 10 (section 2.3). The further increase in the extent and rate of selenium precipitation at 160°C could be due to the combined effect of selenium reduction by sulphurous acid and the cementation of Se by the metallic copper generated from the disproportionation decomposition of the reduced ionic copper (Wang et al., 2003; Weir et al., 1982). The data points for Se precipitation after approximately 60 minutes for the experiment conducted at 80°C could not be presented on Figure 5a due to analytical error in selenium concentration determination.

Using formic acid as precipitating agent, sufficient Se removal is also achievable though only at high operating temperature. The explanation to this could be that the reducing effect of formic acid is temperature dependent (endothermic) and thus a low temperature (80°C) could not provide sufficient energy to cause noticeable selenium reduction. At high temperature, the effect of formic acid may have been complemented by the effect of reduced copper to cause high selenium precipitation. This can also be confirmed from the Cu precipitation behavior by formic acid discussed in section 4.3.

Referring to Figure 5b, tellurium precipitation at low temperature appears to be problematic for all the different reagents investigated. For example a maximum of about 10 % Te was precipitated by thio-urea at 80°C. This behaviour could be ascribed to the fact that precipitation of tellurium by the reduction of ionic tellurium to elemental form using reducing agents is difficult (Wang et al., 2003). At 160°C, however, all the reagents appear to provide better tellurium precipitation (Figure 5d). At this temperature the quantity of Te precipitated by each of these reagents within the first 20 minutes of reaction time were in excess of 60 %. At 160°C the ionic Cu contained in the solution had been reduced to elemental Cu which caused cementation of Te as copper telluride (Crundwell et al., 2011; Wang et al., 2003). This

observation can also be complimented by the SEM analysis results which indicated the presence of metallic copper for the precipitates obtained at 160°C only (section 6.4.1).

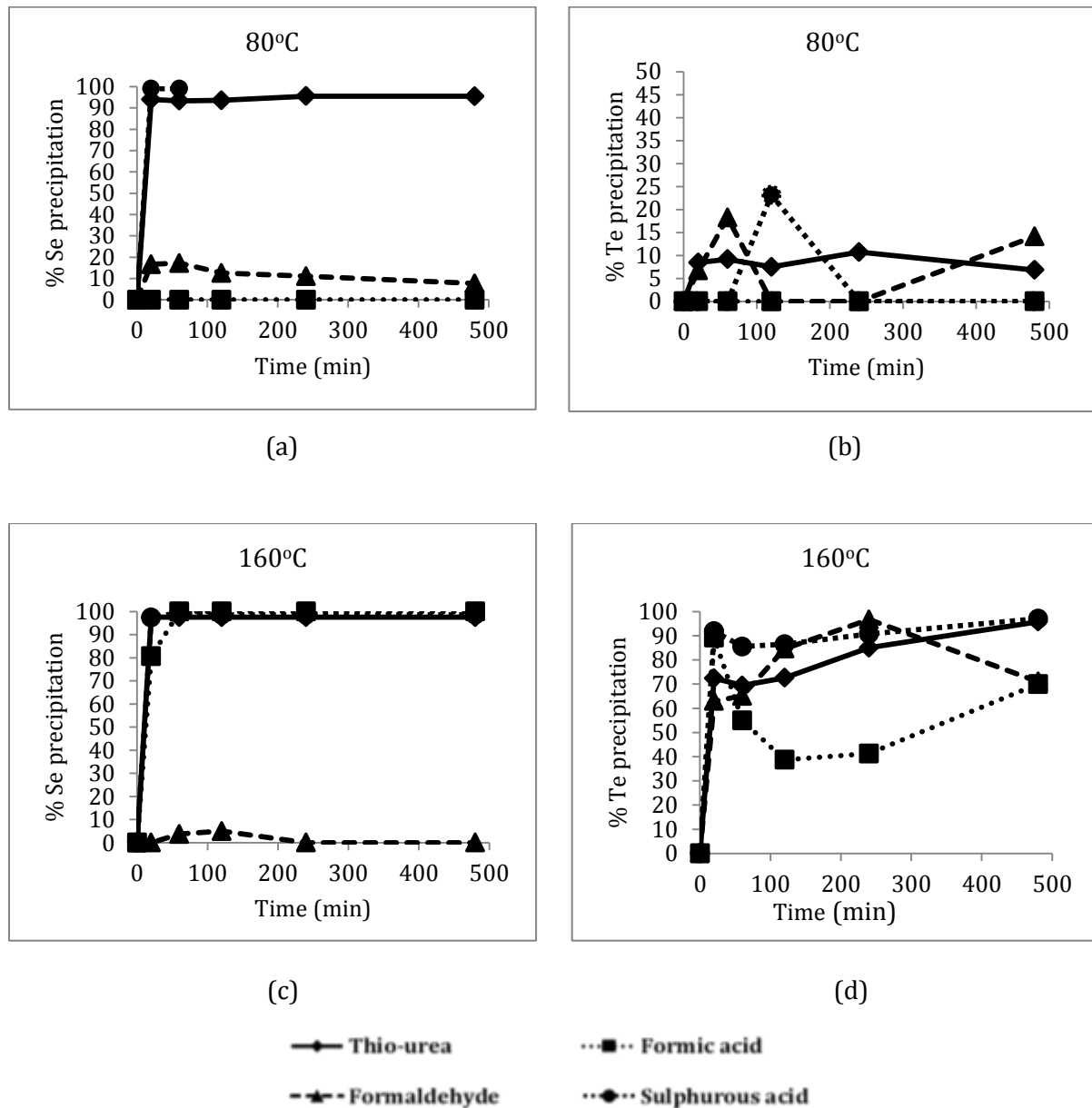


Figure 5: Se and Te precipitation for the different screening test reagents at 80°C and 160°C (250 rpm, ambient pressure)

4.5. Conclusion

The performance of equal excess amount of the screened reagents with regard to the overall quantity of metallic species of interest precipitated from the solution, were analysed in order to obtain information necessary to effect the selection of ideal reagent(s). Using OPMs precipitation as the main criteria to assess performance and effect the selection of ideal reagent, results from reagent screening tests at all conditions studied shows that thio-urea would provide better OPMs recovery in comparison to the other screened reagents. In addition thio-urea also exhibited greater potential of providing minimal Ni co-precipitation with increased temperature and reaction time. Furthermore, it is evident (Figure 5a and c) that using thio-urea would also reduce the concentration of impurities present in the leach solution (particularly selenium) to less than 1 mg/L which is an industrial acceptable limit (Sherritt Gordon Mines Limited, 1983). Based on its performance, thio-urea was selected for further test in order to evaluate the effects of reagent addition, temperature, pressure and agitation speed on the recoveries of OPMs as well as the co-precipitation extent of base metals. It was necessary to understanding the effects of these operating variables for the purposes of generating optimal conditions that would ensure complete recovery of OPMs with minimal base metal co-precipitation.

Although the excess quantity of sulphurous acid used in the screening tests did not provide sufficient OPM recovery sulphurous acid was also considered as an additional reagent for further investigation based on the fact that it is the reagent currently used on the plant for Se and Te removal in base metal refinery at Lonmin (Sherritt Gordon Mines Limited, 1983; Crundwell et al., 2011). Despite not being the best reagent choice from OPM recovery point of view based on reagent screening test results, considering sulphurous acid as additional reagent to further investigate OPM recovery presented several advantages. Using sulphurous acid for the recovery of OPM would require very little modifications of the existing plant equipment. In addition, the aqueous and solid components resulting from the reactions between sulphurous acid and the dissolved metallic species present in the process solution are already known and would thus not present risk of contaminating downstream processes.

5. EFFECTS OF OPERATING PARAMETERS ON THE PRECIPITATION PROCESS

5.1. Characterization of the precipitates

In order to study the nature of the precipitates in this investigation, the experiments were conducted at parameter levels closer to industrial practical operations. The precipitates obtained from the reaction between the process solution (composition given in section 3.1) and the reagent (thio-urea and sulphurous acid) at 80°C and 160°C were analysed using scanning electron microscopy (SEM) and x-ray diffraction (XRD). Examination of the XRD patterns showed that the precipitates generated were characterized by the predominance of amorphous phases. Peaks corresponding to bornite (Cu_5FeS_4), digenite ($\text{Cu}_{1.8}\text{S}$) and wuestite ($\text{Fe}_{0.942}\text{O}$) were of the species identified in the precipitate obtained at 80 °C with bornite being the major compound. At high temperature (160°C) the patterns showed that digenite was the major compound precipitated with minor amounts of tenorite (CuO) and wuestite (Figure 6 and Figure 7). The precipitation of digenite from copper sulphate solution within the studied temperature range using sulphide precipitant was also reported by Jayaweera et al., (1989) (section 2.5). The results also indicated the presence of tenorite (CuO) and elemental copper in the precipitate obtained at 160°C. Because of poor crystallinity of the precipitates, not all the species could be identified. However, the precipitate composition results obtained from scanning electron microscopy (SEM) analysis indicated that the precipitates also contained minor amounts of PGMs and selenium. XRD analysis could not be performed on the precipitates generated from sulphurous acid due to the small amount of the precipitate samples.

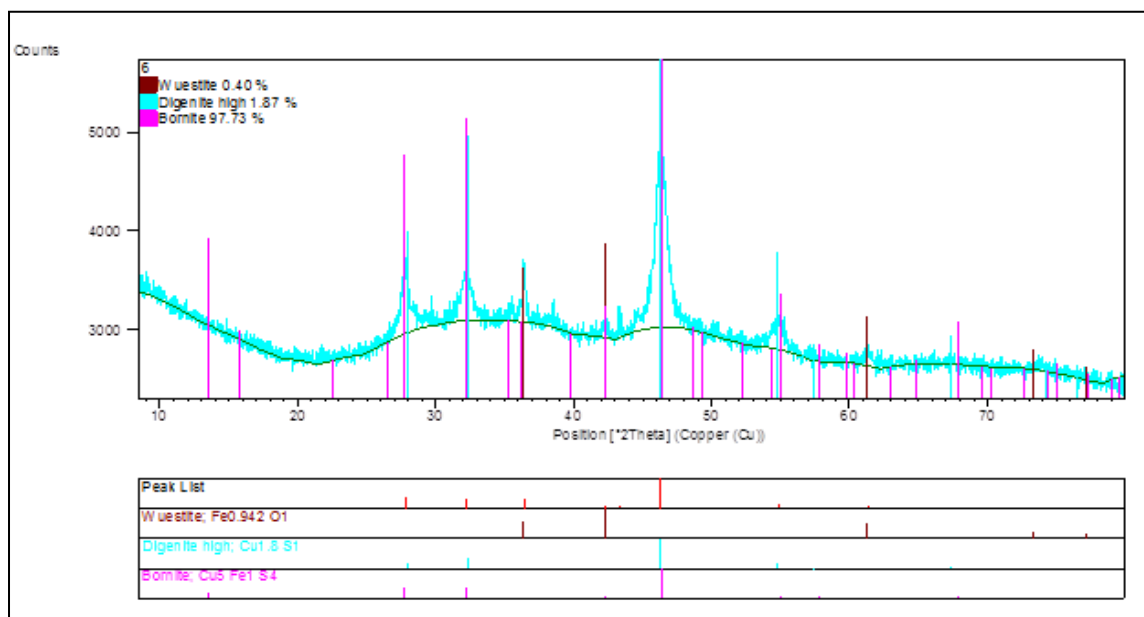


Figure 6: XRD patterns of the precipitate sample (80°C, 200 % excess thio-urea, ambient pressure, and 250 rpm)

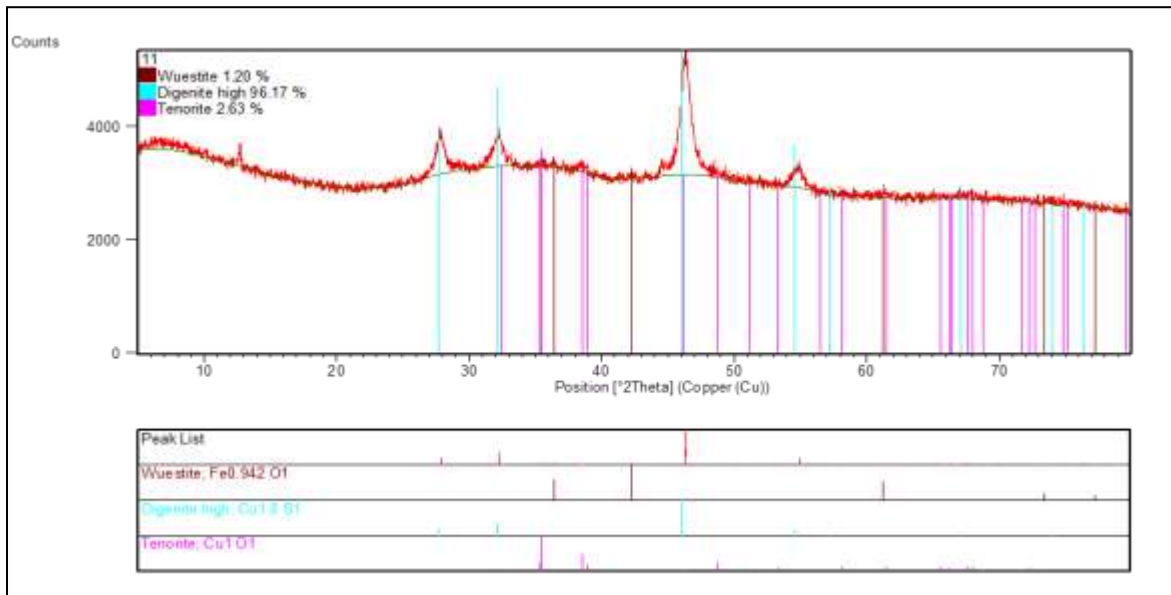


Figure 7: XRD patterns of the precipitate sample (160°C, 200 % excess thio-urea, ambient pressure, and 250 rpm)

The morphology of the precipitates produced using thio-urea and sulphurous acid were also studied using scanning electron microscopy. The results are illustrated in Figure 8 . It can be seen that the precipitates obtained using thio-urea as reagent consisted of clustered small irregular shaped crystals. The observed morphology of generated particles is typical of the sulphide precipitations occurring as a result of dominant homogeneous nucleation resulting from high solution supersaturation. In such precipitation reactions agglomeration is usually the controlling mechanism of crystal growth due to the high number of nuclei produced leading to the formation of fine polycrystalline or amorphous particles (Lewis and van Hille, 2006; Dirksen and Ring, 1991).

The amorphous nature of the particles was also confirmed from XRD analysis. On the other hand, the SEM imaging of precipitates generated from sulphurous acid (Figure 8b) illustrate that the precipitates consisted of a mixture of needle shaped particles and irregular shaped particles appearing to be aggregates of small crystals. The influence of operating variables on the precipitate characteristics presented in section 5.4.

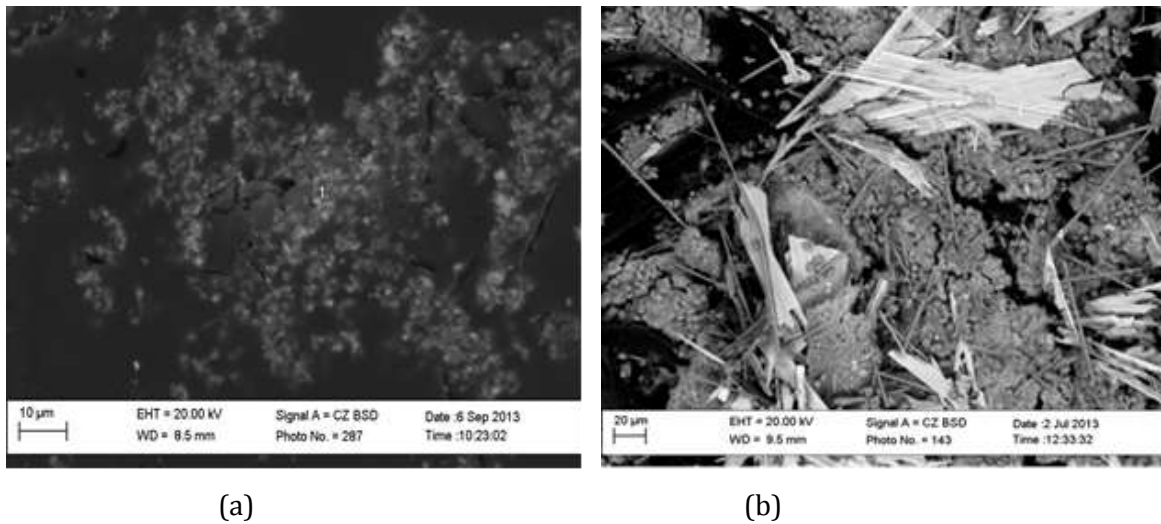


Figure 8: Scanning electron image of precipitates generated from the two reagents at 80°C (a) thio-urea and (b) sulphurous acid

In order to determine the precipitate particle size distribution (PSD), precipitate samples were analysed using light scattering analysis techniques (with Saturn DigiSizer 5200 V1.10 analyzer). The particle size distribution d_{50} among the different experiments performed at various operating conditions using thio-urea ranges from 1.952 μm to 30.81 μm (data shown in appendix D). The PSD analysis, however, could not be performed on the precipitates generated from sulphurous acid due to insufficient amount of precipitate samples.

5.2. Thio-urea based experiments

The influence of operating parameters on the extent and rates of OPMs and base metals precipitation from a copper-nickel sulphate leach solution using thio-urea as precipitating agent were investigated using 2^4 full factorial experimental design. The parameters investigated and their corresponding high and low levels were given section 3.2.1.1. The data reported graphically in this section for each response (Rh, Ru, Ir, Cu, and Ni), are comparisons of the average percent precipitation for 8 experimental tests conducted at low level of a particular variable (temperature, reagent quantity, pressure, and agitation speed) with the average percent precipitation obtained for 8 experimental tests performed at high level of that particular variable.

5.2.1. Rhodium precipitation

The influence of operating parameters on the extent and rate of rhodium recovery are shown in Figure 9. According to this figure, reagent quantity is the most important parameter on the rate of rhodium precipitation while the extent was identical in all cases (Figure 9a). The figure shows that approximately 200 % excess quantity of thio-urea was adequate to precipitate all the

rhodium out of a 1000 ml process solution studied within 60 minutes of reaction time. Further increase in the reagent quantity, however, caused a slight decrease on the rate and quantity of Rh precipitated from the solution within the first 20 minutes. Approximately 94 % Rh recovery on average was achieved using 200 % excess thio-urea within the first 20 minutes of reaction time compared to roughly 88 % Rh recovery when 320 % excess thio-urea was used within the same time range. The observed negative effect of reagent addition on the recovery of Rh is, however, unexpected. The expected scenario was that increasing the quantity of thio-urea would result in increased concentration of the sulphide ions generated by decomposition of the thio-urea reagent (Fang and Muhammed, 1992). Consequently, the likelihood of interactions between the sulphide ions with the Rh ions present in the solution should increase and result in higher rhodium precipitation. The results for the variations in operating temperature, pressure, and agitation speed are displayed in Figure 9b, c, and d respectively where it is apparent that varying these parameters had no significant impact on the rate and extent of rhodium recovery. These results are in agreement with the statistical analysis which showed that reagent addition was the only significant factor at 95 % confidence level (section 6.1.1).

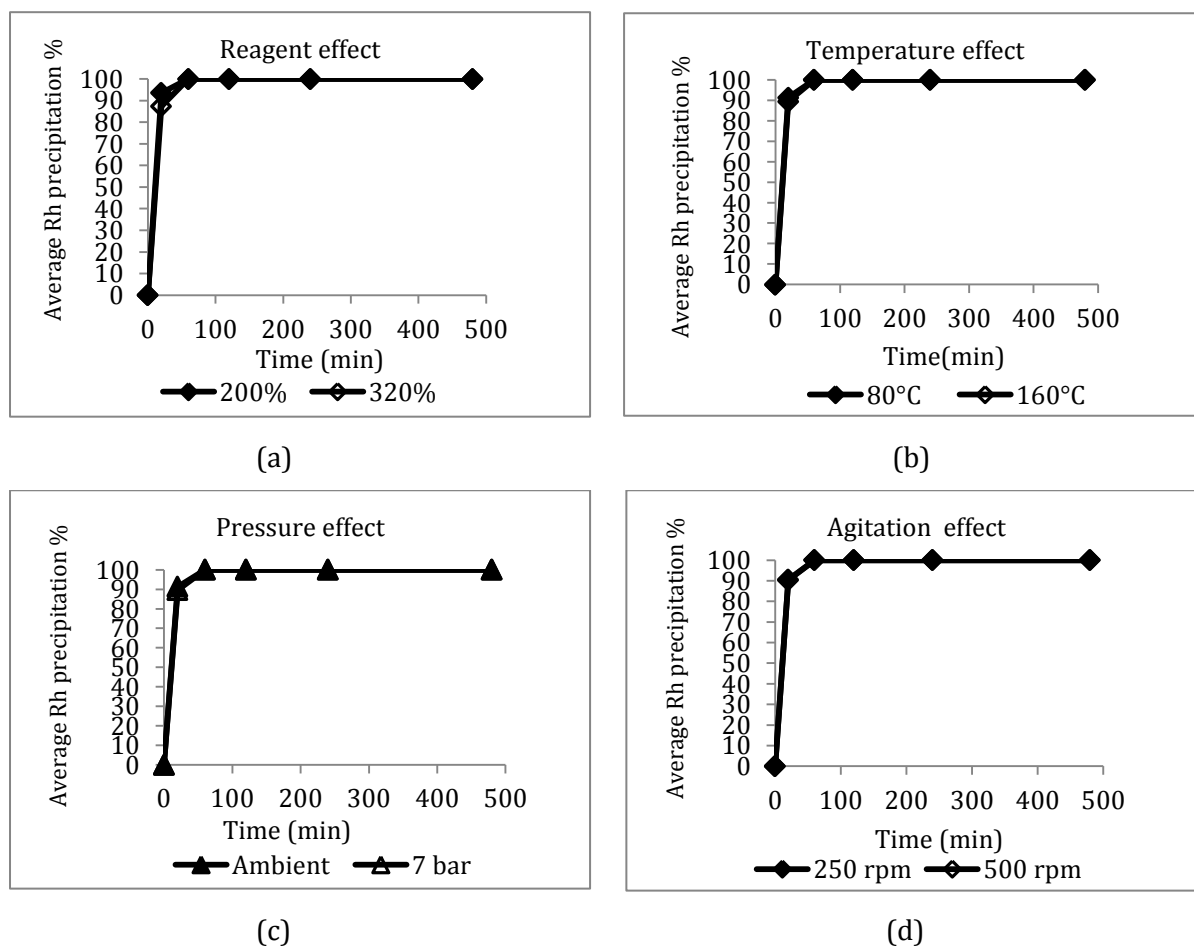


Figure 9: Effects of (a) reagent quantity, (b) temperature, (b) pressure, and (d) agitation speed on the rate and extent of Rh precipitation using thio-urea

5.2.2. Ruthenium precipitation

Results obtained from studying the influence of operating parameters on ruthenium recovery are displayed in Figure 10. The data indicated that reagent quantity, temperature, and pressure had negligible effect on the recovery of ruthenium. Statistical analysis of ruthenium precipitation data showed that agitation speed was the only significant parameter at 95 % confidence level. The observed increase in Ru precipitation due to increased agitation speed can potentially be explained by the fact that increasing the agitation speed increases the contact between the reagent and solution by increasing the speed at which these two solutions are interspersed with one another. This observation is corroborated by the solid particle analysis results presented in section 5.4.4. The results further show that at high temperature the ruthenium precipitated as a function of time appears to re-dissolve back into the solution after about 120 minutes. The reason for the observed Ru dissolution with increasing residence time at high temperature is not very clear at this point. However, the fact that this phenomenon was only observed in the experiments carried out at high temperature (Figures 44 to 59, Appendix B), it could probably mean that the rate of Ru solubility outweighed the rate of Ru precipitation at 160°C with increasing residence time.

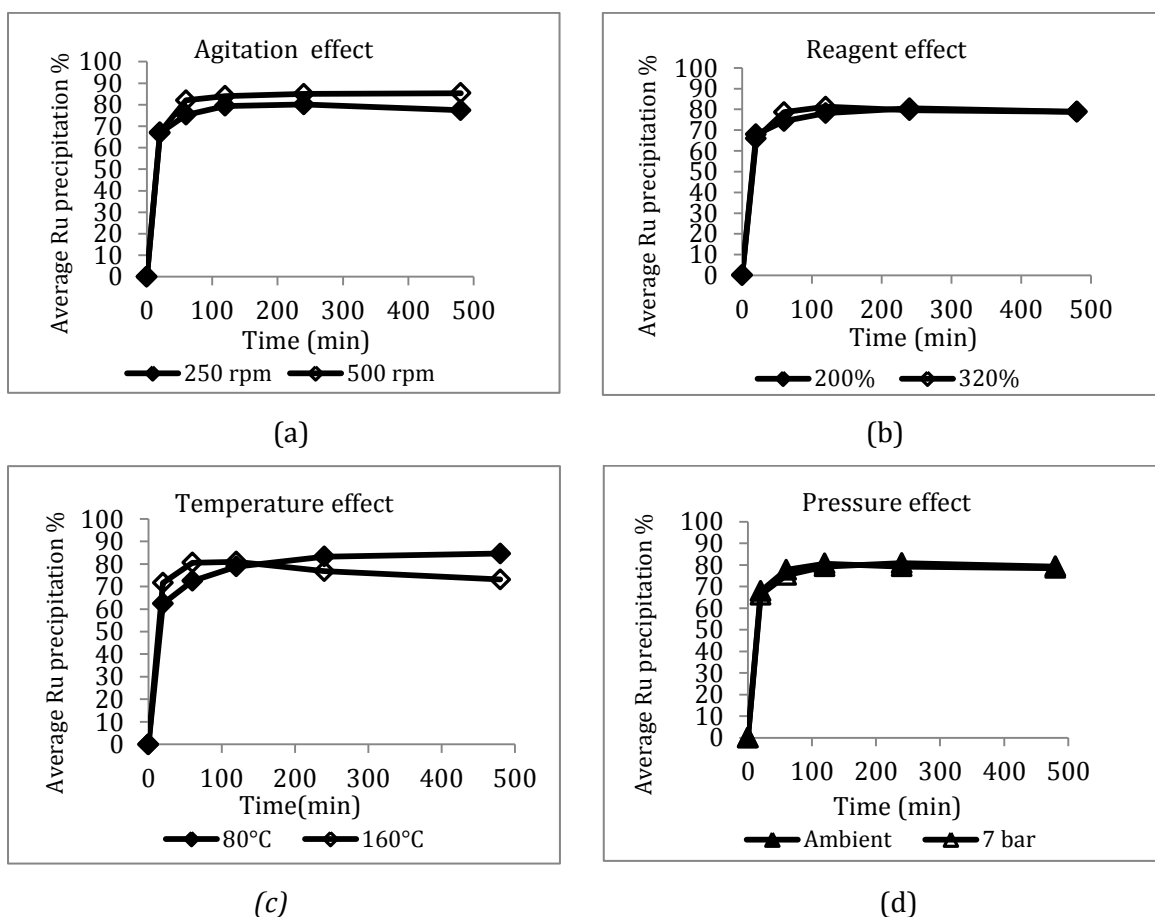


Figure 10: Effects of (a) agitation speed (b) reagent quantity, (c) temperature, and (d) pressure on the rate and extent of Ru precipitation using thio-urea

5.2.3. Iridium precipitation

The effects of varying operating parameters on iridium precipitation from the Ni-Cu sulphate leach solution are shown in Figure 11. The data indicate that the most influential parameter on the rate and extent of Ir precipitation in order of descending importance were: temperature and reagent quantity. Temperature increase caused an increase on the rate of iridium precipitation. At 160°C, iridium precipitation appears to reach equilibrium in about 60 minutes of reaction time while at 80°C the iridium continues to precipitate until after about 250 minutes. The observed increase in the rate of iridium precipitation could be ascribed to the increased kinetic energy of the Ir and thio-urea molecules owing to the temperature increase and subsequent occurrence of collisions with sufficient energy for the molecules to react. Increasing temperature also caused a 10 % average increase in Ir recovery (Figure 11b). The observed effect of temperature on the rate of iridium precipitation could also suggest that the reaction is largely chemically controlled rather than diffusion controlled (Sohnel and Garside, 1992).

Reagent quantity also caused a positive influence on the rate and extent of iridium precipitation. With increased thio-urea quantity (320 %), maximum of roughly 57 % Ir average recovery was achieved in about 2 hours compared to average maximum of 54.7 % Ir recovery obtained in 4 hours using 200 % excess thio-urea quantity (Figure 11a). Increasing agitation speed on the other hand resulted in increased extent of iridium recovery (Figure 11c) whereas increase in pressure had no significant influence on iridium precipitation.

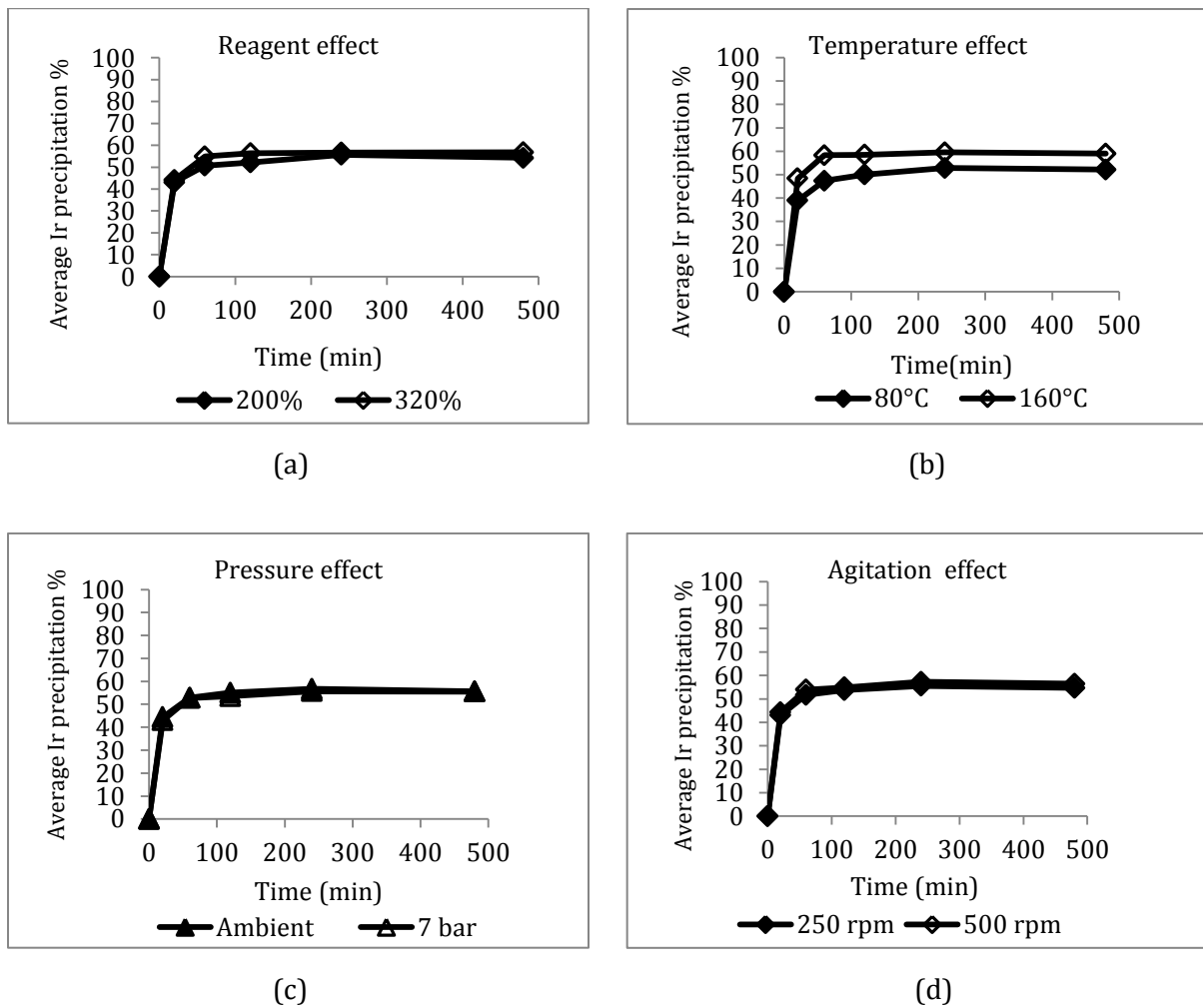


Figure 11: Effects of (a) reagent quantity, (b) temperature, (c) pressure and (d) agitation speed on the rate and extent of Ir precipitation using thio-urea

5.2.4. Copper precipitation

The influence of operating parameters on the rate and extent of copper co-precipitation were also investigated. The results are displayed in Figure 12 where it is evident that increasing temperature and reagent quantity increased the per cent copper precipitation. The maximum quantity of copper precipitated was roughly doubled when the operating temperature was raised from 80°C to 160°C (Figure 12). With variation in thio-urea quantity, the data showed that 22 % maximum average Cu precipitation occurred when 320 % was used compared to 15 % maximum Cu co-precipitation by 200 % excess thio-urea (Figure 12). Referring Figure 12c and d, it can be noticed that the impacts caused by pressure and agitation speed respectively on Cu precipitation were negligible. These observations are in agreement with the statistical analysis presented in section 6.1.

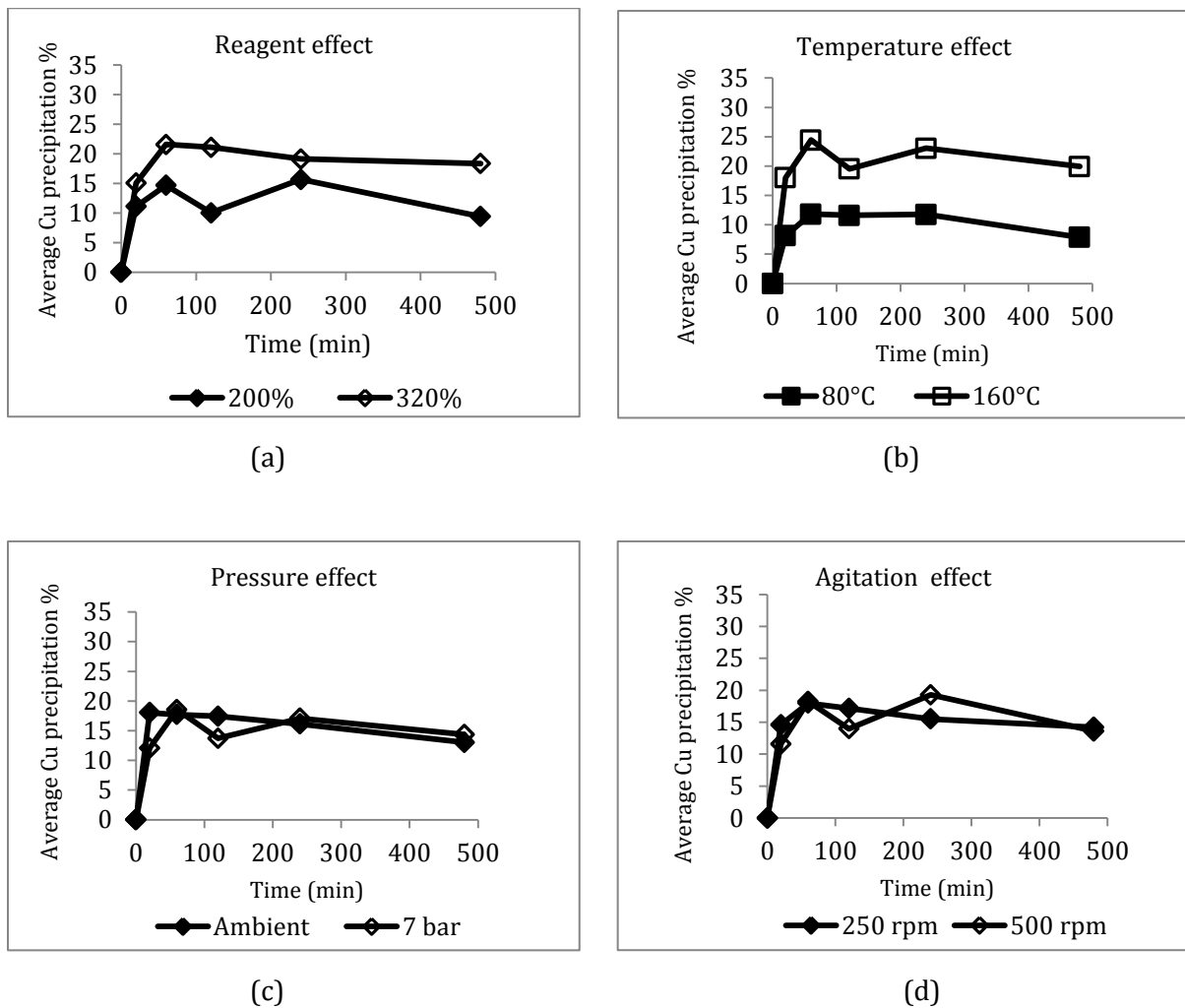


Figure 12: Effects of (a) reagent quantity, (b) temperature, (c) pressure and (d) agitation speed on the rate and extent of Cu precipitation using thio-urea

5.2.5. Nickel precipitation

The influence of operating parameters on nickel co-precipitation using thio-urea are displayed in Figure 13 where it can be seen that variation in thio-urea quantity had the greater impact. It was noted that the influence of thio-urea at all conditions investigated appeared to have less impact on nickel precipitation in comparison to copper precipitation. This could mean that besides the difference in the solubilities of the Cu and Ni precipitates, a portion of the Ni precipitated from the solution were oxidized by the cupric ions present in the solution. Similar trend was also observed in reagent screening test (section 4.3).

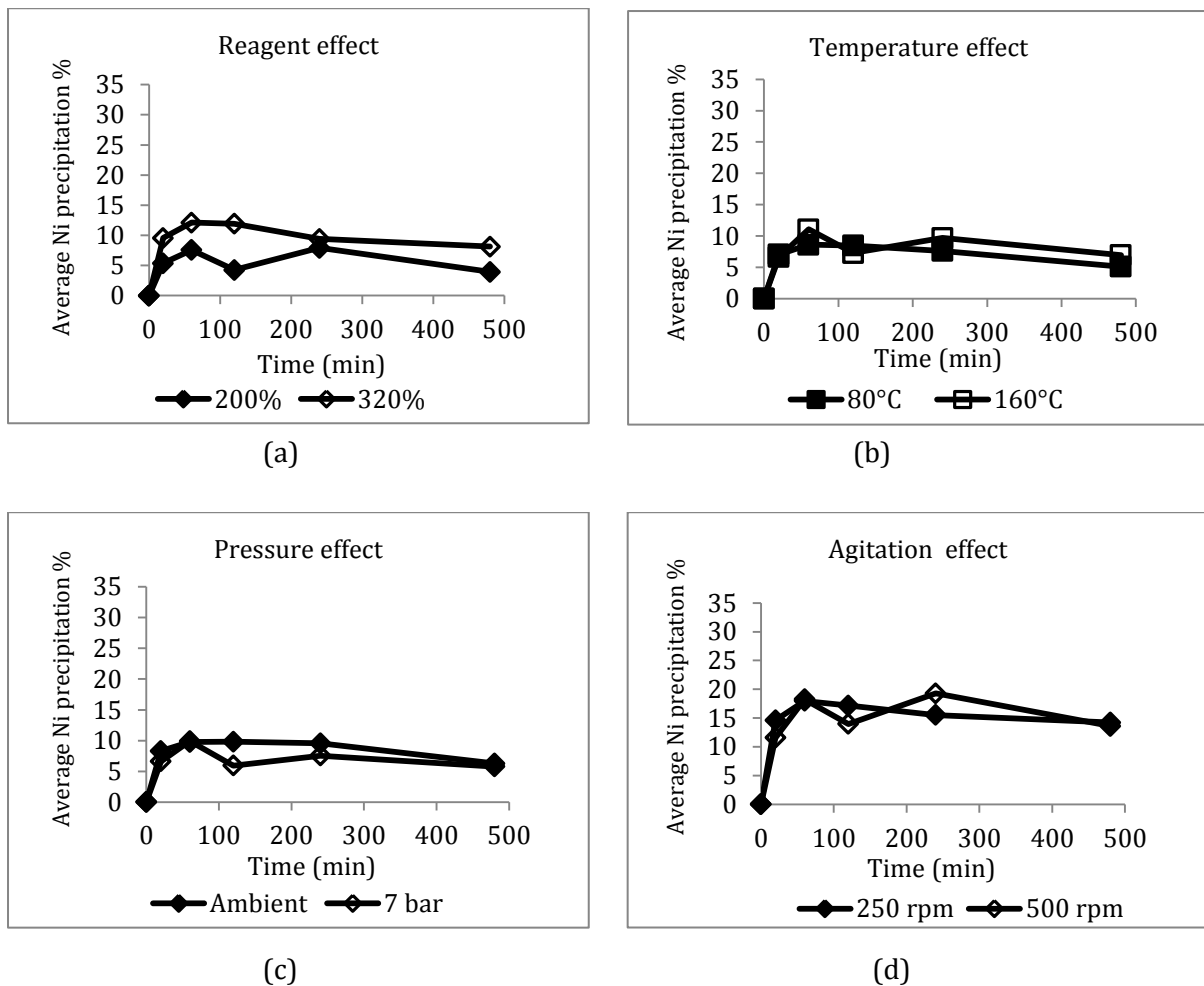


Figure 13: Effects of (a) reagent quantity, (b) temperature, (c) pressure and (d) agitation speed on the rate and extent of Ni precipitation using thio-urea

5.2.6. Selenium and tellurium

Investigating the precipitating behaviour of the impurities (selenium and tellurium) present in our system by reagent addition, was not the primary focus of this research. However, plots illustrating the behaviour of selenium and tellurium in response to variations in operating parameter for both reagents (thio-urea and sulphurous acid) are given in appendix B.

5.3. Sulphurous acid based experiments

The influence of operating parameters on the extent and rates of OPMs and base metals precipitation from a copper-nickel sulphate leach solution using sulphurous acid were investigated. The parameters investigated and their corresponding high and low levels were given section 3.2 (Table 8).

5.3.1. Rhodium precipitation

The results obtained for the effects of operating parameter on rhodium precipitation are shown in Figure 14. This figure shows that the most influential variables on Rh precipitation were: temperature, reagent quantity and reactor pressure. The results show that on average, the rate and extent of Rh recovery increased with increasing temperature and sulphurous acid quantity and decreased when the reactor pressure was increased. The average overall Rh recoveries increased from 17 % at 80°C to 33 % at 160°C, and from 13 % for 720 % excess reagent to about 18 % for the 920 % excess sulphurous acid. The positive influence of operating temperature on the precipitation process has also been reported by other researchers (Ruiz et al., 2007; Awadalla et al., 1994). For the variation in pressure, the average Rh recoveries obtained at ambient and 7 bar pressures were 32 % and 19 % respectively. Agitation speed had negligible influence on Rh recovery (Figure 14d). Based on these findings, it appears that to achieve maximum Rh recovery using sulphurous acid one need to consider operating the process at temperatures higher than 160°C and sulphurous acid excess quantity larger than 960 %. However, operating the process at such temperatures would imply increase in operating cost.

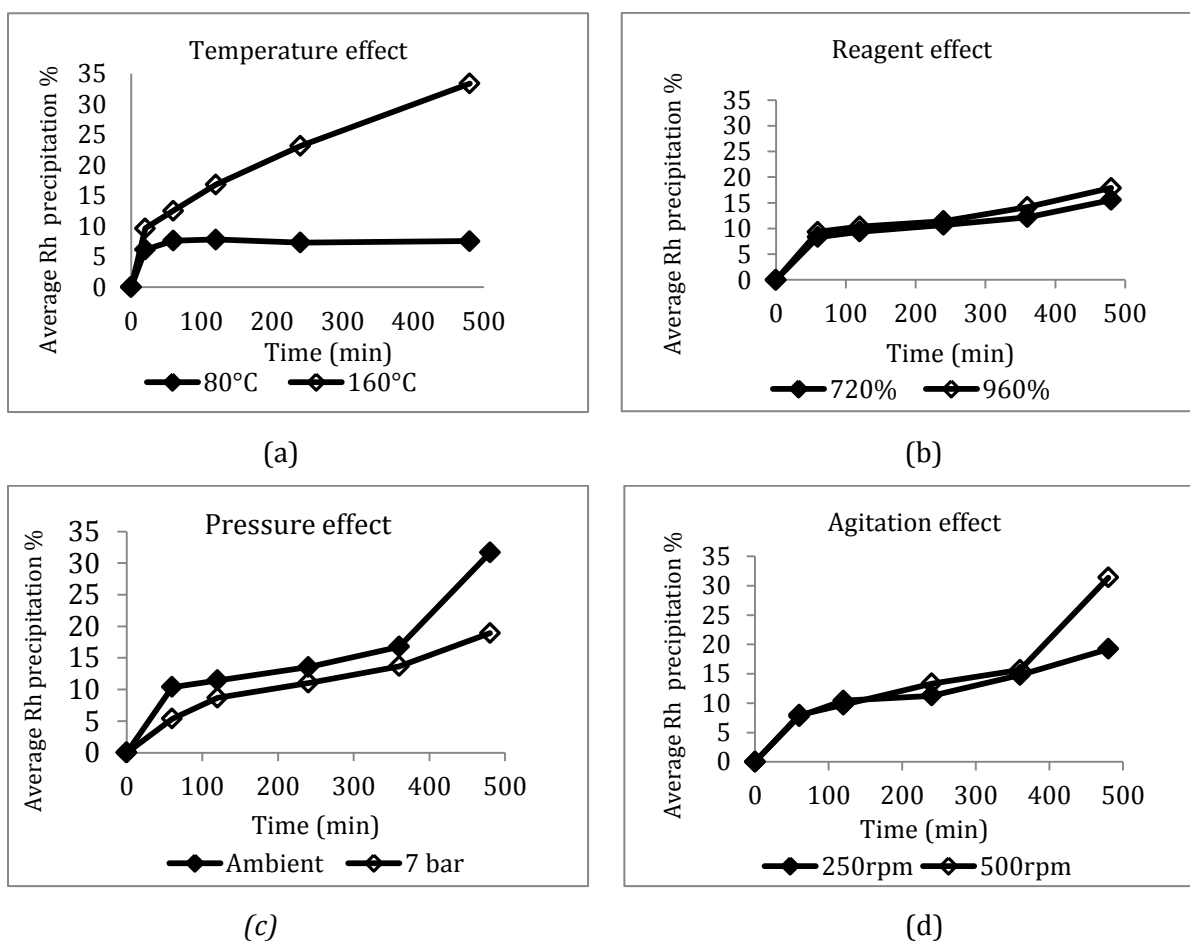


Figure 14: Effects of (a) reagent quantity, (b) temperature (c) pressure, (d) agitation speed on the rate and extent of Rh recovery using sulphurous acid

5.3.2. Ruthenium precipitation

Figure 15 shows the effects of operating parameters on ruthenium recovery. It can be seen that increasing each of the individual variables had negligible influence on ruthenium precipitation. The statistical analysis of the ruthenium precipitation data (section 6.2.2) indicated that the interaction effect between temperature and pressure promoted the precipitation of ruthenium.

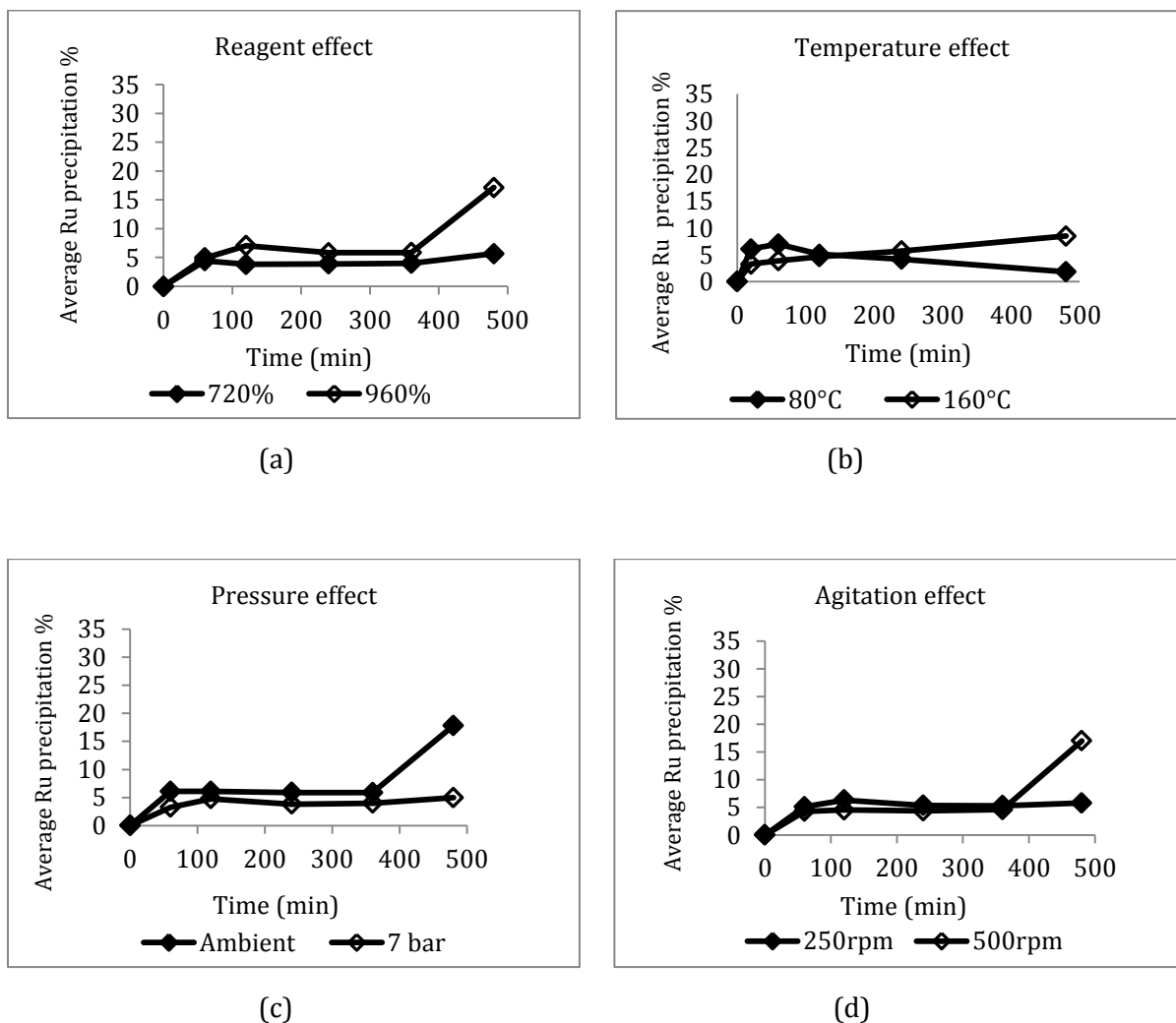


Figure 15: Effects of (a) reagent quantity, (b) temperature (c) pressure, (d) agitation speed on the rate and extent of Ru recovery using sulphurous acid

5.3.3. Iridium precipitation

Figure 16 displays the results from the study of operating parameter effects on iridium recovery. The data showed that the influence of the individual parameters on Ir response were not negligible. Statistical analysis of the results showed that iridium precipitation was favored by the interaction effect between the operating temperature and pressure. This positive effect caused by temperature variation on Ir precipitation using sulphurous acid was also observed when thio-urea was used (section 5.2.3).

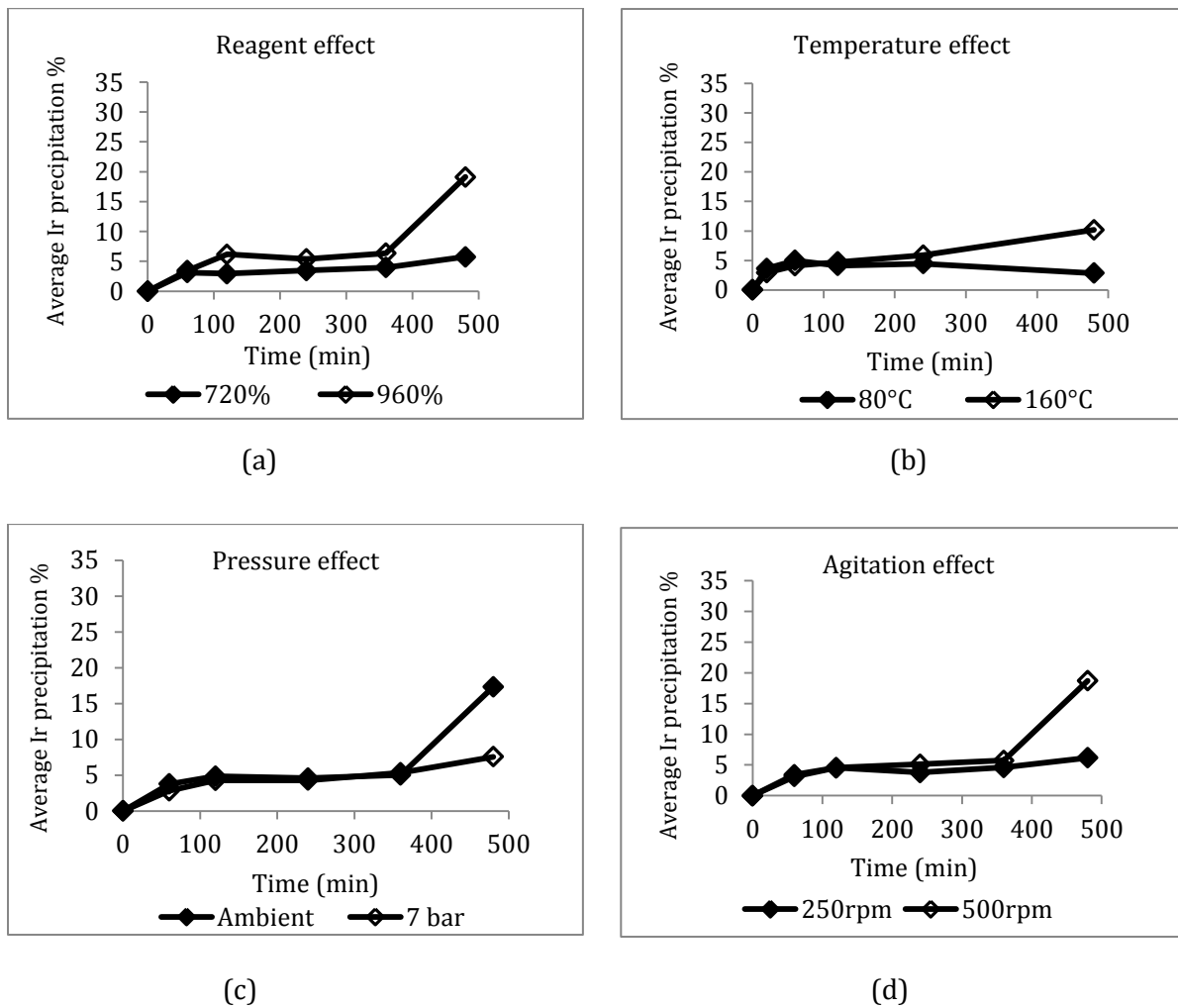


Figure 16: Effects of (a) reagent quantity, (b) temperature (c) pressure, and (d) agitation speed on the rate and extent of Ir precipitation using sulphurous acid

5.3.4. Copper precipitation

The results for the influence of operating parameters on copper co-precipitation using sulphurous acid are displayed in Figure 17. This figure shows that the most influential main variables on the rate and extent of Cu precipitation in order of descending significance were: temperature, reagent quantity, and agitation speed. Increase in temperature (Figure 17a), reagent quantity (Figure 17b), and agitation speed (Figure 17c) resulted in relatively higher Cu co-precipitation percent with faster kinetics. It is thus shown that increasing any of the studied operating parameter in an attempt to improve OPM recovery using sulphurous acid, would as well result in increased Cu co-precipitation.

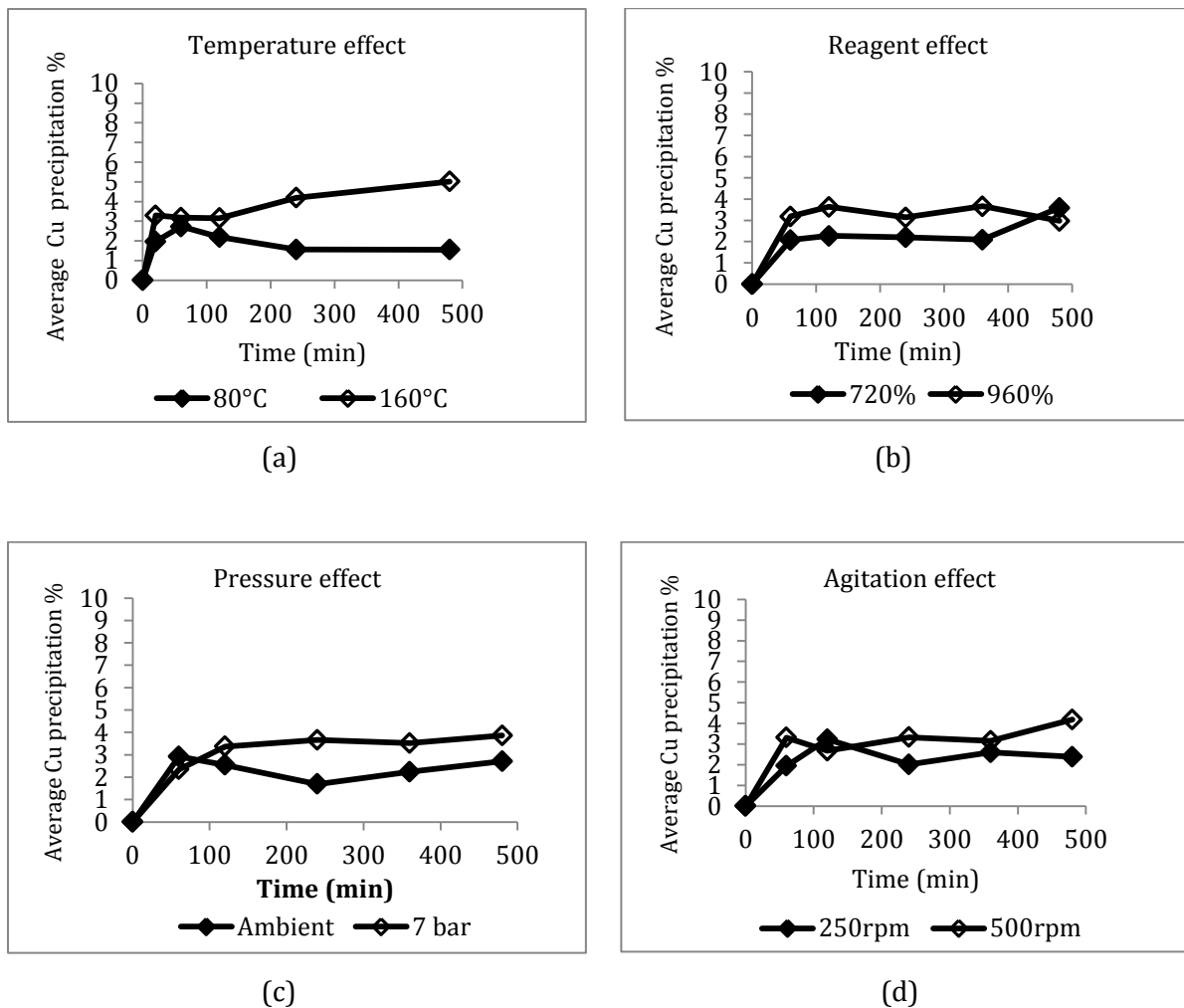


Figure 17: Effects of (a) reagent quantity, (b) temperature (c) pressure, and (d) agitation speed on the rate and extent of Cu precipitation using sulphurous acid

5.3.5. Nickel precipitation

Figure 18 illustrates the average percentage co-precipitation of nickel caused by variations in the studied operating parameters. The results indicated that operating temperature was the only influential effect on nickel precipitation. All the other variables had negligible effect on nickel precipitation.

In summary, the results showed that for a system under current study, operating temperature and its interaction with pressure are the most important effects on OPMs and base metal precipitation by sulphurous acid. Increasing temperature would result in increased Rh and Ir precipitation with excessive Cu and Ni co-precipitation. Similar behaviour in copper precipitation using sulphurous acid at the investigated temperature was reported by Clarke and Rickard (1975).

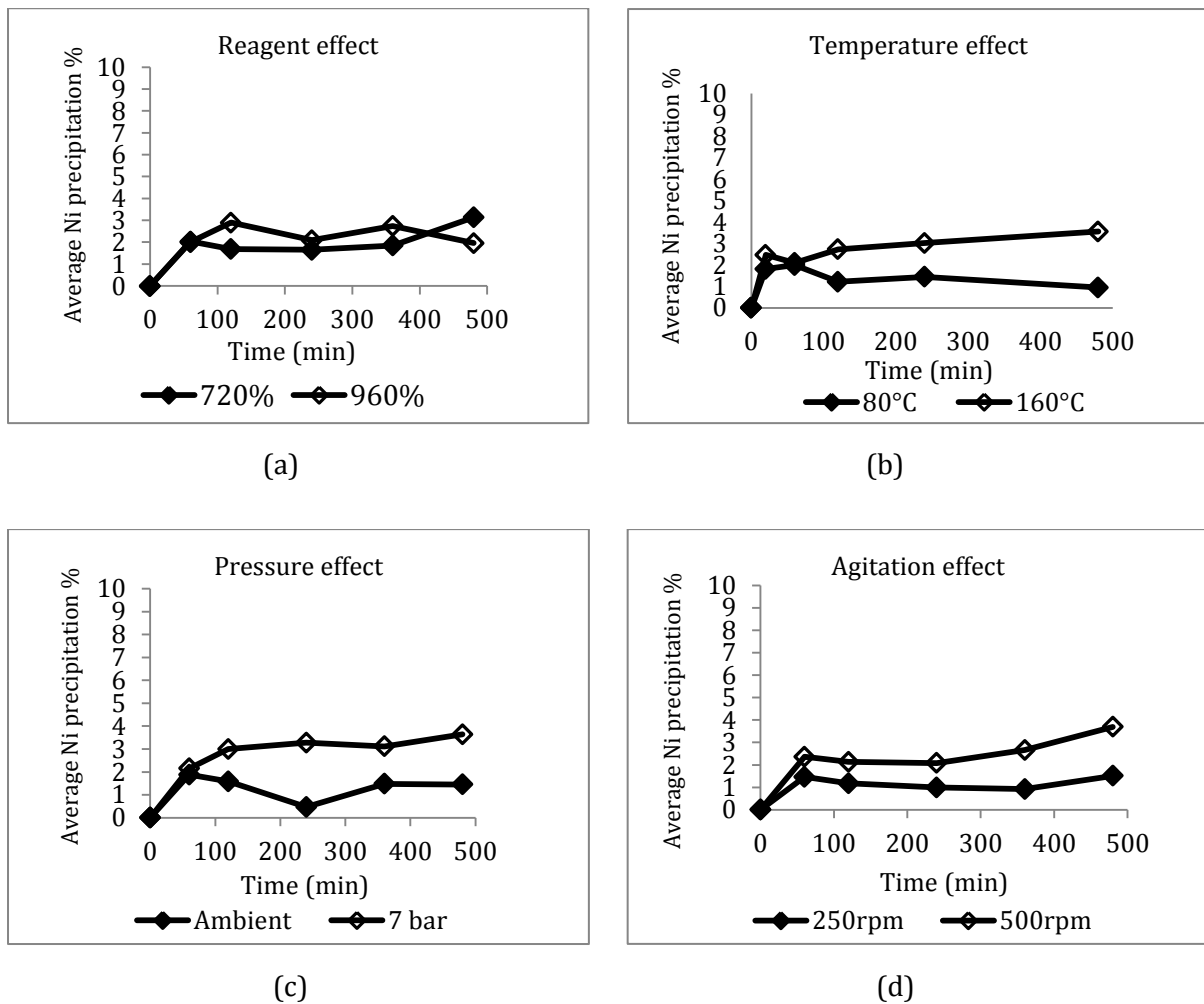


Figure 18: Effects of (a) reagent quantity, (b) temperature (c) pressure, and (d) agitation speed on the rate and extent of Ni precipitation using sulphurous acid

5.3.6. Selenium and tellurium

It was not the main focus of this research to discuss the influence of operating parameters on the precipitation of selenium and tellurium components present in the system. However, reference can be made to Figure 44 to Figure 59 provided in appendix B to see the influence of the studied parameters on Se and Te removal.

5.4. Influence of operating parameters on precipitate characteristics

It was shown in section 2.4 and section 2.5 that the crystallinity, morphology, and size distribution of particles obtained from precipitation processes are influenced by the process operating parameters. This section presents the influence of operating variables (temperature, reagent quantity, pressure and agitation speed) on the composition and size distribution of the precipitate particles generated using thio-urea for a reaction time of 480 minutes. The influence of these operating parameters on the precipitate particles generated using sulphurous acid was not investigated due to insufficient precipitate samples.

5.4.1. Temperature

The effect of operating temperature on the chemical composition of the precipitates was investigated. The precipitates were analysed for PGMs, selenium, tellurium, sulphur and base metal composition. The data showed that variation in temperature caused significant influence on the composition of the precipitates. SEM analysis spectra for the precipitates generated at both 80°C and 160°C showed that the metals precipitated with a relatively large quantity of sulphur indicating that metal sulphides were present in the precipitate (Table 9). This observation is complemented by the XRD results presented in section 5.1 where several metal sulphide peaks for the precipitates were identified. In addition, the presence of metallic copper was observed in the precipitates generated at 160°C.

Although there appear to be no Rh, Ni, and Te in the precipitates generated at 160°C, the ICP-AES analysis results (section 5.2) indicate that these species were significantly precipitated from the solution. The possible explanation for the observed phenomenon could be that these metals (Rh, Ni, and Te) precipitated as fine particles that could not be retained on the 20 - 25 µm filter papers that were used in our study. These findings are in accord with the particle size distribution analysis results presented in Figure 19. These observations are in agreement with the findings reported by Jayaweera et al., (1989) as discussed in section 2.5.

Table 9: Composition of the precipitates formed at both temperatures after 480 minutes (200 % excess thio-urea, ambient temperature and 250 rpm)

Temperature (°C)	Weight %													
	S	Fe	Ni	Cu	Zn	Se	Ru	Rh	Pd	Te	Ir	Pt	Pb	Total
80	21.34	1.01	8.13	31.84	0.00	2.90	2.52	1.12	0.93	0.00	3.03	5.79	21.39	100
160	9.71	0.19	0.00	65.35	0.00	3.57	0.90	0.00	2.68	0.00	2.77	8.38	6.44	100

Furthermore, the effect of operating temperature on particle size distribution (PSD) was studied. The results from PSD analysis were recorded by plotting the cumulative volume finer against the particle size on a semi logarithmic graph. Figure 19 shows the graphical results of the analysis for precipitates obtained at 80°C and 160°C for the reaction time of 8 hours. It can be seen that the result of increasing operating temperature is to decrease the particle size of the precipitates. The particle size distribution d_{50} (medium value of the particle size distribution) was used as a characteristic size of the distribution. The d_{50} is the value in the size distribution where 50 % of the particle size is below this size and 50 % is above it (Wills, 1997). For the data shown in Figure 19, the d_{50} values were 3.7 µm and 17.3 µm for 160°C and 80°C respectively

implying that finer precipitates were formed at high temperature in comparison to that at low operating temperature. The observed large difference between the two d_{50} sizes could be attributed to increased nucleation rate outweighing the agglomeration rate of the nuclei resulting in the formation of smaller particles. The dependence of precipitate particle size on the relative rates of nucleation, crystal growth, and agglomeration resulting from a supersaturated solution is well documented in literature (Ruiz et al., 2007; Dirksen and Ring, 1991). In addition, it is believed that varying operating temperature can significantly induce supersaturation in a solution which may result in high nucleation rates (Dirksen and Ring, 1991).

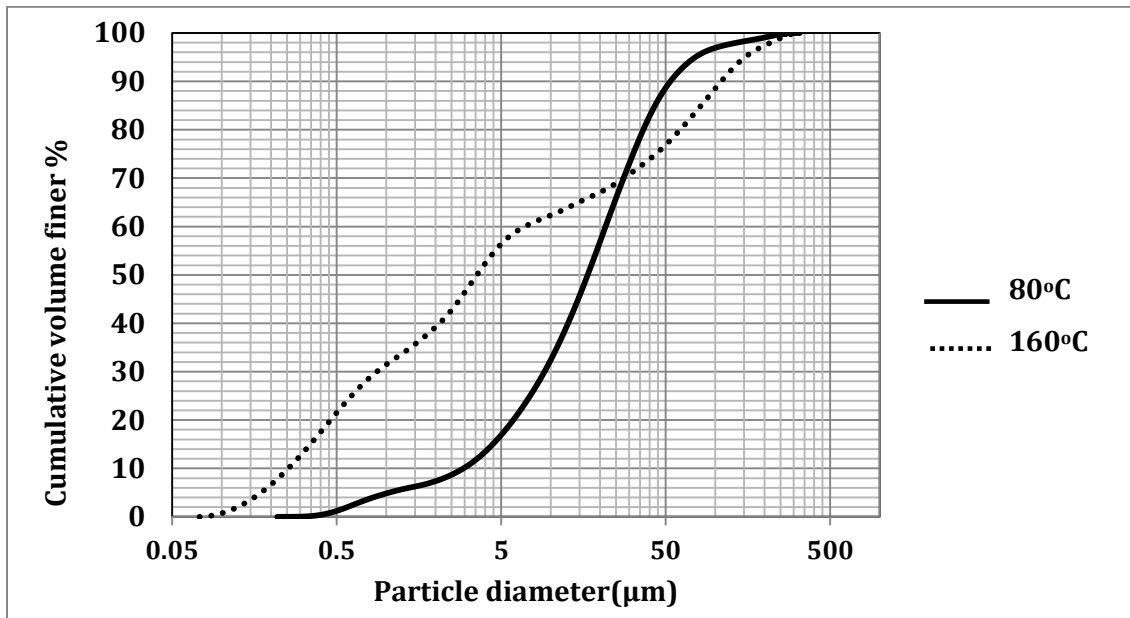


Figure 19: Size distribution of the precipitates obtained at low and high temperature levels (200 % excess thio-urea, ambient pressure, and 250 rpm)

5.4.2. Reagent quantity

The precipitates generated from thio-urea variation experiments were also analysed for PGMs, selenium, tellurium, sulphur, and base metal content. The results are shown in Table 10 where it is evident that variation in thio-urea quantity has negligible influence on precipitate composition.

Table 10: Composition of the precipitates for the variation in reagent excess quantity (80°C, ambient pressure, and 250 rpm)

Reagent (%)	Weight %													Total
	S	Fe	Ni	Cu	Zn	Se	Ru	Rh	Pd	Te	Ir	Pt	Pb	
200	21.34	1.01	8.13	31.84	0.00	2.90	2.52	1.12	0.93	0.00	3.03	5.79	21.39	100
320	27.67	0.91	0.40	23.52	0.00	3.17	12.79	4.32	7.66	0.00	1.46	12.44	5.66	100

Reagent addition did not show significant influence on the particle size of the precipitates. The particle size analysis showed the d_{50} values of 16.3 μm and 17.3 μm for the high and low reagent excess quantity respectively. These results can be seen in Figure 20. It is evident from the small difference in the d_{50} and closeness of the two graphs that reagent addition had no significant effect on particle size distribution of the precipitates.

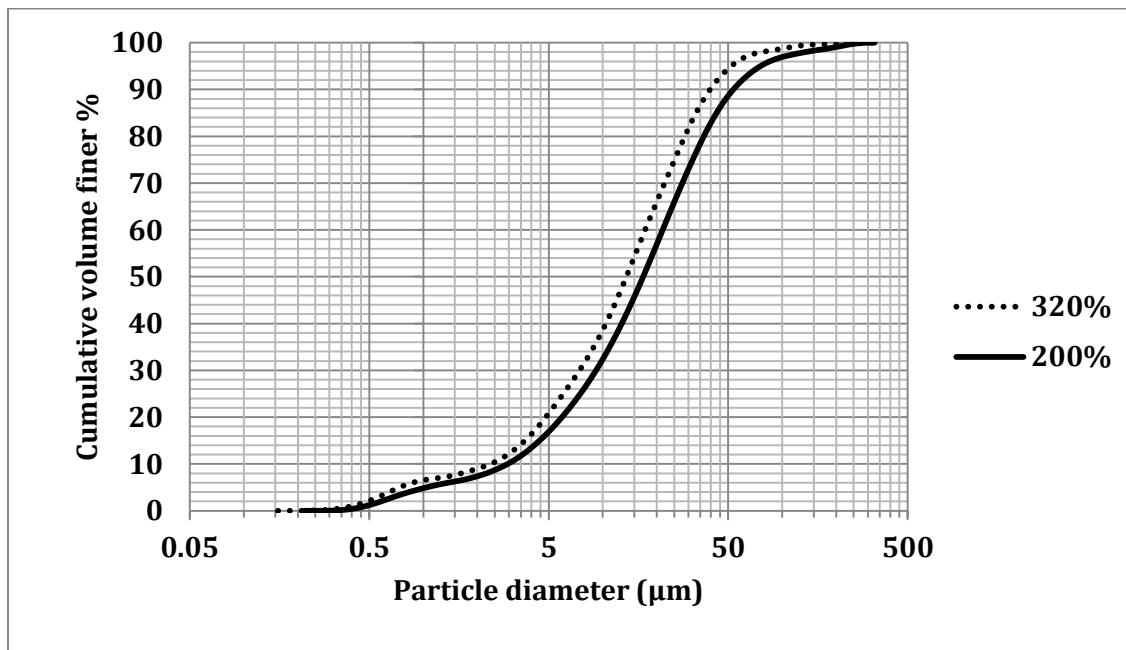


Figure 20: Size distributions of the precipitates obtained using 200 % and 320 % excess thio-urea (80°C, ambient pressure, and 250 rpm)

5.4.3. Pressure

Table 11 is a summary of the effect of varying reactor pressure on the composition of precipitates produced using thio-urea. It is apparent from this table that variation in pressure had no significant influence on the composition of the precipitates.

Table 11: Composition of the precipitates for the variation in reactor pressure (80°C, 200 % excess thio-urea, and 250 rpm)

Pressure(bar)	Weight %													Total
	S	Fe	Ni	Cu	Zn	Se	Ru	Rh	Pd	Te	Ir	Pt	Pb	
Ambient	21.34	1.01	8.13	31.84	0.00	2.90	2.52	1.12	0.93	0.00	3.03	5.79	21.39	100
7	14.03	9.30	11.49	30.66	3.60	5.04	1.99	0.67	0.74	0.17	2.50	4.38	15.42	100

The variation in reactor pressure also showed minor influence in the particle size of the precipitate. It is apparent from the size distribution curves presented in Figure 21 that the precipitates obtained at ambient pressure and 7 bar were of similar size distribution. The corresponding d_{50} values are 17.3 μm and 18.3 μm for the ambient and 7 bar operating pressures, respectively.

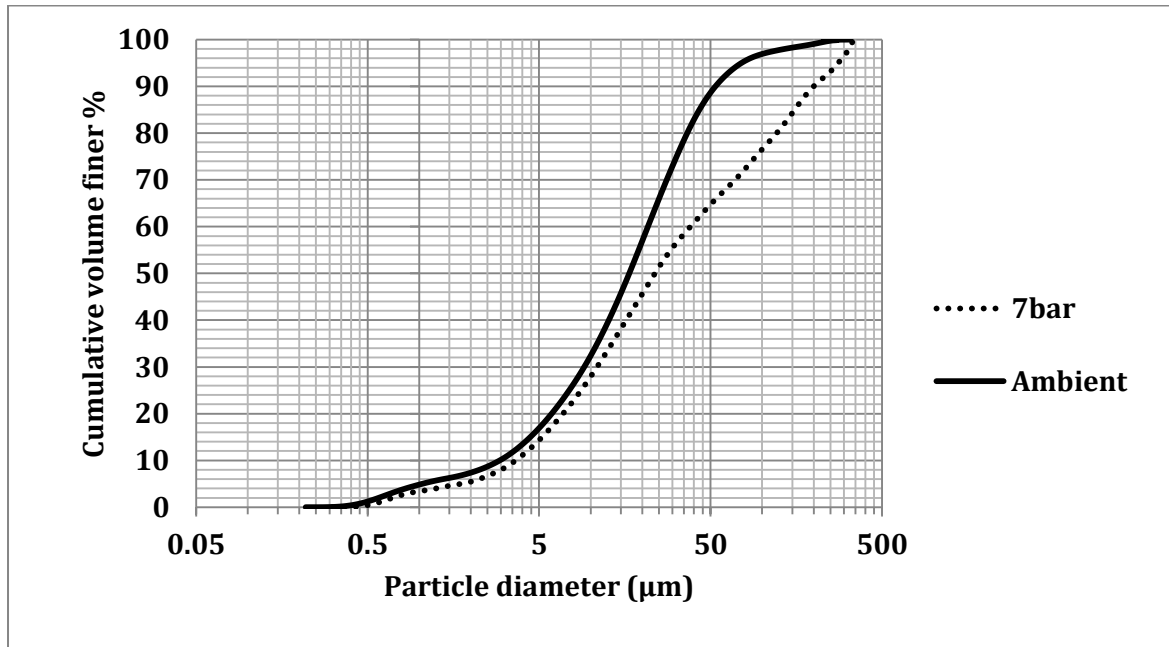


Figure 21: Size distributions of the precipitates obtained at ambient and 7 bar reactor pressure (80°C, 200 % excess thio-urea, and 250 rpm)

5.4.4. Agitation speed

Results from SEM analysis of the precipitates generated at 250 rpm and 500 rpm agitation speeds showed that increasing agitation speed had no significant effect on the composition of the precipitates. These results are shown in Table 12.

Table 12: Composition of the precipitates for the variation in agitation speed (80°C, 200 % excess thio-urea, and ambient pressure)

Agitation(rpm)	Weight %													Total
	S	Fe	Ni	Cu	Zn	Se	Ru	Rh	Pd	Te	Ir	Pt	Pb	
250	21.34	1.01	8.13	31.84	0.00	2.90	2.52	1.12	0.93	0.00	3.03	5.79	21.39	100
500	22.88	0.15	1.03	43.94	5.37	2.56	4.01	0.81	2.04	0.00	1.13	2.43	13.66	100

Agitation speed has also a significant influence on the particle size of the precipitates generated using thio-urea. The size distribution of the precipitates generated with 250 rpm and 500 rpm

agitation speeds are shown in Figure 22. It is evident from this figure that increasing agitation speed resulted in the generation of much smaller sized particle. The d_{50} values for 500 rpm and 250 rpm agitation speeds were 5.1 μm and 17.3 μm , respectively. The observed effect can be attributed to the decrease in the induction time in the system at high agitation speed resulting in a greater number of particles being formed with lower average particle sizes. The faster agitation meant that the likelihood of the reactant components in solution to come into contact with each other increased, leading to high nuclei formation. Consequently, fewer reactant components would be left in solution to contribute to particle growth.

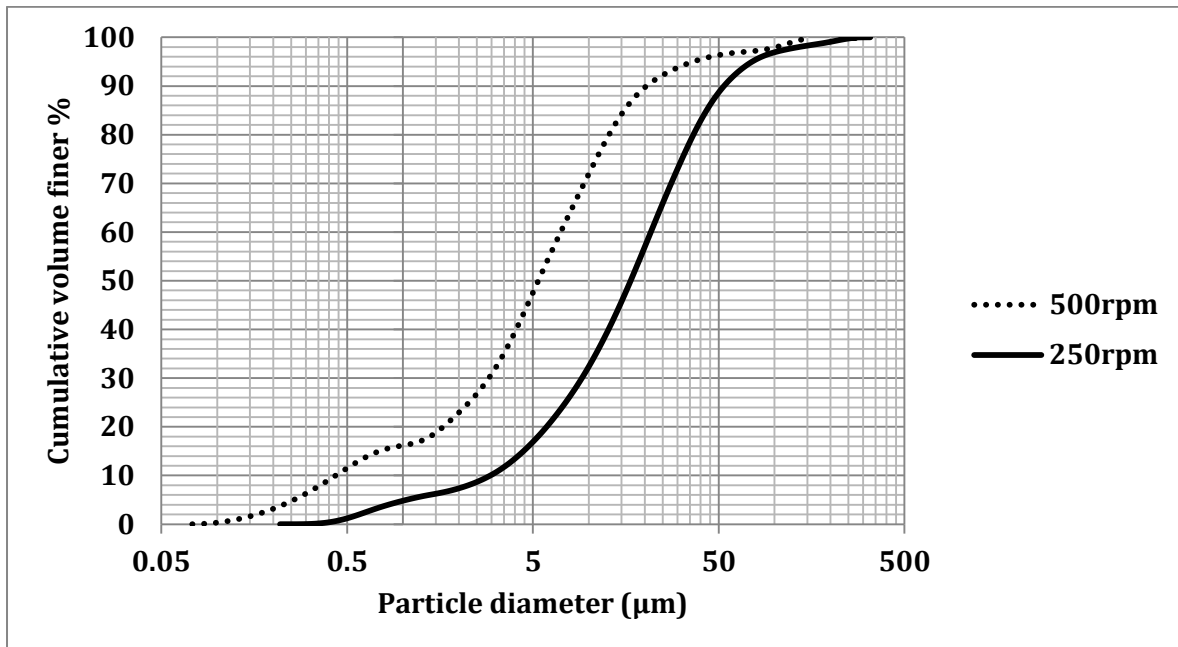


Figure 22: Size distributions of the precipitates obtained at 250 rpm and 500 rpm agitation speed (80°C, 200 % excess thio-urea, and ambient pressure)

6. STATISTICAL ANALYSIS OF EXPERIMENTAL RESULTS

The results obtained from the experiments performed according to a full factorial experimental design have been discussed in chapter 5. This chapter presents the results obtained from a formal statistical analysis of the experimental data, which allowed the author to determine the following:

1. The most influential main or interaction effects on the precipitation performance, and
2. The levels at which the influential parameters should be set to optimise the process performance.

6.1. Thio-urea based experimental data

6.1.1. Model selection

The primary objective was to identify the most influential factors in order to generate the optimum operating conditions for the precipitation process. The responses to be optimised were the average percentage precipitation of OPMs (Rh, Ru and Ir) and base metals (Cu and Ni) calculated over a time period of 8 hours. The main and interaction effects with ANOVA p-value < 0.05 were considered to be statistically significant. The variables studied and their respective levels were presented in Chapter 3 (Table 7).

Selection of the significant model terms for each response of the OPM and base metal precipitation process was effected using half-normal probability plots of effects and Pareto charts (refer to appendix C for Pareto charts). The half-normal plot of effects for the response Rh recovery is shown in Figure 23 where it was observed that the reagent quantity, the second order interaction between pressure and agitation speed as well as the third order between these variables were the significant model terms. The analysis of variance (ANOVA) data presented in Table 13 shows that increasing reagent quantity decreases the recovery of Rh. This was also observed in the data presented in section 5.2.1. Referring to Figure 24 the data indicated that the significant variables for the Ru recovery response were agitation speed, the second order interactions between reagent quantity and temperature; pressure and reagent quantity; and the third order interaction reagent – pressure – agitation speed. Increasing agitation speed resulted in increased Ru recovery. For the Ir recovery response, the data showed that the variables reagent quantity and operating temperature were the only significant model terms (Figure 25). Although the increase in both temperature and reagent improved the recovery of iridium, temperature had the larger effect on iridium precipitation (Table 14). These results are in agreement with the study of parameter effects data presented in section 5.2.3.

The half-normal probability plot of effects for the Cu precipitation response is illustrated in Figure 26 where it is apparent that the variables reagent quantity and operating temperature are the only significant model terms. Increasing temperature and reagent quantity caused excessive copper co-precipitation with temperature having the largest impact. For the Ni precipitation response the data illustrated in Figure 27 showed that the reagent quantity was the only significant main variable model term. Higher thio-urea excess quantity resulted in increased Ni co-precipitation. The quantitative effects of the significant variables on the precipitation of OPMs and base metals have been shown in chapter 5.

Although it was not the main focus of this research to examine the influence of the studied parameters on the selenium and tellurium responses, it was important to note the extent of influence exerted by these variables on Se and Te precipitation. Identifying the significant variables would provide useful information regarding the variables that could be manipulated should one consider the possibility of recovering OPMs along with selenium and tellurium. The half-normal probability plots of effects for the selenium and tellurium responses are displayed in Figure 28 and Figure 29 respectively. These figures indicate that the reagent quantity and temperature were the significant variables for the Se response whereas only the variable temperature was statistically significant for the Te precipitation response. Precipitation of selenium increased with increasing both reagent and temperature whereas, that of tellurium increased with increasing temperature only. Wang et al. (2003) showed that unlike, selenium it is difficult to reduce tellurium to its elemental form in acidic solution by direct addition of sulphur containing agents. But both Te and Se can be cemented using elemental copper. The SEM analysis data (section 5.1) showed that elemental copper was present in the precipitates generated at high temperature. Suggesting that excess Se precipitated by direct reagent addition and cementation on the elemental copper while Te could only be precipitate by cementation. This could explain why statistical results indicated that Te was only dependent on temperature whereas Se was dependent on both temperature and reagent quantity.

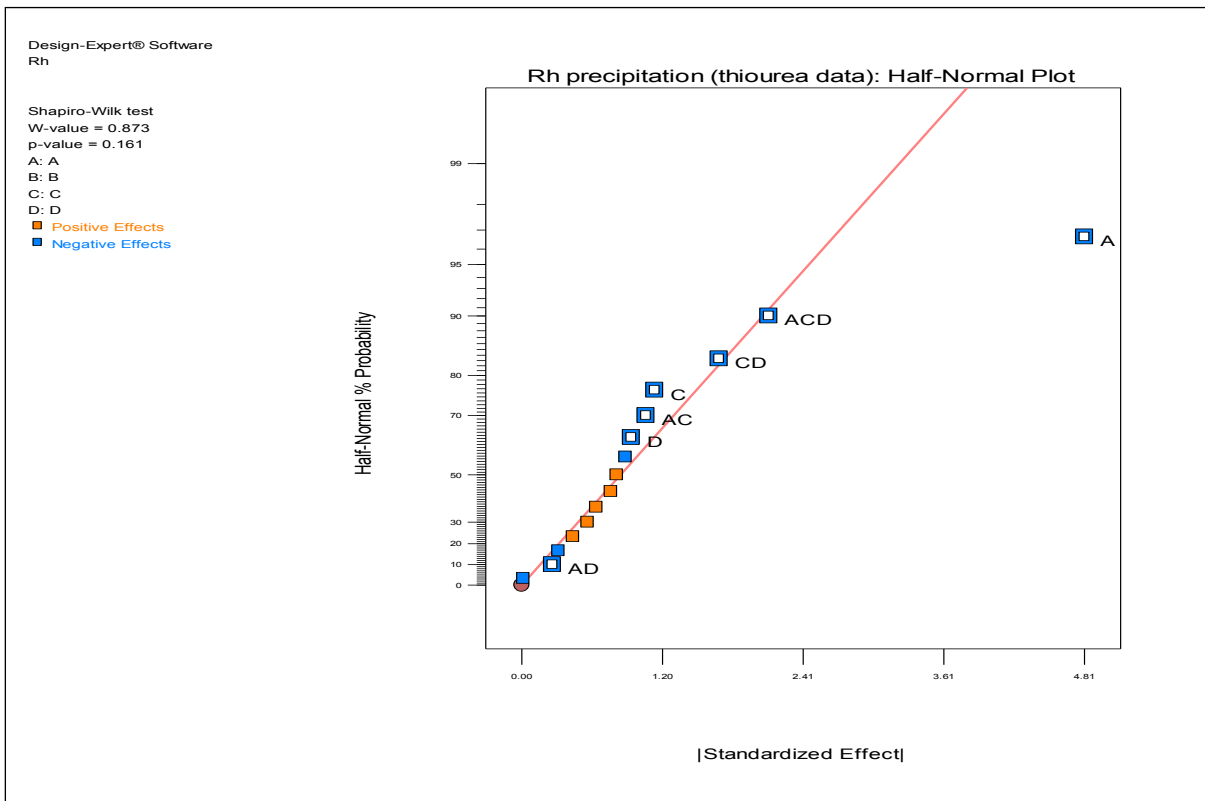


Figure 23: Half-normal probability plot of effects for Rh precipitation by thio-urea

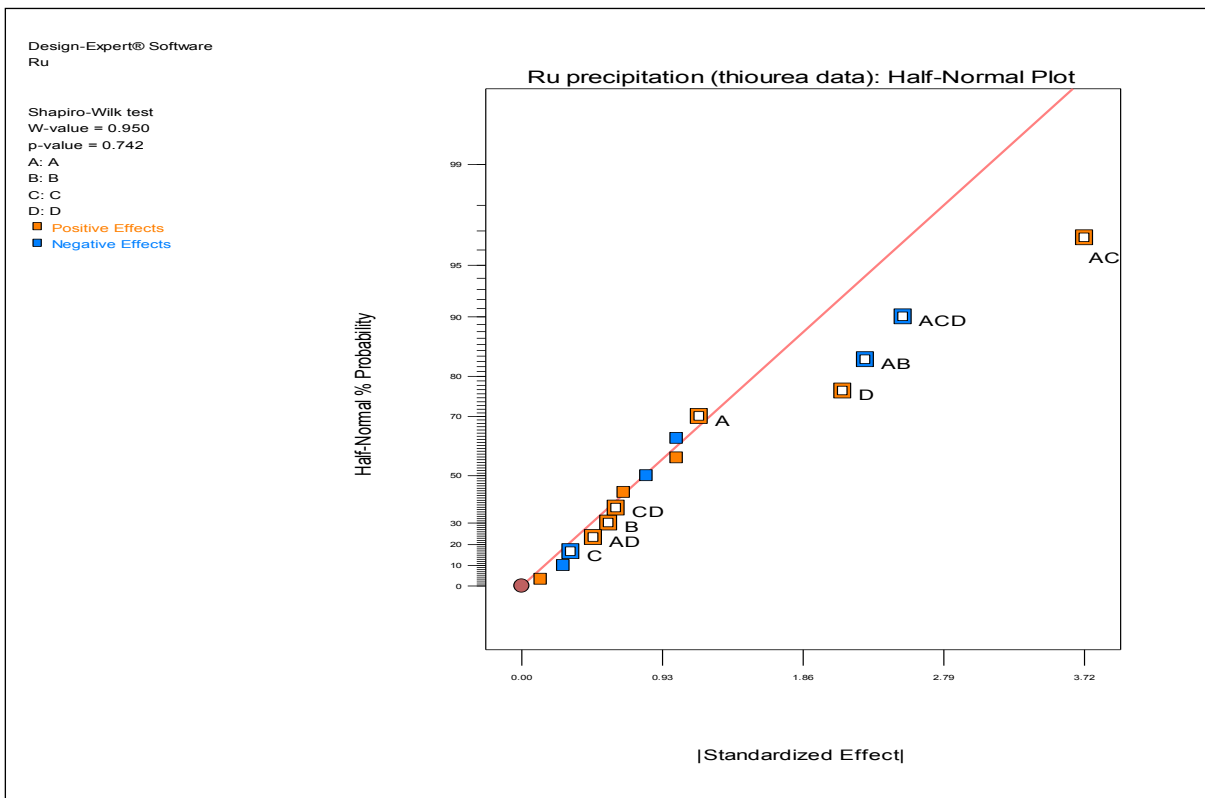


Figure 24: Half-normal probability plot of effects for Ru precipitation by thio-urea

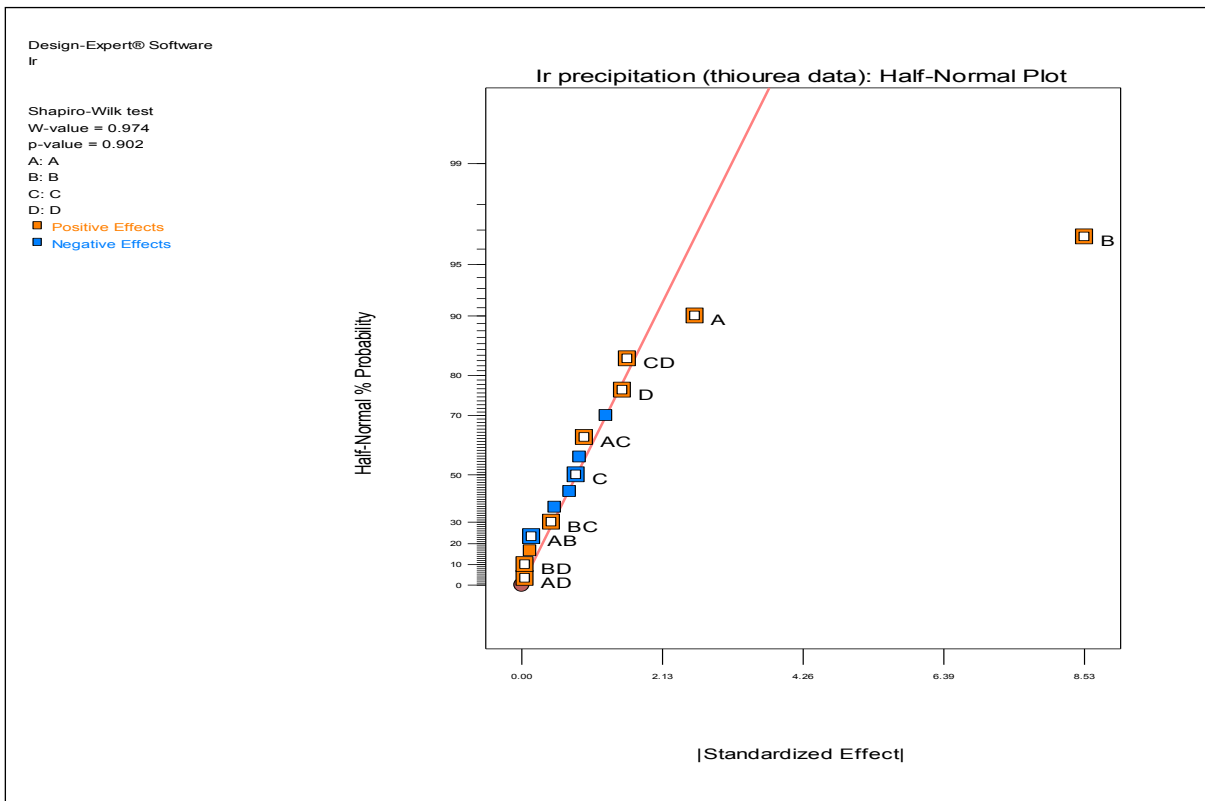


Figure 25: Half-normal probability plot of effects for Ir precipitation by thio-urea.

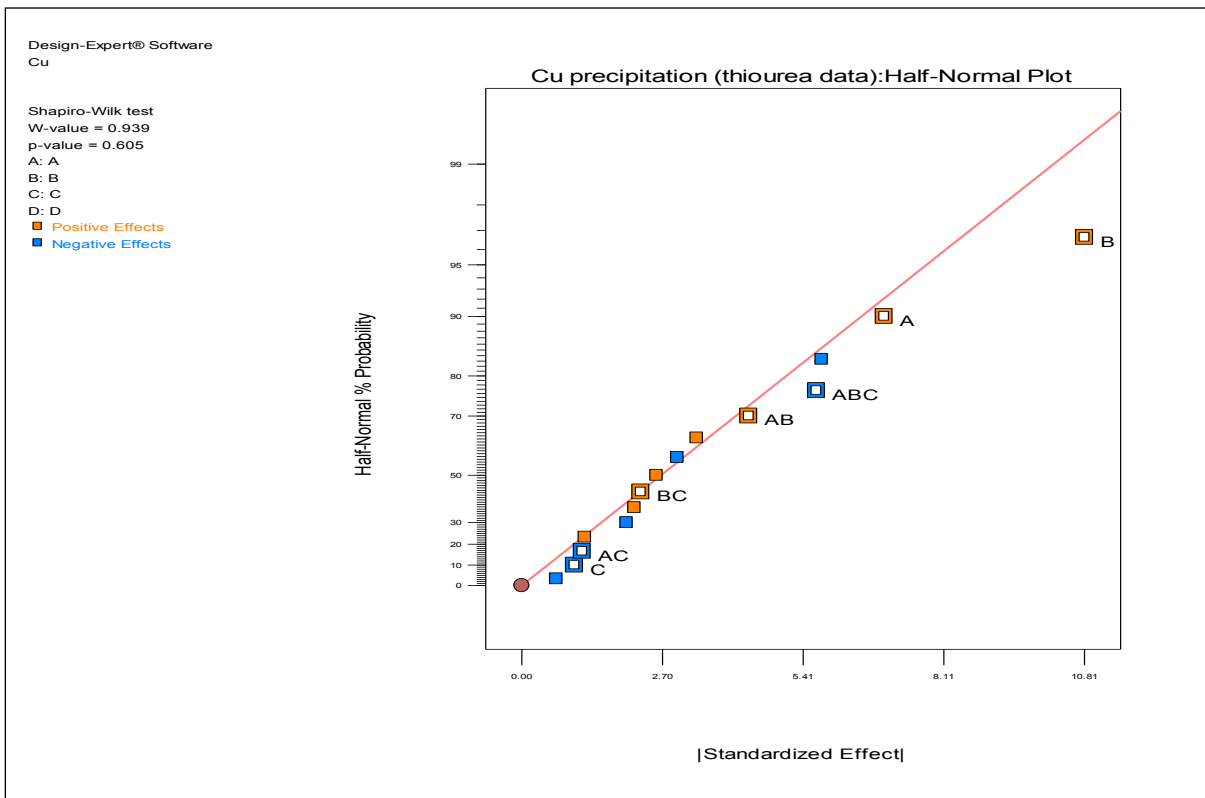


Figure 26: Half-normal probability plot of effects for Cu precipitation by thio-urea

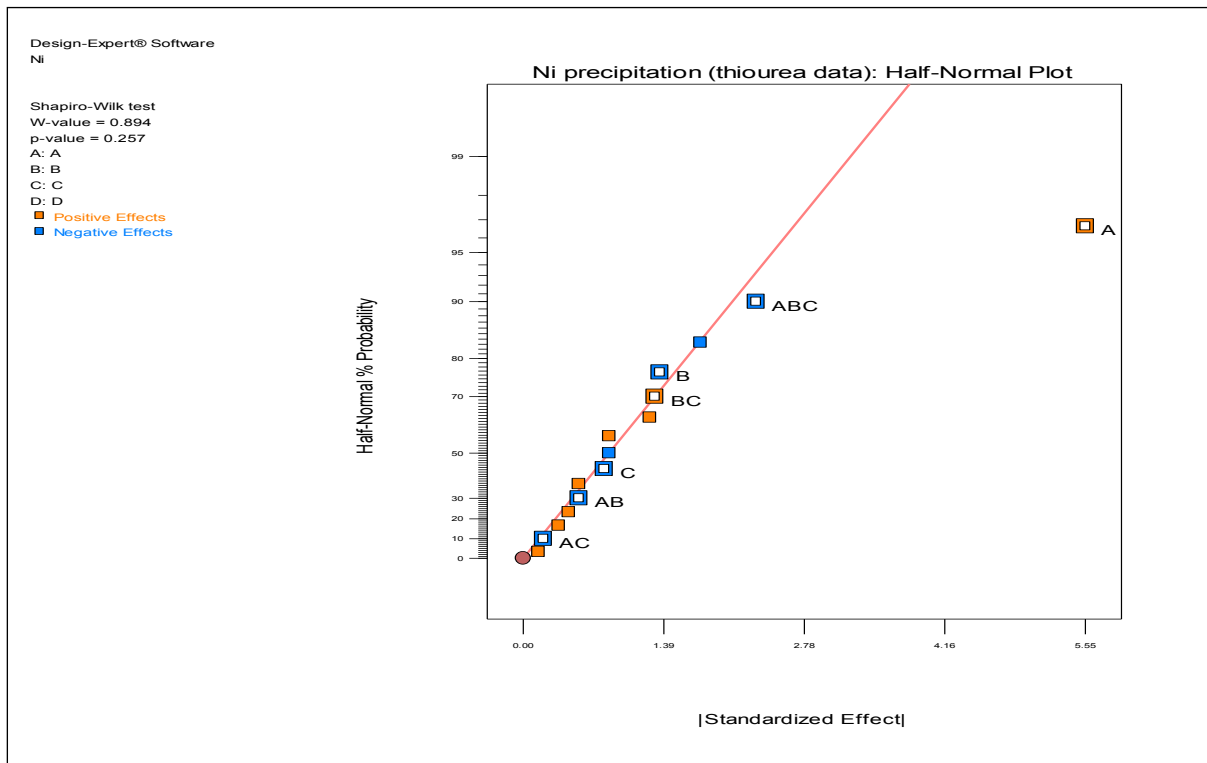


Figure 27: Half-normal probability plot of effects for Ni precipitation by thio-urea.

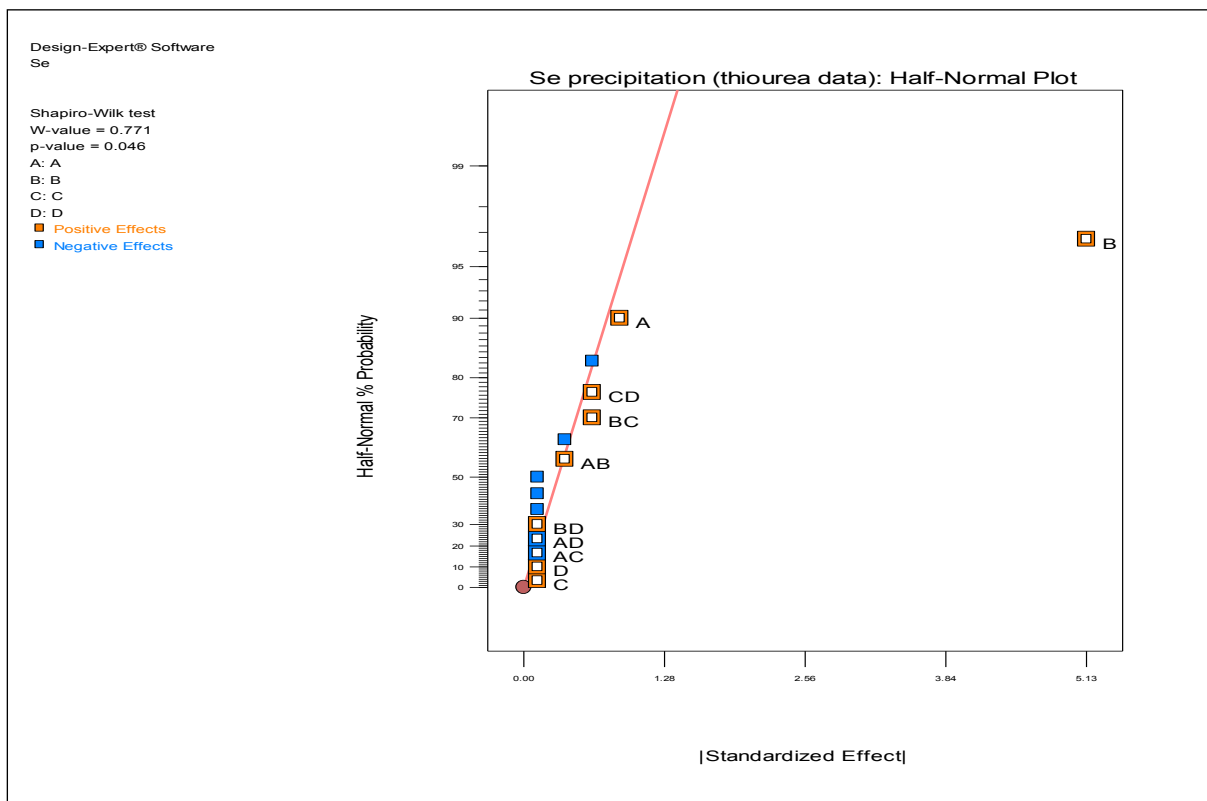


Figure 28: Half-normal probability plot of effects for Se precipitation by thio-urea.

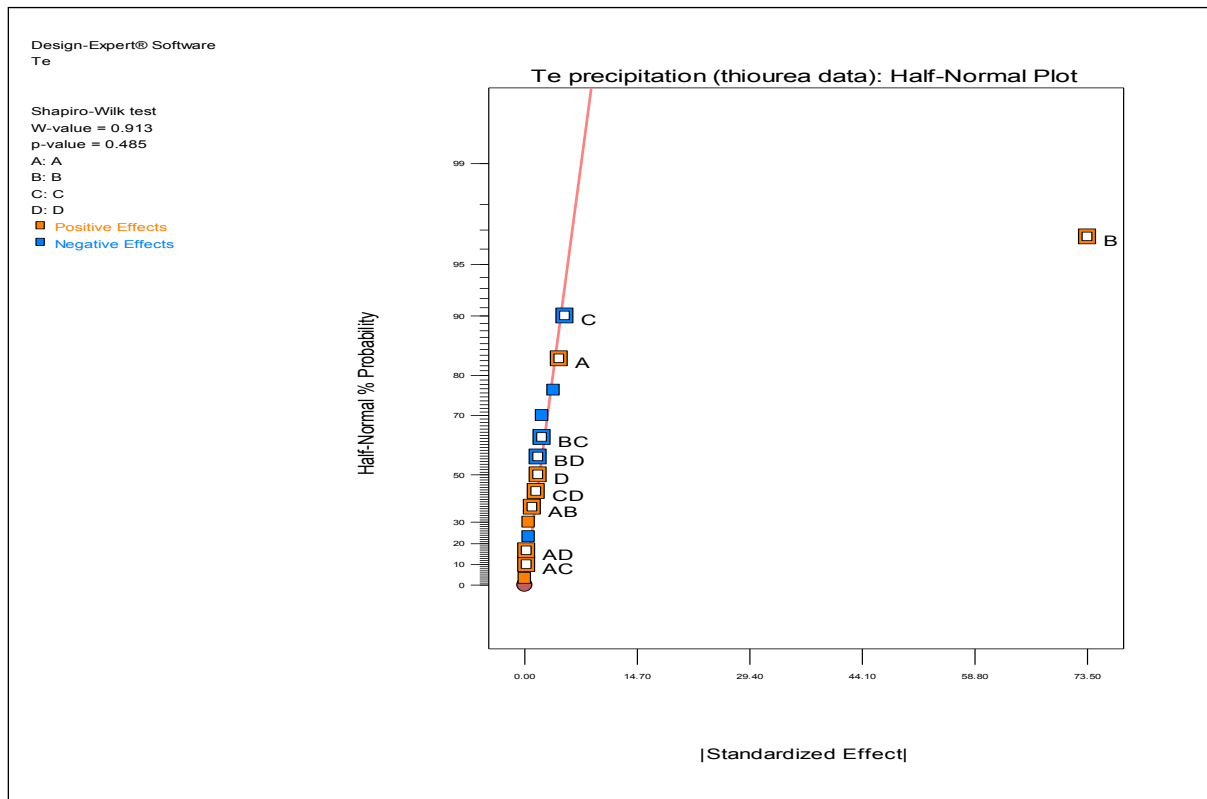


Figure 29: Half-normal probability plot of effects for Te precipitation by thio-urea

The data further showed the presence of significant interaction for the OPMs and Ni responses. The data plotted to illustrate the interaction effects are average values with each data point on the graph resulting from four (4) experiments. Figure 30 displays the statistically significant second order interaction effects involved in the OPMs and Ni precipitation responses. According to Figure 30a, the maximum recovery of Rh is achieved when the reactor pressure is kept at the high level (7 bar) and the agitation speed is set at its low level (250 rpm).

Referring to Figure 30b, it is apparent for the interaction involving the reagent quantity and temperature that attempting to increase the average recovery of Ru by simultaneously increasing the reagent quantity and temperature would be limited by the combined influence of the two parameters. Referring to Figure 30c, the interaction effect involving reagent quantity and pressure indicates that ruthenium recovery is maximized when both the reagent quantity and pressure are set at their high levels. For the process operating at ambient pressure, it is also indicated that using the reagent excess quantities less than 270 % tends to promote Ru recovery Figure 30c. For the Ir response, the second order interaction effect between the pressure and agitation speed suggests that average recovery of iridium increases when both the agitation speed and pressure are kept at their higher levels and decreases when either of pressure or agitation speed is kept at lower level (Figure 30d).

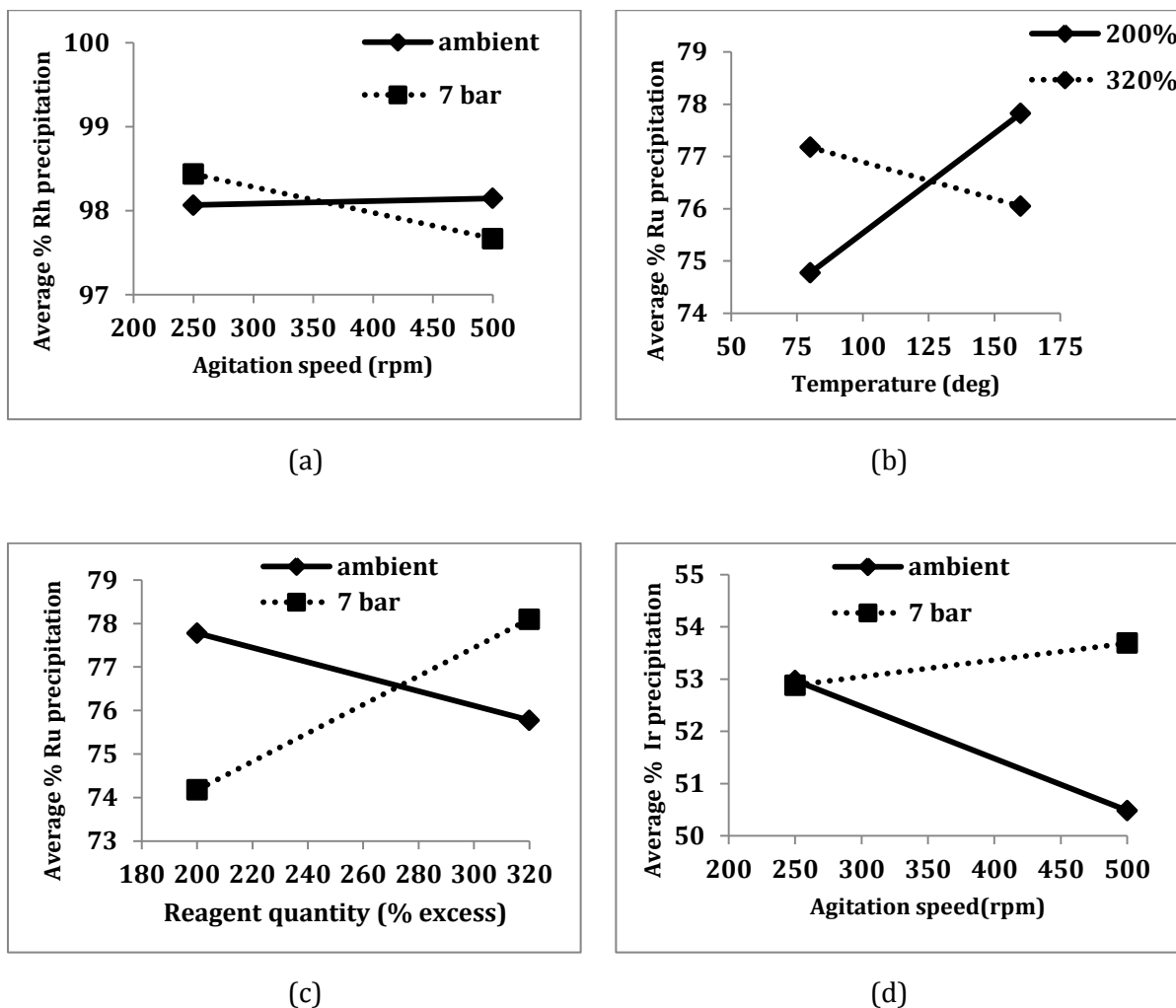


Figure 30: Interaction plots showing the effects of interactions between (a) agitation speed and pressure -Rh (b) temperature and reagent-Ru (c) pressure and reagent - Ru and (d) agitation speed and pressure -Ir on the precipitation responses

6.1.2. Analysis of variance (ANOVA)

Further analysis of the effects through ANOVA was done in order to determine the significance of the models generated and confirm whether the correct model terms were selected. Table 13 and Table 14 show the standardised effects of variables and their percentage contribution to the fitted models respectively. The ANOVA p-values of main and interaction effects are shown in Table 15 where it can be confirmed that the correct model terms for OPMs and base metal precipitation process were selected. The analysis of variance also showed that the insignificant terms pressure, agitation speed, reagent- pressure interaction (AC), and reagent - agitation interaction (AD) included in the Rh precipitation response model where added in order to maintain hierarchy of the model. Similarly, insignificant model terms which are hierarchical were included in the Ru, Ir, Cu, and Ni precipitation predictive models.

Table 13: Standardized effects of factors on various precipitation responses (thio-urea data)

Term	Rh	Ru	Ir	Cu	Ni	Se	Te
Reagent (A)	-4.81	1.18	2.63	6.96	5.55	0.88	4.50
Temperature (B)	-0.89	0.58	8.53	10.81	-1.35	5.13	73.50
Pressure (C)	-1.14	-0.33	-0.83	-1.01	-0.8	0.13	-5.25
Agitation (D)	-0.94	2.13	1.53	-0.66	0.15	0.13	1.75
AB	-0.31	-2.28	-0.15	4.36	-0.55	0.38	1.00
AC	-1.06	3.73	0.95	-1.16	-0.2	-0.13	0.25
AD	-0.26	0.48	0.05	2.59	1.25	-0.13	0.25
BC	0.76	0.68	0.45	2.29	1.3	0.63	-2.25
BD	0.56	-0.83	0.05	-2.01	0.35	0.13	-1.75
CD	-1.69	0.63	1.6	3.36	0.55	0.63	1.50
ABC	0.44	1.03	-0.73	-5.66	-2.3	-0.63	-2.25
ABD	0.64	0.13	-0.88	-5.76	-1.75	-0.13	-3.75
ACD	-2.11	-2.53	-1.28	-2.99	-0.85	-0.13	-0.50
BCD	0.81	-0.28	0.13	1.21	0.45	-0.38	0.00

Table 14: Percentage contribution of standardized effects to the fitted model

Term	Rh	Ru	Ir	Cu	Ni	Se	Te
Reagent (A)	62.79	3.87	7.70	16.44	65.11	2.68	0.37
Temperature (B)	2.14	0.93	81.25	39.65	3.85	91.81	98.50
Pressure (C)	3.51	0.30	0.76	0.35	1.35	0.05	0.50
Agitation (D)	2.38	12.65	2.60	0.15	0.05	0.05	0.06
AB	0.26	14.50	0.03	6.45	0.64	0.49	0.02
AC	3.06	38.86	1.01	0.46	0.08	0.05	0,00
AD	0.19	0.63	0.00	2.27	3.30	0.05	0.00
BC	1.58	1.28	0.23	1.77	3.57	1.37	0.09
BD	0.86	1.91	0.00	1.37	0.26	0.05	0.06
CD	7.72	1.09	2.86	3.83	0.64	1.37	0.04
ABC	0.52	2.94	0.59	10.87	11.18	1.37	0.09
ABD	1.10	0.04	0.86	11.26	6.47	0.05	0.26
ACD	12.10	17.86	1.82	3.03	1.53	0.05	0.00
BCD	1.79	0.21	0.02	0.50	0.43	0.49	0.00

Table 15: ANOVA table of p-values for the responses

Effect	Rh	Ru	Ir	Cu	Ni	Se	Te
Reagent (A)	< 0.0001	0.1658	0.0217	0.0473	0.0003	0.0498	0.0723
Temperature (B)		0.4694	0.0001	0.0066	0.179	< 0.0001	< 0.0001
Pressure (C)	0.1023	0.6779	0.3485	0.7423	0.4082	0.7282	0.0454
Agitation (D)	0.1669	0.0291	0.1142			0.7282	0.4175
AB		0.0224	0.8583	0.1806	0.565	0.3203	0.6352
AC	0.1231	0.0024	0.2872	0.7061	0.8327	0.7282	0.9045
AD	0.6815		0.9525			0.7282	0.9045
BC			0.5971	0.4639	0.1938	0.1255	0.3076
CD	0.0256	0.4336	0.9525			0.1255	0.4831
ABC				0.0934	0.0364		
ABD							
ACD	0.009	0.0147					
R²	0.9175	0.9068	0.9518	0.76	0.858	0.9798	0.9964
Adj. R²	0.8454	0.7669	0.9276	0.55	0.7337	0.9394	0.9893

6.1.3. Mathematical representation of models

Analysis of variance (ANOVA) was employed to determine the model parameters using the data within the interval studied (chapter 3, Table 7). Thus the model generated is essentially empirical and requires validation for conditions outside the studied range. The empirical relationship (in terms of actual factors) between each of the studied responses and the respective parameters for the precipitation process are shown in Equations 35 to 41.

$$\begin{aligned}
 \text{Rh recovery (\%)} = & +119.75 - 0.09*\text{Reagent} - 3.15*\text{Pressure} - 0.04*\text{Agitation} \\
 & + 0.01*\text{Reagent}*\text{Pressure} + 1.70 \times 10^{-4}*\text{Reagent}*\text{Agitation} \\
 & + 9.96 \times 10^{-3}*\text{Pressure}*\text{Agitation} - 4.69 \times 10^{-5}*\text{Reagent}*\text{Pressure}*\text{Agitation}
 \end{aligned}$$

Equation 35

$$\begin{aligned}
 \text{Ru recovery (\%)} = & +92.18 - 0.07*\text{Reagent} + 0.13*\text{Temperature} - 8.53*\text{Pressure} - 0.06*\text{Agitation} \\
 & - 4.74 \times 10^{-4}*\text{Reagent}*\text{Temperature} + 0.03*\text{Reagent}*\text{Pressure} \\
 & + 2.56 \times 10^{-4}*\text{Reagent}*\text{Agitation} + 0.02*\text{Pressure}*\text{Agitation} \\
 & - 5.61 \times 10^{-5}*\text{Reagent}*\text{Pressure}*\text{Agitation}
 \end{aligned}$$

Equation 36

$$\text{Ir recovery (\%)} = +34.05 + 0.02*\text{Reagent} + 0.11*\text{Temperature}$$

Equation 37

$$\begin{aligned}
 \text{Cu precipitation (\%)} = & +63.58 - 0.23*\text{Reagent} - 0.55*\text{Temperature} - 12.74*\text{Pressure} \\
 & + 2.48 \times 10^{-3}*\text{Reagent}*\text{Temperature} + 0.04*\text{Reagent}*\text{Pressure} \\
 & + 0.11*\text{Pressure}*\text{Temperature} \\
 & - 3.93 \times 10^{-4}*\text{Reagent}*\text{Pressure}*\text{Temperature}
 \end{aligned}
 \tag{Equation 38}$$

$$\begin{aligned}
 \text{Ni precipitation (\%)} = & +15.59 - 0.01*\text{Reagent} - 0.17*\text{Temperature} - 5.62*\text{Pressure} \\
 & + 5.24 \times 10^{-4}*\text{Reagent}*\text{Temperature} + 0.019*\text{Reagent}*\text{Pressure} \\
 & + 0.047*\text{Pressure}*\text{Temperature} \\
 & -1.60 \times 10^{-4}*\text{Reagent}*\text{Pressure}*\text{Temperature}
 \end{aligned}
 \tag{Equation 39}$$

$$\text{Se precipitation (\%)} = +86.23 + 0.007*\text{Reagent} + 0.06*\text{Temperature}
 \tag{Equation 40}$$

$$\text{Te precipitation (\%)} = -67.0 + 0.92*\text{Temperature}
 \tag{Equation 41}$$

were temperature is in °C, pressure in bar, agitation speed in rpm, and reagent quantity in percentage excess (refer to section 3.1 for determination of excess quantity).

The corresponding high R² values (Table 15) of all the models indicates that the model prediction was good. The data further showed that the reagent quantity (A) and operating temperature (B) were the most influential parameters on the precipitation process. This can be seen from their larger values of the standardized effects (Table 13) and the corresponding per cent contribution (Table 14) to the fitted models. In addition, the influence of temperature and reagent quantity is corroborated by their contribution to significant interaction effects (Table 15).

6.1.4. Optimization

One of the objectives of this research was to determine the optimum OPM recovery with minimal Ni and Cu co-precipitation from the leach sulphate solution. To achieve this objective, the numerical optimization function of Design Expert software version 8.0.4 was chosen. The numerical optimization function allows the searching of design space using the model created during analysis to find the factor settings that would either maximize or minimize the desirability function. It should, however, be noted that the optimum conditions generated through numerical optimization are merely possible scenarios as the actual optimum conditions depend on the operating philosophy and economics. In the current study two optimisation cases were considered.

In the first case the target criteria were set to maximise the OPMs response and minimise the base metal response while keeping the operating variable values within the ranges under investigation. Setting the parameter values within the ranges being studied also allowed accounting for the interactions effects between the variables. For the second optimisation case the independent variables reagent quantity and temperature were minimised owing to their negative and positive coefficients of standardised effects on Rh and base metal precipitation respectively. This choice, however, caused a negative impact on iridium recovery which was seen to be positively influenced by increase in reagent and temperature (Table 15). The other independent variables pressure and agitation speed were adjusted to be in range and maximum, respectively. This selection criterion was based on the significance influence of the variables as determined from ANOVA. The ANOVA results showed that maximising agitation speed would improve Ru and Ir recoveries and that both the OPMs and base metals yield responses were insensitive to change in pressure (Table 13 and Table 15). The response goal fields for the two optimization cases were set as summarized in Table 16.

Table 16: Constraints varied to obtain optimal conditions

Response	Limits		Case I		Case II	
	Lower	Upper	Setting	Importance	Setting	Importance
Reagent (%excess)	200	320	In range	1	Minimise	5
Temperature (°C)	80	160	In range	1	Minimise	5
Pressure (bar)	Ambient	7	In range	1	In range	3
Agitation (rpm)	250	500	In range	1	Maximise	5
Rh precipitation (%)	90	100	Maximise	5	Maximise	5
Ru precipitation (%)	70	100	Maximise	5	Maximise	5
Ir precipitation (%)	50	100	Maximise	5	Maximise	3
Cu precipitation (%)	0	15	Minimise	1	Minimise	5
Ni precipitation (%)	0	15	Minimise	1	Minimise	5
Se precipitation (%)	-	-	None	-	None	-
Te precipitation (%)	-	-	None	-	None	-

These criteria led to the generation of the numerical solutions given in Table 17 from which the combination for the second optimisation case was chosen and tested to confirm the accuracy of the model.

Table 17: Combinations of optimal conditions for parameters as generated from numerical optimization for two OPMs and base metal precipitation optimization cases

Case	Reagent	Temperature	Pressure	Agitation	Rh	Ru	Ir	Cu	Ni
I	200	160	Ambient	250	100	80	56	11	2
II	200	80	7bar	500	99	75	48	5	2

6.1.5. Confirmatory test results

In order to verify the validity and repeatability of the predicted optimal recoveries, three additional confirmatory experiments were performed using the optimized parameter settings for case II (Table 17). It should be noted that the use of process conditions for case II in confirmatory tests was merely for verification of validity and repeatability of the model prediction, and it is not suggested that these are the optimum conditions to be used in an industrial setting. These process options and practical considerations are discussed in section 6.1.6. The results obtained are displayed in Figure 31 to Figure 33. It can be seen from Figure 31 that for the entire time range, the average recovery of rhodium and ruthenium were very close the respective predicted values while that of iridium was under-predicted. Roughly 70% average Ir recovery was achieved at optimized conditions compared to the predicted 48 %. The results also showed that the average per cent Cu and Ni co-precipitations were well predicted. Average values of 4.2 % Cu and 2.1 % Ni co-precipitated during the confirmatory test compared to the predicted 4.95% and 2.2% average values of copper and nickel precipitation respectively (Figure 32).

Furthermore, the results show that better results were achieved when the process was run for more than 250 minutes at optimized conditions. Running the process at these optimum parameter settings and reaction time above 250 minutes, would also reduce the concentration of selenium contained in the process solution to less than 1.3 mg/L whereas tellurium removal would be poor (Figure 33).

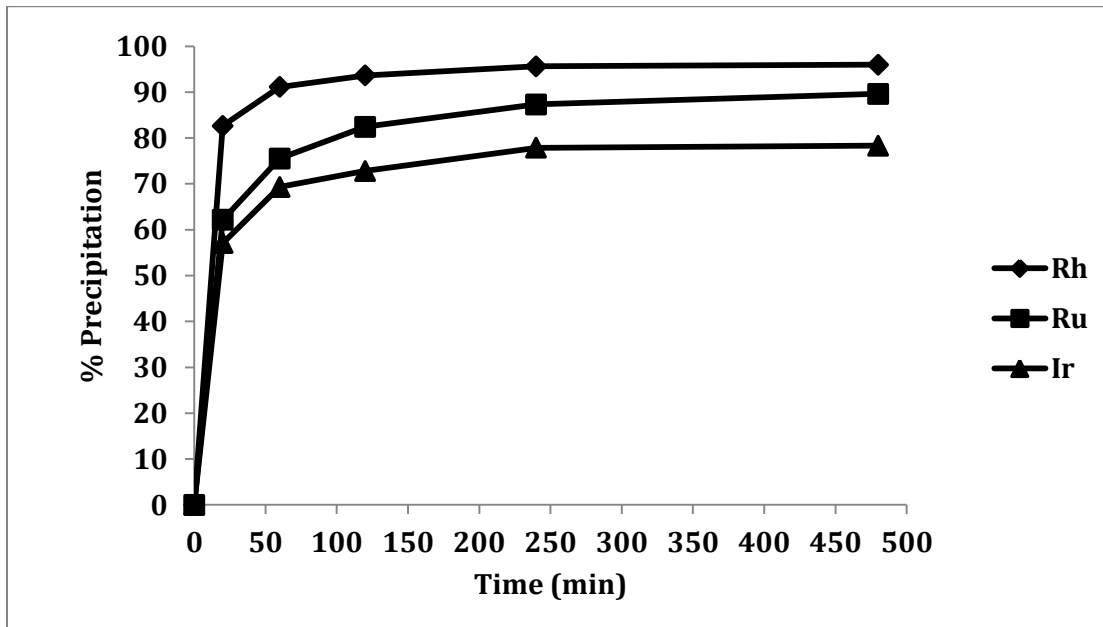


Figure 31: OPMs recovery confirmatory results obtained at optimized process conditions (200 % excess thio-urea, 80°C, 7bar, and 500 rpm)

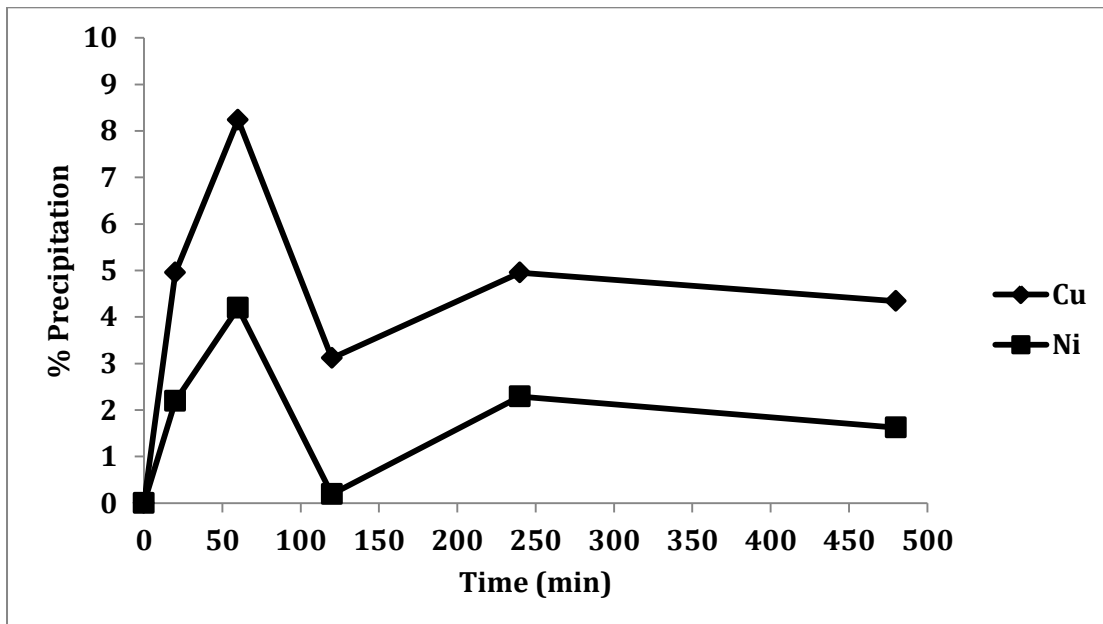


Figure 32: Base metal co-precipitation confirmatory results obtained at optimized process conditions (200 % excess thio-urea, 80°C, 7bar, and 500 rpm)

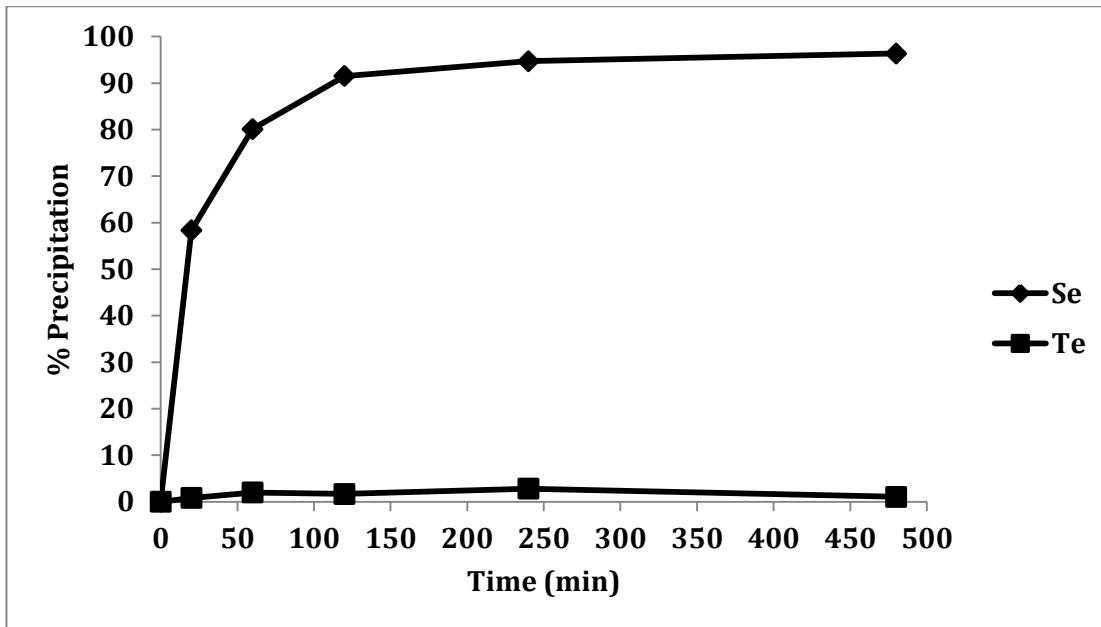


Figure 33: Selenium and tellurium precipitation confirmatory results obtained at optimized process conditions (200 % excess thio-urea, 80°C, 7bar, and 500 rpm)

The confirmatory test results further showed that the experiments have good repeatability in both OPM recovery and base metal precipitation (Figure 34 to Figure 38). The standard deviations for the average Rh, Ru, Ir, Cu, and Ni per cent precipitation for the three confirmatory tests were: 0.33, 1.22, 2.19, 1.06, and 0.78, respectively.

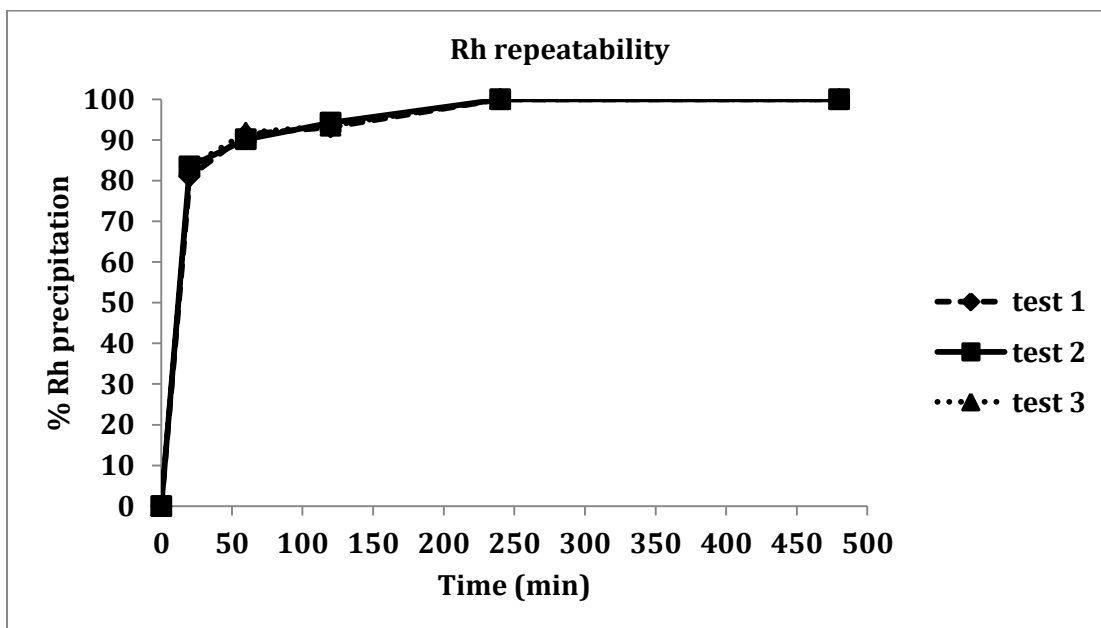


Figure 34: Repeatability of Ru recovery experimental results (200 % excess thio-urea, 80°C, 7bar, and 500 rpm)

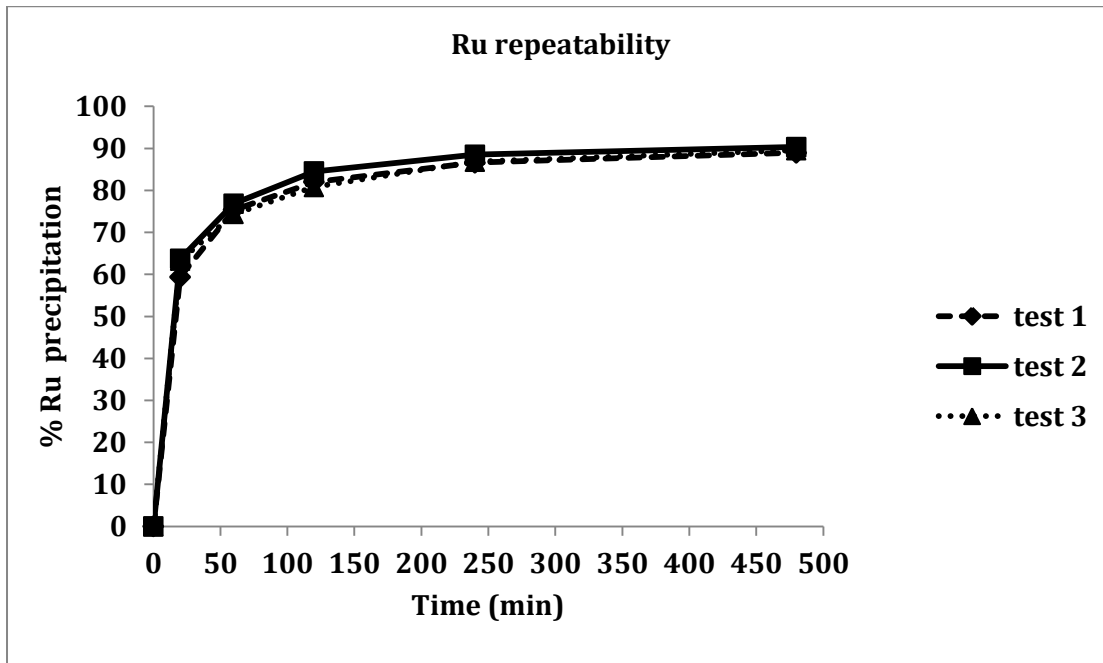


Figure 35: Repeatability of Ru recovery experimental results (200 % excess thio-urea, 80°C, 7bar, and 500 rpm)

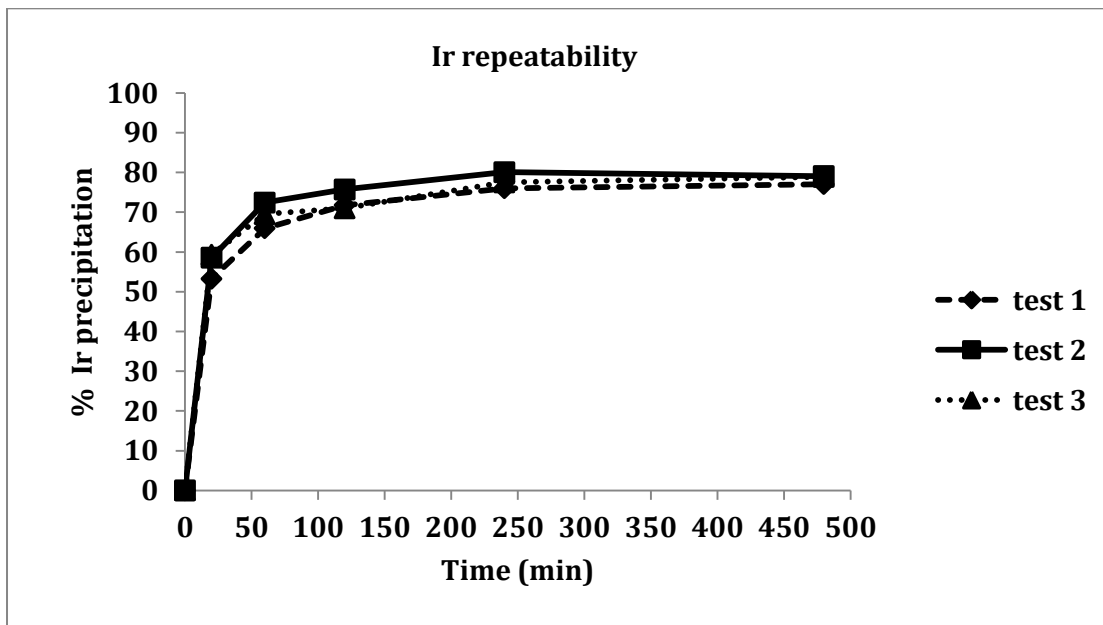


Figure 36: Repeatability of Ir recovery experimental results (200 % excess thio-urea, 80 °C, 7bar, and 500 rpm)

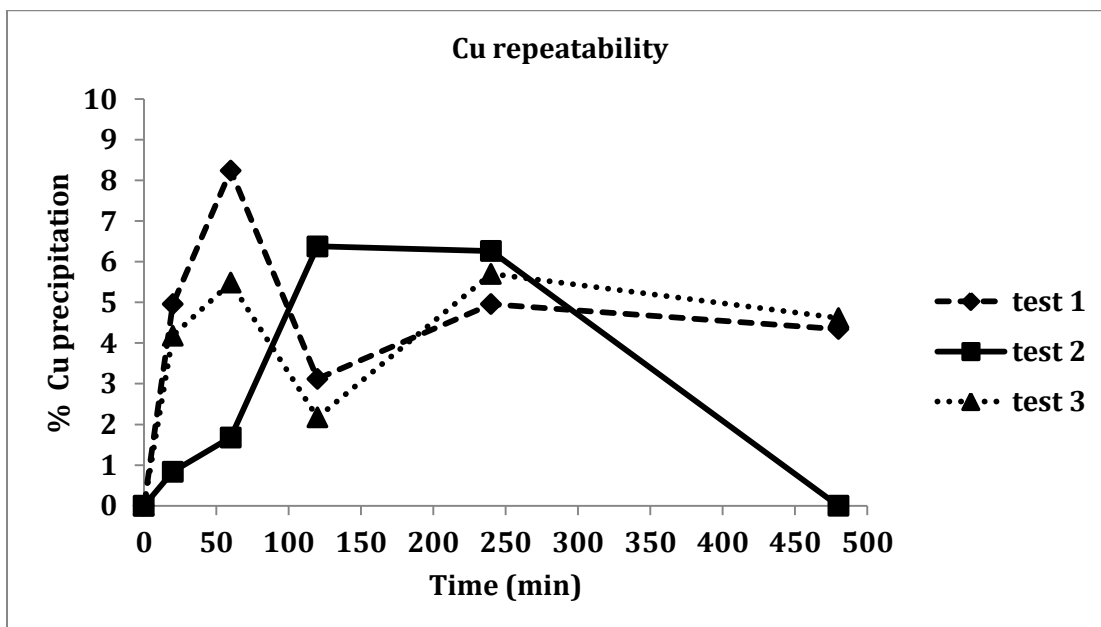


Figure 37: Repeatability of Cu co-precipitation experimental results (200 % excess thio-urea, 80°C, 7 bar, and 500 rpm)

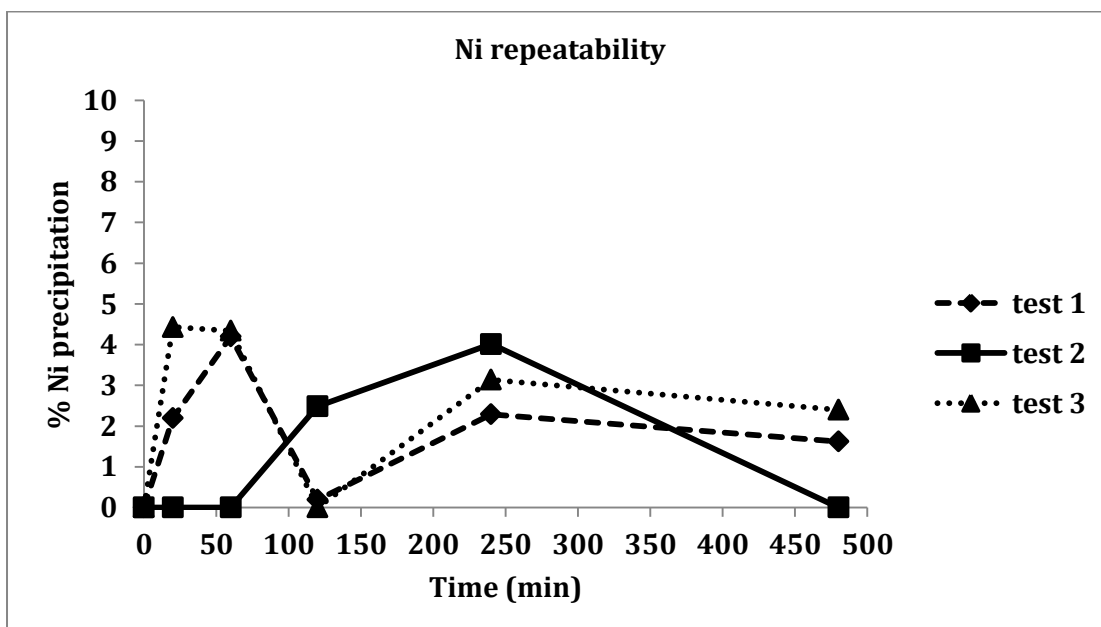


Figure 38: Repeatability of Ni co-precipitation experimental results (200 % excess thio-urea, 80 °C, 7 bar, and 500 rpm)

6.1.6. Process options and practical consideration

The experimental results obtained at all conditions in this study showed that thio-urea has great potential to provide better OPM recovery from process solutions in the BMR process. The effect of thio-urea addition on downstream unit operations does, however, need to be taken into account when discussing the feasibility of using it as a precipitation reagent. Thio-urea is used

as grain refiner in copper electrowinning processes (Schlesinger et al., 2011; Ke et al., 1962). As an electrolyte additive in electrowinning, thio-urea promotes the formation of new copper nuclei and inhibits the crystal growth of existing crystals. This results in the formation of smooth copper deposits with minimum entrapment of electrolyte impurities. The concentration of thio-urea in the electrolyte is usually in the range of 1 to 10 mg/L (Schlesinger et al., 2011). However, if the concentration of thio-urea is too high, its adsorption on the cathode surface results in sulphur contamination of the cathode and passivation of copper electrowinning. The thio-urea concentration in the pregnant leach solution being sent to electrowinning should thus be controlled to within the acceptable limits. The ease of solid-liquid separation is another aspect of the precipitation process that needs to be taken into account when considering different precipitation reagents and operating conditions. In general, the product particles generated in metal sulphide precipitation are very small and separating these particles from the liquid can be challenging. The reagent currently being used for Se and Te removal, sulphurous acid, does result in precipitation of some metal sulphide species. The solid/liquid separation technique currently employed after the selenium and tellurium removal section can hence be considered as a possible feasible technique to achieve solid-liquid separation when using thio-urea as precipitation reagent.

The results generated from the two numerical optimisation cases suggest that two process options are possible to effect optimal recovery of OPMs in the BMR using thio-urea as a precipitating agent. The first option is based on the optimal process conditions generated for numerical optimisation case I (Table 17). For this option, a significant quantity of OPMs with minimal base metal co-precipitation can be recovered from BMR process solutions in a batch reactor. The suggested conditions for this process option are listed in Table 17. The autoclave would be an ideal reactor vessel to use in this case. Based on the experimental data, the required residence time for the optimal recovery of OPMs was estimated to be approximately 250 minutes (refer to Figure 57, Appendix B). This process option has potential for application in the BMR as a replacement for the current Se/Te removal section since under the suggested conditions, higher selenium and tellurium removal is also achievable (refer to Figure 52 to Figure 59, Appendix B). It should, however, be noted that the process will require heating the solution to a temperature as high as 160°C; cost related to energy consumption should thus be considered. The second option (based on case II, Table 17) offers the advantage of operating the process at low temperature (80°C), but requires the precipitation to be conducted at a pressure of 7 bar. The other disadvantage of the second option is that, although selenium removal along with OPMs is satisfactory under the suggested process conditions (Table 17), tellurium removal from the process solution is poor under these conditions.

The results regarding the technical aspects of the precipitation process presented in this thesis cannot be used in isolation to recommend an optimum process solution. The regression models proposed in this study allow the percentage metal precipitation to be predicted for different operating conditions within the investigated ranges of temperature, pressure, reagent addition, and agitation. This can be further utilized to conduct detailed economic analyses. Economic analyses, which fell outside the scope of the current project, are required to compare different technically feasible flow sheets in order to decide on the optimum process solution.

6.2. Sulphurous acid based experimental data

6.2.1. Model selection

The use of half-normal probability and Pareto plots of effects in the selection of model terms have been discussed in chapter 3 (section 3.2.2.2). The half-normal probability plots displayed in Figure 39 indicate that the variables reagent quantity, operating temperature, reactor pressure, and interaction between pressure and reagent have significant impact on Rh precipitation.

According to Figure 40, the second order interactions between reagent and temperature as well as between temperature and pressure were the significant terms for the Ru response. Regarding the recovery of iridium, the half-normal probability plot of effects shows that only the second order interaction between temperature and pressure is a significant model term at 95 % confidence level (Figure 41).

Referring to Figure 42, the data indicated that the operating temperature, second order interaction between temperature and pressure are the significant terms for the Cu co-precipitation response. The half-normal probability for the response Ni precipitation shows that temperature was the significant main variable. Plots summarising the interaction effects variables using sulphurous acid as reagent are given in Appendix C (Figure 88).

The statistical analyses were not performed for the selenium and tellurium data for the reason being OPMs recovery with sulphurous acid was poor. Therefore attempting to study the behaviour of Se and Te in response to variations in parameters for the possibility of recovering OPMs along with Se and Te using sulphurous acid, was not necessary.

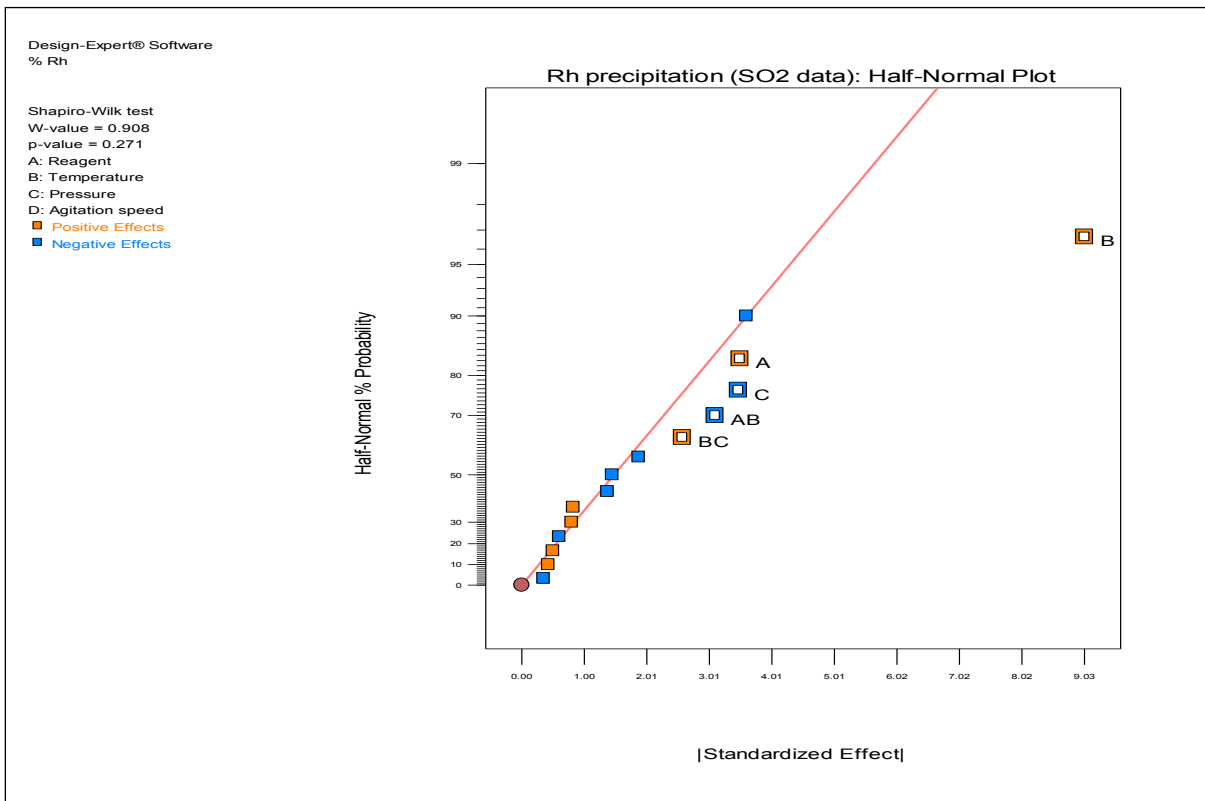


Figure 39: Half-normal probability plot of effects for Rh precipitation by Sulphurous acid

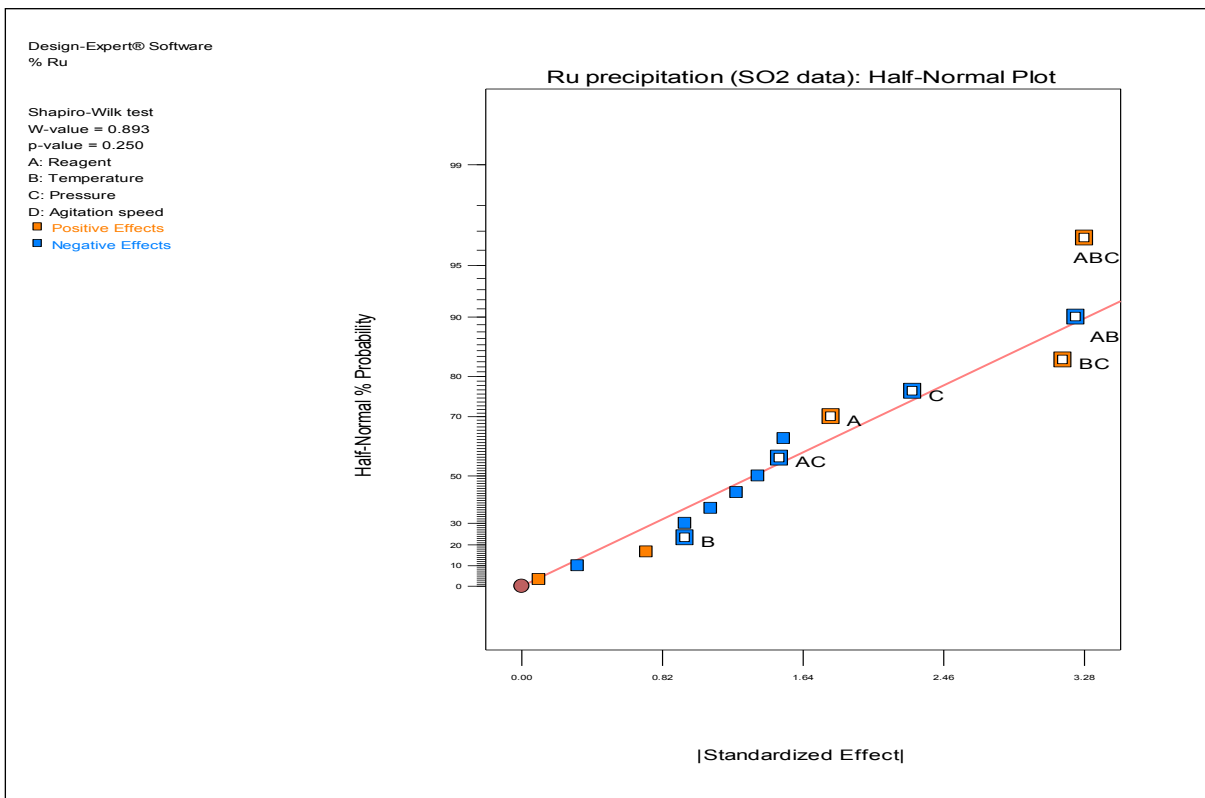


Figure 40: Half-normal probability plot of effects for Ru precipitation by Sulphurous acid

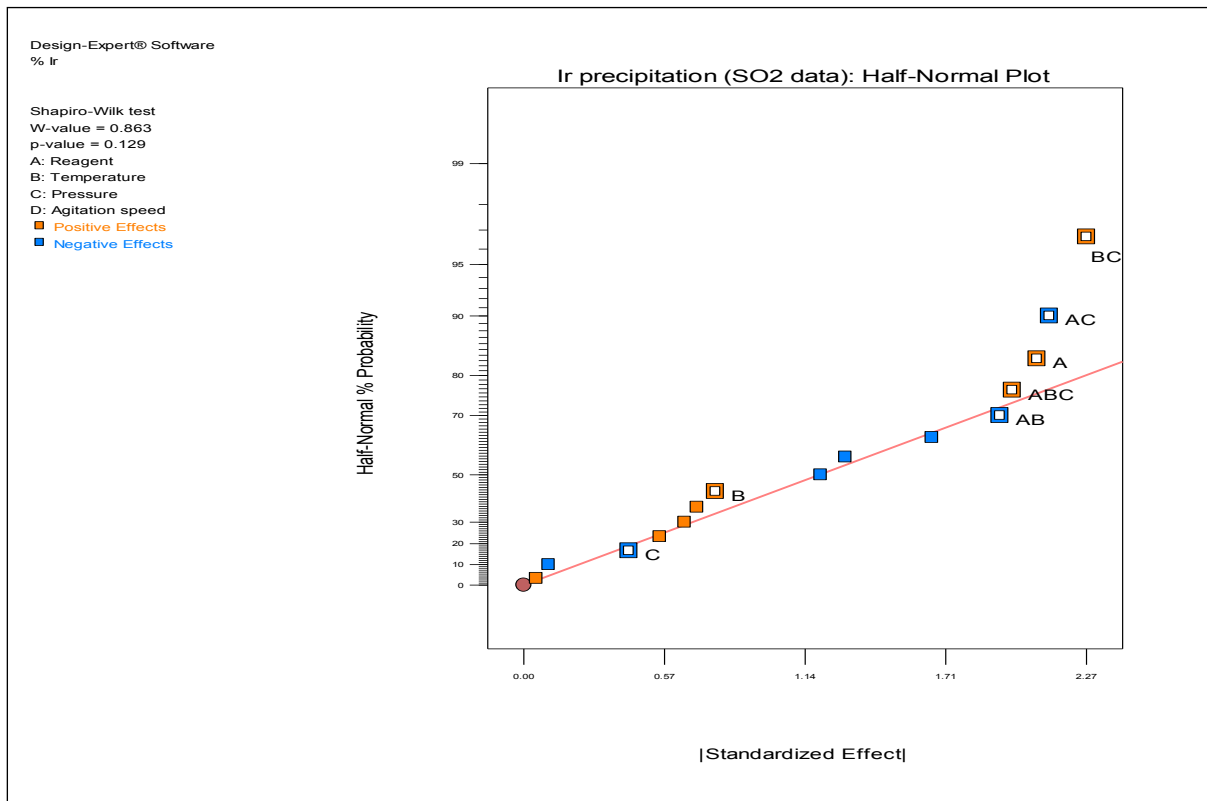


Figure 41: Half-normal probability plot of effects for Ir precipitation by Sulphurous acid

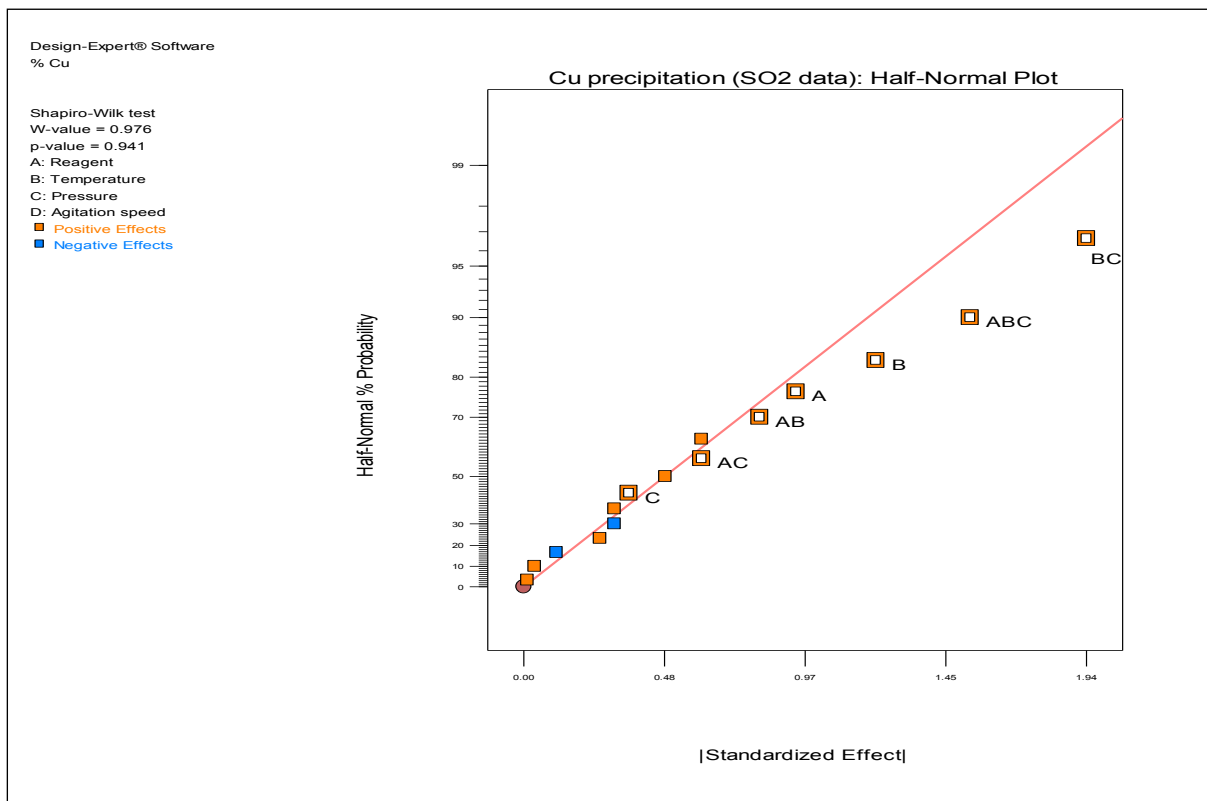


Figure 42: Half-normal probability plot of effects for Cu precipitation by Sulphurous acid

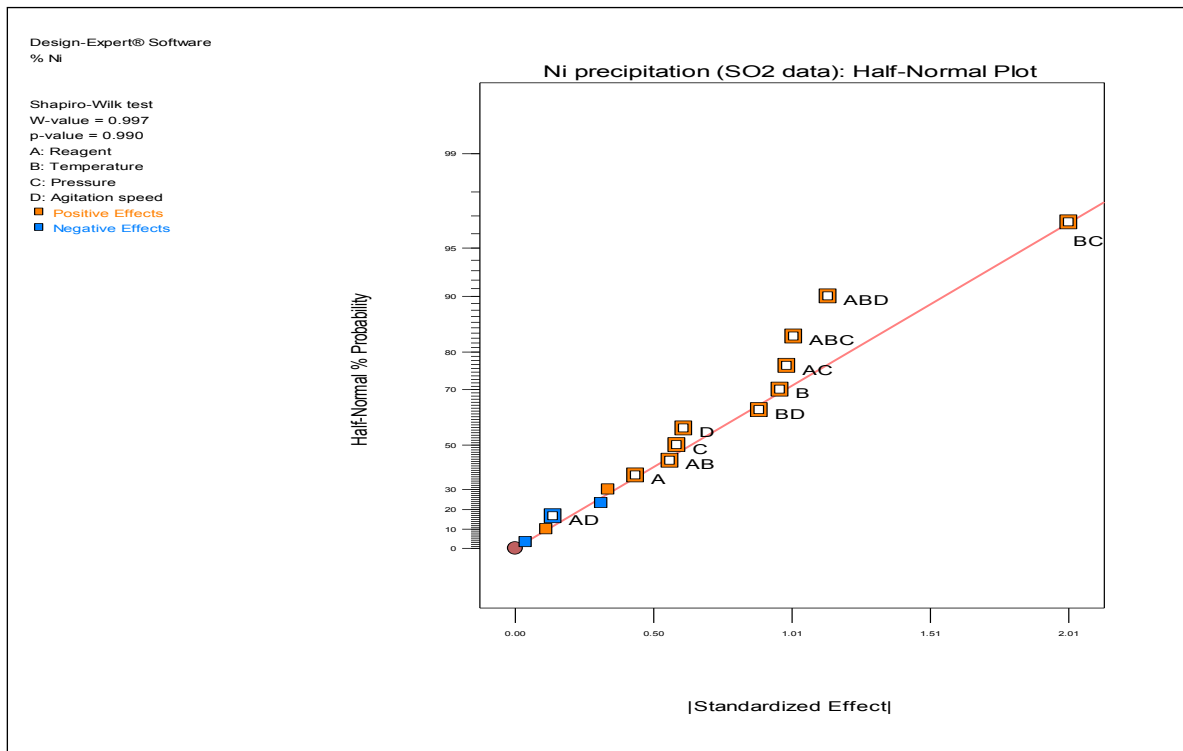


Figure 43: Half-normal probability plot of effects for Ni precipitation by Sulphurous acid

6.2.2. Analysis of variance

The main factors affecting the precipitation of OPMs and base metal using sulphurous acid were determined by analysis of variance (ANOVA). The ANOVA results are displayed in Table 18 to Table 20.

Table 18: Standardized effects of factors on various precipitation responses (sulphurous acid data)

Term	Rh	Ru	Ir	Cu	Ni
Reagent (A)	3.50	1.80	2.08	0.94	0.44
Temperature (B)	9.03	-0.95	0.78	1.21	0.96
Pressure (C)	-3.48	-2.28	-0.43	0.36	0.59
Agitation (D)	0.50	-1.10	0.70	0.49	0.61
AB	-3.10	-3.23	-1.93	0.81	0.56
AC	-3.60	-1.50	-2.13	0.61	0.99
AD	0.83	0.73	0.65	-0.31	-0.14
BC	2.58	3.15	2.28	1.94	2.01
BD	-1.45	-1.38	-1.20	0.26	0.89
CD	-0.35	-1.25	-0.10	0.01	0.11
ABC	0.80	3.28	1.98	1.54	1.01
ABD	0.43	0.10	0.55	0.61	1.14
ACD	-1.38	-0.33	0.05	0.31	-0.04
BCD	-0.60	-1.53	-1.30	0.04	-0.31

Table 19: Percentage contribution of standardized effects to the fitted model (sulphurous acid data)

Term	Rh	Ru	Ir	Cu	Ni
Reagent (A)	8.46	6.33	14.61	8.35	1.82
Temperature (B)	56.28	1.76	2.04	13.97	8.80
Pressure (C)	8.34	10.12	0.61	1.25	3.28
Agitation (D)	0.17	2.37	1.66	2.26	3.56
AB	6.64	20.33	12.58	6.27	3.00
AC	8.96	4.40	15.33	3.56	9.26
AD	0.47	1.03	1.43	0.93	0.18
BC	4.58	19.40	17.57	35.67	38.46
BD	1.45	3.70	4.89	0.65	7.48
CD	0.08	3.05	0.03	0.00	0.12
ABC	0.44	20.97	13.24	22.46	9.73
ABD	0.12	0.02	1.03	3.56	12.29
ACD	1.31	0.21	0.01	0.93	0.01
BCD	0.25	4.55	5.74	0.01	0.93

Table 20: ANOVA p-values for OPMs and base metal precipitation responses (sulphurous acid data)

Effect	Rh	Ru	Ir	Cu	Ni
Reagent (A)	0.0437	0.1195	0.0585	0.0229	0.1393
Temperature (B)	0.0001	0.3845	0.4339	0.0067	0.0154
Pressure (C)	0.0450	0.0587	0.6634	0.3091	0.0687
Agitation (D)				0.0409	0.0614
AB		0.0142	0.0749	0.1038	0.077
AC	0.0390	0.1844	0.0538		0.0142
AD					0.5937
BC		0.0158	0.0420	0.0004	0.0011
BD					0.0202
CD					
ABC		0.0132	0.0690	0.0017	0.013
ABD					0.0087
R²	0.8205	0.8332	0.7597	0.9153	0.9786
Adj. R²	0.7552	0.6872	0.5495	0.8412	0.9197
Std. Dev.	3.0700	2.0700	1.8800	0.6700	0.4700

6.2.3. Mathematical representation of model

Analysis of variance was used for the selected models to generate the following equations in terms of actual factors (Equations 42 to 46):

$$\begin{aligned} \text{Rh recovery (\%)} = & -39.48 + 0.05*\text{Reagent} + 0.34*\text{Temperature} - 1.87*\text{Pressure} \\ & - 3.23 \times 10^{-4}*\text{Reagent}*\text{Temperature} + 0.01*\text{Temperature}*\text{Pressure} \end{aligned} \quad \text{Equation 42}$$

$$\begin{aligned} \text{Ru recovery (\%)} = & -78.96 + 0.11*\text{Reagent} + 0.60*\text{Temperature} + 11.26*\text{Pressure} \\ & - 7.91 \times 10^{-4}*\text{Reagent}*\text{Temperature} - 0.02\text{AC} - 0.08*\text{Temperature}*\text{Pressure} \\ & + 1.14 \times 10^{-4}*\text{Reagent}*\text{Temperature}*\text{Pressure} \end{aligned} \quad \text{Equation 43}$$

$$\begin{aligned} \text{Ir recovery (\%)} = & -57.13 + 0.08*\text{Reagent} + 0.37*\text{Temperature} + 8.18*\text{Pressure} \\ & - 4.75 \times 10^{-4}*\text{Reagent}*\text{Temperature} - 0.01\text{AC} - 0.05*\text{Temperature}*\text{Pressure} \\ & + 6.86 \times 10^{-5}*\text{Reagent}*\text{Temperature}*\text{Pressure} \end{aligned} \quad \text{Equation 44}$$

$$\begin{aligned} \text{Cu recovery (\%)} = & -8.66 + 0.02*\text{Reagent} + 0.09*\text{Temperature} + 3.76*\text{Pressure} \\ & - 1.29 \times 10^{-4}*\text{Reagent}*\text{Temperature} - 5.56 \times 10^{-3}*\text{Reagent}*\text{Pressure} \\ & - 0.04*\text{Temperature}*\text{Pressure} + 5.34 \times 10^{-5}*\text{Reagent}*\text{Temperature}*\text{Pressure} \end{aligned} \quad \text{Equation 45}$$

$$\begin{aligned} \text{Ni recovery (\%)} = & -34.68 + 0.05*\text{Reagent} + 0.31*\text{Temperature} + 1.48*\text{Pressure} + 0.09*\text{Agitation} \\ & - 4.38 \times 10^{-4}*\text{Reagent}*\text{Temperature} - 2.85 \times 10^{-3}*\text{Reagent}*\text{Pressure} \\ & - 1.18 \times 10^{-4}*\text{Reagent}*\text{Agitation} - 0.02*\text{Temperature}*\text{Pressure} \\ & - 7.08 \times 10^{-4}*\text{Temperature}*\text{Agitation} \\ & + 3.52 \times 10^{-5}*\text{Reagent}*\text{Temperature}*\text{Pressure} \\ & + 9.48 \times 10^{-7}*\text{Reagent}*\text{Temperature}*\text{Agitation} \end{aligned} \quad \text{Equation 46}$$

6.2.4. Concluding remarks

The statistical analysis of data for the OPMs and base metal showed that the operating temperature and reagent quantity were the most influential factor on the precipitation process. The influence presented by Factor temperature accounted for 56.28 %, 1.76 %, 2.04 %, 13.97 %, and 8.80 % of the effect contribution to the responses Rh, Ru, Ir, Cu, and Ni precipitation respectively (Table 19). In addition the significance of temperature can be seen from its involvement in many significant interactions effects for the OPMs and base metal responses. The optimisation was not performed for the sulphurous acid reagent because the recovery of OPMs was poor.

7. CONCLUSIONS AND RECOMMENDATIONS

The identification of potential reagent and the most influential process variables allowed the development of a better fundamental understanding of the process configuration and optimal conditions required to maximise OPM recovery from the Ni-Cu sulphate leach solution by precipitation. The objectives of the research outlined in section 1.3 were achieved by performing designed experiments on a laboratory scale. The following conclusions were made in accordance with the specified objectives.

7.1. Reagent identification

The performance of equal excess amount (200 %) of the screened reagents (thio-urea, formic acid and formaldehyde) with regards to OPM precipitation, were compared with that of sulphurous acid. The results showed that at all the conditions studied, thio-urea provided better OPMs recovery in comparison to the other screened reagents. The observed better performance of thio-urea relative to other screened reagents was attributed to the tendency of thio-urea to dissociate into several sulphur-containing species such as formamidine disulphide and hydrogen sulphide. Precipitation reactions effected by hydrogen sulphide and other sulphide species have higher degree of metal removal from solutions with faster kinetics. Though the performance of other reagents with regards to OPM precipitation was generally poor, they showed positive OPM recovery with increasing temperature. This suggested that considering these reagents for the purpose of achieving complete recovery of OPMs from the process solution would require temperatures higher than 160 °C and excess reagent quantities which could be expensive economically.

7.2. Effects operating variables

The influence of operating parameters (temperature, reagent quantity, pressure and agitation speed) on the kinetics, extent and precipitate characteristics for the precipitation of OPMs and base metals were investigated using thio-urea and sulphurous acid as reagents. It was found that the most influential parameters for the OPMs and base metal precipitation rates and extents for both reagents were in order of increasing significance: agitation speed, reagent quantity, and operating temperature.

Agitation speed and operating temperature were also found to be the most influential variables on the precipitates particle size distribution. The precipitate particle size decreased with increasing temperature and agitation speed. The d_{50} values of 3.7 μm and 17.3 μm were determined for the precipitate particles generated at 160 °C and 80 °C, respectively. This

phenomenon was attributed to increased nucleation rate due to temperature-induced supersaturation outweighing the agglomeration rate of the nuclei resulting in the formation of smaller particles. For the increase in agitation speed from 250 rpm to 500 rpm, the d_{50} values determined were 5.7 μm and 17.3 μm respectively. The effect caused by increasing agitation speed was attributed to the decreased induction time in the system resulting in a greater number of particles being formed with lower average particle sizes. The faster agitation meant that the likelihood of the reactant components in solution to come into contact with each other was increased and this led to high nuclei formation. Consequently, fewer reactant components were left in solution to contribute to particle growth.

Temperature was also found to be the only variable affecting the chemical composition of the precipitates. The precipitates generated using thio-urea at 80°C and 160°C were characterized by the XRD as predominantly amorphous phases. Peaks corresponding to bornite (Cu_5FeS_4), digenite ($\text{Cu}_{1.8}\text{S}$) and wuestite ($\text{Fe}_{0.942}\text{O}$) were of the species identified in the precipitates. In addition, the precipitate analysis indicated the presence of tenorite (CuO) and elemental Cu in the precipitate generated at 160°C.

7.3. Process variable optimization

Statistical models were used to define an objective function to determine the optimal operating conditions. A temperature of 80°C, a pressure of 7 bar, and 200 % excess thio-urea were proposed as the optimum operating conditions that would yield 98 % Rh, 75 % Ru, and 48 % Ir precipitation with less than 5 % Cu and Ni co-precipitation. At these conditions approximately 99 % Se and about 5 % Te would also be precipitated from the process solution. Experimental validation tests confirmed the model predicted values and proved repeatability of the experimental data.

7.4. Recommendations for future work

The following are recommended regarding the future work:

- In the current work complete Ru and Ir precipitation was not achieved. It is thus recommended that different reactor configurations should be tried in order to improve the recovery of these components.
- With regards to tellurium removal, thio-urea presented poor performance at low temperature. However, at high temperature tellurium removal increased tremendously. This suggested that at high temperature, the presence of elemental copper caused the observed increase in tellurium removal. It is therefore recommended that experimental

work should be done to investigate the precipitation of tellurium at low temperature using thio-urea and elemental copper.

- It has been shown in this work that thio-urea has great potential to provide higher OPM recovery with minimal Cu and Ni co-precipitation. However, to implement its application on industrial scale, there is a need to perform cost analysis to determine the economic viability of using thio-urea as a precipitating reagent. For the recovery of OPMs in BMR using thio-urea, the cost relating to equipment acquisition and reagent consumption should be evaluated.

References

- Awadalla, F.T., Molnar, R.E., Riteey, G.M., 1994. Recovery of platinum group metals (PGM) from acidic solutions by reduction precipitation with sodium borohydride, United States Patent, Patent number 5304233
- Bhattacharyya, D., Jumawan, A.B., Sun, G., 1981. Precipitation of Heavy Metals with Sodium Sulphide: Bench-Scale and Full-Scale Experimental results. Water-1980 AIChE Symposium series, 77
- Baldyga, J., Podgórska, W., Pohorecki, R., 1995. Mixing-precipitation model with application to double feed semi batch precipitation, Chemical Engineering Science, 50, 1281–1300
- Clarke, F.F., Rickard, R.S., 1975. Method of Removing Selenium from Copper Solution, United States Patent, Patent number: 3 914 375.
- Crear, R., 2001. Engineering and design: Precipitation/flocculation/coagulation manual-EM 1110-1.4012, Department of the Army, U.S. army corps of engineers, Washington DC. 20314-1000
- Crundwell, F.K., Michael, S.M., Venkoba, R., Timothy, G.R., William, G.D., 2011. Extractive metallurgy of nickel, cobalt and platinum group metals, 457 – 488
- Demopoulous, G.P., 2009. Aqueous precipitation and crystallisation for the production of particulate solids with desired properties, Hydrometallurgy, 96, 199 – 214
- Dietz Jr., G., Roberts, M.S., 1978. Aluminium containing precipitating agent for precious metals and method for its use, United States Patent, Patent number 4092154
- Dirksen, J.A., Ring, T.A., 1991. Fundamentals of crystallization: kinetic effects on particle size distributions and morphology, Chemical engineering science, 46, (10), 2389 – 2427.
- Dorfling, C., Akdogan, G., Bradshaw S.M., Eksteen, J.J., 2013. Modelling of an autoclave used for high pressure sulphuric acid/oxygen leaching of first stage leach residue. Part 1: Model development, Minerals Engineering
- Dreisinger, D., Murray, W., Hunter, D., Baxter, K., Ferron, J., Fleming, C., 2005. The application of the PLATSOL™ process to copper-nickel-cobalt-PGE/PGM concentrates from PolyMet mining's NorthMet deposit, presented at ALTA 2005, Perth, WA.
- Fabricius, G., Kontturi, K., Sundholm, G., 1994. Influence of thio-urea on the nucleation of copper from acid sulphate solutions, Electrochimica Acta, 39 (16), 2353 - 2357
- Fang, Z., Muhammed, M., 1992. Leaching of precious metals from complex sulphide ores: on the chemistry of gold lixiviation by thio-urea, Mineral Proc. Extractive Metall. Rev. 2, 39 -60

Flynn, C.M., Jr., T.G. Carnhan, Lindstrom, R.E., 1980. Adsorption of heavy metal ions by xanthated saw dust, Report of investigations – 8427, U.S. Bureau of mines, Reno NV

Fogler, S.H., 2006. Elements of Chemical reaction Engineering, 4th Edition, Pearson Education, Inc., NJ

Gupta, P. C., 1963. Analytical chemistry of thiocarbamides. I. Quantitative determination of thio-urea. Analytical Chemistry, 196, 412

Habashi, F., 1999. Textbook of Hydrometallurgy, Second edition. Les Copies de la Capitale Inc, Quebec City

Habashi, F., 1997. Handbook of extractive metallurgy, edited by Fathi Habashi, volume 3, Wiley-VCH, Weinheim

Hiskey, J. B., 1984. Thiourea leaching of gold and silver technology update and additional applications. Mineral and Metallurgical Process. 11, 173

Hirschkind, W., 1924. Process for recovery of metals from their ores, United States Patent, Patent number 1479542

Holly, J.D., 1990. Process for removal of dissolved copper from solution, United States Patent, Patent number 4950326

Horiba-Scientific, 2012. A guidebook to particle size analysis, www.horiba.com/us/particle

Javet, P.H., Hintermann, H.E., 1969. Electrochimica Acta, 14, 527.

Jayaweera, S.A.A., Moss, J.H., Wearmouth, A., 1989. Formation and reaction of copper sulphide: Part I precipitation, Thermochemica Acta, 152, 277 – 236

Jha, M.C., Wicker, G.R., Meyer, G.A., 1978. Selective precipitation of nickel and cobalt sulphides from acidic sulphate solutions, United States Patent, Patent number 4110400.

Julsing, H.G., and McCrindle, R.I., 2001. The use of sodium formate for the recovery of precious metals from acidic base metal effluents, Journal of Chemical Technology and Biotechnology, 76, 349 – 354

Kayanuma, Y., Okabe, T.H., Mitsuda, Y., Maeda, M., 2004. New recovery process for rhodium using metal vapour, Journal of Alloys and Compounds 365, 211–220

Ke, B., Hoekstra, J.J, Sison Jr., B.C., Trivich, D.J., 1962. Electrochem. Soc., 109 (9), 798–804

Kerfoot, D.G.E., Kofluk, R.P., Weir, D.R., 1986. Recovery of platinum group metals from nickel-copper-iron matte, United States Patent, Patent number 457262

- Kim, B.M., 1981. Treatment of metal containing wastewater with calcium sulphide, *AIChE Symposium Series 77* (209), 39 – 48
- Kraber, S., Whitcomb, P., Anderson, M. 2005. *Handbook for Experimenters, Version 7.2*, Minneapolis: Stat-Ease, Inc.
- Kroschwitz, J.I., Howe-Grant, M., 1991. *Encyclopaedia of chemical technology*, Kirk-Othmer, 4th Edition, Wiley and Sons, New York
- Lacoste-Bouchet, P., Deschênes, G., Ghali, E., 1998. Thio-urea leaching of a copper-gold ore using statistical design, *Hydrometallurgy*, 47, (2-3), 189-203
- Lewis, A.E., 2010. Review of Metal Sulphide Precipitation, *Hydrometallurgy*, 104, 222-234
- Lewis, A., van Hille, R., 2006. An exploration into the sulphide precipitation method and its effect on metal sulphide removal, *Hydrometallurgy*, 81 (3 – 4), 197 – 204
- Lewis, A., Swartbooi, A., 2006. Factors affecting metal removal in mixed sulphide precipitation, *Chemical Engineering & Technology*, 29 (2), 277-280
- Lottering, C., 2011. Rhodium precipitation from copper sulphate solutions in the selenium/tellurium removal section, Final Year Thesis, Stellenbosch University
- Lottering, C., Eksteen, J.J, Steenekamp, N., 2012. Precipitation of rhodium from a copper sulphate leach solution in the selenium/tellurium removal section of a base metal refinery, *Journal of the Southern African Institute of Mining and Metallurgy*, 112 (4), 287 – 294
- Luther III, G.W., et al., 2002. Aqueous copper sulphide clusters as intermediate during copper sulphide formation. *Environmental Science and Technology*, 36 (3), 373 – 379
- Maslowska, J., 1969. Mixed complexes of iron (III) (in Polish), *Zeszyty Naukowe Politechniki Lodzkiej, Chemia*, 20, 5 - 114
- Mathew, S.K., Rajesh, N.P., Ichimura, M., Udayalakshmi, 2008. Preparation and characterisation of copper sulphide particles by photochemical method, *Materials Letters*, 62, 591 – 593
- McGeorge, B., Gaylard, P.G., Lewis, A.E., 2009. Mechanism of Rhodium (III) Co-Precipitation with Copper Sulphide (at Low Rh Concentrations) Incorporating a New Cationic Substitution Reaction Path, *Hydrometallurgy*, 96, 235-245
- Nikolic, C.V., Laferty, J.M., 1977. Precipitation of selenium from copper electrowinning solutions, United States Patent, Patent number 4026797
- Park, J.C., 2008. Purification and recovery of rhodium metal by the formation of intermetallic compounds. *Bull. Korean Chemical Society*, 29, 1787 – 1789.

Peters, D. G., Hayes, J. M., Hieftje, G. M., 1974. Chemical Separations and Measurements, W.B. Saunders Company, 200 – 238.

Peters, R. W., Ku, Y., 1985. Batch precipitation studies for heavy metal removal by sulphide precipitation. *AIChE Symposium series* 243 (81), 9 – 27

Peters, R.W., Shem, L., 1993. Separation of heavy metals: Removal from industrial wastewaters and contaminated soil, Argonne National Lab., IL (United States). Energy Systems Division

Pohorecki, R., Baldyga, J., 1983. The use of a new model of micromixing for determination of crystal size in precipitation, *Chemical Engineering Science*, 38 (1), 79 – 83

Provis, J.L., Van Deventer, J.S.J., Rademan, J.A.M., and Lorenzen, L., 2003. A kinetic model for the acid-oxygen pressure leaching of Ni-Cu matte, *Hydrometallurgy*, 70, 83 - 99

Renner, H., Schlamp, G., Kleinwächter, I., Drost, E., Lüscho, H. M., Tews, P., Panster, P., Diehl, M., Lang, J., Kreuzer, T., Knödler, A., Starz, K. A., Dermann, K., Rothaut, J., Drieselmann, R., Peter, C. and Schiele, R. 2001. Platinum Group Metals and Compounds, *Ullmann's Encyclopedia of Industrial Chemistry*

Roy, P., Srivastava, S.K., 2007. Low-temperature synthesis of CuS nanorods by simple wet chemical method, *Materials Letters*, 61 (8 – 9), 1693 – 1697

Roy, T.K., 1961. Preparing nickel and cobalt concentrate, *Industrial and Engineering Chemistry*, 53 (7) 559 – 566

Ruiz, M.C., Zapata, J., Padilla, R., 2007. Effect of variables on the quality of hematite precipitated from sulphate solutions, *Hydrometallurgy*, 89, 32 – 39

Schlesinger, M.E., King, M.J., Sole, K.C., Davenport, W.G., 2011. *Extractive Metallurgy of Copper*, 5th Edition, Elsevier, UK

Schreier, G., Edtmaier, C., 2003. Separation of Ir, Pd and Rh from secondary Pt scrap by precipitation and calcination, *Hydrometallurgy*, 68, 69 – 75

Serdar, A., 2012. Cementation of rhodium from waste chloride solutions using copper powder, *International Journal of Mineral Processing*, 114–117, 100–105

Serdar, A., 2011. Rhodium recovery from rhodium-containing waste rinsing water via cementation using zinc powder, *Hydrometallurgy*, 104, 71- 75

Sherritt Gordon Mines Limited, 1983. *Base Metal Refinery: Selenium Removal and Residue Treatment Operating Manual*

Siame, J., Kasaini, H., 2010. Sulphur-mediated precipitation of Pt/Fe/Co/Cr ions in liquid – liquid and gas – liquid chloride systems, *World Academy of Science, Engineering and Technology*, 69, 302 – 311

Silberberg, M.S., 2010. *Principles of General chemistry*, 2nd Edition, Mc Graw Hill Higher Education, Boston

Söhnel, O., Garside, J., 1992. *Precipitation: Basic Principles and Industrial Applications*, 1st ed. Butterworth- Heinemann, Oxford

Sutherland, K., 2008. *Filters and Filtration Handbook*, 5th Edition, Elsevier/Butterworth-Heinemann, Oxford

Tuominen, T. and Groenquist, P.O., Hydrogen sulfide as precipitation reagent in hydrometallurgy, *Ertzmetall*, 22 (1969): 81-86

Van der Merwe, A.J.V., 2002. Base metal refinery induction report, Lonmin plc

Wakeman, R. 2007. The influence of particle properties on filtration, *Separation and Purification Technology*, 58, 234–241

Wang, S., Wesstrom, B., Fernadez, J., 2003. A novel process for recovery of Te and Se from copper slims autoclave leach solution, *Journal of Minerals and Materials Characterisation and Engineering*, 2(1), 53 – 64

Weir, R.D., Kerfoot, D.G.E., Hofirek, Z., 1983. Removal of selenium from acidic copper/nickel solutions, United States Patent, Patent number 4374808

Wills, B.A., 1997. *Mineral processing technology: an introduction to the practical aspect of ore treatment and mineral recovery*, 6th ed. Butterworth- Heinemann, Oxford.

Wing, R.E., 1974. Heavy metal removal from wastewater with starch xanthate, *Proceedings 29th Purdue Industrial Waste Conference*, 31, 1068 – 1079

Xiao, Z., Laplante, A.R., 2004. Characterizing and recovering the platinum minerals- a review, *Minerals and Engineering*, 17, 961 – 979

APPENDIX: A**EXPERIMENTAL DATA****Screening experiments***Table 21: Screening test 1*

Screening test 1							
Thio-urea excess : 200% Temperature : 80°C				Pressure : Ambient Agitation:250rpm			
	% precipitation						
Time	Rh	Ru	Ir	Cu	Ni	Se	Te
0	0	0.00	0.00	0.00	0.00	0.00	0.00
20	100	0.66	0.41	0.19	0.16	0.76	0.08
60	100	0.70	0.47	0.25	0.20	0.80	0.09
120	100	0.78	0.51	0.25	0.20	0.83	0.07
240	100	0.82	0.54	0.12	0.06	0.95	0.10
480	100	0.83	0.52	0.18	0.11	1.00	0.07

Table 22: Screening test 2

Screening test 2							
Thio-urea excess : 200% Temperature : 160°C				Pressure : Ambient Agitation:250rpm			
	% precipitation						
Time	Rh	Ru	Ir	Cu	Ni	Se	Te
0	0	0.00	0.00	0.00	0.00	0.00	0.00
20	100	78.92	51.77	31.78	19.10	76.00	72.40
60	100	85.65	57.52	16.32	9.91	80.00	69.42
120	100	83.95	56.44	14.24	8.54	83.00	72.58
240	100	79.84	57.45	12.67	4.43	95.00	85.01
480	100	76.47	58.56	15.15	5.72	100.00	95.82

Table 23: Screening test 3

Screening test 3							
Formic acid : 200% Temperature : 80°C				Pressure : Ambient Agitation:250rpm			
	% precipitation						
Time	Rh	Ru	Ir	Cu	Ni	Se	Te
0	0.00	0.00	0.00	0.00	0.00	0.00	0.00
20	0.00	0.00	0.00	17.46	22.80	0.00	0,00
60	0.00	0.00	0.00	4.06	7.01	0.00	0,00
120	0.00	0.00	0.00	3.74	9.02	0.00	0,00
240	0.00	0.00	0.00	6.25	9.36	0.00	0,00
480	0.00	0.00	0.00	7.02	9.82	0.00	0,00

Table 24: Screening test 4

Screening test 4							
Formic acid: 200% Temperature : 160°C				Pressure : Ambient Agitation:250rpm			
	% precipitation						
Time	Rh	Ru	Ir	Cu	Ni	Se	Te
0	0.00	0.00	0.00	0.00	0.00	0.00	0.00
20	13.95	43.45	0.00	30.40	39.47	80.66	89.21
60	2.33	24.84	0.00	4.08	8.86	100.00	55.00
120	21.63	26.81	0.00	5.25	9.69	100.00	38.68
240	23.02	12.10	0.00	10.30	10.26	100.00	41.32
480	27.67	10.23	0.00	10.30	8.77	100.00	70.00

Table 25: Screening test 5

Screening test 5							
Formaldehyde: 200% Temperature : 80°C				Pressure : Ambient Agitation:250rpm			
	% precipitation						
Time	Rh	Ru	Ir	Cu	Ni	Se	Te
0	0.00	0.00	0.00	0.00	0.00	0.00	0.00
20	0.00	0.00	0.00	5.77	10.01	16.67	6.74
60	0.00	0.00	0.00	4.97	7.52	17.17	18.26
120	0.00	0.00	0.00	1.26	0.00	12.58	0.00
240	0.00	0.00	0.00	0.93	2.94	11.08	0.00
480	0.00	0.00	0.00	4.57	0.73	7.67	14.13

Table 26: Screening test 6

Screening test 6							
Formaldehyde: 200%				Pressure : Ambient			
Temperature : 160°C				Agitation:250rpm			
	% precipitation						
Time	Rh	Ru	Ir	Cu	Ni	Se	Te
0	0.00	0.00	0.00	0.00	0.00	0.00	0.00
20	2.39	0.00	0.00	5.51	4.27	0.00	62.99
60	0.00	0.91	0.00	5.74	3.47	3.70	65.07
120	0.00	28.34	0.00	4.99	0.00	5.00	84.63
240	0.00	27.16	0.00	3.13	0.00	0.00	96.72
480	0.00	26.19	0.00	0.00	0.00	0.00	71.04

Table 27: Screening test 7

Screening test 7							
SO ₂ : 200%				Pressure : Ambient			
Temperature : 80°C				Agitation:250rpm			
	% precipitation						
Time	Rh	Ru	Ir	Cu	Ni	Se	Te
0	0.00	0.00	0.00	0.00	0.00	0.00	0.00
20	5.68	0.00	1.19	4.33	7.00	99.07	0.00
60	2.73	0.00	0.00	4.26	0.46	99.07	0.00
120	1.97	5.20	3.20	12.52	7.64	33.67	23.14
240	0.00	0.12	0.01	3.15	0.00	51.89	0.00
480	0.00	0.00	0.00	2.69	0.00	55.96	0.00

Table 28: Screening test 8

Screening test 8							
SO ₂ : 200%				Pressure : Ambient			
Temperature : 160°C				Agitation:250rpm			
	% precipitation						
Time	Rh	Ru	Ir	Cu	Ni	Se	Te
0	0.00	0.00	0.00	0.00	0.00	0	0.00
20	1.18	2.48	0.00	19.00	15.75	96	12.64
60	3.76	0.41	0.00	5.39	1.62	71	0.38
120	6.48	5.58	0.00	8.05	4.52	68	0.00
240	6.21	0.79	0.00	7.30	3.07	80	3.58
480	6.94	3.38	0.00	20.51	16.24	82	19.25

Optimisation experiments*Table 29: Optimization test 1(thio-urea data)*

Experiment 1							
Thio-urea excess : 320%				Pressure : Ambient			
Temperature : 80°C				Agitation:500rpm			
% precipitation							
Time	Rh	Ru	Ir	Cu	Ni	Se	Te
0	0.00	0.00	0.00	0.00	0.00	0.00	0.00
20	100	70.19	47.86	18.52	14.14	93.32	12.22
60	100	75.41	49.34	19.28	14.90	94.38	11.36
120	100	80.11	50.79	14.21	9.29	93.91	10.97
240	100	83.62	51.26	16.72	12.50	95.09	10.69
480	100	85.20	52.12	17.32	12.33	95.56	12.63

Table 30: Optimization test 2(thio-urea data)

Experiment 2							
Thio-urea excess : 200%				Pressure : Ambient			
Temperature : 80°C				Agitation:250rpm			
% precipitation							
Time	Rh	Ru	Ir	Cu	Ni	Se	Te
0	0	0.00	0.00	0.00	0.00	0.00	0.00
20	100	65.99	41.49	18.97	16.31	93.98	8.42
60	100	70.16	47.28	24.59	20.22	93.34	9.17
120	100	77.62	51.08	25.34	20.46	93.57	7.47
240	100	82.40	54.41	12.21	6.09	95.52	10.72
480	100	84.32	51.96	18.18	10.96	95.45	6.83

Table 31: Optimization test 3 (thio-urea data)

Experiment 3							
Thio-urea excess : 320%				Pressure : Ambient			
Temperature : 80°C				Agitation:250rpm			
	% precipitation						
Time	Rh	Ru	Ir	Cu	Ni	Se	Te
0	0.00	0.00	0.00	0.00	0.00	0.00	0.00
20	80.97	57.25	34.95	3.01	8.82	92.01	0.00
60	100	73.80	46.71	0.00	0.00	94.01	1.82
120	100	81.39	54.59	14.94	17.01	94.69	10.27
240	100	84.31	53.81	2.81	5.32	94.71	8.22
480	100	85.49	52.97	1.81	4.33	94.94	4.96

Table 32: Optimization test 4 (thio-urea data)

Experiment 4							
Thio-urea excess : 200%				Pressure : 7 bar			
Temperature : 80°C				Agitation:250rpm			
	% precipitation						
Time	Rh	Ru	Ir	Cu	Ni	Se	Te
0	0.00	0.00	0.00	0.00	0.00	0.00	0.00
20	79.70	55.15	32.71	8.31	6.36	91.92	0.00
60	100	67.85	43.77	9.07	6.54	92.29	2.43
120	100	72.84	42.94	0.00	0.00	92.35	0.00
240	100	80.48	50.80	6.53	1.77	93.38	1.01
480	100	82.34	49.75	0.10	0.00	93.74	0.00

Table 33: Optimization test 5 (thio-urea data)

Experiment 5							
Thio-urea excess : 320%				Pressure : 7 bar			
Temperature : 80°C				Agitation:500rpm			
	% precipitation						
Time	Rh	Ru	Ir	Cu	Ni	Se	Te
0	0.00	0.00	0.00	0.00	0.00	0.00	0.00
20	85.25	63.67	41.19	12.39	8.21	92.59	5.53
60	100	76.72	53.04	17.69	12.26	93.73	13.24
120	100	81.08	52.21	15.56	9.48	93.83	9.35
240	100	84.90	53.83	13.33	6.60	94.13	12.02
480	100	86.74	56.96	18.04	11.14	94.35	17.53

Table 34: Optimization test 6 (thio-urea data)

Experiment 6							
Thio-urea excess : 200%				Pressure : 7 bar			
Temperature : 80°C				Agitation:500rpm			
% precipitation							
Time	Rh	Ru	Ir	Cu	Ni	Se	Te
0	0.00	0.00	0.00	0.00	0.00	0.00	0.00
20	100	60.74	36.78	3.99	2.61	91.99	3.69
60	100	70.74	46.34	9.30	5.22	93.05	3.41
120	100	78.15	49.47	8.14	4.57	93.42	2.01
240	100	81.66	50.32	8.19	4.10	93.80	4.42
480	100	83.72	51.01	0.00	0.00	94.16	3.24

Table 35: Optimization test 7 (thio-urea data)

Experiment 7							
Thio-urea excess : 200%				Pressure : Ambient			
Temperature : 80°C				Agitation:500rpm			
% precipitation							
Time	Rh	Ru	Ir	Cu	Ni	Se	Te
0	0.00	0.00	0.00	0.00	0.00	0,00	0.00
20	84.98	62.52	36.61	0.00	0.00	92,66	1.41
60	100	71.10	43.47	0.00	0.00	92,40	0.00
120	100	78.75	49.10	3.71	0.00	94,29	6.26
240	100	84.92	56.88	24.25	19.54	95,09	16.59
480	100	83.98	51.26	0.00	0.00	93,79	4.15

Table 36: Optimization test 8 (thio-urea data)

Experiment 8							
Thio-urea excess : 200%				Pressure : 7 bar			
Temperature : 160°C				Agitation:250rpm			
% precipitation							
Time	Rh	Ru	Ir	Cu	Ni	Se	Te
0	0,00	0.00	0.00	0.00	0.00	0.00	0.00
20	100	63.49	39.99	0.00	0.00	92.47	2.49
60	100	73.71	48.75	14.62	9.80	93.35	4.61
120	100	80.69	50.11	11.07	6.96	93.84	2.07
240	100	83.60	51.55	10.07	5.07	95.27	4.90
480	100	85.09	51.03	7.56	2.06	94.29	4.76

Table 37: Optimization test 9 (thio-urea data)

Experiment 9							
Thio-urea excess : 200%				Pressure : 7 bar			
Temperature : 80°C				Agitation:500rpm			
% precipitation							
Time	Rh	Ru	Ir	Cu	Ni	Se	Te
0	0.00	0.00	0.00	0.00	0.00	0.00	0.00
20	100	78.53	49.38	18.84	6.75	87.44	34.19
60	100	66.79	50.53	15.86	2.39	87.44	47.02
120	100	75.55	52.62	7.65	0.00	87.44	90.35
240	100	74.59	55.65	24.22	12.03	87.44	89.39
480	100	68.05	52.76	15.49	1.81	87.44	98.11

Table 38: Optimization test 10 (thio-urea data)

Experiment 10							
Thio-urea excess : 200%				Pressure : Ambient			
Temperature : 160°C				Agitation:500rpm			
% precipitation							
Time	Rh	Ru	Ir	Cu	Ni	Se	Te
0	0.00	0.00	0.00	0.00	0.00	0.00	0.00
20	100	73.98	48.94	9.02	0.00	97.66	63.92
60	100	81.23	56.00	13.63	0.94	97.66	68.52
120	100	79.59	57.04	5.67	0.00	97.66	82.16
240	100	78.60	57.71	12.42	0.00	97.66	94.85
480	100	75.53	56.72	3.44	0.00	97.66	96.56

Table 39: Optimization test 11 (thio-urea data)

Experiment 11							
Thio-urea excess : 200%				Pressure : Ambient			
Temperature : 160°C				Agitation:250rpm			
% precipitation							
Time	Rh	Ru	Ir	Cu	Ni	Se	Te
0	0.00	0.00	0.00	0.00	0.00	0.00	0.00
20	100	78.92	51.77	15.16	3.76	97.56	72.40
60	100	85.65	57.52	17.62	5.97	97.56	69.42
120	100	83.95	56.44	15.21	3.44	97.56	72.58
240	100	79.84	57.45	9.29	0.00	97.56	85.01
480	100	76.47	58.56	11.52	0.00	97.56	95.82

Table 40: Optimization test 12 (thio-urea data)

Experiment 12							
Thio-urea excess : 320%				Pressure : 7 bar			
Temperature : 160°C				Agitation:500rpm			
% precipitation							
Time	Rh	Ru	Ir	Cu	Ni	Se	Te
0	0.00	0.00	0.00	0.00	0.00	0.00	0.00
20	84.68	69.71	49.25	16.75	3.16	97.66	51.82
60	100	81.47	60.16	26.90	11.56	97.66	56.12
120	100	82.06	60.84	24.20	7.57	97.66	86.40
240	100	78.69	60.78	23.08	5.91	97.66	95.47
480	100	73.66	60.44	23.26	5.41	97.66	97.28

Table 41: Optimization test 13 (thio-urea data)

Experiment 13							
Thio-urea excess : 200%				Pressure : 7 bar			
Temperature : 160°C				Agitation:500rpm			
% precipitation							
Time	Rh	Ru	Ir	Cu	Ni	Se	Te
0	0.00	0.00	0.00	0.00	0.00	0.00	0.00
20	83.46	67.73	47.55	14.69	7.05	97.74	53.33
60	100	81.08	60.66	27.34	19.33	97.74	64.87
120	100	79.23	58.58	14.60	5.46	97.74	82.36
240	100	81.41	62.16	28.19	19.86	97.74	91.51
480	100	76.85	62.22	26.73	18.65	97.74	94.44

Table 42: Optimization test 14 (thio-urea data)

Experiment 14							
Thio-urea excess : 320%				Pressure : Ambient			
Temperature : 160°C				Agitation:250rpm			
% precipitation							
Time	Rh	Ru	Ir	Cu	Ni	Se	Te
0	0.00	0.00	0.00	0.00	0.00	0.00	0.00
20	80.39	65.34	46.85	30.88	19.50	100	6.20
60	100	79.87	60.08	34.56	19.34	100	97.38
120	100	79.09	60.61	34.60	19.27	100	91.39
240	100	73.83	60.67	35.79	20.87	100	98.43
480	100	59.97	60.29	35.32	19.88	100	97.53

Table 43: Optimization test 15 (thio-urea data)

Experiment 15							
Thio-urea excess : 320%				Pressure : 7 bar			
Temperature : 160°C				Agitation:250rpm			
% precipitation							
Time	Rh	Ru	Ir	Cu	Ni	Se	Te
0	0.00	0.00	0.00	0.00	0.00	0.00	0.00
20	83.26	69.95	47.05	21.65	9.01	97.62	66.07
60	100	83.88	58.93	27.53	12.29	97.62	75.36
120	100	84.30	61.31	28.52	13.42	97.62	68.12
240	100	81.22	60.07	23.15	6.73	97.62	90.41
480	100	77.30	59.96	23.59	7.28	97.62	96.70

Table 44: Optimization test 16 (thio-urea data)

Experiment 16							
Thio-urea excess : 320%				Pressure : Ambient			
Temperature : 160°C				Agitation:500rpm			
% precipitation							
Time	Rh	Ru	Ir	Cu	Ni	Se	Te
0	0.00	0.00	0.00	0.00	0.00	0.00	0.00
20	83.77	68.62	46.51	17.24	3.89	97.69	58.26
60	100	84.60	62.43	31.98	16.71	97.69	93.53
120	100	84.12	60.78	25.66	8.97	97.69	82.39
240	100	66.30	61.83	28.07	12.11	97.69	91.16
480	100	76.98	61.02	20.05	2.69	97.69	98.45

Sulphurous acid data*Table 45: Optimization test 1 (sulphurous acid data)*

Experiment 1							
Sulphurous acid : 960%				Pressure : Ambient			
Temperature : 80°C				Agitation:250rpm			
% precipitation							
Time	Rh	Ru	Ir	Cu	Ni	Se	Te
0	0.00	0.00	0.00	0.00	0.00	0.00	0.00
20	14.20	12.87	8.42	2.88	2.67	98.45	90.72
60	20.01	19.06	15.25	9.70	9.46	98.46	86.40
120	11.55	11.28	9.34	1.97	0.69	99.52	85.29
240	16.61	13.64	10.08	5.86	4.74	98.46	90.90
480	10.59	7.90	5.34	0.77	0.00	98.46	92.93

Table 46: Optimization test 2 (sulphurous acid data)

Experiment 2							
Sulphurous acid : 960%				Pressure : Ambient			
Temperature : 80°C				Agitation:500rpm			
% precipitation							
Time	Rh	Ru	Ir	Cu	Ni	Se	Te
0	0.00	0.00	0.00	0.00	0.00	0.00	0.00
20	11.27	10.72	6.81	5.20	3.09	97.35	91.85
60	13.76	13.39	9.38	2.53	0.00	99.53	85.53
120	21.18	15.11	10.73	2.72	0.68	98.64	86.49
240	16.76	12.09	10.98	0.00	0.00	98.64	90.72
480	-	-	-	1.78	0.00	98.64	97.08

Table 47: Optimization test 3 (sulphurous acid data)

Experiment 3							
Sulphurous acid : 720% Temperature : 80°C				Pressure : Ambient Agitation:250rpm			
	% precipitation						
Time	Rh	Ru	Ir	Cu	Ni	Se	Te
0	0.00	0.00	0.00	0.00	0.00	0.00	0.00
20	5.68	4.82	0.00	2.47	2.69	97.41	9.39
60	2.73	0.00	0.00	1.40	0.00	33.19	0.00
120	1.97	1.34	0.00	0.00	0.00	99.19	33.97
240	0.00	0.00	0.00	0.00	0.00	97.19	13.05
480	0.00	0.00	0.00	1.44	0.00	99.23	0.00

Table 48: Optimization test 4 (sulphurous acid data)

Experiment 4							
Sulphurous acid : 720% Temperature : 80°C				Pressure : Ambient Agitation:500rpm			
	% precipitation						
Time	Rh	Ru	Ir	Cu	Ni	Se	Te
0	0.00	0.00	0.00	0.00	0.00	0.00	0.00
20	6.98	6.54	3.63	4.14	4.32	88.58	31.59
60	6.19	5.87	4.35	3.89	3.22	91.46	23.05
120	7.12	3.62	2.65	4.65	2.39	91.93	4.09
240	5.78	1.55	1.82	5.27	5.42	91.61	2.88
480	5.52	0.75	1.45	2.66	1.93	91.28	3.02

Table 49: Optimization test 5 (sulphurous acid data)

Experiment 5							
Sulphurous acid : 960% Temperature : 80°C				Pressure : 7 bars Agitation:500rpm			
	% precipitation						
Time	Rh	Ru	Ir	Cu	Ni	Se	Te
0	0.00	0.00	0.00	0.00	0.00	0.00	0.00
20	7.16	7.23	3.56	0.00	0.00	91.19	71.99
60	6.34	6.07	5.56	0.00	0.00	92.06	77.95
120	7.91	3.17	5.10	0.00	0.00	93.96	82.61
240	8.34	2.85	6.51	0.00	0.00	90.69	85.02
480	9.34	2.36	8.92	0.99	0.48	94.23	90.34

Table 50: Optimization test 6 (sulphurous acid data)

Experiment 6							
Sulphurous acid : 960%				Pressure : Ambient			
Temperature : 160°C				Agitation:500rpm			
Time	% precipitation						
	Rh	Ru	Ir	Cu	Ni	Se	Te
0	0.00	0.00	0.00	0.00	0.00	0.00	0.00
20	14.69	3.66	5.12	4.52	4.57	99.25	68.13
60	14.53	2.59	4.83	0.00	0.00	99.25	68.11
120	22.60	4.94	7.21	3.71	2.81	99.25	69.30
240	29.13	5.02	6.64	3.40	2.81	99.25	74.82
480	40.18	5.02	10.23	1.57	1.58	99.25	82.25

Table 51: Optimization test 7 (sulphurous acid data)

Experiment 7							
Sulphurous acid : 720%				Pressure : Ambient			
Temperature : 160°C				Agitation:500rpm			
Time	% precipitation						
	Rh	Ru	Ir	Cu	Ni	Se	Te
0	0.00	0.00	0.00	0.00	0.00	0.00	0.00
20	8.93	2.68	1.31	1.90	0.44	95.64	6.19
60	11.13	1.34	0.56	0.00	0.00	70.68	0.00
120	13.77	3.75	2.51	0.45	0.00	67.53	0.47
240	1822	6.58	2.88	2.15	1.57	79.72	1.72
480	22.75	13.20	8.12	6.95	5.95	82.37	8.90

Table 52: Optimization test 8 (sulphurous acid data)

Experiment 8							
Sulphurous acid : 960%				Pressure : 7 bar			
Temperature : 80°C				Agitation:250rpm			
Time	% precipitation						
	Rh	Ru	Ir	Cu	Ni	Se	Te
0	0.00	0.00	0.00	0.00	0.00	0.00	0.00
20	0.00	0.00	0.00	0.00	0.00	92.05	53.67
60	4.25	1.84	0.00	1.29	2.01	92.67	75.66
120	5.44	0.00	0.00	0.00	0.00	93.99	74.48
240	5.63	0.00	0.00	0.00	0.00	93.97	72.19
480	4.82	0.00	0.00	0.00	0.00	94.52	80.32

Table 53: Optimization test 9 (sulphurous acid data)

Experiment 9							
Sulphurous acid : 720%				Pressure : 7 bar			
Temperature : 80°C				Agitation:500rpm			
% precipitation							
Time	Rh	Ru	Ir	Cu	Ni	Se	Te
0	0.00	0.00	0.00	0.00	0.00	0.00	0.00
20	0.38	1.90	2.05	1.06	1.74	76.91	2.57
60	3.57	3.59	4.34	1.54	1.10	92.33	9.14
120	5.05	1.88	2.94	5.84	4.66	90.17	4.61
240	3.88	2.01	4.47	0.37	1.37	92.37	4.57
480	7.36	3.17	5.13	4.78	5.21	92.64	4.21

Table 54: Optimization test 10 (sulphurous acid data)

Experiment 10							
Sulphurous acid : 960%				Pressure : Ambient			
Temperature : 160°C				Agitation:500rpm			
% precipitation							
Time	Rh	Ru	Ir	Cu	Ni	Se	Te
0	0.00	0.00	0.00	0.00	0.00	0.00	0.00
20	6.79	0.00	0.00	0.00	0.00	94.48	70.15
60	9.56	1.39	2.96	1.60	0.00	98.98	82.08
120	13.17	0.42	0.01	0.00	0.00	99.06	90.77
240	23.78	0.00	0.84	0.00	0.00	99.06	92.90
480	41.06	4.91	8.30	2.03	0.00	99.52	93.56

Table 55: Optimization test 11 (sulphurous acid data)

Experiment 11							
Sulphurous acid : 960%				Pressure : 7 bar			
Temperature : 160°C				Agitation:500rpm			
% precipitation							
Time	Rh	Ru	Ir	Cu	Ni	Se	Te
0	0.00	0.00	0.00	0.00	0.00	0.00	0.00
20	0.00	0.00	0.00	7.20	6.73	99.01	13.25
60	4.24	1.80	3.35	9.19	8.84	99.01	30.47
120	10.50	1.58	4.07	7.82	7.79	99.01	68.53
240	21.24	2.81	6.35	9.95	9.16	98.80	72.82
480	38.00	6.28	12.71	9.86	9.81	99.01	-

Table 56: Optimization test 12 (sulphurous acid data)

Experiment 12							
Sulphurous acid : 960%				Pressure : 7 bar			
Temperature : 160°C				Agitation:250rpm			
% precipitation							
Time	Rh	Ru	Ir	Cu	Ni	Se	Te
0	0.00	0.00	0.00	0.00	0.00	0.00	0.00
20	5.21	5.05	3.60	5.70	3.50	99.40	72.38
60	12.87	10.33	8.06	4.76	2.85	96.79	67.46
120	18.80	10.28	6.72	8.91	7.57	98.73	87.56
240	24.40	10.46	9.53	10.08	8.06	99.01	86.30
480	36.13	10.74	12.50	6.83	4.89	98.73	91.80

Table 57: Optimization test 13 (sulphurous acid data)

Experiment 13							
Sulphurous acid : 720%				Pressure : 7 bar			
Temperature : 80°C				Agitation:250rpm			
% precipitation							
Time	Rh	Ru	Ir	Cu	Ni	Se	Te
0	0.00	0.00	0.00	0.00	0.00	0.00	0.00
20	3.32	4.66	4.51	0.00	0.00	90.50	22.74
60	3.87	6.15	1.14	1.46	0.18	92.65	67.90
120	2.05	4.35	2.32	2.34	1.34	94.38	44.13
240	1.30	1.20	1.72	0.99	0.09	94.94	4.91
480	0.00	0.31	1.92	0.00	0.00	93.86	0.00

Table 58: Optimization test 14 (sulphurous acid data)

Experiment 14							
Sulphurous acid : 720%				Pressure : Ambient			
Temperature : 160°C				Agitation:500rpm			
% precipitation							
Time	Rh	Ru	Ir	Cu	Ni	Se	Te
0	0.00	0.00	0.00	0.00	0.00	0.00	0.00
20	14.52	7.49	4.73	2.24	1.84	94.72	74.03
60	13.55	5.05	1.33	1.22	0.00	98.49	82.25
120	17.02	6.80	4.17	0.00	0.00	98.69	75.22
240	23.81	8.07	6.79	1.22	0.08	98.30	65.18
480	33.02	10.89	10.18	4.48	3.26	99.03	49.92

Table 59: Optimization test 15 (sulphurous acid data)

Experiment 15							
Sulphurous acid : 720%				Pressure : 7 bar			
Temperature : 160°C				Agitation:500rpm			
% precipitation							
Time	Rh	Ru	Ir	Cu	Ni	Se	Te
0	0.00	0.00	0.00	0.00	0,00	0.00	0.00
20	14.51	1.41	4.82	2.52	2,57	99.26	46.91
60	17.81	1.65	3.98	4.27	3,89	98.52	23.98
120	18.41	0.95	5.59	1.45	1,16	98.42	48.94
240	21.90	3.71	6.27	4.07	3,73	98.70	58.06
480	27.57	5.40	8.20	4.90	5,71	98.29	45.09

Table 60: Optimization test 16 (sulphurous acid data)

Experiment 16							
Sulphurous acid : 720%				Pressure : 7 bar			
Temperature : 160°C				Agitation:500rpm			
% precipitation							
Time	Rh	Ru	Ir	Cu	Ni	Se	Te
0	0.00	0.00	0.00	0.00	0.00	0.00	0.00
20	12.32	5.94	3.83	2.26	2.68	99.49	61.96
60	16.40	6.82	7.70	4.43	5.10	99.10	60.60
120	20.10	8.46	7.51	2.90	3.68	99.10	50.06
240	22.65	8.98	7.81	2.66	2.51	99.10	40.13
480	28.15	11.58	11.05	3.54	3.01	98.76	40.94

APPENDIX: B

LIST OF FIGURES

Thio-urea experimental data

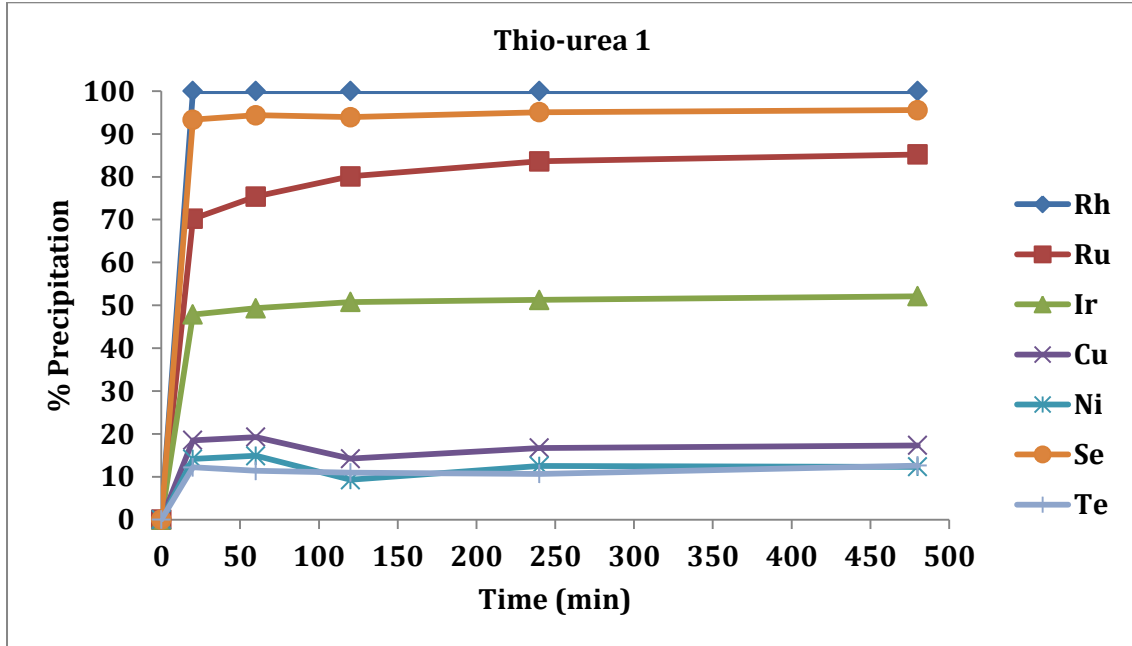


Figure 44: Effect of operating variables on precipitation (80°C, 320% excess, 500rpm, ambient pressure)

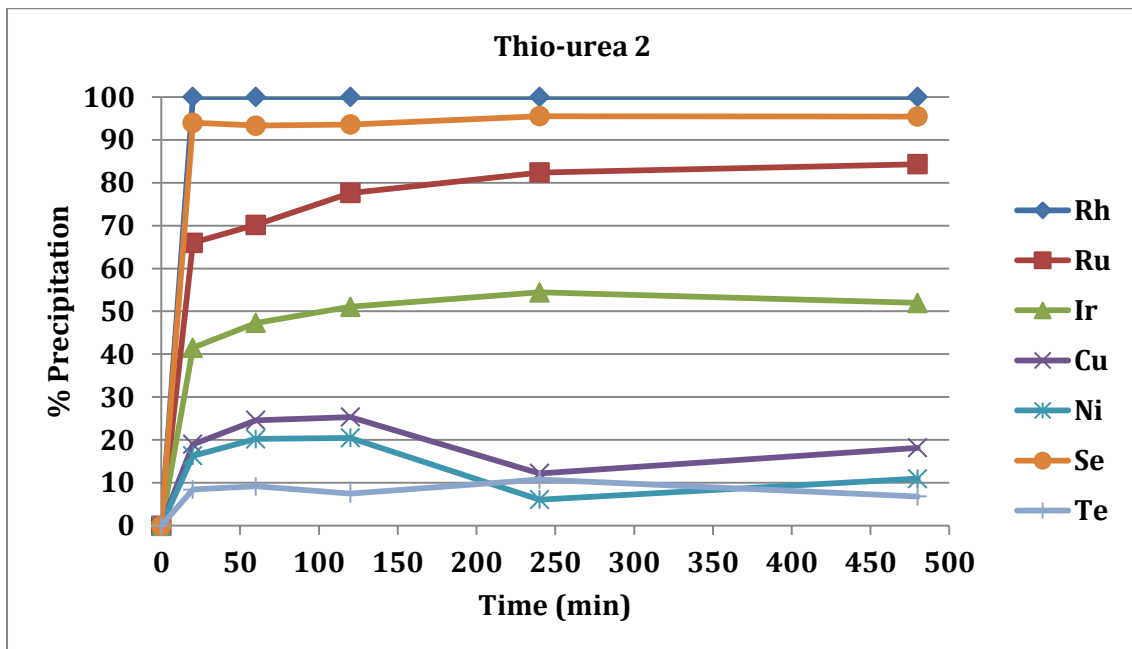


Figure 45: Effect of operating variables on precipitation (80°C, 200% excess, 250rpm, ambient pressure)

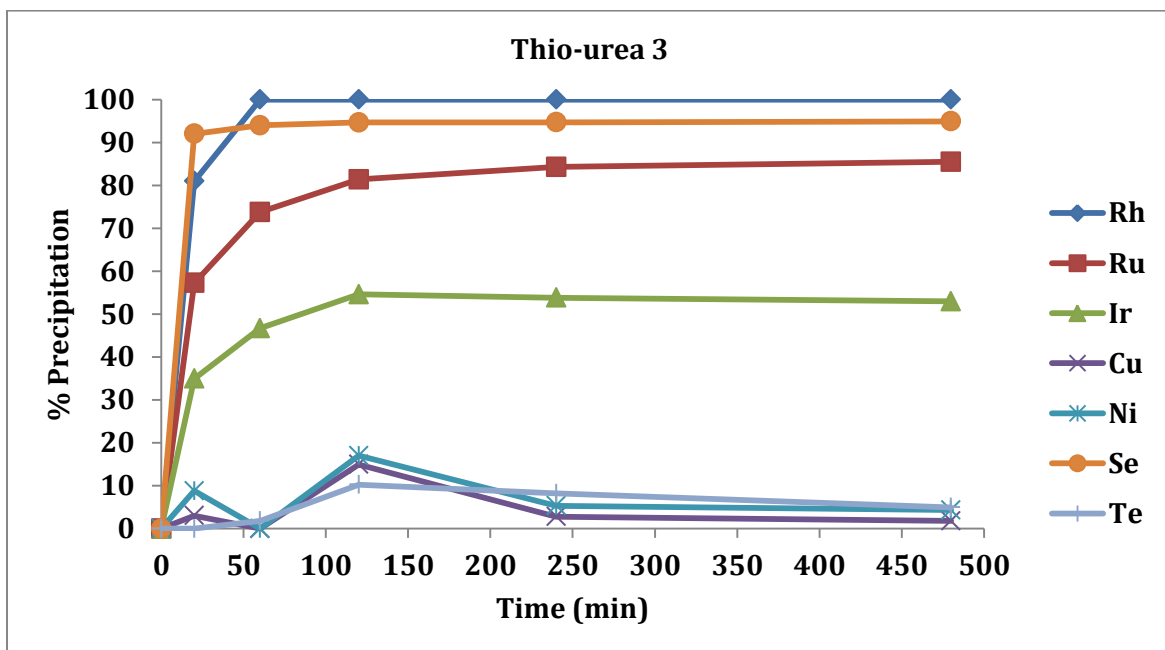


Figure 46: Effect of operating variables on precipitation (80°C, 320% excess, 250rpm, ambient pressure)

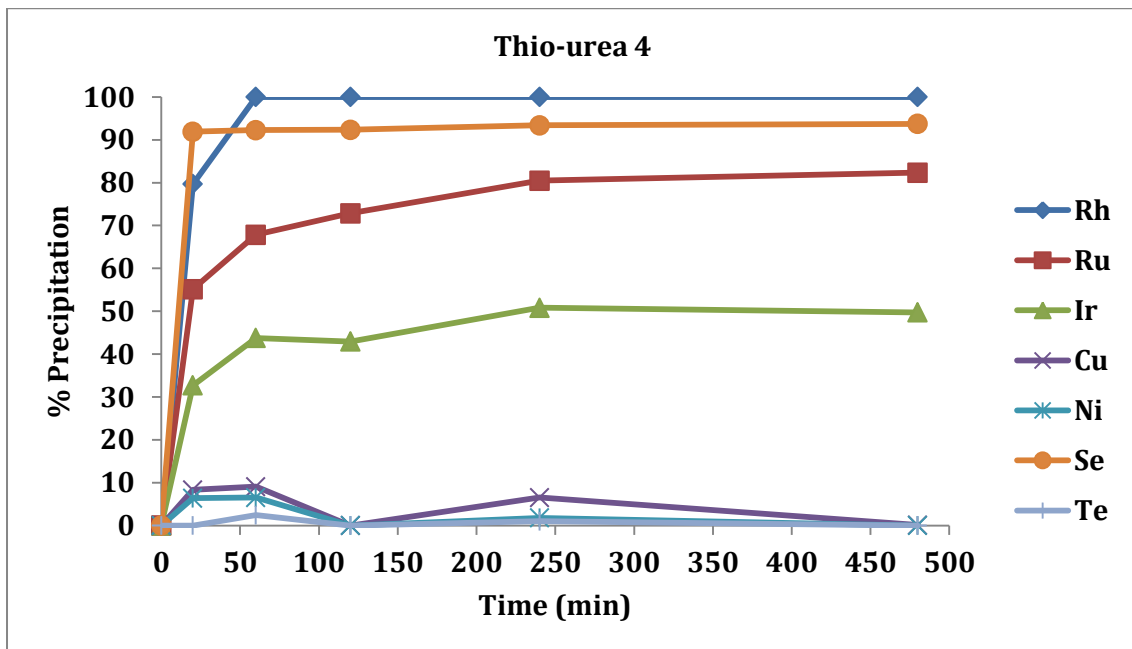


Figure 47: Effect of operating variables on precipitation (80°C, 320% excess, 250rpm, 7 bars)

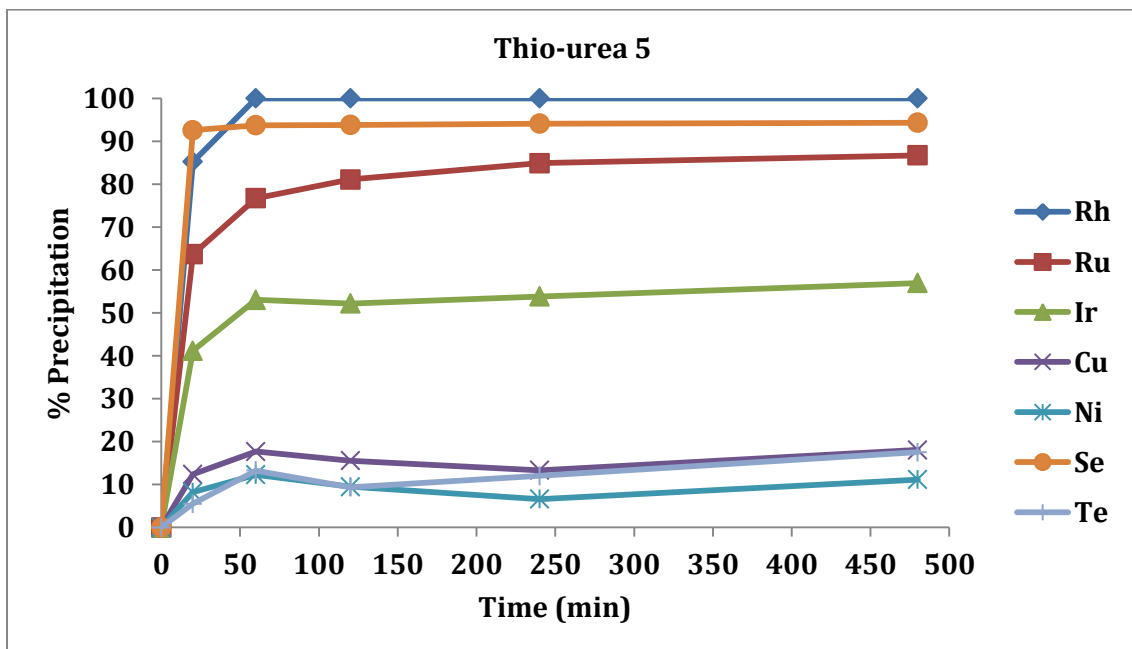


Figure 48: Effect of operating variables on precipitation (80°C, 320% excess, 500rpm, 7bars)

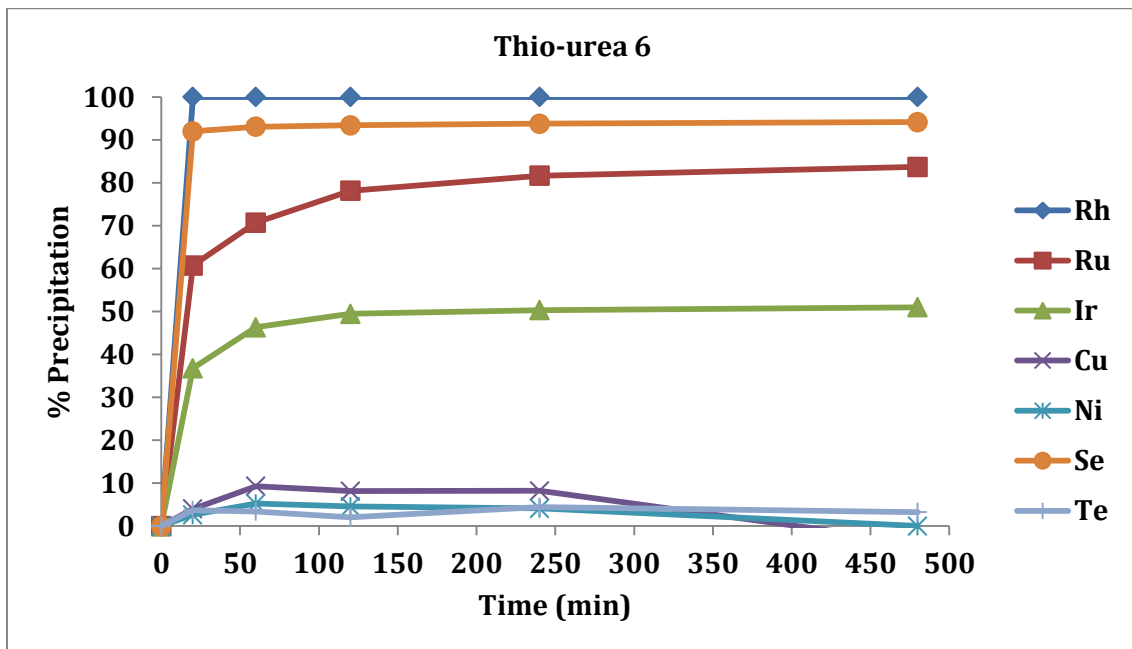


Figure 49: Effect of operating variables on precipitation (80°C, 200% excess, 500rpm, 7 bars)

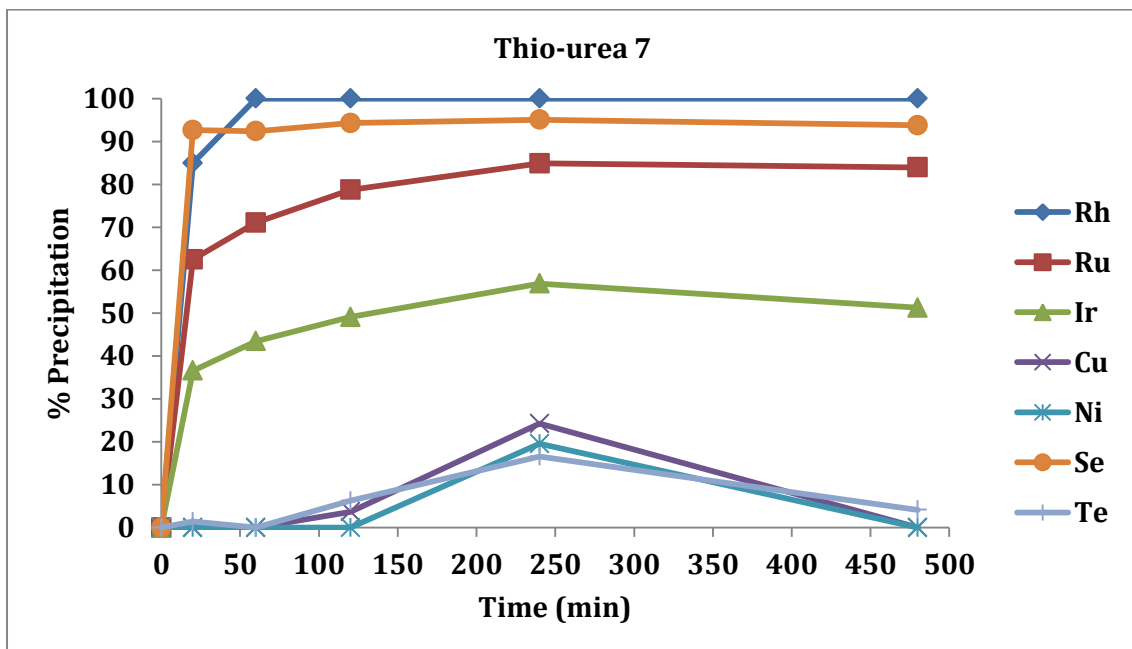


Figure 50: Effect of operating variables on precipitation (80°C, 200% excess, 500rpm, ambient pressure)

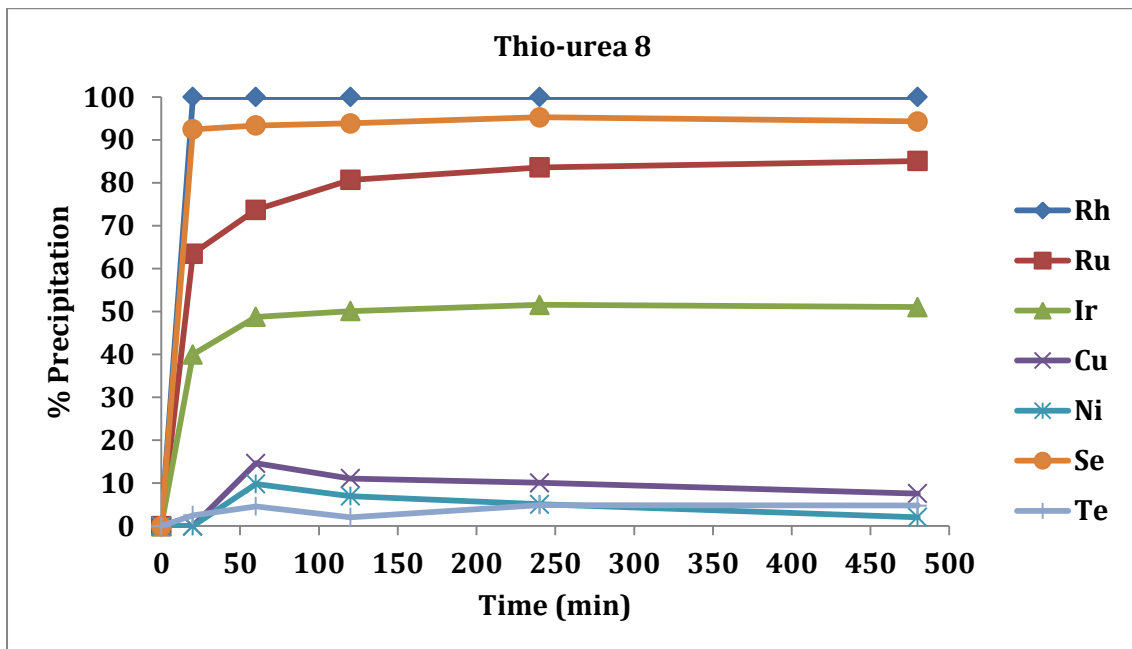


Figure 51: Effect of operating variables on precipitation (80°C, 320% excess, 250rpm, 7 bars)

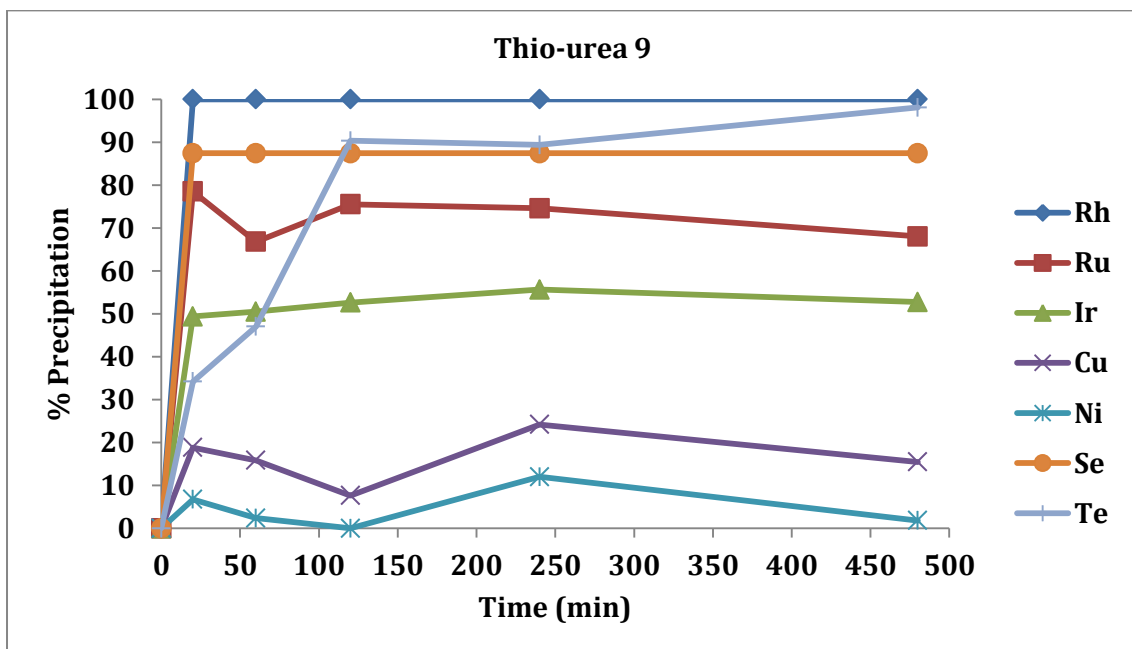


Figure 52: Effect of operating variables on precipitation (160°C, 200% excess, 250rpm, 7 bars)

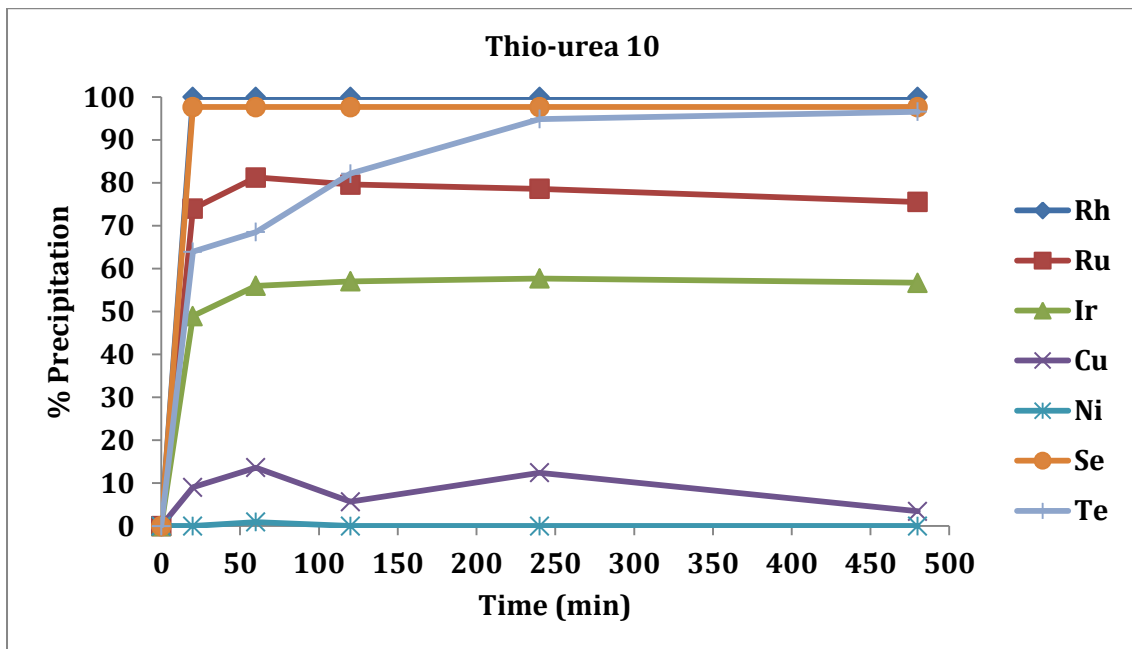


Figure 53: Effect of operating variables on precipitation (160°C, 200% excess, 500rpm, ambient pressure)

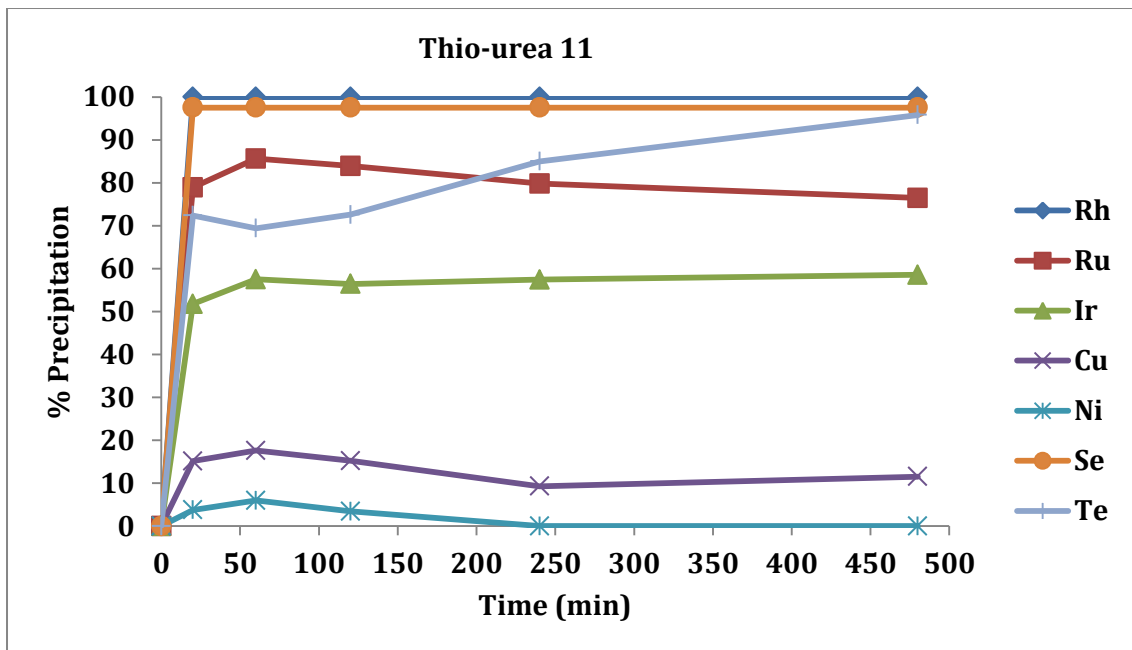


Figure 54: Effect of operating variables on precipitation (160°C, 200% excess, 250rpm, ambient pressure)

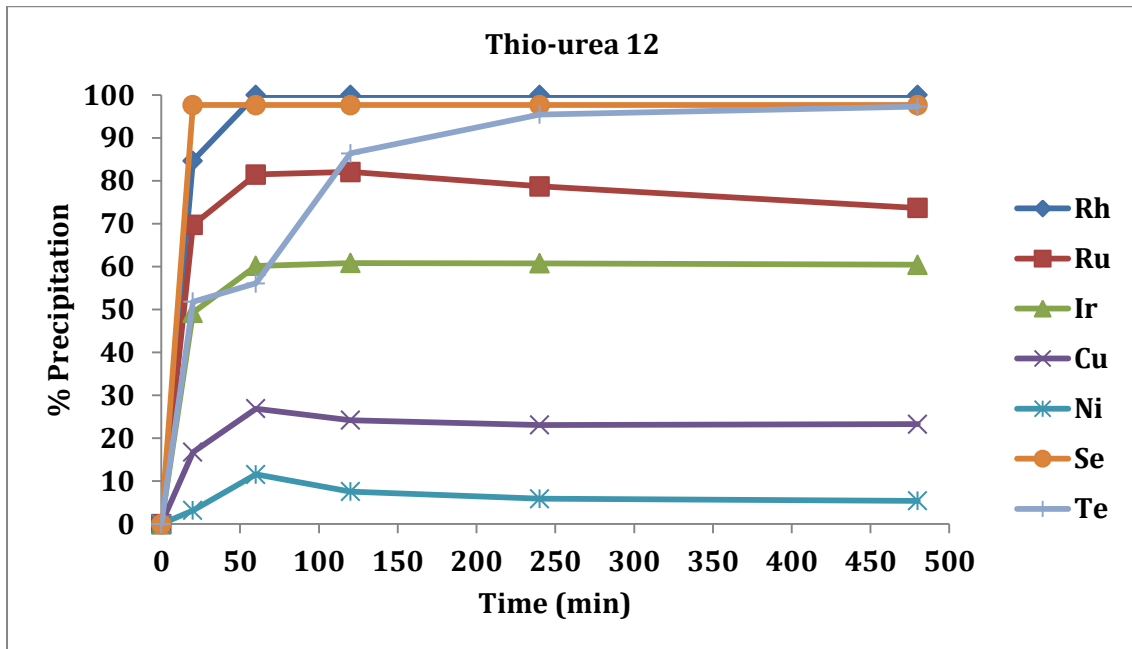


Figure 55: Effect of operating variables on precipitation (160°C, 320% excess, 500rpm, 7 bars)

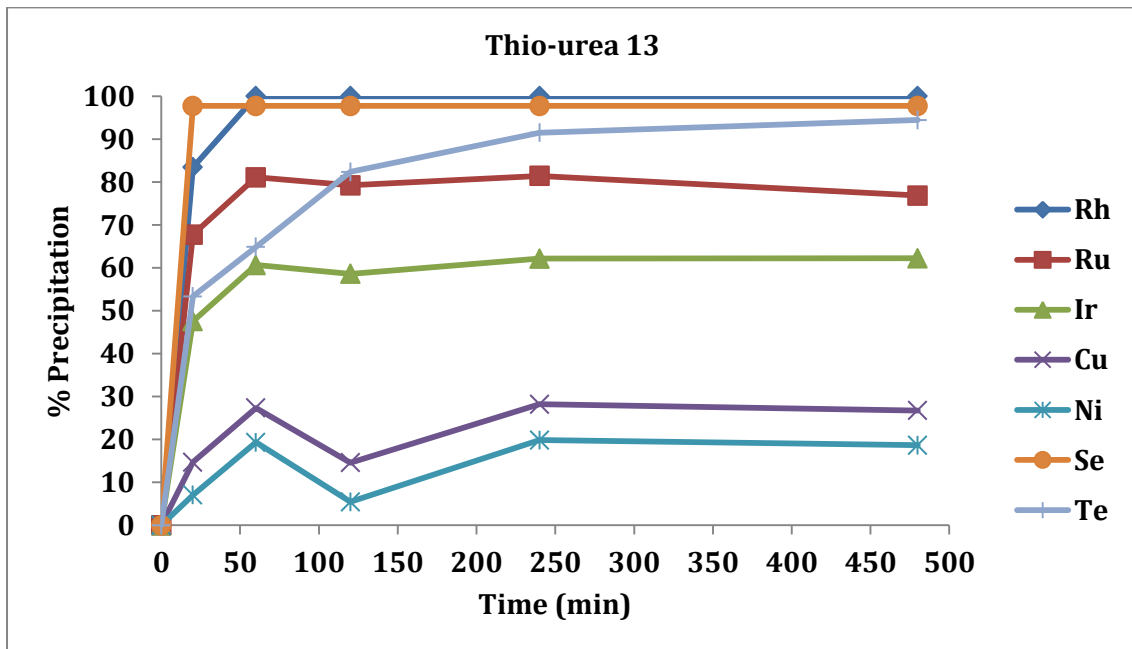


Figure 56: Effect of operating variables on precipitation (160°C, 200% excess, 500rpm, 7 bars)

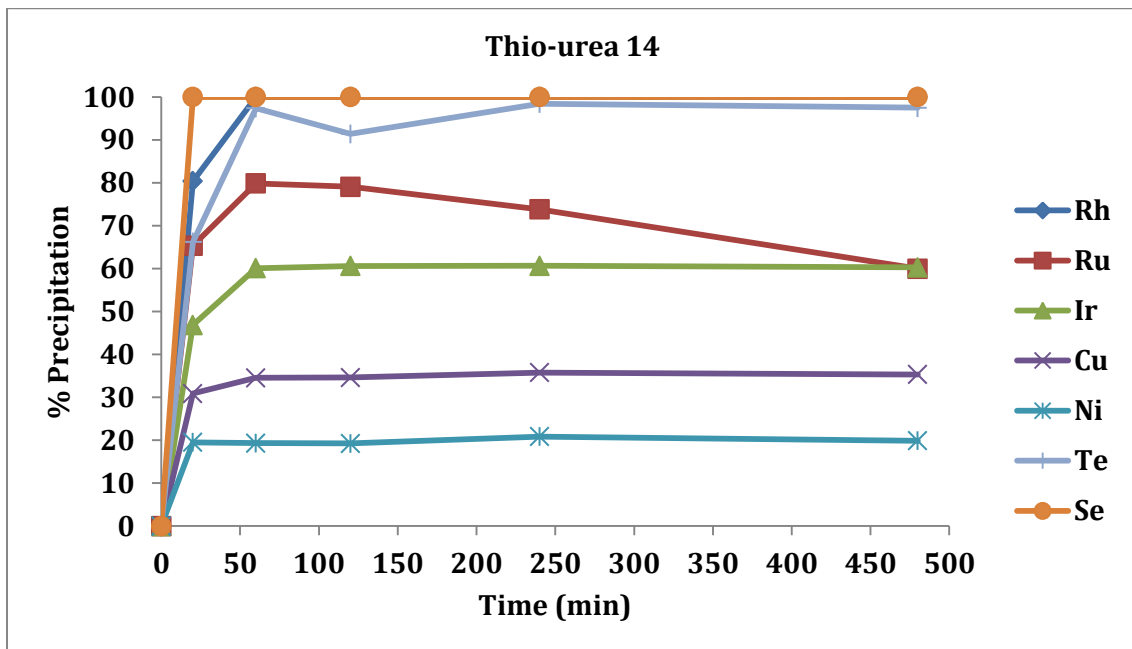


Figure 57: Effect of operating variables on precipitation (160°C, 320% excess, 250rpm, ambient pressure)

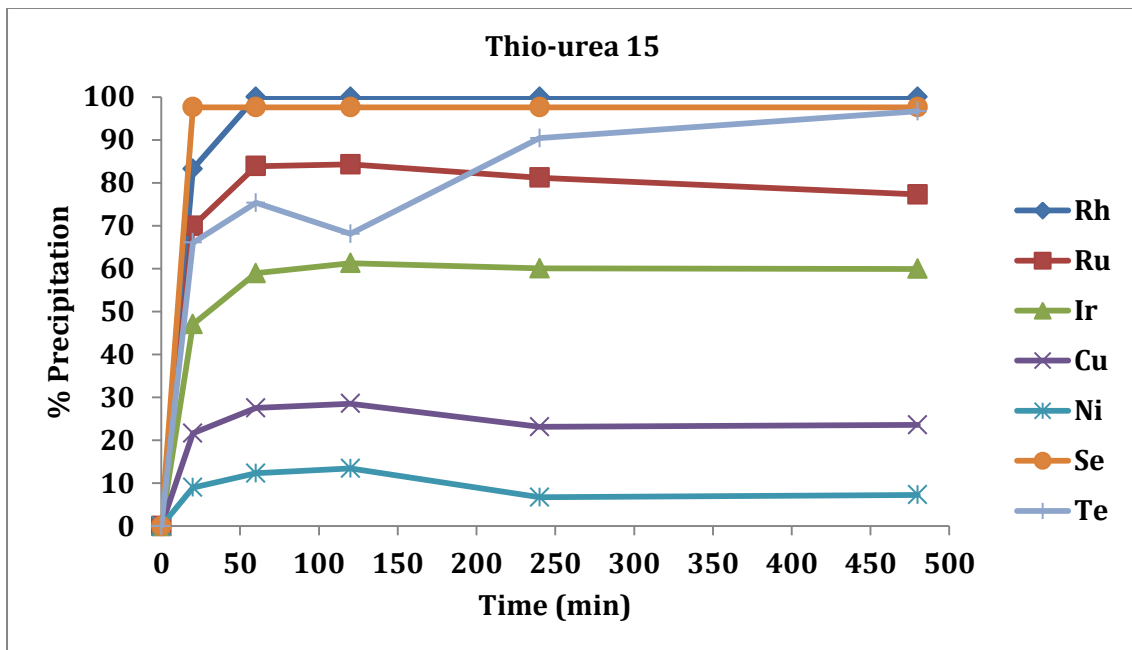


Figure 58: Effect of operating variables on precipitation (160°C, 320% excess, 250rpm, 7 bars)

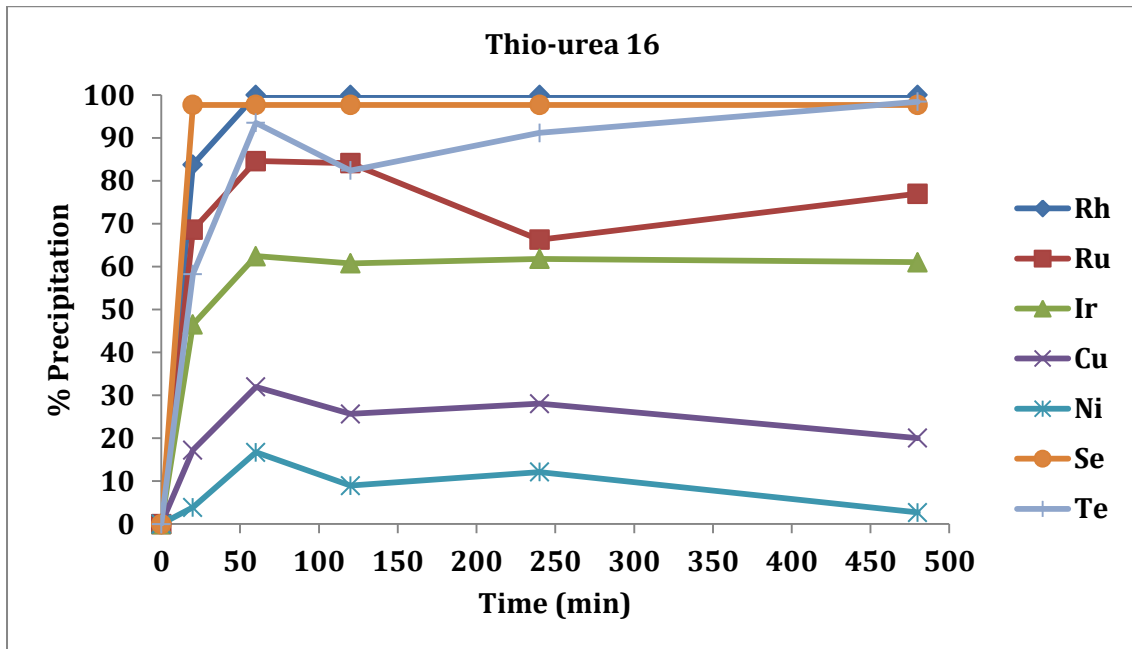


Figure 59: Effect of operating variables on precipitation (160°C, 320% excess, 500rpm, ambient pressure)

Sulphurous acid experimental data

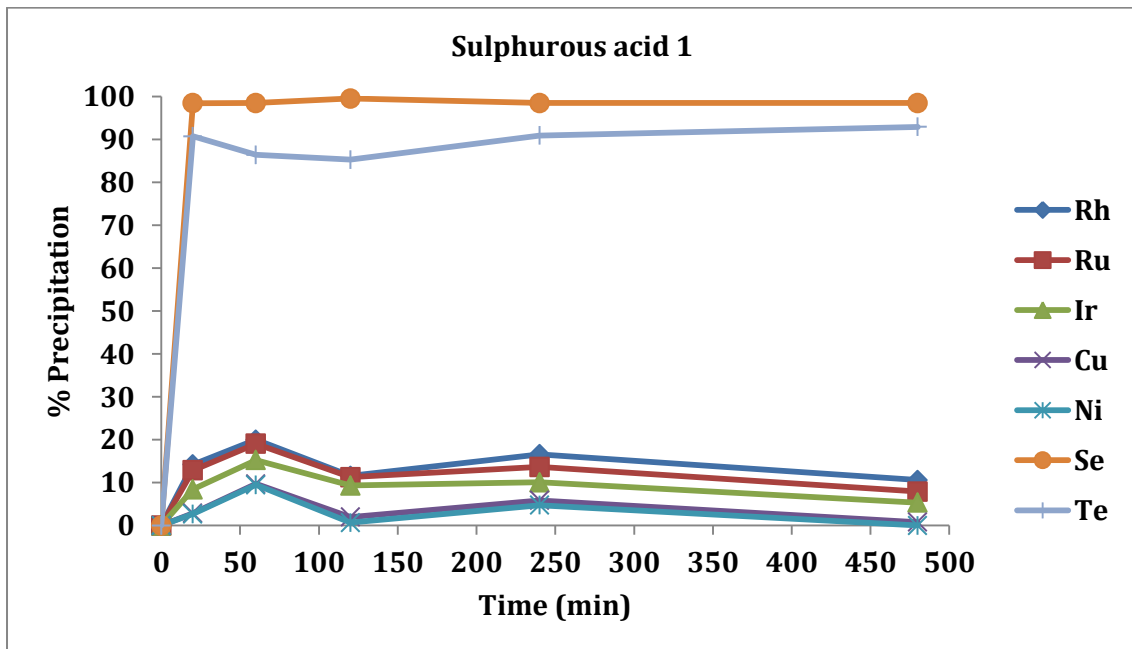


Figure 60: Effect of operating variables on precipitation (80°C, 960% excess, 250rpm, ambient pressure)

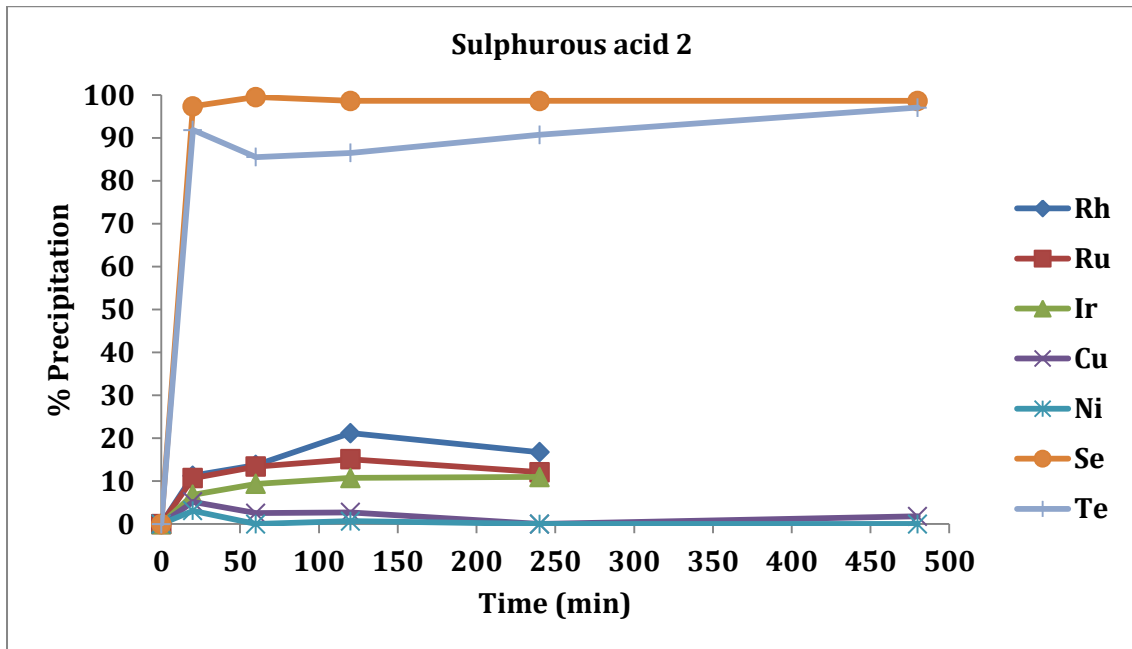


Figure 61: Effect of operating variables on precipitation (80°C, 960% excess, 500rpm, ambient pressure)

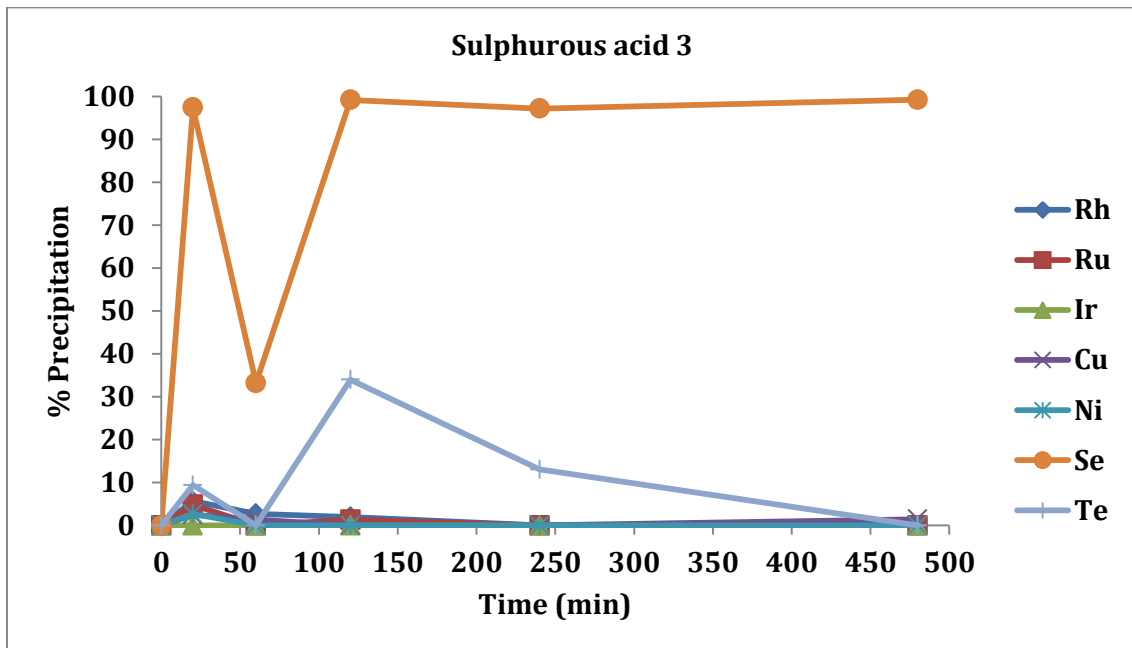


Figure 62: Effect of operating variables on precipitation (80°C, 720% excess, 250rpm, ambient pressure)

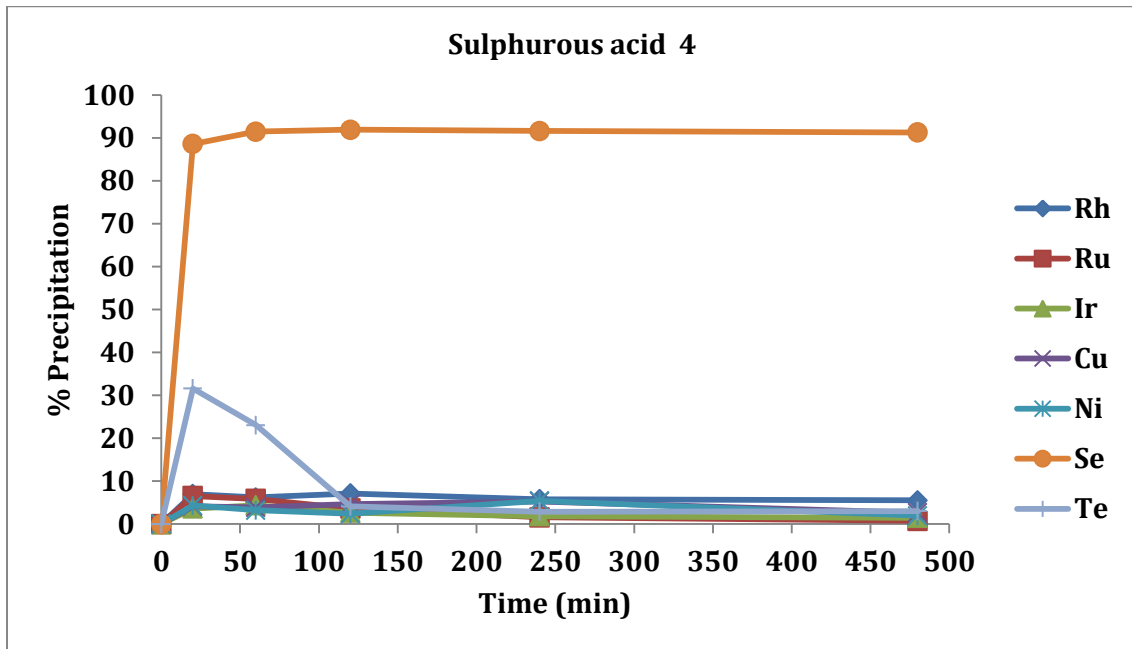


Figure 63: Effect of operating variables on precipitation (80°C, 720% excess, 500rpm, ambient pressure)

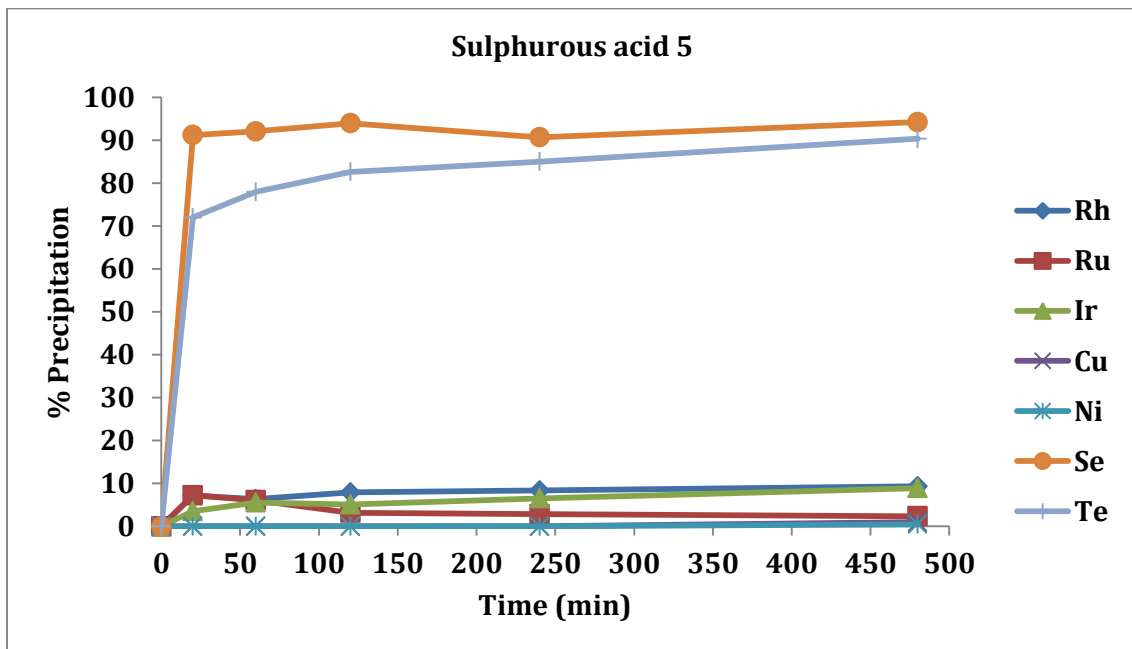


Figure 64: Effect of operating variables on precipitation (80°C, 960% excess, 500rpm, 7 bars)

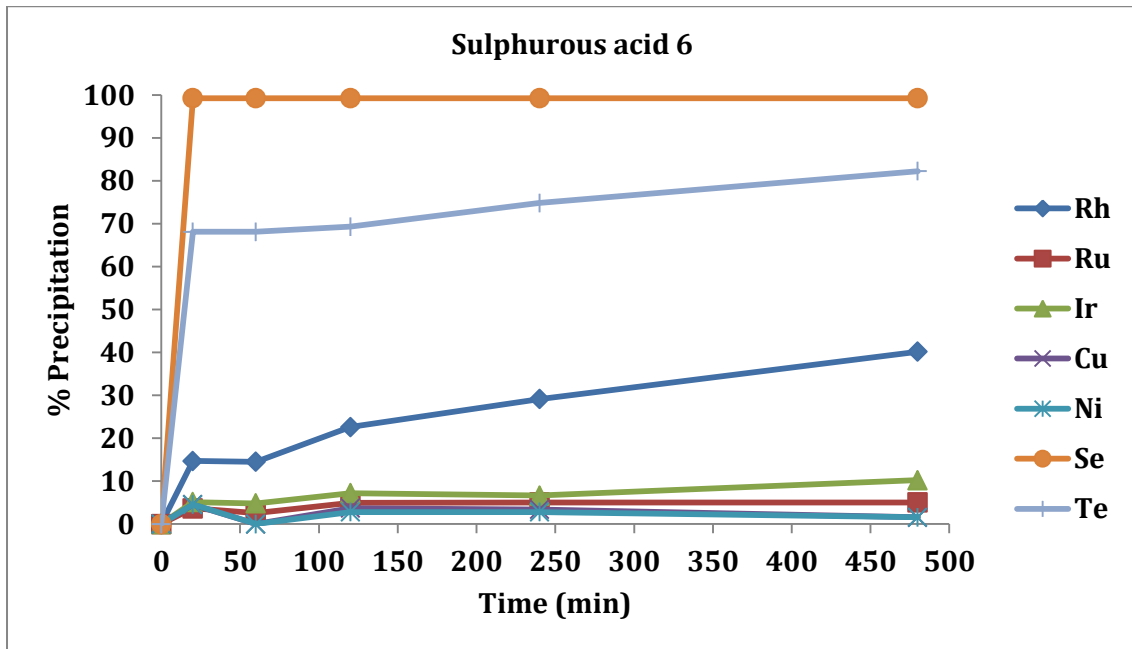


Figure 65: Effect of operating variables on precipitation (160°C, 960% excess, 500rpm, ambient pressure)

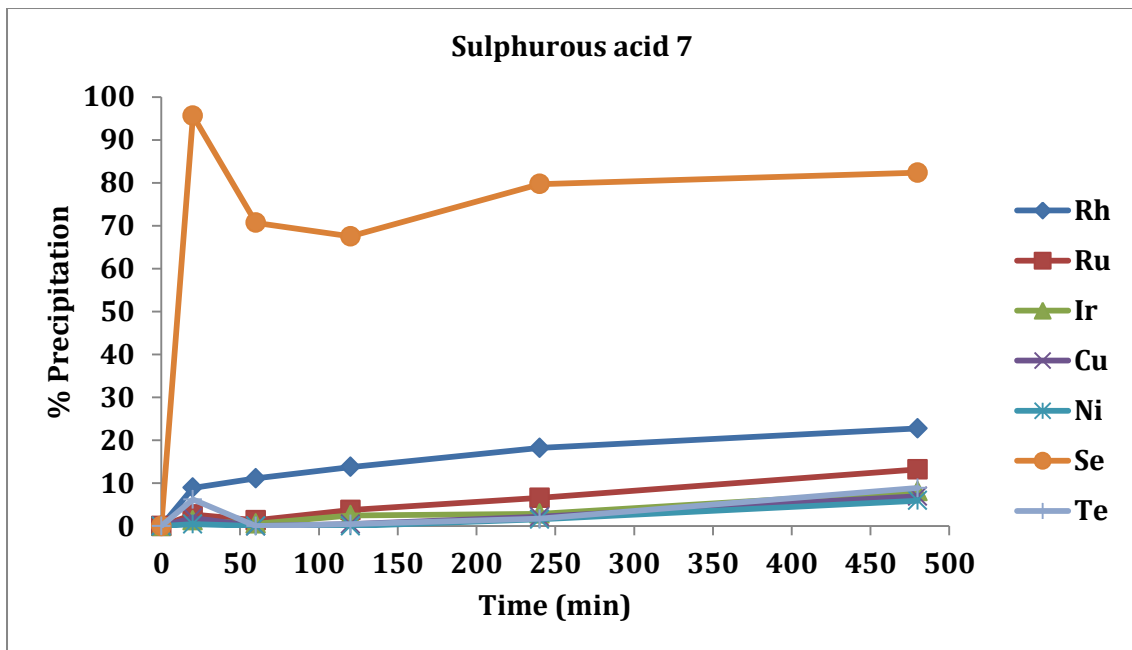


Figure 66: Effect of operating variables on precipitation (160°C, 720% excess, 500rpm, ambient pressure)

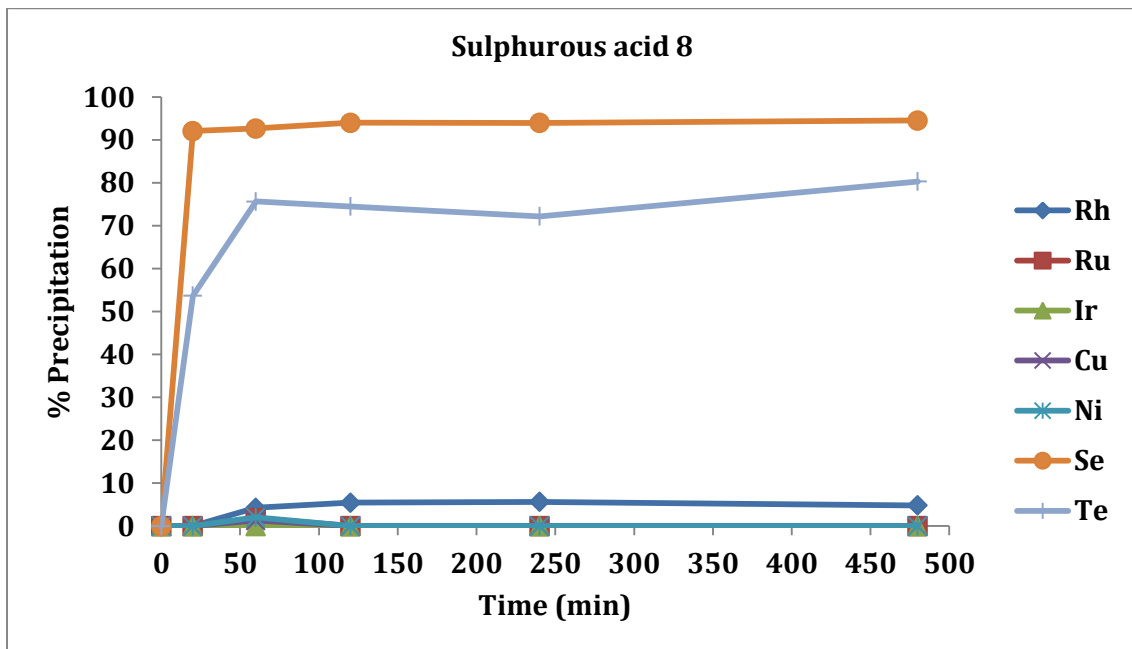


Figure 67: Effect of operating variables on precipitation (80°C, 960% excess, 250rpm, 7 bars)

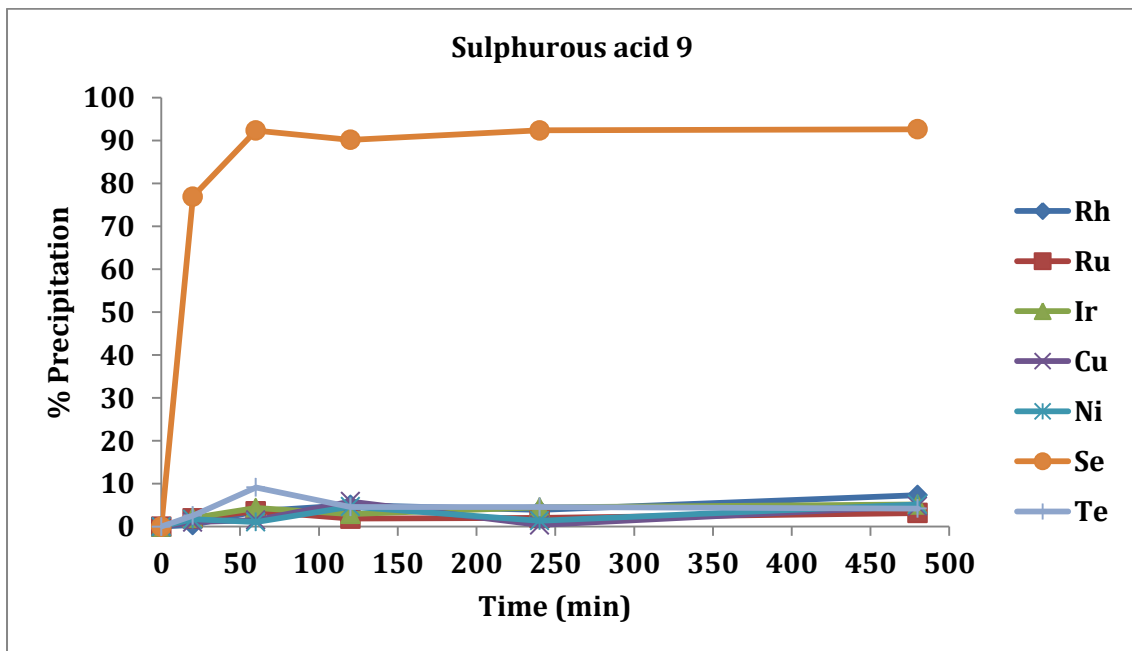


Figure 68: Effect of operating variables on precipitation (80°C, 720% excess, 500rpm, 7 bars)

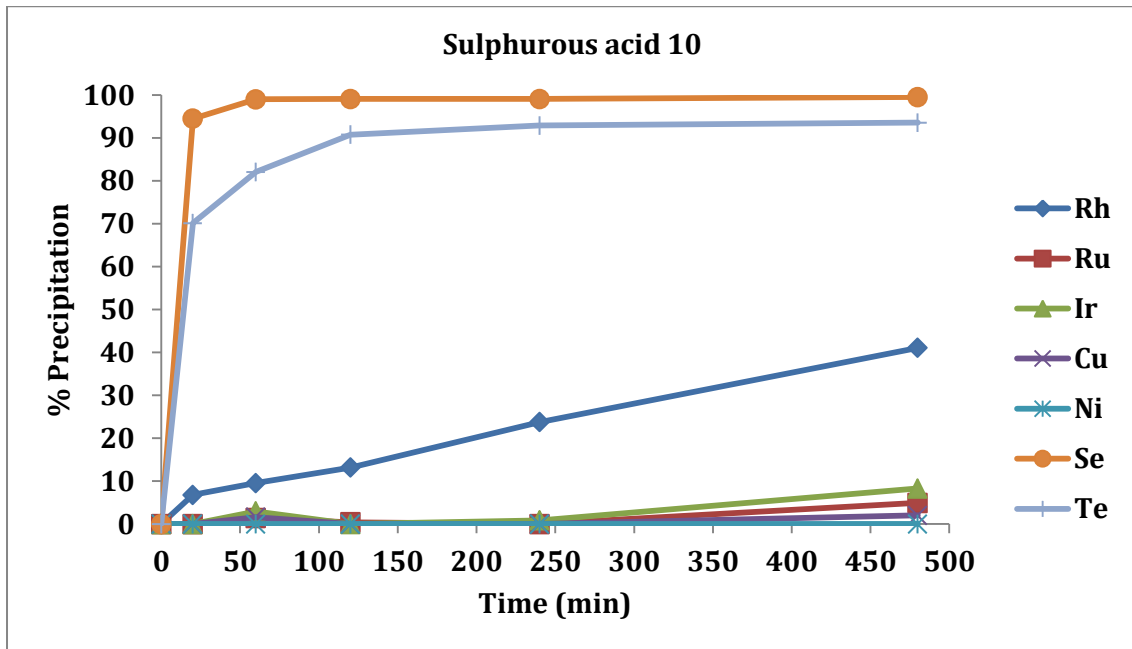


Figure 69: Effect of operating variables on precipitation (160°C, 960% excess, 250rpm, ambient pressure)

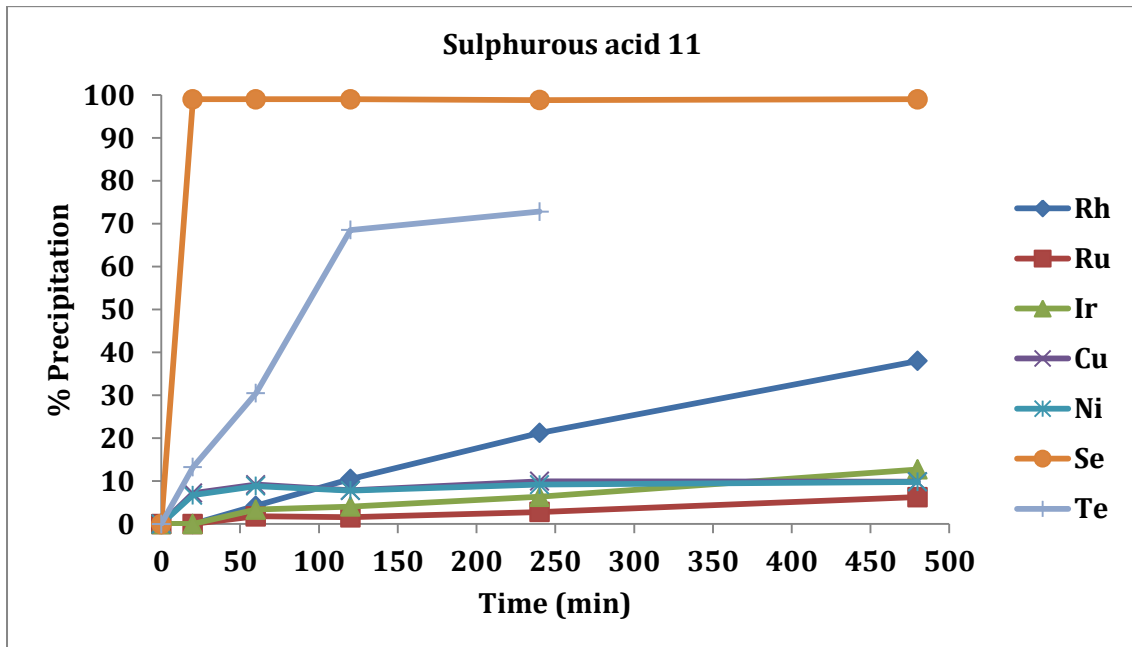


Figure 70: Effect of operating variables on precipitation (160°C, 960% excess, 500rpm, 7 bars)

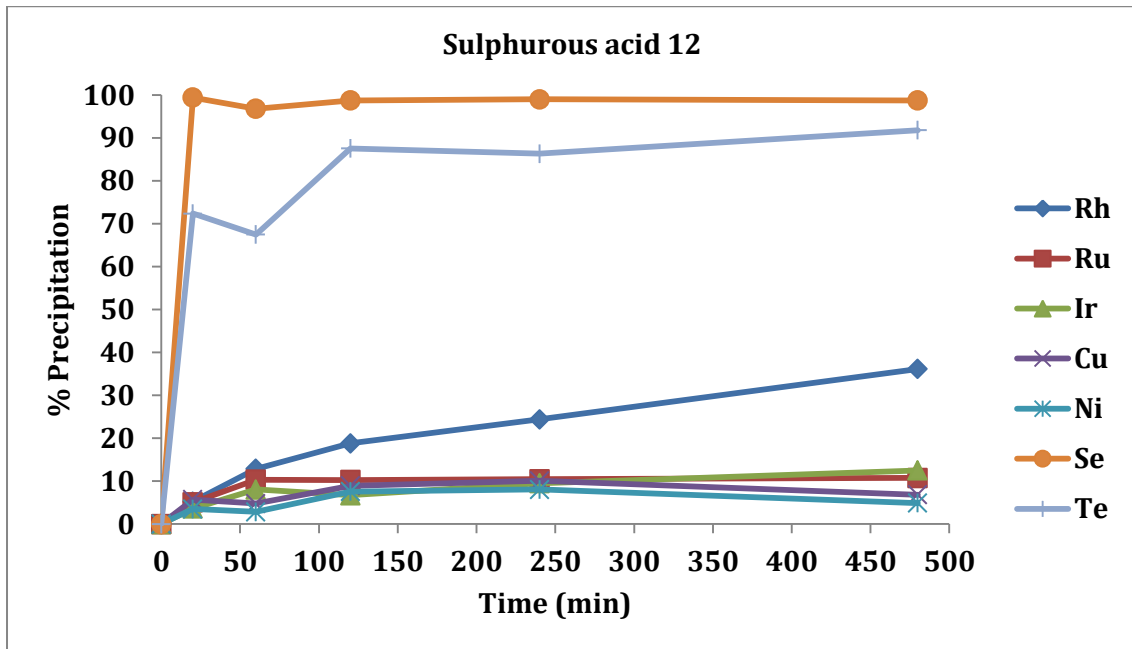


Figure 71: Effect of operating variables on precipitation (160°C, 960% excess, 250rpm, 7 bars)

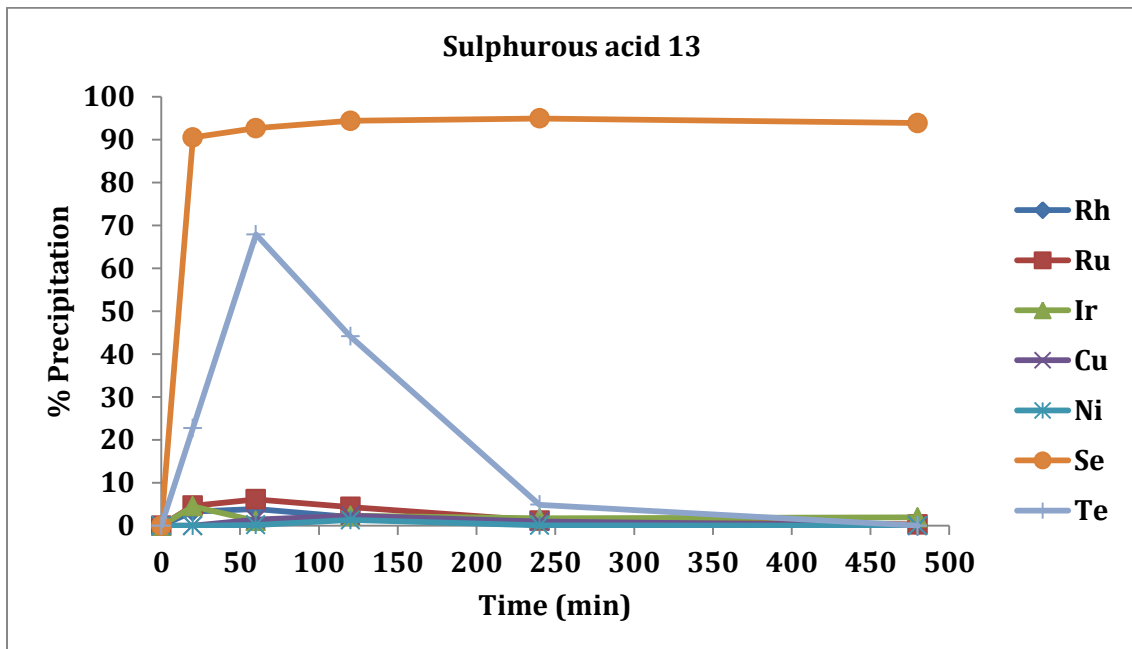


Figure 72: Effect of operating variables on precipitation (80°C, 720% excess, 250rpm, 7 bars)

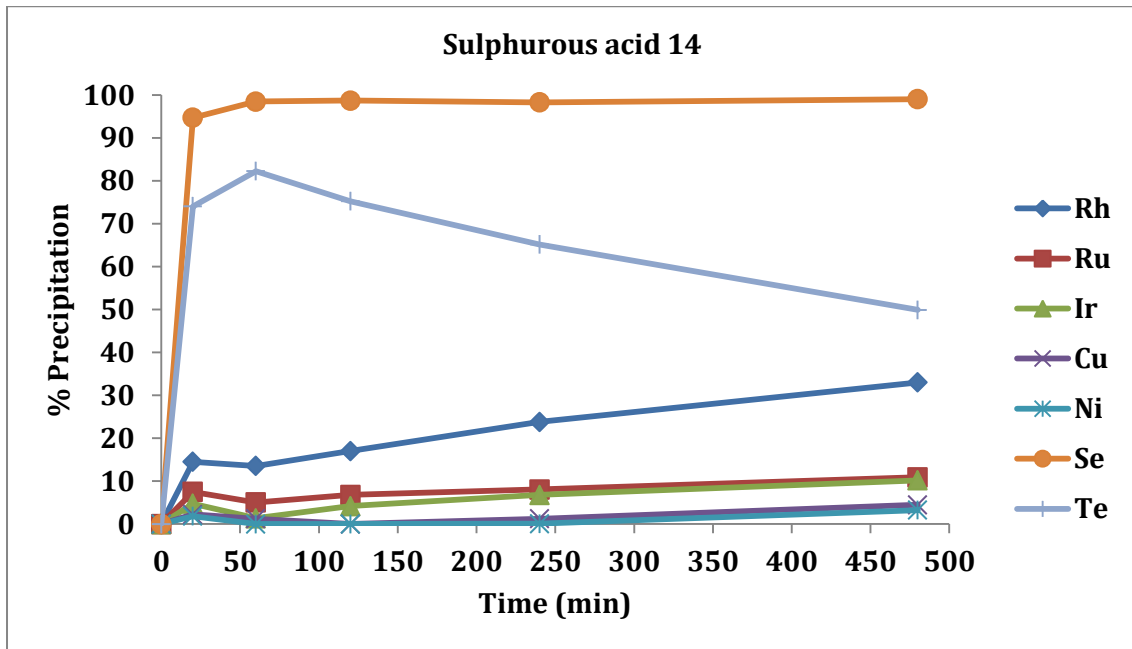


Figure 73: Effect of operating variables on precipitation (160°C, 720% excess, 250rpm, ambient pressure)

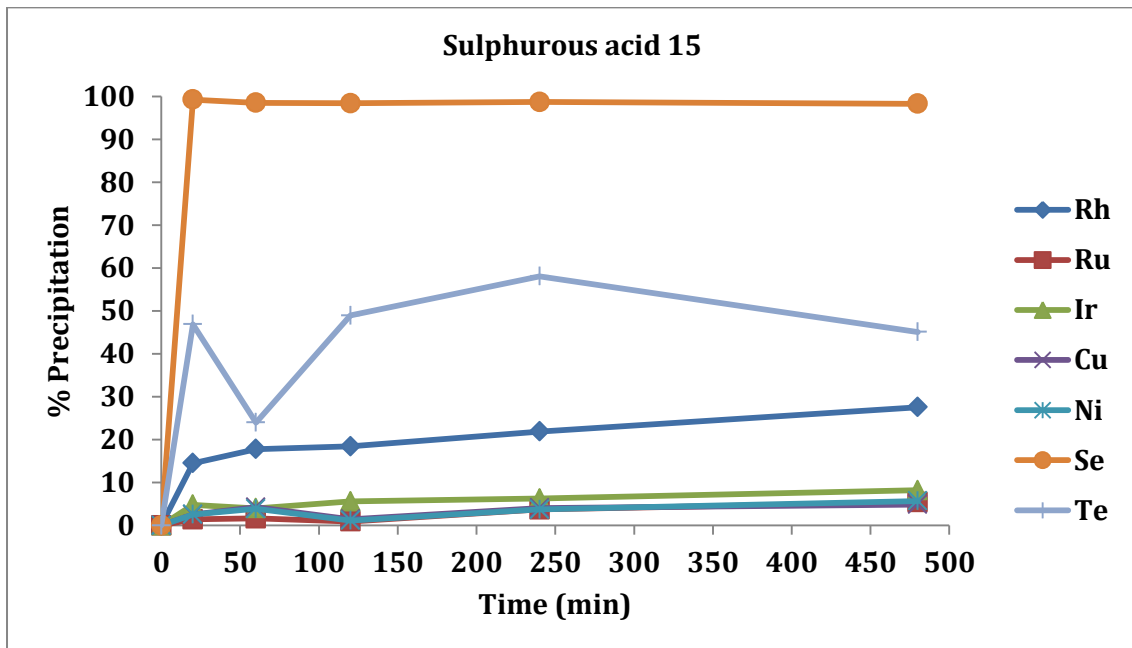


Figure 74: Effect of operating variables on precipitation (160°C, 720% excess, 500rpm, 7 bars)

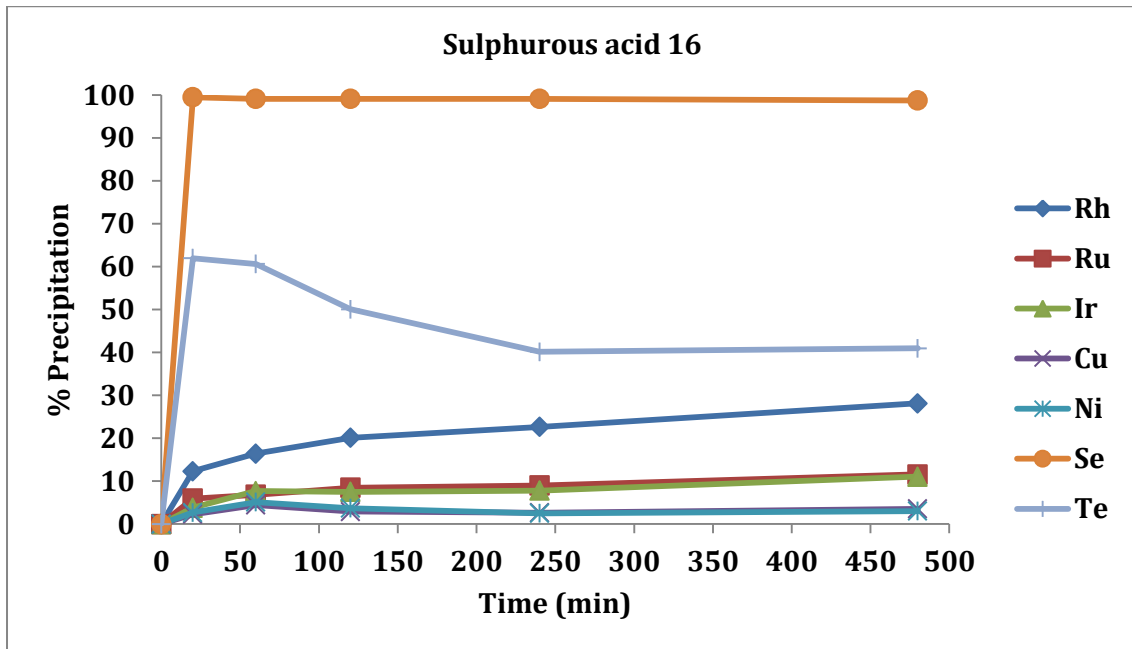


Figure 75: Effect of operating variables on precipitation (80°C, 720% excess, 250rpm, 7 bars)

APPENDIX: C**STATISTICAL ANALYSIS DATA***Table 61: Rh precipitation- ANOVA for selected factorial model (thio-urea data)*

	Sum of		Mean	F	p-value	
Source	Squares	df	Square	Value	Prob > F	
Model	135.36	7	19.34	12.72	0.0009	significant
A-A	92.64	1	92.64	60.92	< 0.0001	
C-C	5.18	1	5.18	3.4	0.1023	
D-D	3.52	1	3.52	2.31	0.1669	
AC	4.52	1	4.52	2.97	0.1231	
AD	0.28	1	0.28	0.18	0.6815	
CD	11.39	1	11.39	7.49	0.0256	
ACD	17.85	1	17.85	11.74	0.009	
Residual	12.16	8	1.52			
Cor Total	147.53	15				

The Model F-value of 12.72 implies the model is significant. There is only a 0.09% chance that a "Model F-Value" this large could occur due to noise.

Std. Dev.	1.23	R-Squared	0.9175
Mean	97.01	Adj R-Squared	0.8454
C.V. %	1.27	Pred R-Squared	0.6702
PRESS	48.66	Adeq Precision	10.322

Table 62: Ru precipitation- ANOVA for selected factorial model (thio-urea data)

Source	Sum of Squares	df	Mean Square	F Value	p-value Prob > F	
Model	129.5	9	14.39	6.48	0.0169	significant
A	5.52	1	5.52	2.49	0.1658	
B	1.32	1	1.32	0.6	0.4694	
C	0.42	1	0.42	0.19	0.6779	
D	18.06	1	18.06	8.14	0.0291	
AB	20.7	1	20.7	9.33	0.0224	
AC	55.5	1	55.5	25.01	0.0024	
AD	0.9	1	0.9	0.41	0.5472	
CD	1.56	1	1.56	0.7	0.4336	
ACD	25.5	1	25.5	11.49	0.0147	
Residual	13.32	6	2.22			
Cor Total	142.82	15				

The Model F-value of 6.48 implies the model is significant. There is only a 1.69% chance that a "Model F-Value" this large could occur due to noise.

Std. Dev.	1.49	R-Squared	0.9068
Mean	76.36	Adj R-Squared	0.7669
C.V. %	1.95	Pred R-Squared	0.337
PRESS	94.68	Adeq Precision	8.534

Table 63: Ir precipitation- ANOVA for selected factorial model (thio-urea data)

Source	Sum of Squares	df	Mean Square	F Value	p-value Prob > F	
Model	345.06	10	34.51	13.55	0.0051	significant
A	27.56	1	27.56	10.83	0.0217	
B	290.7	1	290.7	114.18	0.0001	
C	2.72	1	2.72	1.07	0.3485	
D	9.3	1	9.3	3.65	0.1142	
AB	0.09	1	0.09	0.035	0.8583	
AC	3.61	1	3.61	1.42	0.2872	
AD	1.00E-02	1	1.00E-02	3.93E-03	0.9525	
BC	0.81	1	0.81	0.32	0.5971	
BD	1.00E-02	1	1.00E-02	3.93E-03	0.9525	
CD	10.24	1	10.24	4.02	0.1012	
Residual	12.73	5	2.55			
Cor Total	357.79	15				

The Model F-value of 13.55 implies the model is significant. There is only a 0.51% chance that a "Model F-Value" this large could occur due to noise.

Std. Dev.	1.6	R-Squared	0.9644
Mean	52.52	Adj R-Squared	0.8933
C.V. %	3.04	Pred R-Squared	0.6357
PRESS	130.36	Adeq Precision	11.848

Table 64: Cu precipitation- ANOVA for selected factorial model (thio-urea data)

Source	Sum of Squares	df	Mean Square	F Value	p-value Prob > F	
Model	896.36	7	128.05	3.62	0.0459	significant
A	193.91	1	193.91	5.48	0.0473	
B	467.64	1	467.64	13.22	0.0066	
C	4.1	1	4.1	0.12	0.7423	
AB	76.13	1	76.13	2.15	0.1806	
AC	5.41	1	5.41	0.15	0.7061	
BC	20.93	1	20.93	0.59	0.4639	
ABC	128.26	1	128.26	3.62	0.0934	
Residual	283.08	8	35.38			
Cor Total	1179.44	15				

The Model F-value of 3.62 implies the model is significant. There is only a 4.59% chance that a "Model F-Value" this large could occur due to noise.

Std. Dev.	5.95	R-Squared	0.76
Mean	15.56	Adj R-Squared	0.55
C.V. %	38.24	Pred R-Squared	0.04
PRESS	1132.3	Adeq Precision	5.813

Table 65: Ni precipitation-ANOVA for selected factorial model (thio-urea data)

Source	Sum of Squares	df	Mean Square	F Value	p-value Prob > F	
Model	162.35	7	23.19	6.9	0.0071	significant
A	123.21	1	123.21	36.67	0.0003	
B	7.29	1	7.29	2.17	0.179	
C	2.56	1	2.56	0.76	0.4082	
AB	1.21	1	1.21	0.36	0.565	
AC	0.16	1	0.16	0.048	0.8327	
BC	6.76	1	6.76	2.01	0.1938	
ABC	21.16	1	21.16	6.3	0.0364	
Residual	26.88	8	3.36			
Cor Total	189.23	15				

The Model F-value of 6.90 implies the model is significant. There is only a 0.71% chance that a "Model F-Value" this large could occur due to noise.

Std. Dev.	1.83	R-Squared	0.858
Mean	6.67	Adj R-Squared	0.7337
C.V. %	27.46	Pred R-Squared	0.4318
PRESS	107.52	Adeq Precision	6.481

Table 66: Se precipitation-ANOVA for selected factorial model (thio-urea data)

Source	Sum of Squares	df	Mean Square	F Value	p-value Prob > F	
Model	108.12	2	54.06	111.34	< 0.0001	significant
A	3.06	1	3.06	6.31	0.026	
B	105.06	1	105.06	216.37	< 0.0001	
Residual	6.31	13	0.49			
Cor Total	114.44	15				

The Model F-value of 111.34 implies the model is significant. There is only a 0.01% chance that a "Model F-Value" this large could occur due to noise.

Std. Dev.	0.7	R-Squared	0.9448
Mean	95.81	Adj R-Squared	0.9364
C.V. %	0.73	Pred R-Squared	0.9164
PRESS	9.56	Adeq Precision	19.885

Table 67: Te precipitation-ANOVA for selected factorial model (thio-urea data)

Source	Sum of Squares	df	Mean Square	F Value	p-value Prob > F	
Model	21609	1	21609	922.34	< 0.0001	significant
B	21609	1	21609	922.34	< 0.0001	
Residual	328	14	23.43			
Cor Total	21937	15				

The Model F-value of 922.34 implies the model is significant. There is only a 0.01% chance that a "Model F-Value" this large could occur due to noise.

Std. Dev.	4,84	R-Squared	0,985
Mean	43,25	Adj R-Squared	0,984
C.V. %	11,19	Pred R-Squared	0,9805
PRESS	428,41	Adeq Precision	42,95

Table 68: Rh precipitation- ANOVA for selected factorial model (sulphurous acid data)

Source	Sum of Squares	df	Mean Square	F Value	p-value Prob > F	
Model	488.07	5	97.61	10.75	0.0009	significant
A	49	1	49	5.4	0.0426	
B	325.8	1	325.8	35.88	0.0001	
C	48.3	1	48.3	5.32	0.0438	
AB	38.44	1	38.44	4.23	0.0667	
BC	26.52	1	26.52	2.92	0.1182	
Residual	90.81	10	9.08			
Cor Total	578.88	15				

The Model F-value of 10.75 implies the model is significant. There is only a 0.09% chance that a "Model F-Value" this large could occur due to noise.

Std. Dev.	3.01	R-Squared	0.8431
Mean	11.39	Adj R-Squared	0.7647
C.V. %	26.46	Pred R-Squared	0.5984
PRESS	232.47	Adeq Precision	8.67

Table 69: Ru precipitation- ANOVA for selected factorial model (sulphurous acid data)

Source	Sum of Squares	df	Mean Square	F Value	p-value Prob > F	
Model	170.47	7	24.35	5.71	0.0127	significant
A	12.96	1	12.96	3.04	0.1195	
B	3.61	1	3.61	0.85	0.3845	
C	20.7	1	20.7	4.85	0.0587	
AB	41.6	1	41.6	9.75	0.0142	
AC	9	1	9	2.11	0.1844	
BC	39.69	1	39.69	9.3	0.0158	
ABC	42.9	1	42.9	10.06	0.0132	
Residual	34.13	8	4.27			
Cor Total	204.6	15				

The Model F-value of 5.71 implies the model is significant. There is only a 1.27% chance that a "Model F-Value" this large could occur due to noise.

Std. Dev.	2.07	R-Squared	0.8332
Mean	4.81	Adj R-Squared	0.6872
C.V. %	42.92	Pred R-Squared	0.3327
PRESS	136.52	Adeq Precision	7.258

Table 70: Ir precipitation- ANOVA for selected factorial model (sulphurous acid data)

Source	Sum of Squares	df	Mean Square	F Value	p-value Prob > F	
Model	89.54	7	12.79	3.61	0.0461	significant
A	17.22	1	17.22	4.87	0.0585	
B	2.4	1	2.4	0.68	0.4339	
C	0.72	1	0.72	0.2	0.6634	
AB	14.82	1	14.82	4.19	0.0749	
AC	18.06	1	18.06	5.1	0.0538	
BC	20.7	1	20.7	5.85	0.042	
ABC	15.6	1	15.6	4.41	0.069	
Residual	28.32	8	3.54			
Cor Total	117.86	15				

The Model F-value of 3.61 implies the model is significant. There is only a 4.61% chance that a "Model F-Value" this large could occur due to noise.

Std. Dev.	1.88	R-Squared	0.7597
Mean	4.24	Adj R-Squared	0.5495
C.V. %	44.4	Pred R-Squared	0.0388
PRESS	113.28	Adeq Precision	6.088

Table 71: Cu precipitation- ANOVA for selected factorial model (sulphurous acid data)

Source	Sum of Squares	df	Mean Square	F Value	p-value Prob > F	
Model	38.53	7	5.5	12.35	0.001	significant
A	3.52	1	3.52	7.89	0.0229	
B	5.88	1	5.88	13.2	0.0067	
C	0.53	1	0.53	1.18	0.3091	
AB	2.64	1	2.64	5.93	0.0409	
AC	1.5	1	1.5	3.37	0.1038	
BC	15.02	1	15.02	33.7	0.0004	
ABC	9.46	1	9.46	21.22	0.0017	
Residual	3.57	8	0.45			
Cor Total	42.1	15				

The Model F-value of 12.35 implies the model is significant. There is only a 0.10% chance that a "Model F-Value" this large could occur due to noise.

Std. Dev.	0.67	R-Squared	0.9153
Mean	2.94	Adj R-Squared	0.8412
C.V. %	22.68	Pred R-Squared	0.6613
PRESS	14.26	Adeq Precision	11.652

Table 72: Ni precipitation- ANOVA for selected factorial model (sulphurous acid data)

Source	Sum of Squares	df	Mean Square	F Value	p-value Prob > F	
Model	41.22	11	3.75	16.61	0.0077	significant
A	0.77	1	0.77	3.39	0.1393	
B	3.71	1	3.71	16.42	0.0154	
C	1.38	1	1.38	6.12	0.0687	
D	1.5	1	1.5	6.65	0.0614	
AB	1.27	1	1.27	5.61	0.077	
AC	3.9	1	3.9	17.29	0.0142	
AD	0.076	1	0.076	0.34	0.5937	
BC	16.2	1	16.2	71.8	0.0011	
BD	3.15	1	3.15	13.96	0.0202	
ABC	4.1	1	4.1	18.17	0.013	
ABD	5.18	1	5.18	22.94	0.0087	
Residual	0.9	4	0.23			
Cor Total	42.12	15				

The Model F-value of 16.61 implies the model is significant. There is only a 0.77% chance that a "Model F-Value" this large could occur due to noise.

Std. Dev.	0.47	R-Squared	0.9786
Mean	2.52	Adj R-Squared	0.9197
C.V. %	18.86	Pred R-Squared	0.6572
PRESS	14.44	Adeq Precision	17.26

Table 73: Se precipitation- ANOVA for selected factorial model (sulphurous acid data)

Source	Sum of Squares	df	Mean Square	F Value	p-value Prob > F	
Model	392.75	4	98.19	5.66	0.01	significant
A	351.56	1	351.56	20.28	0.0009	
B	3.06	1	3.06	0.18	0.6823	
C	27.56	1	27.56	1.59	0.2334	
D	10.56	1	10.56	0.61	0.4515	
Residual	190.69	11	17.34			
Cor Total	583.44	15				

The Model F-value of 5.66 implies the model is significant. There is only a 1.00% chance that a "Model F-Value" this large could occur due to noise.

Std. Dev.	4.16	R-Squared	0.6732
Mean	94.31	Adj R-Squared	0.5543
C.V. %	4.41	Pred R-Squared	0.3085
PRESS	403.44	Adeq Precision	6.23

Table 74: Te precipitation- ANOVA for selected factorial model (sulphurous acid data)

Source	Sum of Squares	df	Mean Square	F Value	p-value Prob > F	
Model	14448.47	10	1444.85	8.53	0.0144	significant
A	7774.83	1	7774.83	45.89	0.0011	
B	708.89	1	708.89	4.18	0.0962	
C	40.64	1	40.64	0.24	0.645	
D	1070.93	1	1070.93	6.32	0.0536	
AB	1570.14	1	1570.14	9.27	0.0286	
AC	1070.93	1	1070.93	6.32	0.0536	
AD	606.39	1	606.39	3.58	0.1171	
BC	154.38	1	154.38	0.91	0.3836	
BD	1415.64	1	1415.64	8.36	0.0342	
CD	35.7	1	35.7	0.21	0.6655	
Residual	847.07	5	169.41			
Cor Total	15295.54	15				

The Model F-value of 8.53 implies the model is significant. There is only a 1.44% chance that a "Model F-Value" this large could occur due to noise.

Std. Dev.	13.02	R-Squared	0.9446
Mean	52.66	Adj R-Squared	0.8339
C.V. %	24.72	Pred R-Squared	0.4329
PRESS	8674.03	Adeq Precision	8.578

Pareto plots of effects

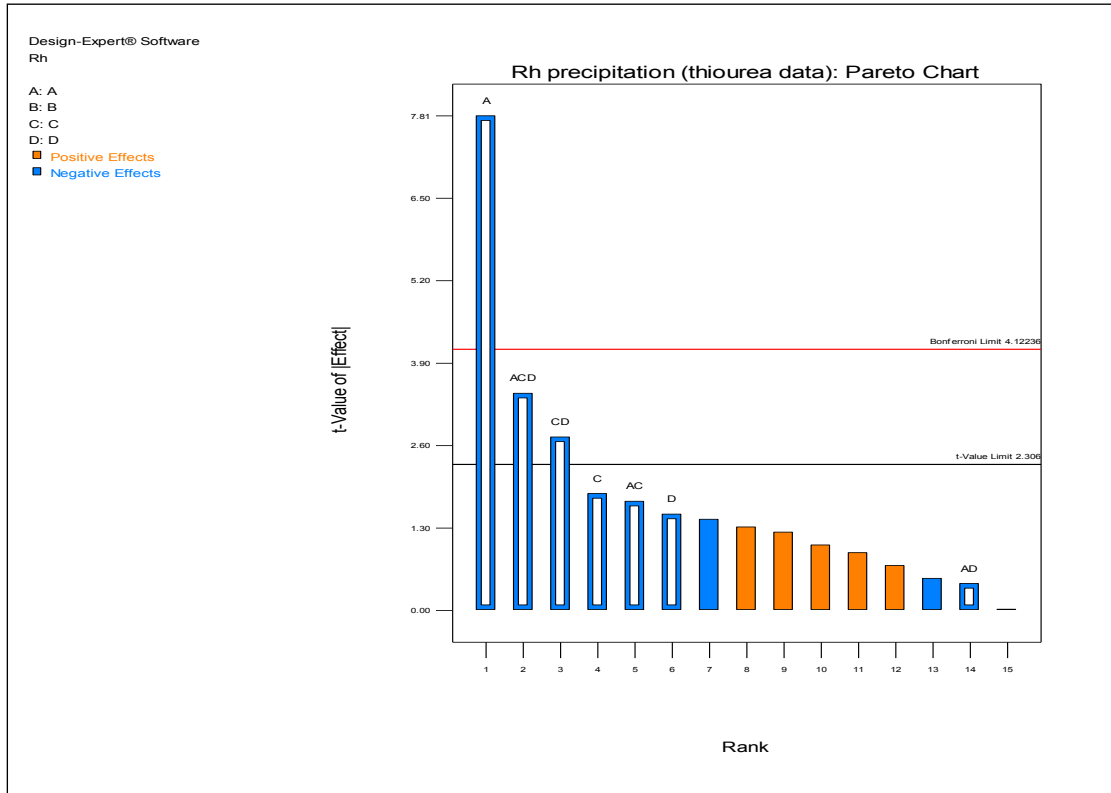


Figure 76: Pareto plots of effects for the Rh response (thio-urea data)

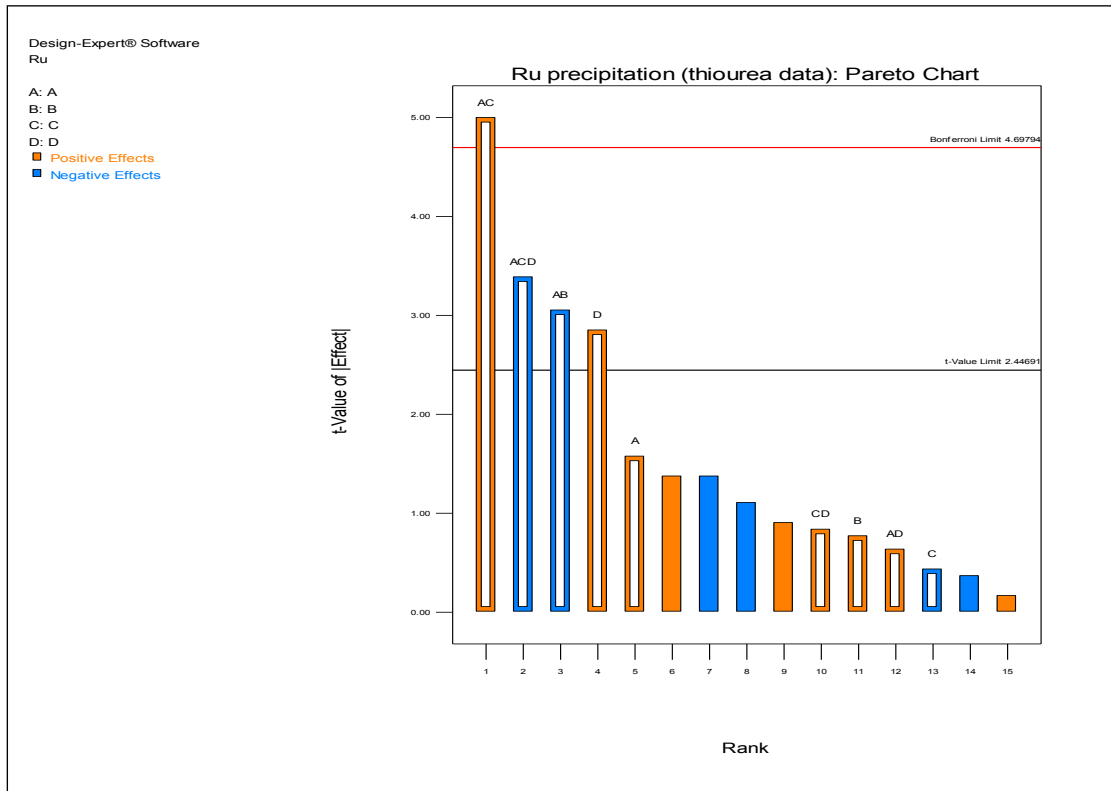


Figure 77: Pareto plots of effects for the Ru response (thio-urea data)

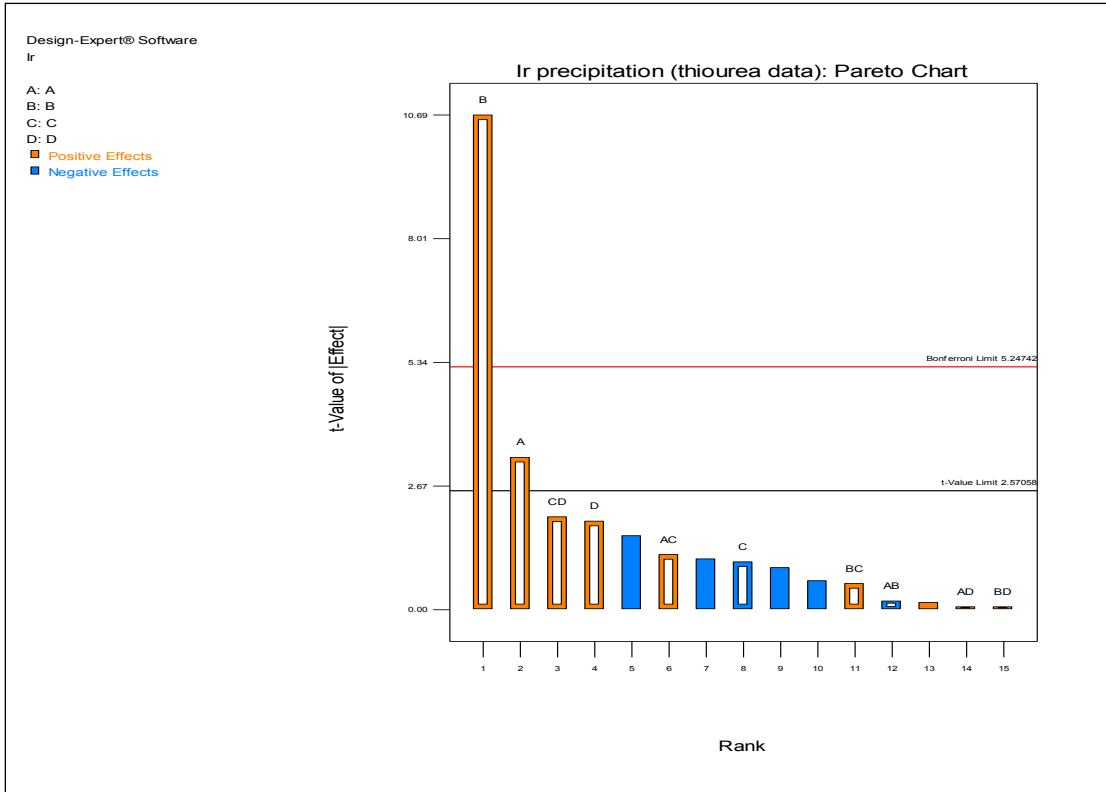


Figure 78: Pareto plots of effects for the Ir response (thio-urea data)

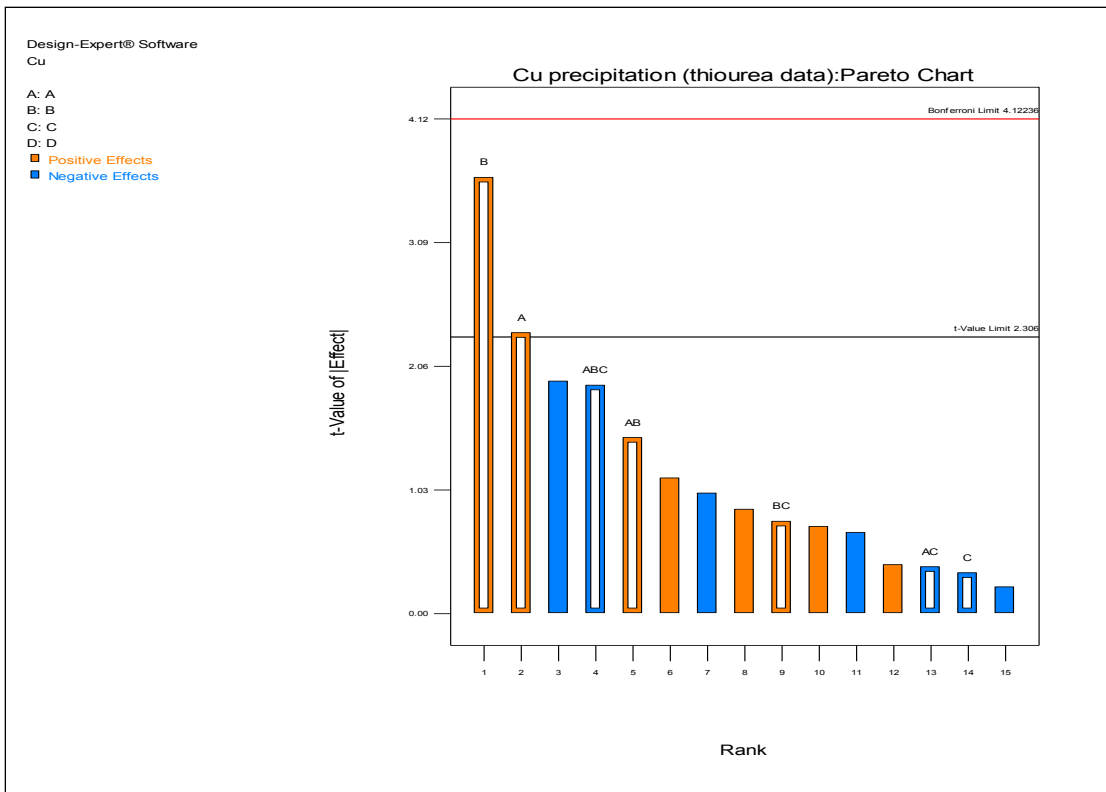


Figure 79: Pareto plots of effects for the Cu response (thio-urea data)

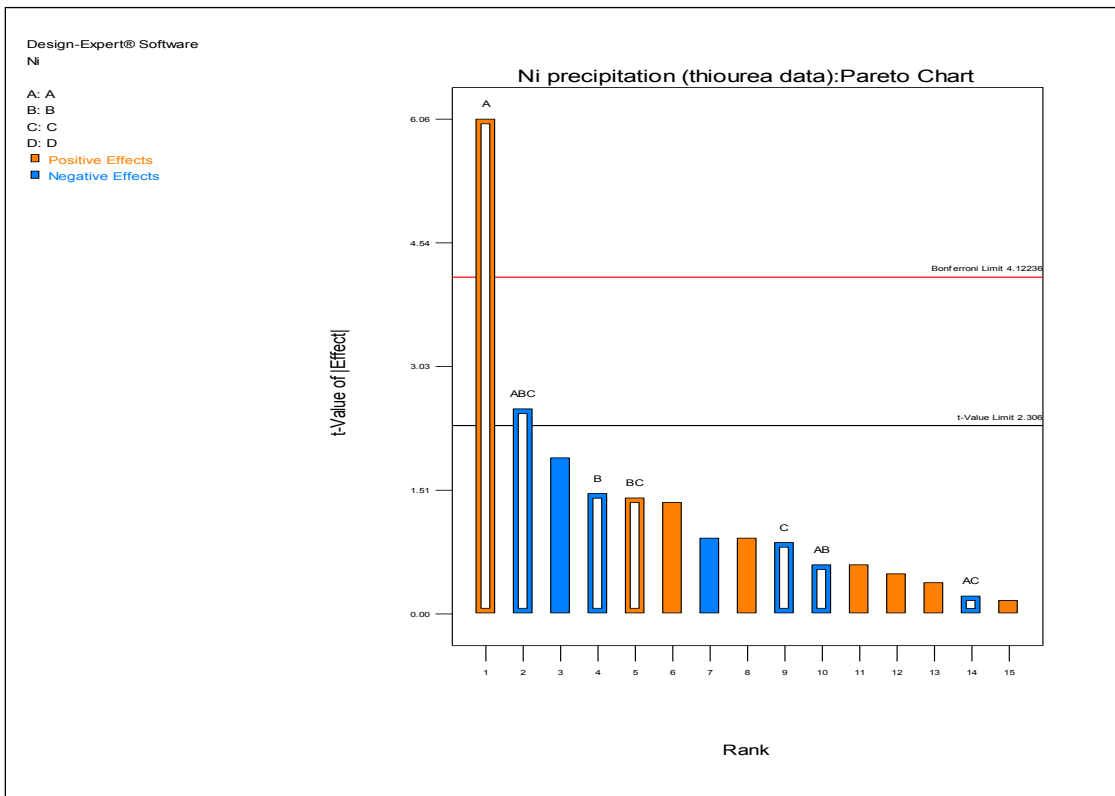


Figure 80: Pareto plots of effects for the Ni response (thio-urea data)

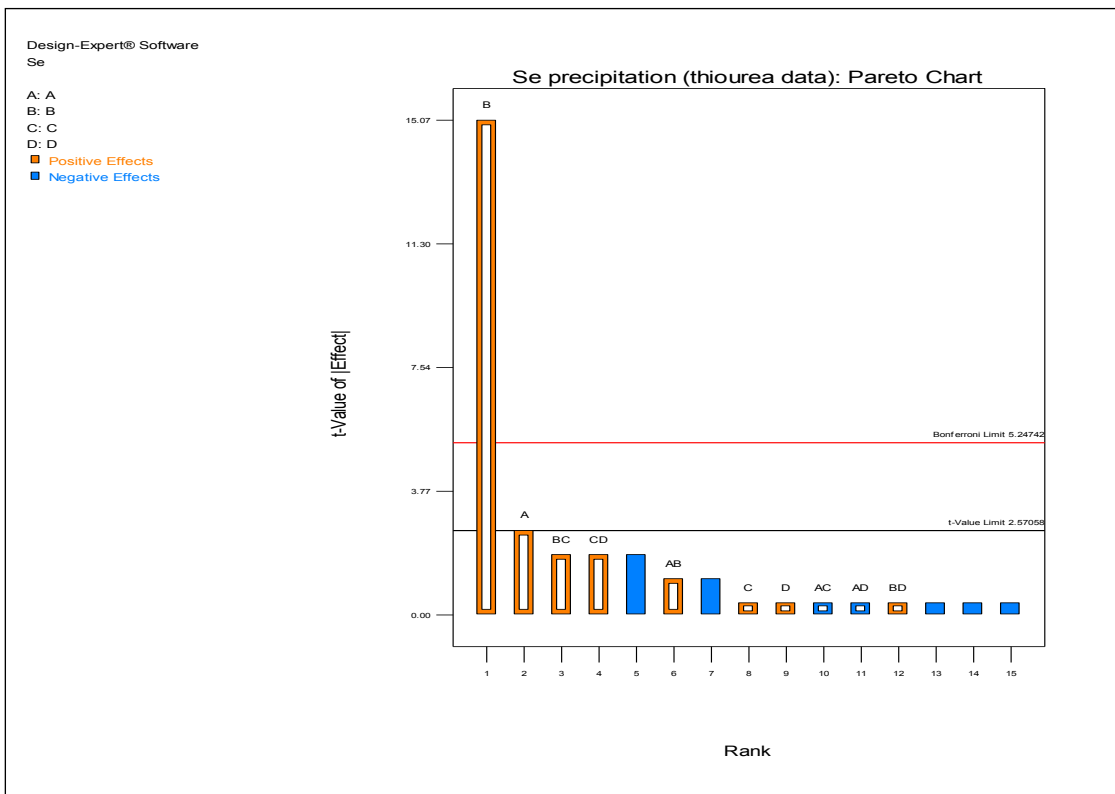


Figure 81: Pareto plots of effects for the Se response (thio-urea data)

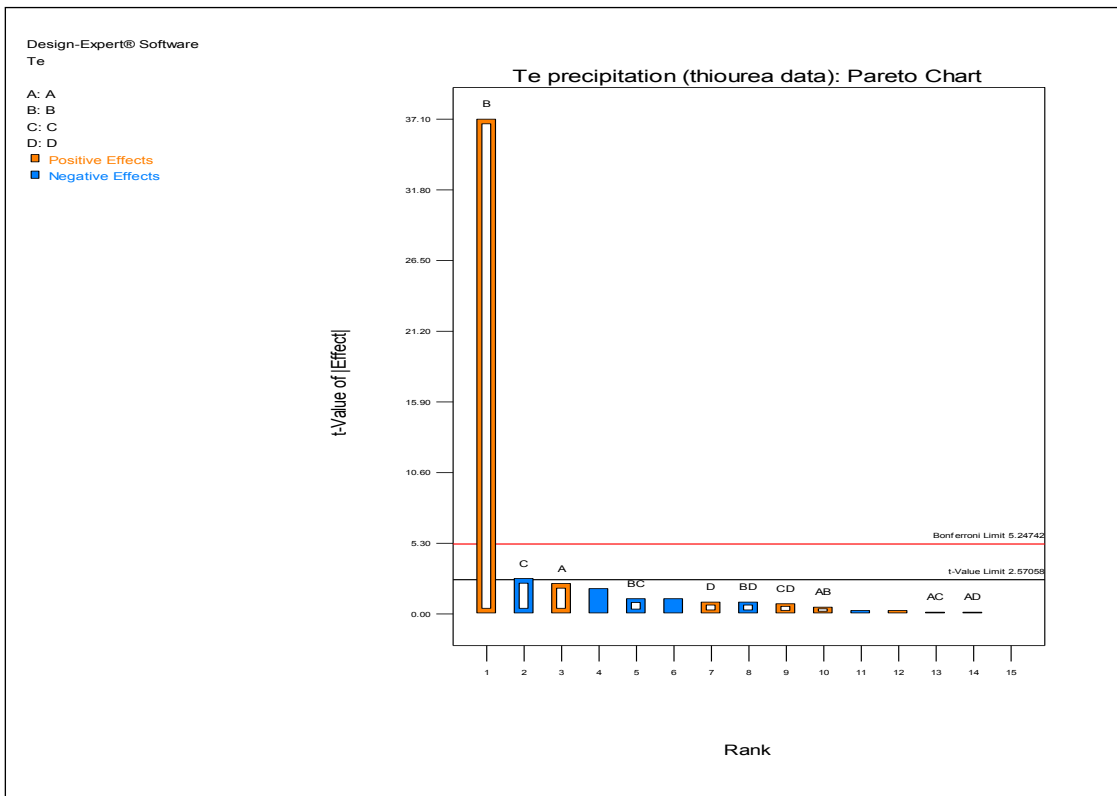


Figure 82: Pareto plots of effects for the Te response (thio-urea data)

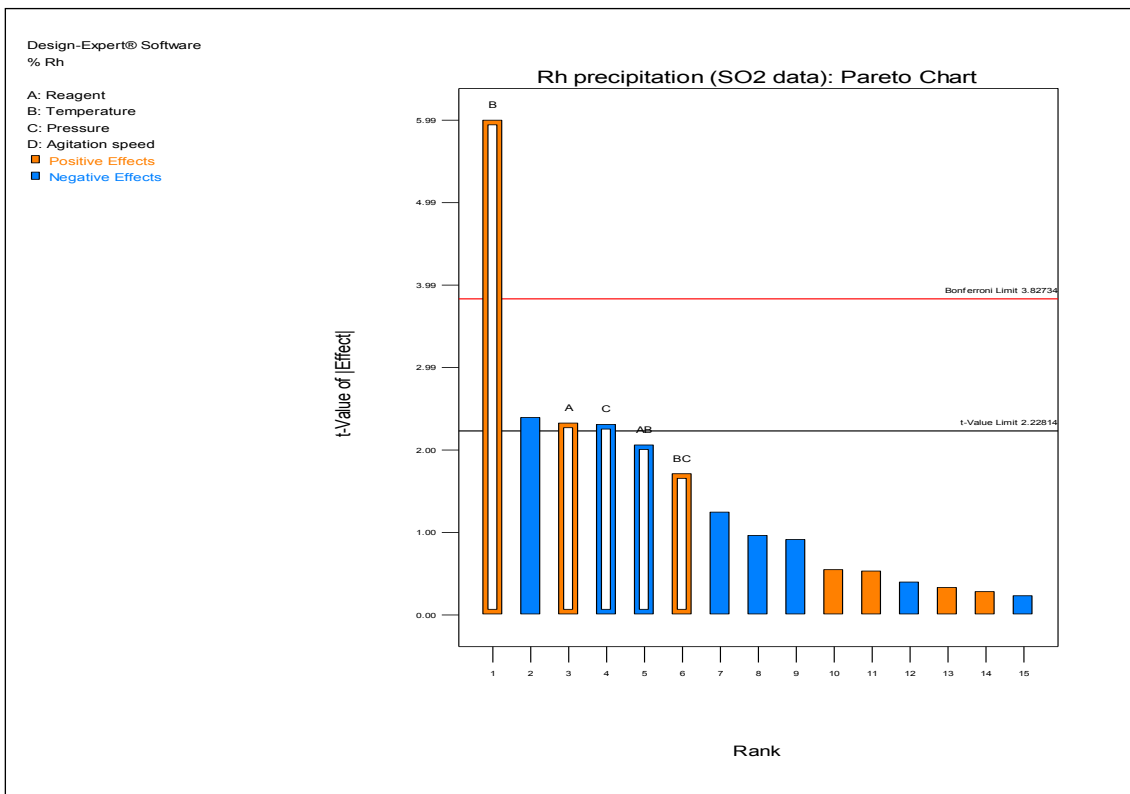


Figure 83: Pareto plots of effects for the Rh response (sulphurous acid data)

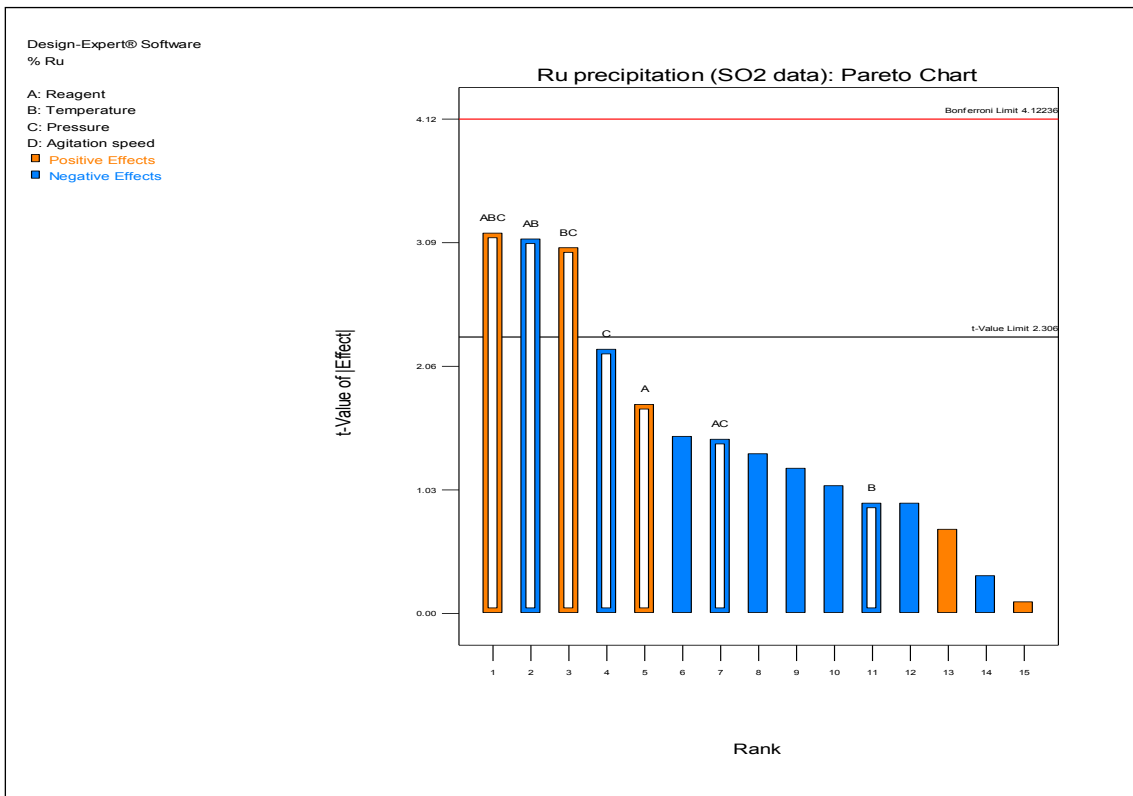


Figure 84: Pareto plots of effects for the Ru response (sulphurous acid data)

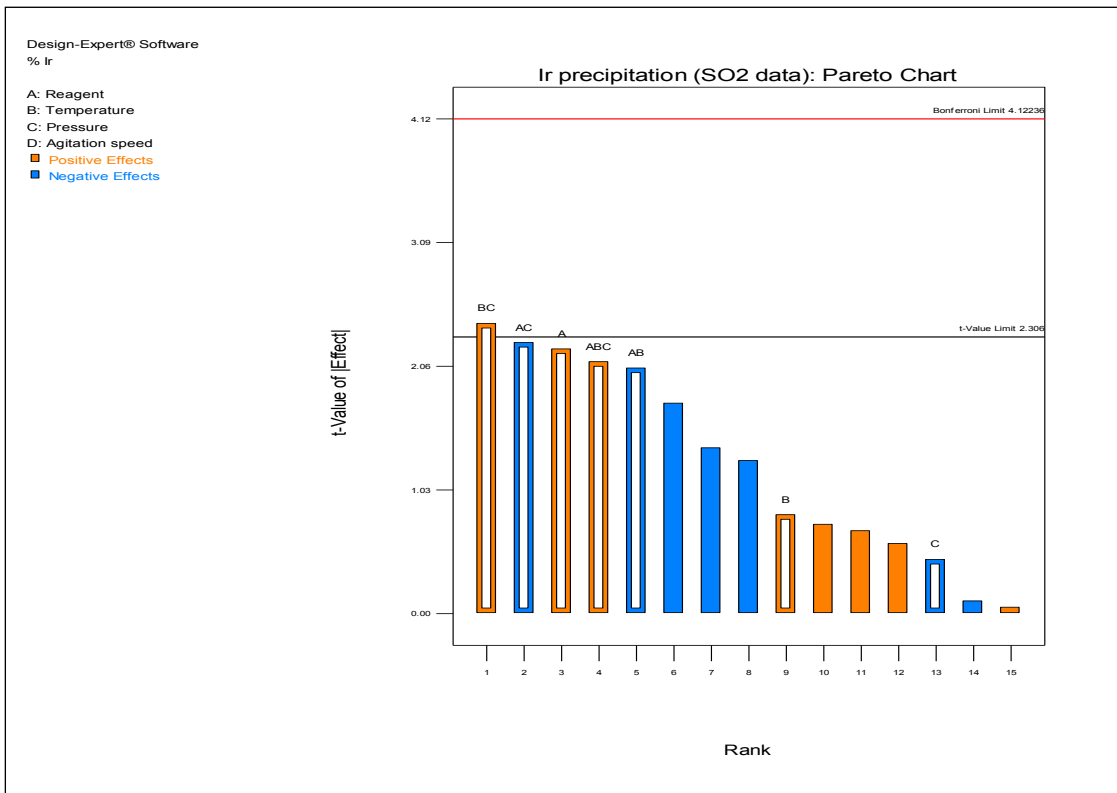


Figure 85: Pareto plots of effects for the Ir response (sulphurous acid data)

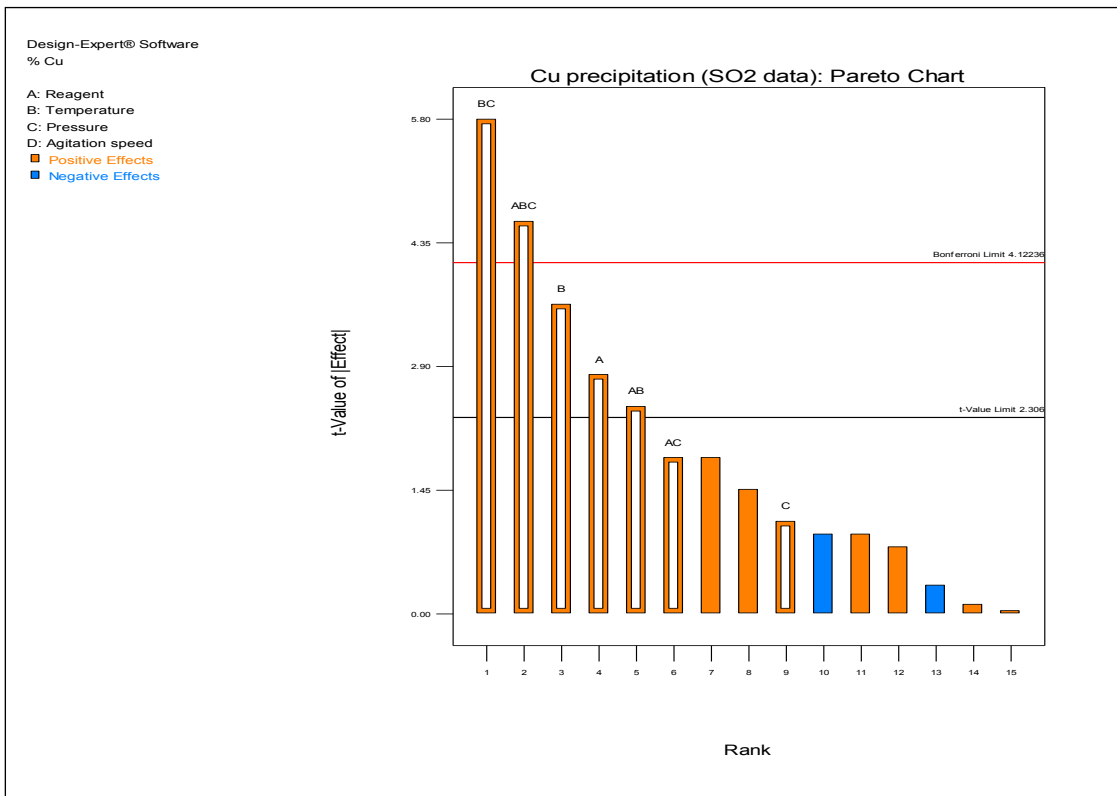


Figure 86: Pareto plots of effects for the Cu response (sulphurous acid data)

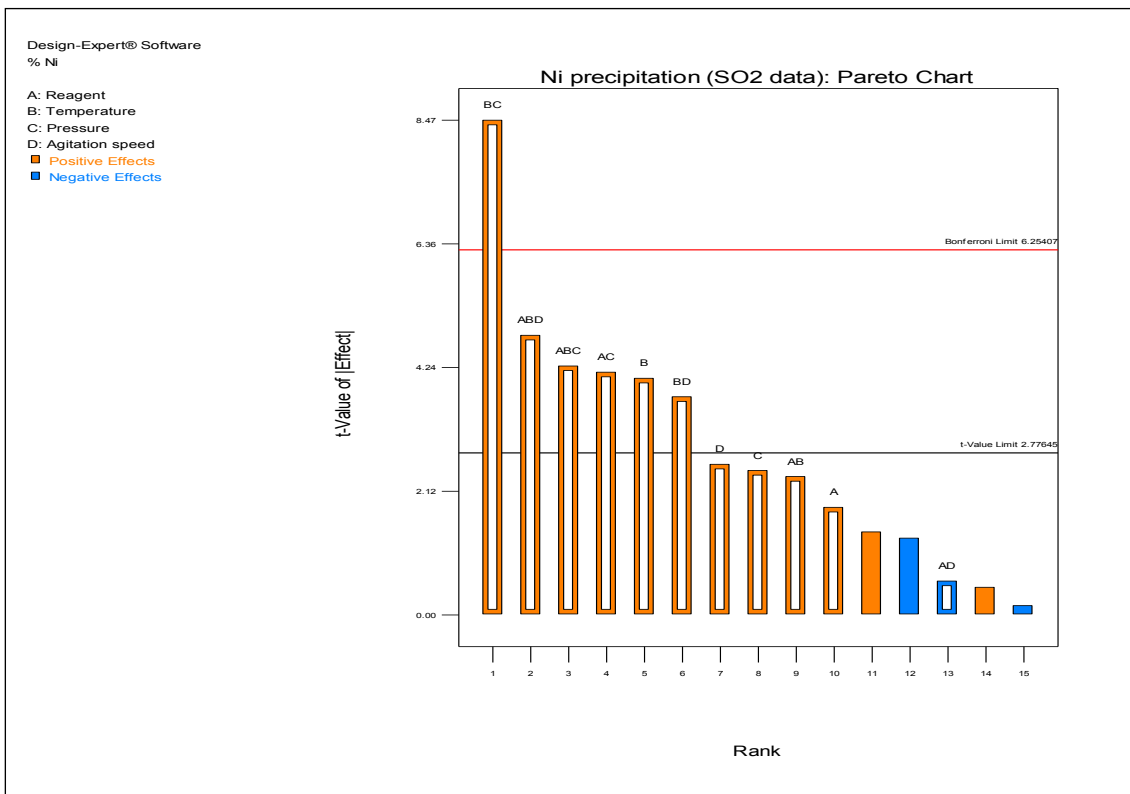
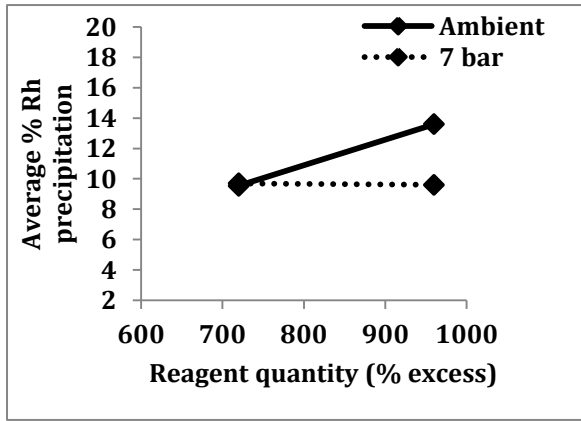
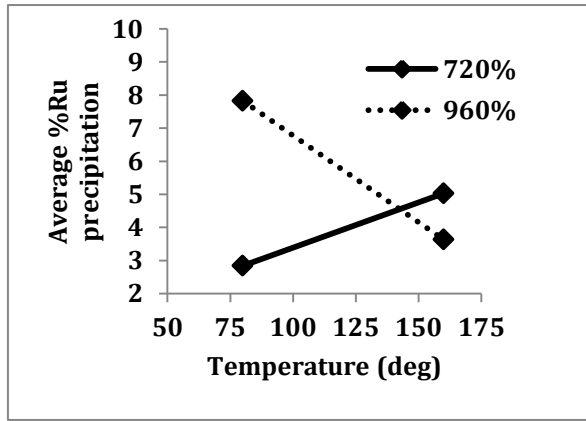


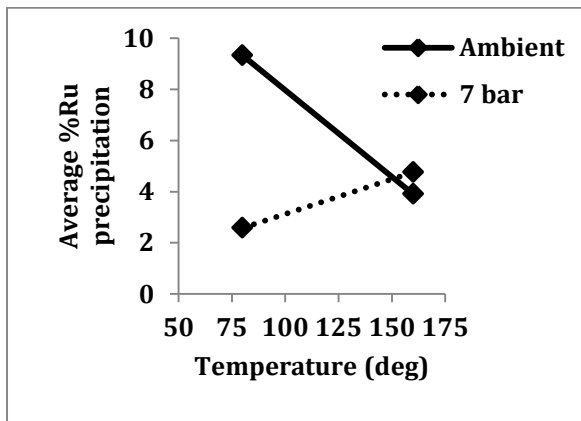
Figure 87: Pareto plots of effects for the Ni response (sulphurous acid data)



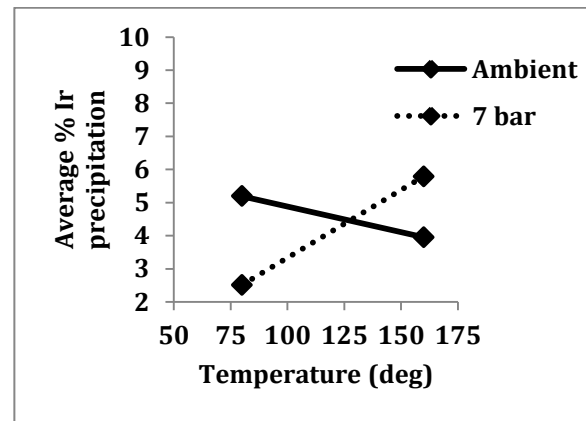
(a)



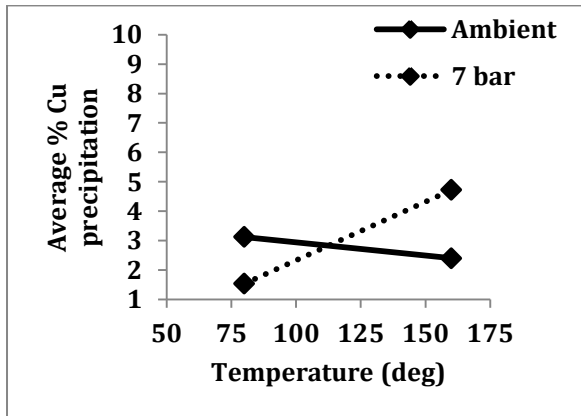
(b)



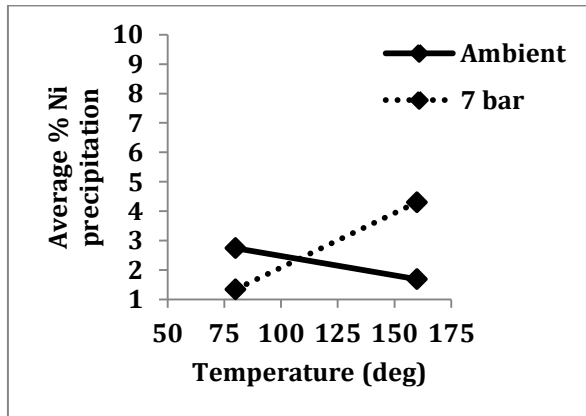
(c)



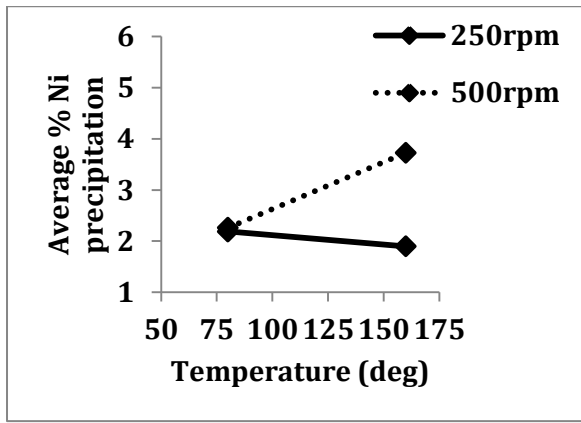
(d)



(e)



(f)



(g)

Figure 88: Interaction plots showing the effects of interactions between (a) reagent quantity and pressure -Rh (b) temperature and reagent-Ru (c) pressure and temperature - Ru and (d) pressure and temperature-Ir (e) pressure and temperature-Cu, (f) pressure and temperature-Cu, (f) pressure and temperature-Ni, and (g) temperature and agitation-Ni on the precipitation responses